



PhD-No PhD-FSTM-2023-086
The Faculty of Science, Technology and Medicine

DISSERTATION

Presented on 27/09/2023 in Luxembourg
to obtain the degree of

DOCTEUR DE L'UNIVERSITÉ DU LUXEMBOURG EN PHYSIQUE

by

Jorge Alfonso CHARRY MARTÍNEZ

Born on 12 October 1989 in Bogotá (Colombia)

CHEMISTRY AND PHYSICS OF POSITRONS INTERACTING WITH ATOMS, MOLECULES, AND FIELDS

Dissertation defense committee

Dr. Alexandre Tkatchenko, supervisor
Professor, University of Luxembourg

Dr. Aurélia Chenu, Chairman
Professor, University of Luxembourg

Dr. Neil Drummond, Vice-Chairman
Professor, University of Lancaster

Dr. Stefan Yoshi Buhmann
Professor, University of Kassel

Dr. Michele Casula
Professor, Sorbonne University

The content of this thesis is dedicated to any curious mind that wants to know what we have found in our journey to learn about positrons. All my efforts during my Ph.D. studies are dedicated to my family and to all the loved ones who have supported me along the way.

Abstract

The positron is the antiparticle of the electron, possessing the same mass and obeying the same spin statistics but with an opposite charge. When a positron and an electron collide, both annihilate within a few nanoseconds, emitting two or three photons. However, positrons can also form energetically metastable states with atoms and molecules before the pair annihilation.

The relatively long positronic lifetime, on a nanosecond time scale, allows a positron to interfere with the faster molecular vibrational motions or with molecular reactions, which are typically in the range between femto- and picoseconds. Therefore, such positronic systems expand the field of physical chemistry, which is still vastly unexplored theoretically and experimentally, and it could lead to new and exciting applications.

In recent decades, significant efforts have been made in the development of theoretical methods to accurately describe the interactions of positrons with matter, which often requires explicit many-body correlation effects, posing a substantial challenge for quantum-chemical methods based on single-particle atomic orbitals. Despite many creative and accurate approaches, most of them are extremely computationally expensive. Therefore, their application is limited to small and highly polar molecular systems, where the binding is mainly driven by the strong attractive electrostatic interaction.

This thesis aims to attain a robust understanding of positrons interacting with molecular systems, starting from first principles of quantum mechanics. To this end, new variational electron-positron wave function ansatzes are proposed and discussed, which are based on a combination of electron-positron geminal orbitals and a Jastrow factor that explicitly includes three- and four-body electron-positron correlations in the field of the nuclei, that is fully optimized within the framework of the Variational Monte Carlo (VMC) method. The performance of this approach is validated in combination with the Diffusion Monte Carlo (DMC) method by calculating total energies and binding energies of a set of positronic atomic and molecular systems, demonstrating that a representation in terms of electron-positron orbitals for the fermionic and Jastrow wave functions is an accurate and efficient approach for studying the interactions of positrons with matter.

Moreover, the developed methodology is applied here to study electronic and positronic response properties such as dipole polarizabilities, annihilation lifetimes, and expectation values of interparticle distances as a function of an external electric field, aiming to gain further physical insights into the electron-positron wave function structure. Through the Quantum Monte Carlo (QMC) method, non-trivial variations of the polarizabilities with respect to the interatomic length were unveiled. A further decomposition of the polarizability into electronic and positronic contributions revealed that the positronic cloud in the outer regions is highly polarizable and screens the response of the electrons to the same external electric field.

Furthermore, the QMC methodology was employed to investigate the stability of a system consisting of two positrons and three hydride anions, discovering the formation of a three-center two-positron bond, analogous to the well-known three-center two-electron counterpart in Li_3^+ , thus extending the concept of positron-bonded molecules, in which two or more repelling anions are stabilized by one or more positrons.

The final section is dedicated to the exploration of using positron-bonded diatomic systems as an alternative approach for estimating interacting atomic sizes, in which it was found that their equilibrium distance is connected to the sum of van der Waals radii of the corresponding neutral atoms, and to a lesser extent to the sum of anionic radii.

Overall, this thesis presents the development of a computational methodology based on QMC techniques to compute and analyze the wave function of positrons interacting with atoms, molecules, and external electric fields. The methods and analysis developed in the presented work will pave the way for further study of complex positronic systems of physical and chemical interest, encouraging new theoretical and experimental investigations in the field of positron-matter interactions.

Keywords: positrons, electron-positron correlation, quantum Monte Carlo, variational Monte Carlo, diffusion Monte Carlo, polarizability, annihilation lifetimes, positron-bond, three-center bonds, atomic radius.

Acknowledgments

Working on science is like navigating into a vast unexplored ocean to discover new lands. We do not know what we will discover, so we will need to have an open mind and sharp eyes. Sometimes we will pass through seas visited by previous travelers, reading their maps will be our guide. We do not know how much time it will take us, so we will be patient, persistent, and methodic. Curiosity will be the wind that drives us. We do not know which direction to take, so we will pay attention to our surroundings: the tides and the stars, then we will adjust the plan. In a navigation logbook, we will record the route. Discovering a new land will be our gift to science. Enjoying the journey with the crew members will be the treasure for our hearts, those memories we must record too. And then, we will go back to tell others what we found and how to get there. Hoping for more people to embark from the new lands, to further expand the horizon.

Therefore, I would like to dedicate the next words to express my gratitude to all the people who helped me, who supported me, to all who traveled with me on the ship. Doing a PhD felt like traveling on a new ocean. I prepared myself in the best way I knew, I was afraid of the unknown, I was sure that many challenges would appear. But still, I decided to start this adventure because I knew that I was having the support of my family, and that I would meet wonderful people along the way. I was right, the journey was full of pleasant surprises.

First of all, I would like to express gratitude to my supervisor, Prof Alexandre Tkatchenko, for providing me the opportunity to join his research group, and for sharing with me your research interests and scientific questions, which helped me to continue paving my way in science. I also appreciate the time and efforts you dedicated to my project, which you trusted from the start. Additionally, I appreciate all your efforts and time dedicated to carefully reviewing my project proposals, conference abstracts, papers, and thesis.

I acknowledge the financial support from the Luxembourg National Research Fund (AFR PhD/19/MS, 13590856) and from the University of Luxembourg, as well as the High-Performance Computing facilities of the University of Luxembourg for providing me the computational resources to perform all the calculations for the thesis.

I would also like to thank all the thesis committee members for accepting to be jury members of this dissertation. Furthermore, I would like to thank Dr. Matteo Barborini and Dr. Dmitry Fedorov for carefully proofreading the thesis, and to Dr. Carolin Müller for the feedback on the introduction section.

Dr. Matteo Barborini greatly helped in the scientific discussions of the introduction, theoretical background, and all the other chapters of this dissertation. In addition, Chapter 6 is the result of an external collaboration project with professor Andrés Reyes, professor Marcio Varela, Dr. Felix Moncada, and Dr. Laura Pedraza.

All the QMC calculations, developments, and implementations were performed with the QMeCha code, developed by Dr. Matteo Barborini. The multi-component MP2 calculations were carried out with the openLowdin code, developed under the supervision of professor Andrés Reyes. I appreciate the excellent work performed by the developers of both codes.

I want to express my deep gratitude to the thesis committee for accepting the invitation to be part of my thesis committee. It was an honor to meet you and to receive feedback from someone with such vast experience in QMC and quantum mechanics in general. Thanks for reviewing my thesis in detail and for showing interest in my topic, in particular to professor Drummond for his careful revision of the document. All of your questions and comments were very relevant to the discussion and it will help us to improve on the following research and publications. As a young scientist, I deeply appreciate that my work and effort were interesting to the more experienced community.

A special thanks go to my colleagues at the Theoretical Chemical Physics (TCP) group for sharing their research work, for fruitful discussions, and for keeping high scientific standards within the group. Working in a multidisciplinary and multicultural group as the TCP was a fascinating and challenging experience. I'm sure I learned something valuable from each of you, academic and personal. Despite sailing on different ships, it was a pleasure to navigate common seas with all of you. Thanks and congratulations to all of you for the great work. Additionally, I want to express my gratitude to all of you for the amazing gifts and great support for my PhD defense. I feel incredibly happy every time that I look at the hat. I love it! all the colorful lights, the representation of the Ps- and antiPs- is a great summary of our work, also the chocolates in blue and red wrappers, the racing cars which represent all the weekends that I spend chilling at home watching F1, the cat is also a good symbol of quantum mechanics to go along with the Ps- and because I love cats! And, of course, all the photos of great moments with the TCP people. Kudos to the hat makers! Finally, big thanks for the F1 McLaren Lego! I was not expecting that, and especially so big and amazing. Lego was my favorite toy when I was a kid. That was the first thing that I wrote in my Christmas card to baby Jesus (yep, Santa Claus does not have jurisdiction for Christmas gifts in Colombia, although he is welcome for decorations). Thank you for this lovely gift, it would help me to bring back memories from my great time

in Luxembourg. You are the most valuable part of my PhD adventure. Thank you TCP, my heart is completely filled with all your affection

I joined the PhD with two goals, the first was to learn more about science, and the second was to know great people with great human values. Matteo B., in you, I found both. Therefore I feel happy and satisfied with the PhD. Thanks for teaching me in detail about Quantum Monte Carlo; this is an amazing field, within an error bar, of course. Thanks for accepting to sail on this mixed positronic and QMC journey. QMC was our method of transportation, and QMeCha code was the ship. Many storms and tricky waters were a challenge, but thanks to your efforts and dedication, the ship was capable to continue sailing. Thanks for listening me, thanks for supporting my passion for positrons. Thanks for your great emotional support and for the life lessons. Thanks for our long conversations, thanks for waiting for the next tram, or the second one, or the third one. Thanks for all the fruitful scientific discussions, and for the long, long audios, thanks for helping me to understand physics a bit more. Thanks for sharing your life story, your perspective of science and life. It would be an honor to embark again with you, in search of new adventures. In any case, my best wishes for your next journey. Thank you Matteo B.

I highly appreciate the kindness of Yolande Edjogo, Erik Pillon, Dmitry Fedorov, and Ali Hakami during my first weeks in Luxembourg, those weeks were a bit frenetic and intimidating, but all of you kindly helped me to feel more comfortable in different aspects.

Thanks to Igor Polstavsky for the PhD interview, which counts as the first scientific discussion with the group, and the first step to start the PhD. Thanks to Dima for our scientific discussions about positrons, polarizability, and van der Waals interactions. I highly appreciate all your efforts and dedication in reviewing many of my manuscripts and slides. Thanks to all coauthors on our papers, Peter Szabo, Dmitry Fedorov, Szabolcs Goger, Reza Karimpour, Matteo Barborini, Félix Moncada, Laura Pedraza, Marcio Varella, Andrés Reyes, and Alexandre Tkatchenko, thanks for your great work.

Thanks Yolande, for all your administrative assistance and for sharing with us many delicious cakes and desserts!

Teaching was a new experience for me, and I was terrified. Therefore, I would like to thank Peter Szabo and Matteo Gori for your help during the quantum mechanics course. Thanks also to professor Jörg Baller and Sergey Ershov for your kind help and guidance during my teaching experience in the physics labs. As a chemist, it was a fun experience to go back to the lab! Thanks to all the students of the quantum mechanics and physics lab course, thanks for your great patience and comprehension.

I want to thank the support from many members of group: Erik Pillon, Somayeh Khazaei, Reza Karimpour, Szabolcs Goger, Peter Szabo, Mirela Puleva, Ariadni Boziki, and Carolin Müller. Thanks to all of you for listening to me and for giving me kind words of support.

On many occasions you helped me to stay on track when I was feeling a bit lost.

Gracias a Valentin Vassilev y Leonardo Medrano por todos aquellos agradables momentos en los que conversamos en nuestro idioma, me hicieron sentir cerca a mi casa, a nuestra gente, a nuestra cultura. Aprecio muchísimo esos momentos.

Thanks to Leonardo, Peter, Mario Galante, Kyunghoon Han, Matteo B., and Ariadni for kindly inviting me to your places for dinner, all of you are great chefs and hosts! Thanks to my office mates: Szabi, Gregory Cordeiro, Matej Ditte, Kyunghoon Han, Anton Charkin, and Tobias Henkes, thanks for keeping a fun spirit in the office. Every time I remember my time during the PhD, the first memory that comes to mind is the image and voices of all of you.

I want to express a special gratitude to Carolin and Ariadni for your friendship in the last months of the PhD. Thanks for opening the door of your office, those were great times, I will treasure many memories from such lovely moments. Thanks for your friendship Ariadni, thanks for sharing your story. A big koala hug for you. As I told you once, I find admirable your affection towards the most valuable aspects of your life; emotions, memories, and connections with people, which shows your greatness as a person. σου εύχομαι τα καλύτερα.

Within the TCP, my last gratitude message is to Mirela, thanks for your great support, kindness, and affection during the chaotic days before the defense. It would be an honor to return the favor and to be present at the culmination of your PhD. But since I probably won't be there, I just hope that the special wizard hat could help you to achieve your own legendary PhD hat.

Once more, I would like to thank my chemist colleagues, "el equipo". With all of you, we shared a common interest in chemistry. With all of you, I developed my skills as a professional. With you, I took those first steps in science that have led me to where I am today. A special thanks to Félix and Laura for your friendship, for our travels in Europe, and for your great support, thank you for always watching over me. Visiting me in Luxembourg was the best gift I have received for my birthday! Félix, we need to finish Cuphead!. Thanks to Nicolás and Diana for your support from Colombia and for caring about me. Yina, I will never forget our friendship, especially our long conversation on whatsapp, I always remember that time with great affection. I wish you the best in life.

Thanks to professor Andrés Reyes, thanks for still being my supervisor, my academic "father". Thanks for all your personal and academic teachings, especially for your passion for quantum chemistry, which was the foundation of my current research interest and motivation. And, of course, thanks for encouraging me to start this PhD adventure.

I would also like to thank Dr. Cristina. Thanks for your work; thanks for dedicating your life to helping others. You helped me in one of my most difficult times.

Finally, the last part of the acknowledgment section is dedicated to my family. Thanks to all my cousins, uncles, and aunts for your affection, it is always heartwarming to come back to Colombia and see the family. All of you remind me of my childhood, my origins. Luli, before starting the PhD I was hoping to tell you stories of my journey, but we did not have the chance to do that, rest in peace.

To my closest family: Leonor, Alfredo, Manuel, Nikita, Pinina, and Tani. Every day of my life, you have taught me love, affection, kindness, and empathy. Thanks for always being present. Despite the distance, I always feel your love. Thanks to you, I have a lovely place to call home, where I came from, and where I can return.

(Now in Spanish the last two paragraphs): Finalmente, la última parte de la sección de agradecimientos está dedicada a mi familia. Gracias a todos mis primos, tíos y tías por su cariño, siempre ha sido grato y reconfortante volver a Colombia y ver a toda la familia. Todos ustedes me recuerdan a mi infancia, a mis orígenes. Luli, antes de empezar el doctorado you esperaba poder contarte todas las historias de mi viaje, pero no tuvimos la oportunidad de hacer tener esos momentos, descansa en paz.

A mi familia más cercana: Leonor, Alfredo, Manuel, Nikita, Pinina y Tani. Cada día de mi vida ustedes me han enseñado amor, afectión, amabilidad, y empatía. Gracias por siempre estar presentes. A pesar de la distance siempre sentí su cariño. Gracias a ustedes tengo un maravilloso lugar al que llamar hogar, el lugar de donde vengo y a donde puedo volver.

Now, the journey is coming to an end. This thesis logs my adventures and findings on the quest to learn more about positrons and matter interactions. Thanks to all the people who accompanied and supported me, it was a pleasure to travel together. My best wishes on your personal journeys.

Preface

Note on publications

This thesis is partly based on the previously published articles:

- [1] J. Charry, M. Barborini, A. Tkatchenko. "Correlated Wave Functions for Electron-Positron Interactions in Atoms and Molecules" *J. Chem. Theory Comput.* **18**, 4, 2267-2280, 2022.
- [2] J. Charry, F. Moncada, M. Barborini, L. Pedraza-González, M. T. do N. Varella, A. Tkatchenko, A. Reyes. "The three-center two-positron bond" *Chem. Sci.* **13**, 13795, 2022.

The author's contribution to each paper is given at the beginning of a chapter or section where the main results are included.

Other publications:

- [1] P. Szabó, S. Góger, J. Charry M. R. Karimpour, D. V. Fedorov, A. Tkatchenko, "Four-Dimensional Scaling of Dipole Polarizability in Quantum Systems" *Phys. Rev. Lett.* **128**, 070602, 2022.

Papers published during the course of the PhD studies related to previous research.

- [1] F. Moncada, L. Pedraza-González, J. Charry, M. T. do N. Varella, A. Reyes. "Covalent bonds in positron dihalides". *Chem. Sci.* **11**, 42, 2019.
- [2] M. Bergami, A. L. D. Santana, J. Charry, A. Reyes, K. Coutinho, M. T. do N. Varella. "Multicomponent Quantum Mechanics/Molecular Mechanics Study of Hydrated Positronium" *J. Phys. Chem. B.* **126**, 14, 2699-2714, 2022.

Contents

Abstract	v
Acknowledgments	ix
Preface	xv
List of Figures	xxiii
List of Tables	xxvi
List of Abbreviations	xxvii
List of Symbols and Notation	xxxix
1 Introduction	1
2 Theoretical Background	9
2.1 Electron/Positron Hamiltonian	9
2.1.1 Born-Oppenheimer approximation	10
2.2 Multicomponent molecular orbital approach	11
2.2.1 Hartree-Fock method	11
2.2.2 Second-order Möller-Plesset perturbation theory	13
2.3 Quantum Monte Carlo	14
2.3.1 Monte Carlo integration	15
2.3.2 Variational Monte Carlo	19
2.3.3 Optimization methods	22
2.3.4 Diffusion Monte Carlo	23
2.3.5 Basic fixed-node DMC algorithm	28
2.4 Software	30
2.4.1 QMeCha code	30
2.4.2 LOWDIN code	31
3 Correlated Electron-Positron Wave Functions	33
3.1 Wave function	34
3.1.1 Generalized cusps conditions	34
3.1.2 Electron-positron wave functions	35
3.1.3 Electronic wave function	35
3.1.4 Positronic wave function	36
3.1.5 Jastrow factor	37
3.1.6 Computational details	40
3.2 Total Energies of Atomic-Positron System	41

3.2.1	Electron affinities	41
3.2.2	Total energies of atomic-positron system	43
3.2.3	Positron affinities and positronium binding energies with atoms	46
3.2.4	Dissociation channels of $e^+ \cdot H_2^-$ molecule	49
3.3	Summary	54
4	Dynamical Electron-Positron Jastrow Factor	57
4.1	Electron-positron wave functions	58
4.2	Electron-positron Jastrow factor	59
4.2.1	Atomic dynamical Jastrow factor	60
4.2.2	Geminal dynamical Jastrow factor	62
4.2.3	Mixed atomic-geminal dynamical Jastrow factor	63
4.2.4	Computational details	64
4.3	Results and discussion	65
4.3.1	Pure electron-positron systems	65
4.3.2	Jastrow basis set effect	67
4.3.3	Atoms and molecules	67
4.3.4	Dissociation energies	71
4.3.5	Scaling	75
4.4	Summary	75
5	Electric Response Properties of Positronic Systems	79
5.1	Methods	81
5.1.1	Wave function	81
5.1.2	External electric field	82
5.1.3	Polarizabilities	83
5.1.4	Annihilation rate	84
5.1.5	Computational details	84
5.2	Results and discussion	85
5.2.1	Dipole polarizabilities	85
5.2.2	Interparticle expectation distances and annihilation rates	91
5.3	Summary	92
6	Three-center Two-positron Bond	95
6.1	Methods	96
6.1.1	Quantum Monte Carlo wave function	97
6.1.2	Computational details	98
6.2	Results and discussion	99
6.2.1	Energy stability analysis	99
6.2.2	Comparison with analogous purely electronic systems	103
6.2.3	Densities	104
6.3	Summary	107
7	Positron-Bonded Diatomics: Estimating the Size of Interacting Atoms	111
7.1	Methods	112
7.2	Positron-bond systems	112
8	Summary and Outlook	119
	Appendix A: Correlated Electron-Positron Wave Functions	125

<i>CONTENTS</i>	xix
Appendix B: Dynamical Jastrow Factor for Electron-Positron Interactions	129
Appendix C: Electric Response Properties of Positronic Systems	133
Appendix D: The Three-Center Two-Positron Bond	135
Appendix E: Positron Bonded Diatomics: Relative Size of Interacting Atoms	139
Bibliography	158

List of Figures

1.1	Electronic and positronic density of tryptophan	4
3.1	Correlation energies ratios for atoms	42
3.2	Positron affinities and positronium binding energies of neutral atoms	46
3.3	Positron affinities and positronium binding energies of anionic atom	47
3.4	Potential energy curve of $e^+ \cdot H_2^{2-}$	50
3.5	Dissociation energy curves of $e^+ \cdot H_2^{2-}$	52
4.1	Schematic representation of the dynamical Jastrow factor	61
4.2	Comparison of VMC energies for different dynamical Jastrow factors	70
4.3	Comparison of DMC energies for different dynamical Jastrow factors	72
4.4	Positronic dissociation energies for different dynamical Jastrow factors at VMC	74
4.5	Positronic dissociation energies for different dynamical Jastrow factors at DMC	76
5.1	Dipole polarizability of positronic systems	86
5.2	Dipole polarizability as a function of internuclear distance in PsH dimer . .	89
5.3	Density change on PsH dimer under external electric field	90
5.4	Decomposition of dipole polarizability	91
5.5	Effect of external electric field on interparticle distances	92
6.1	Coordinate system for triatomic system	100
6.2	MP2 potential energies surface for triatomic systems	101
6.3	Potential energy curves for $2e^+[H_3^{3-}]$ and vertical detachment channels . .	103
6.4	Electronic and positronic density cuts of $2e^+[H_3^{3-}]$	105
6.5	Comparison of 2D binding densities for triatomic singlet systems	106
6.6	Comparison of 2D binding densities for triatomic triplet systems	107
7.1	Correlation between positron-bonded equilibrium distance and atomic radii	115

B1	DMC reblocking technique comparison	130
C1	Density change on Lithium dimer under external electric field	133
E1	Potential energy curves of positron-bond diatomics $e^+[A^-B^-]$	140

List of Tables

3.1	Relative errors for electron affinities and ionization potentials of atoms . . .	43
3.2	Non-relativistic total energies of positronic atoms	44
4.1	Mass effect on the dynamical Jastrow	65
4.2	Basis set effect on the dynamical Jastrow	68
5.1	Molecular properties of Ps, Ps ₂ , PsH, and (PsH) ₂	87
6.1	Vibrational parameters of 2e ⁺ [H ₃ ³⁻]	100
6.2	Comparison of vibrational parameters of triatomic systems	104
7.1	Atomic radii	113
7.2	Equilibrium distances of positron-bond diatomics	114
7.3	Comparison between positron-bonded equilibrium distance and atomic radii	114
A1	Non-relativistic total energies of atoms	125
A2	Non-relativistic total energies of atomic ions	126
A3	Electron affinities and ionization potentials of atoms	126
A4	Positron affinities and positronium binding energies of atoms	127
B1	Jastrow factor comparison of VMC and DMC energies	129
D1	Total energies of triatomic systems at VMC	135
D2	Total energies of triatomic systems at DMC	135
D3	Total energies of triatomic dissociated species	136
D4	Vertical dissociation channels for 2 e ⁺ H ₃ ³⁻	137
D5	Addiabatic dissociation channels for 2 e ⁺ H ₃ ³⁻	138

List of Abbreviations

3c2e	Three-center Two-electron
3c2p	Three-center Two-positron
AGP	Antisymmetrized Geminal Power
APMO	Any Particle Molecular Orbital
BE	Bond Energy
BOA	Born-Oppenheimer Approximation
CAS	Complete Active Space
CC	Coupled Cluster
CI	Configuration Interaction
DFT	Density Functional Theory
DMC	Diffusion Monte Carlo
EA	Electron Affinity
EPO	Electron-Positron Orbitals
FCI	Full Configuration Interaction
FN	Fixed-Node
FN-DMC	Fixed-Node Diffusion Monte Carlo
GTF	Gaussian Type Function
GTFs	Gaussian Type Functions

GTO Gaussian Type Orbital
GTOs Gaussian Type Orbitals
IP Ionization Potential
MBPT Many-body Perturbation Theory
MCMO Multi-Component Molecular Orbital
MD Multideterminant
MP Multi-Pairing
MP2 Second-Order Möller-Plesset
MRCI Multi-Reference Configuration Interaction
PA Positron Affinity
PALS Positron Annihilation Lifetime Spectroscopy
PEC Potential Energy Curve
PES Potential Energy Surface
PMO Positronic Molecular Orbitals
QMC Quantum Monte Carlo
QTAIM Quantum Theory of Atoms In Molecules
SD Single-Determinant
SNR Signal-to-Noise Ratio
SP Single-Pairing
SRC Stochastic Reconfiguration
SVM Stochastic Variational Method
TDSE Time-Dependent Schrödinger Equation
TISE Time-Independent Schrödinger Equation
vdW van der Waals
VFR Vibrational Feshbach Resonance
VMC Variational Monte Carlo
ZPE Zero Point Energy

List of Symbols and Notation

Γ	Annihilation rate
E_h	Atomic energy unit
a_0	Atomic distance unit
q	Charge
R	Classical nuclei position
ρ	Particle density
\det	Determinant of a matrix
μ	Dipole moment
\mathcal{A}	Dipole polarizability
E	Energy
\exp	Exponential function
Eq.	Equation
∇	Gradient
H	Hamiltonian
\mathcal{J}	Jastrow factor
Δ, ∇^2	Laplacian
m	Mass
ϕ	Orbital
r	Particle position
e^+	Positron
Ps	Positronium
\prod	Product of a sequence
\sum	Summatory
α	Variational parameter
ν	Vibrational frequency
Ψ	Wave function

Chapter 1

Introduction

One of the important milestones of 20th century physics was the discovery of the positron, an elementary particle with the same mass and same spin statistics of the electron but with opposite electric charge [1], hence its antiparticle counterpart. The first experimental evidence of this particle was attained by Anderson in 1933 [2]. While studying cosmic radiation in a cloud chamber, Anderson observed a particle's trail with a curvature matching the one obtained by electrons, but going in the opposite direction, revealing that its charge was positive, like a positively charged electron. Before this observation, one of the theoretical arguments to support the existence of an antiparticle of the electron was implied by the relativistic quantum mechanics of Dirac's equation [3], allowing particles like electrons to have either positive or negative energy solutions. However, due to the natural tendency of systems towards equilibrium and thus lower energy, these negative states would lead the energy to be unbound from below [4]. To overcome this issue, Dirac proposed a model of vacuum, described as an infinite sea filled with particles of negative energy, and thus impeding an electron from occupying those states. In this model, a hole in the sea could be seen as a particle with positive energy and positive charge, which Dirac initially identified as a proton. However, shortly after, it was pointed out that if that was the case, then stable atoms would not exist, therefore the mass of the positively charged particle should be the same as the electron, but no such particle was observed at the time until Anderson's discovery. Years later, Stueckelberg and Feynman reinterpreted the negative energy solutions as positive energy states of a particle with inverse charge, in a mirrored space, and moving backward in time [5], thus disregarding the notion of electron sea and holes.

Following the discovery of the positron, the phenomenon of electron-positron annihilation was observed experimentally [6, 7]. When an electron and a positron get in contact with each other, both can form a pseudo-atom called Positronium (Ps), a system similar to a Hydrogen atom but with the notable difference of having half of the reduced mass, and where both particles equally orbit their center of mass. Once the electron and the positron in Ps get into contact at a distance of approximately $\hbar/mc \approx 10^{-13}\text{m}$, the particles annihilate,

converting their total rest mass m into a pair of photons with an energy of 511 keV, which move in opposite directions according to the conservation of momentum [8]. This phenomenon was also predicted by Dirac's model, in which he proposed that an electron of positive energy could make a transition into an unoccupied negative-energy state, leading to the simultaneous disappearing of both the electron and a 'proton', emitting their energy in the form of electromagnetic radiation [9]. The lifetime of Ps also depends on its total spin state, going from 125 ps for antiparallel spins, for which the two particles decay through a two-photon channel as mentioned before, to 142 ns for parallel spin particles that decay into three photons with a total energy of 1022 keV [8]. However, once the particles are in contact, the time of the annihilation event is very short, of just 10^{-21} seconds.

Since the discovery of the positron, many exciting applications have been emerging in several fields, most of them based on electron-positron pair annihilations. For example, in medicine, positron emission tomography (PET) is a well-established functional imaging technique employed for cancer detection and for the visualization of metabolic processes in living tissues. It is based on the detection of gamma rays produced from a positron-emitting radionuclide, which is incorporated into a molecule that will be involved in a biochemical reaction [10, 11, 12]. In materials science, the Positron Annihilation Lifetime Spectroscopy (PALS) [8, 13, 14] is a non-destructive technique used to study defects and voids in solids, which is based on the principle that in the bulk of a material the positron will annihilate promptly with an electron, while if the positron resides in a vacancy defect, its lifetime will be longer, due to the absence of a close electron to annihilate. The production of positrons in both applications is based on the same principle; the β^+ radioactive decay of a neutron-poor isotope, in which a proton of a radionuclide atom is converted into a neutron, releasing a positron and an electron neutrino [8]. The most common positron sources for PALS and PET techniques are the isotopes ^{22}Na and ^{18}F , decaying into ^{22}Ne and ^{18}O , respectively.

Prior to the pair annihilation process, positrons and electrons are capable to form energetically metastable systems. As was mentioned above, the simplest bound state is the Ps atom, which was predicted by Mohorovičić in 1934 [15] and detected experimentally in 1951 by Deutsch [16]. Other electron-positron systems are the positronium anion Ps^- and positronium dimer Ps_2 , both speculated in 1946 by Wheeler [17]. Theoretically, these species are remarkably fascinating systems because they expose the complexity of stable three- and four-body systems, interacting through a Coulomb potential [18, 19]. However, due to the short lifetime of Ps and the technical difficulty of obtaining low-energy positrons in large numbers, the experimental observation of these species was achieved many years later, in 1981 [20] and 2007 [21], for Ps^- and Ps_2 , respectively. Larger species, such as Ps_3 have been predicted to be unbound [22].

For decades, several enthusiastic physicists and chemists have dedicated themselves to studying the interactions between positrons and regular matter [23, 24], finding some energetically stable bound states between a positron and an atom or a molecule. About 50

atoms have already been theoretically identified to bind a positron in the ground states of their neutral or anionic forms [25, 26], while for others, unbound states are mostly guaranteed, according to empirical predictions based on the correlation between highly accurate positron or positronium binding energies with other electronic properties of atoms such as polarizabilities, ionization potentials, or numbers of valence electrons. Nevertheless, no experimental evidence for positron-atom bound states has been found so far, with the remarkable exception of Positronium Hydride (denoted as PsH or e^+H^-), which was indirectly observed by analyzing the products of the collisions between $e^+ + CH_4$ and their dissociation energies threshold [27].

Regarding positron-molecule interactions, during the last two decades, the experimental evidence of such positronic complexes has only been obtained via vibrational Feshbach resonances (VFR) [28, 29]. In this technique, higher annihilation rates are observed at resonant frequencies of the incident positron energy with the vibrational motions of the positronic molecular complex, a process mainly explained through dipole coupling. Under this approach, the positron binding energies are inferred from the redshifts between the positron annihilation spectra and selected vibrational modes in the infrared spectra of the corresponding molecule. This innovative methodology has allowed the measurement of positron binding energies for over 90 molecules, mostly small organic nonpolar or weakly polar species [29], which has led to the following relationship

$$\epsilon = 12.4(\alpha_1 + 1.6\mu + 2.4N_\pi - 5.6), \quad (1.1)$$

between the positronic binding energies (in meV), and the dipole polarizabilities α_1 (in \AA^3), dipole moment μ (in Debye), and the number of π bonds N_π (for aromatic compounds) of the isolated molecule. Figure 1.1 illustrates the positronic and electronic density distribution for a polar molecule, showing that the positron localizes around the most negative region of the molecule, since the interaction is mainly driven by the electrostatic attraction between the positron and permanent dipoles in the molecule.

In general, the addition of a positron induces a slight change in the electronic structure. However, due to the coupling between the vibrational motions and enhanced annihilation rates, it is suggested that positron binding should also include molecular structures deviated from the equilibrium [30]. Apart from these findings, other types of coupling mechanisms are presumed to exist for nonpolar molecules [31, 32, 33] beyond dipole coupling, and thus further physical and chemical understanding remains to be unveiled.

The interest in metastable positronic states lies in the fact that, due to the somewhat relative long positronic lifetime, within the nanosecond, they can interfere with the faster molecular vibrational motions or with molecular reactions that are typically in the range between femto- and picoseconds [34]. Thus, the positronic binding phenomena can be envisioned as a useful mechanism for controlling chemical reactivity. Furthermore, the techniques to accumulate and manipulate positrons [35] and positronium atoms [36] at low energies have

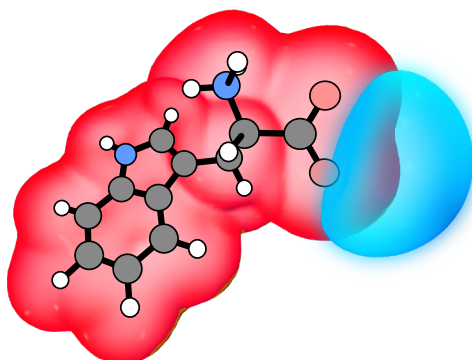


Figure 1.1: Electronic density (in red) and positronic density (in blue) for the positronic tryptophan system obtained at HF level. A contour value of 0.001 a.u. was used for both densities.

significantly advanced, allowing the possibility of a more careful study of the interaction between matter and antimatter, as well as achieving remarkable breakthroughs, such as the production of dipositronium (Ps_2) [21], the development of positronium gamma-ray lasers [37], and the production of long-lived positronium beams to study gravitational interactions [38].

In molecular physics, such experimental and technical advancements have stimulated a wide range of theoretical investigations, mostly aimed at developing accurate methods for predicting positron binding to atoms or molecules [29, 39]. Other related studies are focused on the calculation of scattering cross-sections [40, 41, 42, 43, 44], annihilation rates [40, 45, 46, 47, 48, 49, 50, 51, 52, 53], excited states [54, 55, 56, 57], electric response properties [58, 59, 60, 61, 62, 63], positron dynamics [30, 64, 65], or chemical reactions [66, 67, 68, 69, 70]. Among some recent theoretical discoveries, one could remark a new type of chemical binding in which the positron is directly responsible for binding and stabilizing two or more electronic species [71, 72, 73, 74]. Furthermore, it has been shown that positrons can act as a chemical mediator by drastically changing energy profiles of proton-transfer reactions in aminoacid compounds [69]. Nevertheless, further experimental work is necessary to confirm such findings.

Despite the aforementioned advancements, the field of positronic chemistry is still in its early stage, requiring further efforts to narrow the gap between experiment and theory [29, 39, 49, 75, 76]. Experimentally, the main challenge is accumulating and manipulating positrons before pair annihilation. On the other hand, the prediction of positron binding to atoms and molecules requires robust theoretical methods that can handle both localized and delocalized positronic and electronic states, and at the same time accurately capture electron-positron correlation energies. For this purpose, one can rely on the well-

established hierarchy of quantum-chemical methods. However, these methods, based on a single-particle atomic orbital representation, cannot explicitly capture the correlation arising from the attractive electron-positron Coulomb interaction [40], making them incapable to predict correct bound states in comparison to experiments. As a result, the methods based on the Multi-Component Molecular Orbital (MCMO) reference, including Many-body Perturbation Theory (MBPT) and Configuration Interaction (CI), still struggle to describe positron-matter systems accurately [76] and have to rely on large basis set extrapolations and multireference approaches at an extreme computational cost, limiting their applicability to relatively small systems [29, 77]. Recent progress has been achieved in this direction through the use of GW approaches [39, 78, 79], which correct the positron-molecule self-energy by including the contribution of virtual-positronium terms. Yet, their applicability is limited to positron binding energies only, and there is no guarantee of a monotonic convergence at higher orders. Nevertheless, these approaches represent the best agreement with experiment to date [39]. Given that, an accurate systematic description of electron-positron interactions can be obtained with highly accurate approaches such as explicitly correlated methods [80, 81, 82] and the Stochastic Variational Method (SVM) [83, 84], where the dependence on interparticle distances is explicitly introduced in the wave function.

In the direction of theoretical predictions, a successful computational approach to accurately describe the ground state of positronic complexes is represented by the family of QMC methods [85], which have already been applied to study positron interactions with atoms [45, 86, 87, 88, 89, 90, 91], small molecules [46, 92, 93], and solids [94]. The QMC techniques correspond to a family of stochastic integration approaches commonly used to solve Schrödinger's equation and to compute ground-state properties of quantum systems. The main advantage of these approaches lies in the versatility to work with elaborated wave functions that are capable of including explicit many-body interactions between the spatial degrees of freedom in the system, greatly enhancing the accuracy and improving the convergence with respect to the basis set size. Therefore, over the decades, for many physicists and chemists, QMC has been a powerful tool for proposing and testing sophisticated variational ansatzes. Additionally, for QMC calculations, the 3rd to 4th order scaling of the computational operations with respect to the number of fermions makes these techniques promising for the study of large systems with respect to the many correlated electronic methods, and due to the intrinsic parallel nature of their algorithms, it can fully exploit the progress of modern high-performance computing facilities despite their large computational prefactor [90, 95]. Thus, the main challenge for QMC remains the definition of an efficient variational ansatz, which for positron-matter systems should also include the electron-positron correlation interactions [96], besides the standard electronic correlation effects and cusp conditions.

This thesis presents contributions related to the development and applications of methodologies aimed at expanding the current computational tools and understanding of positron

interactions with atomic and molecular systems, mainly employing QMC techniques. The aforementioned topics serve as a general introduction and motivation for the subjects presented in the following chapters and a more specific introductory paragraph is given at the beginning of each chapter. The structure of the thesis is organized as follows:

Chapter 2 briefly summarizes the theoretical background employed in this work to tackle the problem of positron-matter interactions and describes the methodological approaches, highlighting all important points that should be taken into account for the inclusion of a positron into a quantum-mechanical system.

Chapter 3 describes in detail a new proposal for a variational ansatz of the total electron-positron wave function based on a combination of electron-positron geminal orbitals and a Jastrow factor, which are optimized at the level of VMC. This approach, in combination with DMC, is applied to calculate binding energies for either a positron e^+ or a Ps, bound to a set of atomic systems, as well as to study the Potential Energy Surface (PES) of two hydrogen anions H^- mediated by a positron, comparing the results to most accurate reference data available in the literature.

Furthermore, Chapter 4 presents an improved version of the Jastrow factor for the study of electron-positron interactions that explicitly includes three- and four-body correlations between pairs of positive charges (positrons, nuclei) and pairs of negative charges (electrons), expanded in a set of atomic and positronic orbitals. The performance of this Jastrow factor is analyzed through a systematic study of its components on the convergence of total energies and dissociation energies for the most relevant positronic compounds, computed by means of VMC and DMC.

Once the methodology is established and analyzed in Chapters 3 and 4, the following chapters 5, 6, and 7 present further studies and applications aimed to expand the current understanding of the positron behavior in atomic and molecular systems.

More specifically, Chapter 5 provides a detailed QMC study of the effects of an external electric field on the properties of positronic systems such as dipole polarizabilities, expectation values of interparticle distances, and two-photon annihilation rates for the most common positronic species, aiming to gain valuable insights into the electron-positron wave function structure, and their electric response to an external environment.

Next, Chapter 6 presents a QMC computational study on how two positrons can stabilize three repelling atomic anions through the formation of a three-center positronic bond, analyzing the local stability of the system against the vertical detachment and adiabatic energy dissociation channels, as well as comparing its bonding properties with those of the purely electronic H_3^+ and Li_3^+ systems.

Chapter 7 discusses how the equilibrium distance of positron bonded dimers, similarly to the one described in Chapter 6, can be connected to the sum of their atomic radii, presu-

ably serving as a new way to estimate atomic sizes.

Finally, Chapter 8 presents concluding remarks covering all preceding chapters, pointing out the main developments in the methods presented, the most relevant results obtained by studying the proposed applications, and a general outlook on future studies based on the findings and methodology discussed in this thesis.

Theoretical Background

This chapter provides a brief introduction to the basics of quantum mechanics in the context of a system comprised of electrons and positrons as quantum particles within the framework of a non-relativistic Time-Independent Schrödinger Equation (TISE) as described in Section 2.1. In addition to covering the essential steps of the methodologies used in this thesis, the current chapter will also highlight all the modifications required to extend the well-known electronic structure theory to the case of multiple electrons and positrons. Section 2.2 summarizes the most relevant expressions of MCMO, starting from HF to Second-Order Möller-Plesset (MP2) theories. A major emphasis will be given to Section 2.3 that covers the fundamental aspects of QMC techniques, since later in this thesis novel developments based on QMC will be described. Finally, Section 2.4 briefly summarizes technical aspects of the computational packages used in this work. In this thesis, atomic units were employed for all formulas, in essence: $\hbar = 1$, $m_e = 1$, and $q_e^- = e = 1$. Although, in some equations the variables of mass and charge are reintroduced to remark different terms coming for electrons and positrons, aiming for future generalizations to other particles with different mass and charge.

2.1 Electron/Positron Hamiltonian

Under the framework of the Born-Oppenheimer Approximation (BOA) [97], the non-relativistic Hamiltonian of a system comprised of N_f fermionic quantum particles and N_c classical point charges is written as:

$$\hat{H} = - \sum_i^{N_f} \frac{1}{2m_i} \nabla_i^2 + \sum_i^{N_f} \sum_J^{N_c} \frac{q_i Z_J}{R_{iJ}} + \sum_i^{N_f} \sum_{j>i}^{N_f} \frac{q_i q_j}{r_{ij}} + \sum_I^{N_c} \sum_{J>I}^{N_c} \frac{Z_I Z_J}{r_{IJ}}. \quad (2.1)$$

For the specific case of N_{e^-} electrons, N_{e^+} positrons, and N_c classical nuclei, the Hamiltonian correspond to:

$$\begin{aligned} \hat{H} = & -\sum_i^{N_{e^-}} \frac{1}{2m_{e^-}} \nabla_i^2 + \sum_i^{N_{e^-}} \sum_J^{N_c} \frac{q^{e^-} Z_J}{R_{iJ}} + \sum_i^{N_{e^-}} \sum_{j>i}^{N_{e^-}} \frac{q^{e^-} q^{e^-}}{r_{ij}} \\ & -\sum_k^{N_{e^+}} \frac{1}{2m_{e^+}} \nabla_k^2 + \sum_k^{N_{e^+}} \sum_J^{N_c} \frac{q^{e^+} Z_J}{R_{kJ}} + \sum_k^{N_{e^+}} \sum_{l>k}^{N_{e^+}} \frac{q^{e^+} q^{e^+}}{r_{kl}} \\ & + \sum_i^{N_{e^-}} \sum_k^{N_{e^+}} \frac{q^{e^-} q^{e^+}}{r_{ik}} + \sum_I^{N_c} \sum_{J>I}^{N_c} \frac{Z_I Z_J}{r_{IJ}}. \end{aligned} \quad (2.2)$$

Here, i - j and k - l are indexes for the electrons and positrons, respectively, while capital letters are used to denote nuclear indices. The masses and charges of the quantum particles are expressed with m and q , while Z is used for the nuclear charges. In Eq. 2.2, the first and fourth terms correspond to the kinetic energy, the second and fifth terms to the Coulomb potential with the nuclear charges, and the third and sixth terms are the repulsive Coulomb potential between fermionic particles of the same type. Finally, the second last term is the attractive Coulomb potential between electrons and positrons, and the last is the classical Coulomb potential between fixed point charges.

2.1.1 Born-Oppenheimer approximation

The previous molecular Hamiltonian is based on the BOA [97], one of the cornerstones of molecular physics and quantum chemistry. This is based on the fact that the nuclear motion is much slower than the motion of the electrons due to the large difference between their masses by at least a factor of 1800. Considering that, at first instance, the electronic and nuclear degrees of freedom can be decoupled, allowing to separate the molecular TISE into electronic and nuclear parts

$$\hat{H}_e(\mathbf{r}, \mathbf{R})\Psi(\mathbf{r}; \mathbf{R}) = E_e\Psi(\mathbf{r}; \mathbf{R}) \quad (2.3)$$

$$[\hat{T}_n + E_e(\mathbf{R})]\Phi(\mathbf{R}) = E\Phi(\mathbf{R}), \quad (2.4)$$

which converts the problem into solving an electronic Hamiltonian (Eq. 2.3) that explicitly depends on all electronic coordinates \mathbf{r} and parametrically on all nuclear coordinates \mathbf{R} . By extension, this approximation can also be applied to positrons with respect to the nuclei since $m_{e^+} = m_{e^-}$. Numerous electronic structure methods based on the BOA have been developed to solve the electronic Schrödinger equation (Eq. 2.3) [98]. The nuclear part can be solved in a second step by solving the nuclear equations with kinetic energy operator \hat{T}_n

for all nuclei N_n in a potential generated by the electronic part $E_e(R)$. The next sections of this thesis describe some methodologies employed to solve the TISE for electron-positron molecular systems.

2.2 Multicomponent molecular orbital approach

This section summarizes the expressions of MCMO methods for the specific case of multi electron-positron quantum systems based on the Any Particle Molecular Orbital (APMO) approach; a more detailed description can be found in a recent review of the method in reference [76]. Within this subsection, the Greek letters α and β are used to identify a quantum species, for example electrons or positrons.

2.2.1 Hartree-Fock method

The APMO/HF level wave function for an electron-positron molecular system in the ground state, Ψ_0 , is constructed as a product of a single-configurational electronic wave function, Φ^{e^-} , and a single-configurational positronic wave function, Φ^{e^+} ;

$$\Psi_0 = \Phi^{e^-} \Phi^{e^+}. \quad (2.5)$$

In the most common case, Φ^{e^-} and Φ^{e^+} are built as a Single-Determinant (SD) of single-particle spin molecular orbitals χ_i as

$$\Psi_{\text{SD}}(\bar{\mathbf{x}}) = \frac{1}{\sqrt{N_\alpha!}} \begin{vmatrix} \chi_1(\mathbf{x}_1) & \chi_1(\mathbf{x}_2) & \dots & \chi_1(\mathbf{x}_{N_\alpha}) \\ \chi_2(\mathbf{x}_1) & \chi_2(\mathbf{x}_2) & \dots & \chi_2(\mathbf{x}_{N_\alpha}) \\ \dots & \dots & \dots & \dots \\ \chi_{N_\alpha}(\mathbf{x}_1) & \chi_{N_\alpha}(\mathbf{x}_2) & \dots & \chi_{N_\alpha}(\mathbf{x}_{N_\alpha}) \end{vmatrix}, \quad (2.6)$$

here α symbol is used to represent either electrons or positrons, \mathbf{x} corresponds to their spin-coordinates vector, and $\bar{\mathbf{x}}$ is the full set of $4N$ coordinates. The spatial part of these spin orbitals, ϕ , is written as a linear combination of atomic orbitals φ with a basis set of size B (notice that the number of atomic centers can be greater than the number of classical nuclei N_c) as

$$\phi(\mathbf{r}_i) = \sum_{a=1}^B c_a \varphi_a(r_{i,q}). \quad (2.7)$$

Commonly these atomic orbitals are constructed with Gaussian Type Functions (GTFs) that depend on the spatial coordinate of one single particle r_i and are centered on a fixed position

r_a for each atomic center. The molecular orbitals are obtained by solving the coupled Fock equations

$$f^\alpha(i)\phi_i^\alpha = \varepsilon_i^\alpha \phi_i^\alpha, \quad \alpha = e^-, e^+, \quad (2.8)$$

where ε_i are the single particle orbital energies. The effective one-particle Fock operators, $f^\alpha(i)$, for the quantum species e^- and e^+ are expanded as

$$f^\alpha(i) = h^\alpha(i) + \sum_j^{N_\alpha} [J_j^\alpha - K_j^\alpha] - J^\beta. \quad (2.9)$$

In the above equation $h^\alpha(i)$ is the single-particle core Hamiltonian

$$h^\alpha(i) = -\frac{1}{2}\nabla_i^2 + \sum_J^{N_c} \frac{q^\alpha Z^\alpha}{R_{iJ}}, \quad (2.10)$$

and J^α and K^α are the Coulomb and exchange operators defined as

$$J_j^\alpha(1)\phi_i^\alpha(1) = q^\alpha q^\alpha \left[\int d\mathbf{r}_2 \phi_j^{\alpha*}(2) \frac{1}{r_{12}} \phi_j^\alpha(2) \right] \phi_i^\alpha(1), \quad (2.11)$$

$$K_j^\alpha(1)\phi_i^\alpha(1) = \left[\int d\mathbf{r}_2 \phi_j^{\alpha*}(2) \frac{1}{r_{12}} \phi_i^\alpha(2) \right] \phi_j^\alpha(1). \quad (2.12)$$

In addition, J^β is the operator which accounts for the Coulomb potential between particles of different quantum species, thus is the term which couples the electronic and positronic Fock equations, and is defined as

$$J_j^\beta(1)\phi_i^\alpha(1) = q^\beta q^\alpha \left[\int d\mathbf{r}_2 \phi_j^{\beta*}(2) \frac{1}{r_{12}} \phi_j^\beta(2) \right] \phi_i^\alpha(1). \quad (2.13)$$

In practice, these expressions are implemented in a matrix form [99] as

$$\begin{aligned} S_{\mu\nu}^\alpha &= \int dr_1 \phi_\mu^\alpha(1) \phi_\nu^\alpha(1) \\ F_{\mu\nu}^\alpha &= H_{\mu\nu}^\alpha + G_{\mu\nu}^\alpha + G_{\mu\nu}^\beta \\ H_{\mu\nu}^\alpha &= \int dr_1 \phi_\mu^\alpha(1) h^\alpha(1) \phi_\nu^\alpha(1) \\ G_{\mu\nu}^\alpha &= \sum_{\lambda\sigma} P_{\lambda\sigma}^\alpha [(\mu^\alpha \nu^\alpha | \sigma^\alpha \lambda^\alpha) - (1/2) (\mu^\alpha \lambda^\alpha | \sigma^\alpha \nu^\alpha)] \\ G_{\mu\nu}^\beta &= \sum_{\lambda\sigma} P_{\lambda\sigma}^\beta (\mu^\alpha \nu^\alpha | \sigma^\beta \lambda^\beta), \end{aligned} \quad (2.14)$$

where $S_{\mu\nu}$, $F_{\mu\nu}$, $H_{\mu\nu}$, and $G_{\mu\nu}$ correspond to the overlap, Fock (Eq. 2.9), one-core Hamiltonian (Eq. 2.10), and two-particles (Eqs. 2.11, 2.12, 2.13) element matrices, which run over the total number of atomic orbitals μ, ν . Here, the chemistry notation of two-particles integrals ($\phi_\mu\phi_\nu|\phi_\sigma\phi_\lambda$) has been simplified to $(\mu\nu|\sigma\lambda)$. In addition, the density matrix elements are defined from the coefficient matrix \mathbf{C} of the molecular orbitals expansion in Eq. 2.7 and the fermionic orbital occupation η

$$P_{\mu\nu}^\alpha = \eta^\alpha \sum_\lambda C_{\mu\lambda}^\alpha C_{\lambda\nu}^{*\alpha}. \quad (2.15)$$

These coefficient matrices are found by diagonalizing the Roothan-Hall equations

$$\mathbf{FC} = \epsilon\mathbf{SC}. \quad (2.16)$$

Finally, the total Hartree-Fock energy is computed from

$$E_0 = \frac{1}{2} \sum_\mu \sum_\nu P_{\mu\nu}^\alpha (H_{\mu\nu}^\alpha + F_{\mu\nu}^\alpha). \quad (2.17)$$

2.2.2 Second-order Möller-Plesset perturbation theory

The APMO/MP2 energy of a molecular system containing N^{e^-} electrons and N^{e^+} positrons is given by [76]

$$E^{\text{APMO/MP2}} = E^{(0)} + E_{\alpha\alpha}^{(2)} + E_{\alpha\beta}^{(2)}, \quad (2.18)$$

where $E^{(0)}$ is the APMO/HF energy (Eq. 2.17), while $E_{\alpha\alpha}^{(2)}$ and $E_{\alpha\beta}^{(2)}$ are the second-order same fermion (electron-electron and positron-positron) and different fermion correlation energies, respectively. These second-order corrections are written in the physicist notation [99] as

$$E_{\alpha\alpha}^{(2)} = \frac{1}{4} \sum_a^{\text{occ}^\alpha} \sum_b^{\text{occ}^\alpha} \sum_r^{\text{vir}^\alpha} \sum_s^{\text{vir}^\alpha} \frac{|\langle ab | rs \rangle - \langle ab | sr \rangle|^2}{\epsilon_a + \epsilon_b - \epsilon_r - \epsilon_s}, \quad (2.19)$$

and

$$E_{\alpha\beta}^{(2)} = \frac{1}{4} \sum_a^{\text{occ}^\alpha} \sum_b^{\text{occ}^\beta} \sum_r^{\text{vir}^\alpha} \sum_s^{\text{vir}^\beta} \frac{|\langle ab | rs \rangle|^2}{\epsilon_a + \epsilon_b - \epsilon_r - \epsilon_s}, \quad (2.20)$$

where occ^α and vir^α are, respectively, the number of occupied ($a - b$) and virtual ($r - s$) molecular orbitals for the fermionic type particle $\alpha = e^-, e^+$. Here, it should be noted that the two-particles integrals are built in terms of molecular orbitals as

$$\langle ij | kl \rangle = \sum_\mu \sum_\nu \sum_\kappa \sum_\lambda C_{\mu i} C_{\nu j} C_{\kappa k} C_{\lambda l} \langle \mu\nu | \kappa\lambda \rangle. \quad (2.21)$$

The second-order correction to the APMO/HF energy has contributions from double electronic or positronic excitations, according to Eq. 2.19, and from double excitations comprising of single excitations of the electronic and positronic subspaces, as given by Eq. 2.20. Both the direct (rs) and exchange (sr) contributions are accounted for in Eq. 2.19, and the MP2 perturbation potential, namely the difference between the sum of the Coulomb interactions and the sum of the single-particle Fock potentials [99], is implied in the above expressions.

2.3 Quantum Monte Carlo

QMC methods [85, 100, 101] are a family of stochastic techniques used to numerically integrate the many-body Schrödinger equation on a chosen trial wave function in order to calculate the mean value of physical observables for molecules, surfaces, and bulk materials. All these methods are characterized for using random samplings to integrate multi-dimensional functions that appear in many-body problems.

The difficulty of handling the Schrödinger equation lies in the correct description of an antisymmetric many-body wave function, which has a complexity that grows exponentially with the number of fermionic particles and explicitly depends on the two-particle distances. Traditionally, the approximations for the wave function are based on a linear combination of one-body Gaussian Type Orbital (GTO)s like in HF, see Section 2.2, due to the relative simplicity and low computational cost of the analytic integrals that arise in its formulation. Under this approach, the correlation effects can be introduced by using many-body perturbative expansion such as MBPT or Green functions approaches or by configuration state expansions in the Coupled Cluster (CC) and CI based methods, which usually dominate the field of quantum chemistry simulations. In these formulations, the accuracy is determined by the uncorrelated mean field reference provided by the single particle orbitals, which can only be systematically improved by increasing the many-body expansion. In practice, this orbital expansion is typically slowly convergent, quickly increasing the computational time and storage demands. Alternatively, methods based on Density Functional Theory (DFT) are generally not strongly limited by the system size, but the incomplete or unknown treatment of exchange and correlation effects decreases the accuracy [98], which are approximated by the use of empirical functionals, especially for mixed systems of electrons and positrons [64, 102, 103]. Nevertheless, DFT is fundamental in the PALS methodology for materials [94].

On the other hand, QMC methods are not necessarily constrained by the choice of the wave function, such as basis set type and size, or many-particle expansions, since more intricate explicitly correlated effects can be introduced in the wave function ansatz without relying on analytically available integrals or expensive spatial grid numerical integration

techniques. In addition, the highly parallelizable nature of Monte Carlo algorithms allows to efficiently exploit the advantages of large supercomputer resources. Therefore, over the decades QMC has been a powerful tool to study highly correlated systems, in which the accuracy can be improved by including novel and sophisticated variational ansatzes defined through physical intuition, while the precision can be systematically improved by increasing the number of samples.

The following subsections discuss the basic ideas of Monte Carlo stochastic integration and how this method is applied to evaluate the energy functional for a given approximate trial wave function of the Schrödinger equation, starting with the VMC method, which is considered as the most popular application of Monte Carlo integration technique for quantum mechanics, as well as describing the technical aspects of the optimization techniques of the variational parameters of the wave function. Finally, the basic concepts behind the DMC procedures within the Fixed-Node (FN) approximation Fixed-Node Diffusion Monte Carlo (FN-DMC), which is further employed to overcome the limitations of the VMC trial wave function.

2.3.1 Monte Carlo integration

Monte Carlo methods encompass a large number of numerical algorithms which can be used to solve integration problems through random sampling [85]. The common issue in solving an integral is the large number of evaluations of the integrand over many coupled degrees of freedom. However, in Monte Carlo, the idea is to create random samples of configurations that will be added together to give an accurate estimate of the desired exact quantity.

To recall the basic concepts of the Monte Carlo integration procedure [85, 100], let us consider a set of $3N$ -dimensional coordinates $\bar{\mathbf{r}}$ for a system of N fermions

$$\bar{\mathbf{r}} = \{\mathbf{r}_1, \mathbf{r}_2, \dots, \mathbf{r}_N\}. \quad (2.22)$$

A particular value of $\bar{\mathbf{r}}$ is sometimes called a walker or a configuration. The normalized probability density of finding the fermions in a given configuration $\bar{\mathbf{r}}$ has to satisfy the properties

$$\Pi(\bar{\mathbf{r}}) \geq 0, \quad \int \Pi(\bar{\mathbf{r}}) d\bar{\mathbf{r}} = 1. \quad (2.23)$$

Now, for a set of \mathcal{N} mutually independent configurations (uncorrelated) distributed according to the probability distribution $\Pi(\bar{\mathbf{r}})$, a new random variable $\mathcal{Z}[f(\bar{\mathbf{r}})]$ will be introduced

$$\mathcal{Z}_f = \frac{1}{\mathcal{N}} \sum_{i=1}^{\mathcal{N}} f(\bar{\mathbf{r}}), \quad (2.24)$$

where $f(\bar{\mathbf{r}})$ is a function with mean value m_f and variance σ_f^2 which are exactly defined by the finite integrals

$$m_f = \int d\bar{\mathbf{r}} f(\bar{\mathbf{r}}) \Pi(\bar{\mathbf{r}}) \quad , \quad \sigma_f^2 = \int d\bar{\mathbf{r}} (f(\bar{\mathbf{r}}) - m_f)^2 \Pi(\bar{\mathbf{r}}).$$

Due to the central limit theorem, it can be demonstrated that for a large number of configurations \mathcal{N} , the random variable \mathcal{Z}_f follows a normal distribution with mean m_f and standard deviation $\sigma_f/\sqrt{\mathcal{N}}$. Implying that, in general, the mean value of independent measurements of a given function f over a large number of configurations $\bar{\mathbf{r}}$ can be a good estimator of the exact mean value m_f , with an error that decreases as $1/\sqrt{\mathcal{N}}$, independently of the number of integration variables and independently of the form of the probability distribution $\Pi(\bar{\mathbf{r}})$. This idea can be extended to evaluate integrals over generic multidimensional functions. In essence, in order to compute the integral of a function $g(\bar{\mathbf{r}})$, as

$$I = \int d\bar{\mathbf{r}} g(\bar{\mathbf{r}}), \quad (2.25)$$

a distribution function $\Pi(\bar{\mathbf{r}})$ is introduced to guide the exploration of the integration space of $f(\bar{\mathbf{r}})$ over the most probable region; this procedure is called the importance sampling technique.

$$I = \int d\bar{\mathbf{r}} g(\bar{\mathbf{r}}) = \int d\bar{\mathbf{r}} f(\bar{\mathbf{r}}) \Pi(\bar{\mathbf{r}}) \quad f(\bar{\mathbf{r}}) \equiv \frac{g(\bar{\mathbf{r}})}{\Pi(\bar{\mathbf{r}})}. \quad (2.26)$$

As seen before, the above integral can be obtained as the average of discrete evaluations of $f(\bar{\mathbf{r}})$ over an infinite set of random configurations $\bar{\mathbf{r}}$ generated according to the distribution $\Pi(\bar{\mathbf{r}})$ as

$$I = \lim_{\mathcal{N} \rightarrow \infty} \left\{ \frac{1}{\mathcal{N}} \sum_{i=1}^{\mathcal{N}} f(\bar{\mathbf{r}}) \right\}, \quad (2.27)$$

then, a stochastic estimation of the integral can be obtained by averaging over a large but finite sample of configurations drawn from $\Pi(\bar{\mathbf{r}})$ as

$$I \approx \langle f(\bar{\mathbf{r}}) \rangle_{\Pi} = \frac{1}{\mathcal{N}} \sum_{i=1}^{\mathcal{N}} f(\bar{\mathbf{r}}), \quad (2.28)$$

with an associated error of

$$\frac{\sigma_f}{\sqrt{\mathcal{N}}} \approx \sqrt{\frac{1}{\mathcal{N}(\mathcal{N}-1)} [\langle f(\bar{\mathbf{r}})^2 \rangle_{\Pi} - \langle f(\bar{\mathbf{r}}) \rangle_{\Pi}^2]}. \quad (2.29)$$

According to this way, a better choice of the distribution function $\Pi(\bar{\mathbf{r}})$ reduces to the variance of fixed sample size, more specifically, the best choice for $\Pi(\bar{\mathbf{r}})$ would be to make it as close as possible to $|g(\bar{\mathbf{r}})/I|$, when $f(\bar{\mathbf{r}})$ becomes constant. However, I is unknown for this problem.

Metropolis algorithm

As described before, when using Monte Carlo integration, it is necessary to sample probability distributions in multidimensional spaces, which are generally very complicated and highly correlated, and of which its normalization is unknown, as in the case of quantum mechanics problems. To overcome this issue, the Metropolis algorithm was introduced [104] to generate a collection of configurations according to a desired distribution $\Pi(\bar{\mathbf{r}})$. Before enumerating the basic steps of the method, it is necessary to start by introducing some quantities. The Metropolis algorithm is based on the *detailed balance principle*, which establishes that to maintain a stable stationary relationship, the number of processes undergoing a transition $\bar{\mathbf{r}}' \rightarrow \bar{\mathbf{r}}$ has to be exactly compensated by the same amount of reverse processes $\bar{\mathbf{r}} \rightarrow \bar{\mathbf{r}}'$. Then, in order to define a Markov process (a process in which the probability of each event depends only on the state attained in the previous event), according to a desired distribution $\Pi(\bar{\mathbf{r}})$, the transition probability $\omega(\bar{\mathbf{r}}', \bar{\mathbf{r}})$ of being in a state $\bar{\mathbf{r}}$ transitioning to state $\bar{\mathbf{r}}'$ must be equal to the probability of being in state $\bar{\mathbf{r}}'$ transitioning to state $\bar{\mathbf{r}}$, such that

$$\omega(\bar{\mathbf{r}}', \bar{\mathbf{r}}) \Pi(\bar{\mathbf{r}}) = \omega(\bar{\mathbf{r}}, \bar{\mathbf{r}}') \Pi(\bar{\mathbf{r}}'). \quad (2.30)$$

In the Metropolis algorithm, the transition probability ω is split into two parts: the proposal and the acceptance-rejection as

$$\omega(\bar{\mathbf{r}}', \bar{\mathbf{r}}) = T(\bar{\mathbf{r}}', \bar{\mathbf{r}}) A(\bar{\mathbf{r}}', \bar{\mathbf{r}}), \quad (2.31)$$

where $T(\bar{\mathbf{r}}', \bar{\mathbf{r}})$ defines a trial probability that proposes the new configuration $\bar{\mathbf{r}}'$ and $A(\bar{\mathbf{r}}', \bar{\mathbf{r}})$ is the acceptance probability of that move. Therefore, an acceptance ratio can be written as

$$\frac{A(\bar{\mathbf{r}}', \bar{\mathbf{r}})}{A(\bar{\mathbf{r}}, \bar{\mathbf{r}}')} = \frac{T(\bar{\mathbf{r}}, \bar{\mathbf{r}}') \Pi(\bar{\mathbf{r}}')}{T(\bar{\mathbf{r}}', \bar{\mathbf{r}}) \Pi(\bar{\mathbf{r}})}. \quad (2.32)$$

The next step is to choose an acceptance probably, which in the Metropolis algorithm is given by

$$A(\bar{\mathbf{r}}', \bar{\mathbf{r}}) = \min \left(1, \frac{T(\bar{\mathbf{r}}, \bar{\mathbf{r}}') \Pi(\bar{\mathbf{r}}')}{T(\bar{\mathbf{r}}', \bar{\mathbf{r}}) \Pi(\bar{\mathbf{r}})} \right), \quad (2.33)$$

In this way, the *detailed balance principle* is satisfied either when $A(\bar{\mathbf{r}}, \bar{\mathbf{r}}') = 1$ or $A(\bar{\mathbf{r}}', \bar{\mathbf{r}}) = 1$. If $A(\bar{\mathbf{r}}', \bar{\mathbf{r}}) > 1$ the move is always accepted, otherwise it is compared to a random number μ uniformly extracted between $[0,1]$, so that if $A(\bar{\mathbf{r}}', \bar{\mathbf{r}}) > \mu$ then it will be accepted, otherwise refused. When the move is accepted the new position $\bar{\mathbf{r}}'$ becomes the new starting point from which to continue the *random walk*, otherwise a new move must be extracted again with the probability $T(\bar{\mathbf{r}}', \bar{\mathbf{r}})$ from the old position $\bar{\mathbf{r}}$. This procedure is repeated until the chosen number \mathcal{N} of fermionic configurations are generated. In most cases (as in

the original work by Metropolis and collaborators), it is useful to consider symmetric trial probabilities $T(\bar{\mathbf{r}}, \bar{\mathbf{r}}') = T(\bar{\mathbf{r}}', \bar{\mathbf{r}})$ simplifying the acceptance probability to

$$A(\bar{\mathbf{r}}', \bar{\mathbf{r}}) = \min\left(1, \frac{\Pi(\bar{\mathbf{r}}')}{\Pi(\bar{\mathbf{r}})}\right), \quad (2.34)$$

Considering the above definitions, the Metropolis algorithm is summarized in the following steps:

1. Initial setup: set initial random configuration $\bar{\mathbf{r}}$.
2. Propose a move according to a transition probability $T(\bar{\mathbf{r}}, \bar{\mathbf{r}}')$, for example as:

$$\bar{\mathbf{r}}' = \bar{\mathbf{r}} + \frac{1}{2}\eta[-1, 1]\Delta t, \quad (2.35)$$

where $\eta[-1, 1]$ is a set of $3N_f$ random numbers extracted uniformly in the interval $[-1, 1]$, and Δt is an initial Metropolis step that defines the maximum length of the move. Here, it should be noted that in practice, this variable is allowed to be different for electrons and positrons.

3. Evaluate the acceptance probability $A(\bar{\mathbf{r}}', \bar{\mathbf{r}})$.
4. Acceptance or rejection criteria
 - Generate a random number $u \in [0, 1]$.
 - If $A(\bar{\mathbf{r}}', \bar{\mathbf{r}}) \geq u$ the move is accepted and $\bar{\mathbf{r}}'$ will become the new configuration.
 - If $A(\bar{\mathbf{r}}', \bar{\mathbf{r}}) < u$ the move is rejected and the new configuration will remain the previous position $\bar{\mathbf{r}}$.

The above process is repeated until generating the desired number of configurations \mathcal{N} . In order for a random walk to move according to the *detailed balance principle* imposed by the acceptance probability, it is necessary to perform a certain number of thermalization steps to equilibrate the Markov process according to $\Pi(\bar{\mathbf{r}})$. Each walker moving in a new configuration of the space will depend on the Δt parameter that appears in Eq. 2.33. The smaller Δt , the more configurations visited by each walker will be correlated, leading to an error in the estimation of the variance of $f(\bar{\mathbf{r}})$. On the other hand, using values of Δt which are too large, would lead to a small acceptance probability, with the consequence that the majority of the moves proposed would be refused. Empirically, Δt (also called thermalization time step) is chosen so that the acceptance rate of the moves is around 50% along all the random walks.

One of the main advantages of this algorithm is that the normalization of $\Pi(\bar{\mathbf{r}})$ is never required since it only depends on the ratio of two different configurations $\frac{\Pi(\bar{\mathbf{r}}')}{\Pi(\bar{\mathbf{r}})}$, therefore

the normalization condition $\int \Pi(\bar{\mathbf{r}}) d\bar{\mathbf{r}} = 1$ will appear on both numerator and denominator of the ratio, canceling out itself. This allows for arbitrarily sampling complex distribution in a straightforward way without knowledge of its normalization.

Binning technique

An issue of the Metropolis algorithm is the fact that in a random walk, the walkers moving towards a new configuration in space will have a memory of their previous position that will depend on the Δt amplitude of the step; they are serially correlated, leading to autocorrelation of the configurations and thus to an underestimation of the variance of the functions estimated over the sampling. To decorrelate the variables, the so-called binning method (or reblocking) is used [105]. This method is based on the division of the \mathcal{N} consecutive samplings into N_{bin} segments (bins) of length $L_{bin} = \mathcal{N}/N_{bin}$.

For each bin j , in $j = 1 \dots N_{bin}$, the partial average of a property x is defined as

$$x^j = \frac{1}{L_{bin}} \sum_{i=(j-1)L_{bin}+1}^{jL_{bin}} x_i, \quad (2.36)$$

which are equal to the original average \bar{x} . However, the distribution of each binned variables x^j is different from the one of the x_i 's. Therefore, the total variance will also change and can be estimated as

$$s_{bin}^2 = \frac{1}{N_{bin} - 1} \sum_{j=1}^{N_{bin}} (x^j - \bar{x})^2. \quad (2.37)$$

Notice that in the case when the N_{bin} increases, therefore the length of each bin decreases, the average of each bin x^j goes further away from the real average \bar{x} leading to an increase of their variance. In contrast, the error bar $\sqrt{s_{bin}^2/N_{bin}}$ goes lower due to the larger number of bins. Thus, in practice, it is recommended to plot the estimated standard error in the mean energy against the number of blocks. It should converge to a constant value for large enough blocks, which is a better standard error in the mean.

2.3.2 Variational Monte Carlo

In quantum mechanics, the simplest QMC method is VMC [85], where Monte Carlo integration is applied to compute the energy functional

$$E[\Psi_T(\bar{\alpha})] = \frac{\int \Psi_T^*(\bar{\alpha}; \bar{\mathbf{r}}) \hat{H} \Psi_T(\bar{\alpha}; \bar{\mathbf{r}}) d\bar{\mathbf{r}}}{\int |\Psi_T(\bar{\alpha}; \bar{\mathbf{r}})|^2 d\bar{\mathbf{r}}}, \quad (2.38)$$

over a trial wave function $\Psi_T(\bar{\alpha}; \bar{\mathbf{r}})$, where $\bar{\alpha}$ is a set of variational parameters. In the above-normalized expectation value, the integrand can be rewritten as the product of two functions by dividing and multiplying by the function $\Psi_T(\bar{\alpha}; \bar{\mathbf{r}})$ on the left of the operator \hat{H} , leading to

$$E[\Psi_T(\bar{\alpha})] = \int E_{loc}(\bar{\alpha}; \bar{\mathbf{r}}) \Pi(\bar{\alpha}; \bar{\mathbf{r}}) d\bar{\mathbf{r}}, \quad (2.39)$$

where the first function corresponds to the local energy

$$E_{loc}(\bar{\alpha}; \bar{\mathbf{r}}) = \frac{\hat{H}\Psi_T(\bar{\alpha}; \bar{\mathbf{r}})}{\Psi_T(\bar{\alpha}; \bar{\mathbf{r}})}, \quad (2.40)$$

which is the energy of a particular electronic configuration $\bar{\mathbf{r}}$, and

$$\Pi(\bar{\alpha}; \bar{\mathbf{r}}) = \frac{|\Psi_T(\bar{\alpha}; \bar{\mathbf{r}})|^2}{\int |\Psi_T(\bar{\alpha}; \bar{\mathbf{r}})|^2 d\bar{\mathbf{r}}}, \quad (2.41)$$

is the probability density, which is proportional to the square modulus of the wave function $\Psi_T(\bar{\alpha}; \bar{\mathbf{r}})$, according to which the fermionic configurations $\bar{\mathbf{r}}$ are distributed.

In the Monte Carlo method (see Section 2.3.1) the estimation of the energy functional corresponds to the mean value of the local energies computed for a certain number \mathcal{N} of fermionic configurations extracted through the Metropolis-Hastings (see Section 2.3.1) algorithm according to $\Pi(\bar{\alpha}; \bar{\mathbf{r}})$

$$E[\Psi_T(\bar{\alpha})] = \langle E_{loc}(\bar{\alpha}; \bar{\mathbf{r}}) \rangle_{\Pi(\bar{\alpha}; \bar{\mathbf{r}})} \approx \frac{1}{\mathcal{N}} \sum_{i=1}^{\mathcal{N}} E_{loc}(\bar{\alpha}; \bar{\mathbf{r}}_i). \quad (2.42)$$

With the notation $\langle \dots \rangle_{\Pi(\bar{\alpha}; \bar{\mathbf{r}})}$ from now on indicating the Monte Carlo average of a quantity on the configurations extracted according to $\Pi(\bar{\alpha}; \bar{\mathbf{r}})$. Because of their stochastic nature, the estimation of the observable is always accompanied by an error that is proportional to the square root of the variance of the local quantity

$$\text{Var}[E_{loc}(\bar{\alpha}; \bar{\mathbf{r}})] = \langle E_{loc}(\bar{\alpha}; \bar{\mathbf{r}})^2 \rangle_{\Pi(\bar{\alpha}; \bar{\mathbf{r}})} - \langle E_{loc}(\bar{\alpha}; \bar{\mathbf{r}}) \rangle_{\Pi(\bar{\alpha}; \bar{\mathbf{r}})}^2, \quad (2.43)$$

and inversely proportional to the square root of the number of samplings \mathcal{N} allocated during the random walk:

$$\sigma_E = \sqrt{\frac{1}{\mathcal{N}} \left[\langle E_{loc}(\bar{\alpha}; \bar{\mathbf{r}})^2 \rangle_{\Pi(\bar{\alpha}; \bar{\mathbf{r}})} - \langle E_{loc}(\bar{\alpha}; \bar{\mathbf{r}}) \rangle_{\Pi(\bar{\alpha}; \bar{\mathbf{r}})}^2 \right]}. \quad (2.44)$$

Here it should be noted that the above error bar does not include the uncertainty due to the stochastic optimization of the variational parameters $\bar{\alpha}$. As discussed before while describing the principles of importance sampling and Monte Carlo integration, it also holds the *zero variance principle*, which affirms that when the trial wave function is exactly an eigenfunction of the Hamiltonian, the variance of the local energies Eq. 2.43 goes to zero, *i.e.* the local energy is a constant function.

Variational principle

The variational principle represents one of the most important features when searching for reliable approximations of the ground state wave function for quantum systems [99]. Given an approximate trial wave function Ψ_T for the exact ground state Ψ_0 of a given Hamiltonian \hat{H} , the variational energy of Eq. 2.38 in Dirac notation is written as

$$E_T = \frac{\langle \Psi_T | \hat{H} | \Psi_T \rangle}{\langle \Psi_T | \Psi_T \rangle}. \quad (2.45)$$

Within the Hilbert space, any state can be expanded in terms of a linear combination of eigenstates of the Hamiltonian, which forms a complete orthonormal basis set

$$\Psi_T = \sum_i a_i |\Psi_i\rangle, \quad a_i = \langle \Psi_i | \Psi_T \rangle. \quad (2.46)$$

By introducing this expansion in the variational energy expression, and assuming the orthonormalization conditions $\langle \Psi_i | \Psi_j \rangle = \delta_{ij}$ and $\sum_i |a_i|^2 = 1$, it follows that

$$E_T = \sum_i |a_i|^2 \langle \Psi_i | \hat{H} | \Psi_i \rangle = \sum_i |a_i|^2 E_i, \quad (2.47)$$

which can be split in

$$E_T = |a_0|^2 E_0 + \sum_{i>0} |a_i|^2 E_i. \quad (2.48)$$

Similarly, the normalization condition can be rewritten as

$$|a_0|^2 = 1 - \sum_{i>0} |a_i|^2 \quad (2.49)$$

Combining both expressions leads to

$$E_T = (1 - \sum_{i>0} |a_i|^2) E_0 + \sum_{i>0} |a_i|^2 E_i = E_0 + \sum_{i>0} |a_i|^2 (E_i - E_0). \quad (2.50)$$

Since the second term on the right-hand side is always positive due to $E_i - E_0 > 0$, it follows that

$$E_T = \langle \Psi_T | \hat{H} | \Psi_T \rangle \geq E_0, \quad (2.51)$$

and thus, the expectation value of the energy for any trial wave function is greater or equal to the true ground-state electronic energy. Considering this variational principle and the zero variance principle previously described, it is possible to approximate the correct ground state of the system of interest, by finding the most optimal variational parameters of the trial wave function to lower the VMC energy or its variance, that will be computed through Monte Carlo integration.

2.3.3 Optimization methods

The quality of the trial wave function controls the statistical efficiency of the VMC and DMC algorithms and determines the final accuracy obtained. For this reason, by performing an optimization of its variational parameters at VMC level, it is possible to reach the lowest-energy state, which is expected to capture the correct ground-state behavior as previously discussed in the variational principle (see Section 2.3.2). The following lines will briefly describe two common optimization techniques applied to VMC, namely Stochastic Reconfiguration (SRC) and Signal-to-Noise Ratio (SNR) [85, 95], although other successful approaches have also been proposed [90].

Stochastic Reconfiguration

A straightforward technique to optimize a wave function is to employ the steepest descent method, where the variational parameters are iteratively updated as follows

$$\bar{\alpha} \rightarrow \bar{\alpha}' = \bar{\alpha} + \Delta \bar{f}_\alpha, \quad (2.52)$$

here $\bar{\alpha}$ is the set of variational parameters, Δ is a small constant to control the minimization process, and $f_\alpha = -\frac{\delta E}{\delta \alpha}$ are the generalized forces, here defined as the partial derivatives of the energy functional of Eq. 2.42 with respect to a parameter, that in Monte Carlo are computed as

$$f_\alpha = -2 \{ \langle E_{loc} \mathcal{O}_\alpha \rangle_\Pi - \langle E_{loc} \rangle_\Pi \langle \mathcal{O}_\alpha \rangle_\Pi \}, \quad (2.53)$$

which are based on the derivatives of the logarithm of the wave function $\mathcal{O}_\alpha = \partial_\alpha \ln \Psi_T$. However, in their straightforward implementations, this method and more sophisticated ones, such as the Newton-Raphson method and the conjugate gradient, do not work efficiently within the stochastic approach of VMC [95]. To improve the situation, one can introduce a positive-definite matrix \mathcal{S} that takes into account the non-linearity of the variational space. In the SRC approach introduced by Sorella [85], the Matrix \mathcal{S} defines essentially a metric for the parameters' space as

$$\mathcal{S}_{\alpha_i \alpha_j} = \langle \mathcal{O}_{\alpha_i} \mathcal{O}_{\alpha_j} \rangle_\Pi - \langle \mathcal{O}_{\alpha_i} \rangle_\Pi \langle \mathcal{O}_{\alpha_j} \rangle_\Pi, \quad (2.54)$$

which corresponds to the covariance matrix of the derivatives of the logarithmic wave function. Therefore, the problem of finding the optimal parameter variation $\delta\alpha$ that minimizes the energy reduces to solving the linear systems of equations $\mathcal{S}\delta\bar{\alpha} = \bar{f}$. Additionally, to avoid numerical instabilities in the new parameters caused by small eigenvalues of the matrix, or for elements in different scales, a shift in the diagonal elements of the matrix can be introduced $\mathbf{S}_{\alpha_i \alpha_j} = \mathbf{S}_{\alpha_i \alpha_j} + \epsilon \delta_{\alpha_i \alpha_j}$. Then the parameters are updated as

$$\bar{\alpha} \rightarrow \bar{\alpha} + \Delta \delta \bar{\alpha}. \quad (2.55)$$

Signal-to-noise ratio

As show in reference [85], the SRC method is parent to the SNR approach, in which the \mathcal{S} matrix is substituted with the covariance matrix of the forces. The generalized force defined before (Eq. 2.53) has a corresponding statistical noise, which can also be estimated in conjunction with its correlation function, namely the correlation between two parameters. This procedure can be done by calculating the covariance matrix

$$\sigma_{\alpha_i \alpha_j}^2 \approx \langle f_{\alpha_i} f_{\alpha_j} \rangle_{\Pi} - \langle f_{\alpha_i} \rangle_{\Pi} \langle f_{\alpha_j} \rangle_{\Pi}. \quad (2.56)$$

Now, the new parameters set can be expressed as $\bar{\alpha} \rightarrow \bar{\alpha} + \Delta \delta \bar{\alpha}$ where Δ parametrizes a line change of the parameters in the pointing out in the direction of $\delta \bar{\alpha}$ vector starting from $\bar{\alpha}$. Therefore, one could define a new force vector in the direction of $\boldsymbol{\tau}$ as

$$f_{\boldsymbol{\tau}} = -\frac{\partial E_{loc}}{\partial \Delta} = -\sum_i \frac{\partial E_{loc}}{\partial \alpha_i} \frac{\partial \alpha_i}{\partial \Delta} = \bar{f} \cdot \delta \bar{\alpha}, \quad (2.57)$$

with a standard deviation given by

$$\sigma_{\boldsymbol{\tau}} = \sqrt{\sum_{i,j} \delta \alpha_i \sigma_{i,j}^2 \delta \alpha_j}. \quad (2.58)$$

These two definitions can be used together within the signal-to-noise ratio technique to find the direction where the force (the signal) is the largest compared to its standard deviation (the noise), providing a direction that guarantees to lower the energy if the following ratio:

$$\Sigma^2(\boldsymbol{\tau}) = \frac{\sum_{i,j} \delta \alpha_i f_{\alpha_i} f_{\alpha_j} \delta \alpha_j}{\sum_{i,j} \delta \alpha_i \sigma_{\alpha_i, \alpha_j}^2 \delta \alpha_j}, \quad (2.59)$$

is much larger than one. Then, to obtain the vector of the parameter variation $\delta \bar{\alpha}$ the problem reduces to the inversion of σ^2 , so that $\delta \bar{\alpha} = (\boldsymbol{\sigma}^2)^{-1} \bar{f}$.

2.3.4 Diffusion Monte Carlo

Although considerable research focuses on developing high-quality trial functions at VMC level, their accuracy will always be limited by the trial wave function's form, flexibility, and parametrization. To improve the treatment of quantum many-body effects and overcome the limitations of the variational wave function, a common approach consists of applying the DMC method [85, 100, 106] over a trial wave function, which in practice is prepared by a preceding VMC calculation. DMC is a projection technique based on wave function propagation in imaginary time that is able to converge to the ground state of a fermionic system

within the Fixed-Node (FN-DMC) approximation. The FN-DMC overcomes the standard DMC algorithm's sign problem by fixing the projected wave function's nodal surface to that of the trial wave function and relaxing its amplitudes. In this way, one obtains the best estimation of the ground state for a particular nodal surface, recovering dynamical correlation between fermions and obtaining a more accurate estimation of the corresponding observables.

The foundations of the DMC method are based on the transformation of the Time-Dependent Schrödinger Equation (TDSE) into a diffusion equation in imaginary time with shifted energy. In the standard TDSE

$$i\frac{\partial}{\partial t}\varphi(\bar{\mathbf{r}}, t) = \hat{H}\varphi(\bar{\mathbf{r}}, t). \quad (2.60)$$

For a time-independent Hamiltonian operator, the space and time variables of Eq. 2.60 can be separated, allowing to express the solution of the integrodifferential equation as a product of spatial and temporal wave functions $\varphi(\bar{\mathbf{r}}, t) = \varphi(\bar{\mathbf{r}}, t_0)a(t)$ where the initial state $\varphi(\bar{\mathbf{r}}, t_0)$ can be expressed as a linear combination of a complete orthonormal basis in the Hilbert space, corresponding to the stationary eigenstates of the Hamiltonian as

$$\varphi(\bar{\mathbf{r}}, t_0) = \sum_{k=0}^{\infty} a_k(t) \Psi_k(\bar{\mathbf{r}}), \quad (2.61)$$

where the temporal function is a phase factor of the form:

$$a_k(t) = a_k(t_0) e^{-iE_k(t-t_0)}. \quad (2.62)$$

The two critical steps behind the DMC methods correspond to transforming the real-time variable t to an imaginary time $t = -i\tau$ and adding a constant shift in the energies E_R , thus transforming Eq. 2.60 into a diffusion equation of the form:

$$-\frac{\partial\varphi(\bar{\mathbf{r}}, \tau)}{\partial\tau} = (\hat{H} - E_R)\varphi(\bar{\mathbf{r}}, \tau). \quad (2.63)$$

The solution of this modified version of the Schrödinger equation here will be convergent in imaginary time instead of being oscillatory, which can still be expanded as linear combinations of the stationary states of the TISE as

$$\varphi(\bar{\mathbf{r}}, \tau) = \sum_{k=0}^{\infty} a_k e^{-(E_k - E_R)\tau} \Psi_k(\bar{\mathbf{r}}). \quad (2.64)$$

The above equation exhibits interesting properties. First, if the energy shift E_R is equal to the ground state energy E_0 , the time-dependent function will be null, so that the term associated to the ground state Ψ_0 will be constant during the time evolution. However, in the other cases, where E_R is higher than the ground state, each stationary state will

be multiplied by an exponential function that decays as $\tau \rightarrow \infty$ according to the energy differences $E_k - E_R$, thus, by letting the solution to evolve in time, the only component that will survive in the expansion will be the one corresponding to the ground state $\Psi_0(\bar{\mathbf{r}})$. In addition, all the excited states with $E_k > E_R$ will decay faster in time, while all the states with $E_k \leq E_R$ will gain more and more weight in the linear combination.

Based on these properties, Eq. 2.63 gives a way to determine the ground state energy by observing how the amplitude of the wave function propagates in time depending on the choice of the energy shift E_R , which will be changed during the time evolution to maintain the total weight of the wave function constant. If the amplitude increases, then decrease the estimation of E_R ; if the amplitude decreases, then increase the offset energy. In general, for $\tau \rightarrow \infty$ the algorithm will project out the ground state wave function $\Psi_0(\bar{\mathbf{r}})$ from a general trial wave function $\varphi(\bar{\mathbf{r}}, \tau_0)$, for any given Hamiltonian.

In order to define the algorithm procedure behind DMC, the first step is to define the integral form of the time evolution of an initial wave function written in terms of a Green's function:

$$\varphi(\bar{\mathbf{r}}', \tau) = \int_V G(\bar{\mathbf{r}}', \tau; \bar{\mathbf{r}}, \tau_0) \varphi(\bar{\mathbf{r}}, \tau_0) d\bar{\mathbf{r}}, \quad (2.65)$$

that defines the time propagation from $\bar{\mathbf{r}}$ to $\bar{\mathbf{r}}'$ between a time interval $\tau - \tau_0$, and is expressed as

$$G(\bar{\mathbf{r}}', \tau; \bar{\mathbf{r}}, \tau_0) = \langle \bar{\mathbf{r}}' | e^{-(\tau - \tau_0)(\hat{T} + \hat{V} - E_R)} | \bar{\mathbf{r}} \rangle. \quad (2.66)$$

The following step is to separate the operators that appear in the exponent of the above equation. Unfortunately, since $e^{\hat{A} + \hat{B}} = e^{\hat{A}} e^{\hat{B}}$ is valid only if $[\hat{A}, \hat{B}] = 0$, and this is not the case for the kinetic \hat{T} and potential \hat{V} operators, such procedure is not straightforward. Nevertheless, the Trotter-Suzuki decomposition [107] provides a clever workaround through the discretization of the time interval in \mathcal{M} intervals of length $\delta\tau = (\tau - \tau_0)/\mathcal{M}$, allowing to express the full operator as the product

$$e^{-(\tau - \tau_0)(\hat{T} + \hat{V} - E_R)} = \lim_{\mathcal{M} \rightarrow \infty} (e^{-(\hat{V} - E_R)\frac{\delta\tau}{2}} e^{-\hat{T}\delta\tau} e^{-(\hat{V} - E_R)\frac{\delta\tau}{2}})^{\mathcal{M}}. \quad (2.67)$$

For finite small enough intervals, this time discretization of the Green function (Eq. 2.66) allows approximating the propagation in an infinitesimal time with an error of $\mathcal{O}(\delta\tau)^3$ as:

$$G(\bar{\mathbf{r}}', \bar{\mathbf{r}}; \delta\tau) = \langle \bar{\mathbf{r}}' | e^{-\delta\tau(\hat{T} + \hat{V} - E_R)} | \bar{\mathbf{r}} \rangle \approx e^{-(V(\bar{\mathbf{r}}') + V(\bar{\mathbf{r}}) - 2E_R)\frac{\delta\tau}{2}} \langle \bar{\mathbf{r}}' | e^{-\hat{T}\delta\tau} | \bar{\mathbf{r}} \rangle, \quad (2.68)$$

where $|\bar{\mathbf{r}}\rangle$ is the position basis vector, normalized such that $\langle \bar{\mathbf{r}} | \bar{\mathbf{r}} \rangle = \delta(\mathbf{r} - \mathbf{r}')$. The above equation can be expressed as a product of two functions:

$$G(\bar{\mathbf{r}}', \bar{\mathbf{r}}; \delta\tau) \approx P(\bar{\mathbf{r}}', \bar{\mathbf{r}}; \delta\tau) W(\bar{\mathbf{r}}', \bar{\mathbf{r}}; \delta\tau),$$

where $\langle \bar{\mathbf{r}}' | e^{-\hat{T}\delta\tau} | \bar{\mathbf{r}} \rangle$ is the Green function for non-interacting systems, defined by a diffusion function

$$P(\bar{\mathbf{r}}', \bar{\mathbf{r}}; \delta\tau) = \left(\frac{m_f}{2\pi\delta\tau} \right)^{3N_f/2} e^{-\frac{m_e}{2\delta\tau} |\bar{\mathbf{r}}' - \bar{\mathbf{r}}|^2}, \quad (2.69)$$

and the second function is the so-called *weighting, branching, or growth/decay* function

$$W(\bar{\mathbf{r}}', \bar{\mathbf{r}}; \delta\tau) = e^{-\frac{\delta\tau}{2}(V(\bar{\mathbf{r}}') + V(\bar{\mathbf{r}}) - 2E_R)}. \quad (2.70)$$

To understand the basic procedure to stochastically solve the integral in Eq. 2.65 with the approximate Green function in Eq. 2.3.4, it is necessary to consider a set of all the coordinates positions $\bar{\mathbf{r}}^{n,0}$ in a configuration n at time τ_0 initially distributed according to $\varphi(\bar{\mathbf{r}}, \tau_0)$, for a total of \mathcal{N} configurations. Each configuration, will evolve in the time interval $\tau - \tau_0$ from $\bar{\mathbf{r}}^{n,0}$ to the final one, $\bar{\mathbf{r}}^{n,\mathcal{M}}$.

For each walker the total probability of a certain path will be defined as the product of the single diffusion probabilities

$$\mathcal{P}(\bar{\mathbf{r}}^{n,\mathcal{M}}, \tau; \bar{\mathbf{r}}^{n,0}, \tau_0) = \prod_{m=1}^{\mathcal{M}} P(\bar{\mathbf{r}}^{n,m}, \bar{\mathbf{r}}^{n,m-1}; \delta\tau), \quad (2.71)$$

and each walker will accumulate a weight given by the product

$$\mathcal{W}(\bar{\mathbf{r}}^{n,\mathcal{M}}, \tau; \bar{\mathbf{r}}^{n,0}, \tau_0) = \prod_{m=1}^{\mathcal{M}} W(\bar{\mathbf{r}}^{n,m}, \bar{\mathbf{r}}^{n,m-1}; \delta\tau). \quad (2.72)$$

At the end of the time evolution the wave function $\varphi(\bar{\mathbf{r}}, \tau)$ will be represented through the distribution of the walkers, each multiplied by its weight:

$$\varphi(\bar{\mathbf{r}}', \tau) = \sum_{i=1}^{\mathcal{N}} \mathcal{W}(\bar{\mathbf{r}}^{i,\mathcal{M}}, \tau; \bar{\mathbf{r}}^{i,0}, \tau_0) \delta(\bar{\mathbf{r}}^{i,\mathcal{M}} - \bar{\mathbf{r}}'). \quad (2.73)$$

Finally, inserting these expression in Eq. 2.3.4 back into the convolution integral in Eq. 2.65 leads to

$$\varphi(\bar{\mathbf{r}}', \tau) = \int_V \left[\prod_{m=1}^{\mathcal{M}} d\bar{\mathbf{r}}^{m-1} \delta(\bar{\mathbf{r}}' - \bar{\mathbf{r}}^{\mathcal{M}}) P(\bar{\mathbf{r}}^m, \bar{\mathbf{r}}^{m-1}; \delta\tau) W(\bar{\mathbf{r}}^m, \bar{\mathbf{r}}^{m-1}; \delta\tau) \right] \varphi(\bar{\mathbf{r}}^0, \tau_0), \quad (2.74)$$

which corresponds to the propagation of $\varphi(\bar{\mathbf{r}}^0, \tau_0)$ in infinitesimal time steps. Because of this time discretization, DMC calculations always suffer from the so-called **time-step** error, affecting the estimation of its observables. In practice, this effect is alleviated by extrapolating the values obtained for different time steps $\delta\tau$ to the zero time-step limit $\delta\tau \rightarrow 0$. The next step is to stochastically evaluate Eq. 2.74, but before that, it is necessary to mention two limitations of the simple DMC algorithm. First, the Coulomb potential term in the exponential part $V(\mathbf{R}) - E_T$, can diverge, causing large fluctuations in the probability distributions. Secondly, this approach also lacks the antisymmetry conditions of the wave

function since the time-dependent wave function $\varphi(\bar{\mathbf{r}}, \tau_0)$ acts as a probability density, and thus it must be a positive function in all the volume (see Eq. 2.74). Then, for fermionic systems, the original DMC algorithm suffers from a sign problem. Both issues are alleviated by incorporating a trial function to guide the sampling and to impose the nodal surface of the fermionic wave function forcing the DMC solution to be antisymmetric. This constraint method is known as the **fixed-node approximation**.

The fixed-node approximation

The FN-DMC algorithm employs a time-independent trial function $\Psi_T(\bar{\mathbf{r}})$ to steer the importance sampling to the wave function [108] constraining the nodal surface and removing the sign problem that affects the original DMC algorithm. In FN-DMC the idea is to evolve the product

$$f(\bar{\mathbf{r}}, \tau) = \varphi(\bar{\mathbf{r}}, \tau) \Psi_T(\bar{\mathbf{r}}), \quad (2.75)$$

by multiplying the right and left sides of the imaginary TDSE (Eq. 2.63) by $\Psi_T(\bar{\mathbf{r}})$, leading to

$$\frac{\partial}{\partial \tau} \varphi(\bar{\mathbf{r}}, \tau) \Psi_T(\bar{\mathbf{r}}) = \left[\frac{1}{2m_f} \nabla^2 \varphi(\bar{\mathbf{r}}, \tau) - (\mathbf{V}(\bar{\mathbf{r}}) - E_R) \varphi(\bar{\mathbf{r}}, \tau) \right] \Psi_T(\bar{\mathbf{r}}), \quad (2.76)$$

which can be rewritten as

$$\frac{\partial}{\partial \tau} f(\bar{\mathbf{r}}, \tau) = \frac{1}{2m_e} \nabla^2 f(\bar{\mathbf{r}}, \tau) - \frac{1}{m_e} \nabla [f(\bar{\mathbf{r}}, \tau) \bar{\mathbf{v}}_D(\bar{\mathbf{r}})] - (E_{loc}(\bar{\mathbf{r}}) - E_R) f(\bar{\mathbf{r}}, \tau). \quad (2.77)$$

In such a way, two time-independent quantities appear, the local energy $E_{loc}(\bar{\mathbf{r}}) = \frac{\hat{H}\Psi_T(\bar{\mathbf{r}})}{\Psi_T(\bar{\mathbf{r}})}$ as defined in VMC (Eq. 2.42) and the *drift velocity* $\bar{\mathbf{v}}_D(\bar{\mathbf{r}}) = \frac{\nabla \Psi_T(\bar{\mathbf{r}})}{\Psi_T(\bar{\mathbf{r}})}$. In Eq. 2.77, the last term now is proportional to the excess energy $(E_{loc} - E_R)$, which helps to control the branching in low probability regions, unlike the singularities caused by $(\hat{V} - E_R)$ in the original branching term of DMC. On the other hand, the drift velocity helps to guide the diffusion process by pushing away the walkers from low probability regions, according to the form of the trial wave function.

As seen before, the solution of Eq. 2.77 will still be of the form

$$f(\bar{\mathbf{r}}', \tau) = \int_V \tilde{G}(\bar{\mathbf{r}}', \tau; \bar{\mathbf{r}}, \tau_0) f(\bar{\mathbf{r}}, \tau_0) d\bar{\mathbf{r}}, \quad (2.78)$$

where now the Green function includes the importance sampling function, and is written as

$$\tilde{G}(\bar{\mathbf{r}}', \tau; \bar{\mathbf{r}}, \tau_0) = \Psi_T(\bar{\mathbf{r}}') G(\bar{\mathbf{r}}', \tau; \bar{\mathbf{r}}, \tau_0) \frac{1}{\Psi_T(\bar{\mathbf{r}})}. \quad (2.79)$$

Similarly to Eq. 2.67, the Trotter-Suzuki decomposition can be applied to approximate the Green function into a product of a diffusion (with the addition of a drift component) and reweighting process through an infinitesimal time variation $\delta\tau$, leading to the approximation

$$\tilde{G}(\mathbf{r}', \bar{\mathbf{r}}; \delta\tau) \approx P(\mathbf{r}', \bar{\mathbf{r}}; \delta\tau)W(\mathbf{r}', \bar{\mathbf{r}}; \delta\tau), \quad (2.80)$$

with the diffusion process defined by the function

$$P(\mathbf{r}', \bar{\mathbf{r}}; \delta\tau) = \left(\frac{m_f}{2\pi\delta\tau}\right)^{3N_e/2} e^{-\frac{m_f}{2\delta\tau}[\mathbf{r}' - \bar{\mathbf{r}} - \frac{\delta\tau}{m_e}\mathbf{v}_D(\bar{\mathbf{r}})]^2}, \quad (2.81)$$

and the reweighting

$$W(\mathbf{r}', \bar{\mathbf{r}}; \delta\tau) = e^{-\frac{\delta\tau}{2}(S(\mathbf{r}') + S(\bar{\mathbf{r}}))}, \quad S(\bar{\mathbf{r}}) = E_{loc}(\bar{\mathbf{r}}) - E_R. \quad (2.82)$$

As seen in the Monte Carlo integration section (2.3.1), if $\Psi_T(\bar{\mathbf{r}})$ resembles the exact eigenfunction of the system, the variance on the local energy will reduce to zero, thus the branching term $E_{loc} - E_R$ becomes independent on the configuration $\bar{\mathbf{r}}$. For FN-DMC, the choice of a good approximate trial function that correctly describes any information about the exact wave function, such as cusp conditions, will yield averages with lower statistical uncertainties than those obtained without the importance sampling technique [108].

2.3.5 Basic fixed-node DMC algorithm

The basic procedure to stochastically solve integral in Eq. 2.78, requires to define an initial set of configurations $\bar{\mathbf{r}}^{n,0}$ with $n = 1, 2, \dots, \mathcal{N}$. Each configuration is assumed to be the initial position of an independent random walk that evolves in the time interval $\tau - \tau_0$ from $\bar{\mathbf{r}}^{n,0}$ to the final one, $\bar{\mathbf{r}}^{n,\mathcal{M}}$. The complete algorithm used to perform a FN-DMC calculation requires many technical considerations, but the main elements can be summarized in the following steps:

- I. Initialize a set of \mathcal{N} walkers distributed according to the probability density of the guiding function $|\Psi_T(\bar{\mathbf{r}})|^2 = f(\bar{\mathbf{r}}, \tau_0)$. Set initial weights to one: $W^{n,0} = 1$. Set the initial reference energy E_R to the VMC energy estimate.
- II. For each walker of the \mathcal{N} configuration set
 - For every fermionic particle i in the configuration
 - * Propose a new position based on the drift/diffusion equation

$$\bar{\mathbf{r}}^{n,m+1} = \bar{\mathbf{r}}^{n,m} + \frac{\delta\tau}{m_e}\mathbf{v}_D(\bar{\mathbf{r}}^{n,m}) + \sqrt{\frac{\delta\tau}{m_e}}\bar{\rho}, \quad (2.83)$$

where $\bar{\rho}$ is a vector of random variables extracted with a Gaussian distribution.

- * Check the sign of $\Psi_T(\bar{\mathbf{r}}^{m+1})$ compared to $\Psi_T(\bar{\mathbf{r}}^m)$, if a node has been crossed, reject the move of fermion i
- * Accept the move according to the Metropolis acceptance probability ratio

$$\mathcal{A}^n \Rightarrow \mathcal{A}(\bar{\mathbf{r}}_{m+1}^n, \bar{\mathbf{r}}_m^n; \delta\tau) = \min \left[1, \frac{|\Psi_T(\bar{\mathbf{r}}_{m+1}^n)|^2 P(\bar{\mathbf{r}}_m^n, \bar{\mathbf{r}}_{m+1}^n; \delta\tau)}{|\Psi_T(\bar{\mathbf{r}}_m^n)|^2 P(\bar{\mathbf{r}}_{m+1}^n, \bar{\mathbf{r}}_m^n; \delta\tau)} \right], \quad (2.84)$$

III. Once all \mathcal{N} walkers are moved, update their weights by the factor:

$$W(\bar{\mathbf{r}}_{m+1}^n, \bar{\mathbf{r}}_m^n; \delta\tau) = e^{-\frac{\delta\tau}{2}(S(\bar{\mathbf{r}}_{m+1}^n) + S(\bar{\mathbf{r}}_m^n))}, \quad (2.85)$$

IV. After each reweighting process, accumulate the local quantities to compute the weighted averages of each observable (e.g., the local energy). Update the trial reference energy E_R , to bring it closer to that of the current ensemble.

Repeat steps from II to IV until the projection has evolved for a chosen time $\tau = \mathcal{M}\delta\tau$.

For direct applications to fermionic problems, the FN-DMC algorithm needs to deal with further considerations such as: i) singularities near the nodal surface [109], usually addressed by introducing cut-offs function in the values of both the local energy and the drift velocity that depend on the time step $\delta\tau$; ii) singularities near the nuclear cusps [110]; iii) efficient branching procedure [110, 111]; iv) updates of the reference energy E_R ; v) size consistency error correction [112].

Mixed averages

For a QMC calculation, it is possible to define different estimators for a quantity described by an operator \hat{A} [85]. First of all, the variational energy estimator (the VMC energy estimator) from the trial wave function Ψ_T that imposes the nodal surface is given by

$$E_{\text{VMC}} = \langle E \rangle_T = \frac{\langle \Psi_T | \hat{H} | \Psi_T \rangle}{\langle \Psi_T | \Psi_T \rangle}. \quad (2.86)$$

If Ψ_T is appropriately constructed, the method usually provides a good estimation for the true quantum-mechanical expectation value of \hat{H} . As seen before, in FN-DMC, the time evolution generates the mixed distribution $f(\bar{\mathbf{r}}, \tau) = \varphi(\bar{\mathbf{r}}, \tau)\Psi_T(\bar{\mathbf{r}})$, where $\varphi(\bar{\mathbf{r}}, \tau)$ is the best (lower energy) wave function for the ground state with the same nodes as the trial function $\Psi_T(\bar{\mathbf{r}})$. To obtain the exact energy with respect to the distribution $|\varphi(\bar{\mathbf{r}}, \tau)|^2$,

$$E_{\text{FN}} = \langle E \rangle_\varphi = \frac{\langle \varphi | \hat{H} | \varphi \rangle}{\langle \varphi | \varphi \rangle}, \quad (2.87)$$

it is necessary to project by means of a mixed estimator (which corresponds to the FN-DMC estimation)[113, 114] in the limit when $\tau \rightarrow \infty$,

$$\begin{aligned} \langle E \rangle_{\text{mix}} &= \frac{\langle \varphi | \hat{H} | \Psi_T \rangle}{\langle \varphi | \Psi_T \rangle} \\ &= \lim_{\tau \rightarrow \infty} \frac{\int \varphi(\bar{\mathbf{r}}, \tau) \hat{H} \Psi_T(\bar{\mathbf{r}}) d\bar{\mathbf{r}}}{\int \varphi(\bar{\mathbf{r}}, \tau) \Psi_T(\bar{\mathbf{r}}) d\bar{\mathbf{r}}} \\ &= \lim_{\tau \rightarrow \infty} \frac{\int \varphi(\bar{\mathbf{r}}, \tau) \Psi_T(\bar{\mathbf{r}}) E_{\text{loc}} d\bar{\mathbf{r}}}{\int \varphi(\bar{\mathbf{r}}, \tau) \Psi_T(\bar{\mathbf{r}}) d\bar{\mathbf{r}}} \end{aligned} \quad (2.88)$$

$$\approx \frac{1}{\mathcal{N}} \sum_i^{\mathcal{N}} E_{\text{loc}}(\bar{\mathbf{r}}_i), \quad (2.89)$$

which is a biased estimation of $\langle E \rangle_{\varphi}$, since φ satisfies the equation $\hat{H}\varphi = E_{\text{FN}}\varphi$ within the nodal surface of Ψ_T . The calculation of this mixed average is possible for any type of operator \hat{A} that commutes with \hat{H} , due to the fact that the operator \hat{A} is also defined in the ground state $\hat{A}|\varphi\rangle = A_{\text{FN}}|\varphi\rangle$. For all other operators, an approximated scheme to evaluate the ground-state expectation value can be used if the trial wave function differs from ground-state wave function by a small difference [85]

$$\varphi = \Psi_T + \delta\Psi,$$

where $\delta\Psi$ should be normalized and orthogonal to Ψ_T . Then the ground-state average can be written as

$$\langle \hat{A} \rangle_{\text{pure}} = \langle \varphi | \hat{A} | \varphi \rangle = \langle \Psi_T | \hat{A} | \Psi_T \rangle + 2 \langle \varphi | \hat{A} | \delta\Psi \rangle + \langle \delta\Psi | \hat{A} | \delta\Psi \rangle.$$

If $\delta\Psi$ is small enough, the second order term $\langle \delta\Psi | \hat{A} | \delta\Psi \rangle$ can be neglected. After substitution $\langle \varphi | \hat{A} | \delta\Psi \rangle = \langle \Psi_T | \hat{A} | \varphi \rangle - \langle \Psi_T | \hat{A} | \Psi_T \rangle$ the extrapolation formula becomes

$$\langle \hat{A} \rangle \approx 2 \langle \hat{A} \rangle_{\text{mix}} - \langle \hat{A} \rangle_T.$$

Such combinations of variational $\langle \hat{A} \rangle_T$ (VMC) and mixed $\langle \hat{A} \rangle_{\text{mix}}$ (DMC) estimators are often called extrapolated estimators.

2.4 Software

2.4.1 QMeCha code

The QMeCha (Quantum MeCha) code is a quantum Monte Carlo package to study many-body interactions between electrons, positrons, and an embedding environment of classical

charges and quantum Drude oscillators. The main developer and scientific supervisor of the code is Dr. Matteo Barborini. It has been written in FORTRAN03 following an object-oriented programming philosophy. The QMeCha package has been designed to integrate many-particle Hamiltonians under the VMC and FN-DMC techniques for molecular systems of many-electron, positrons, or drudons. Regarding the wave function, the code has implemented single- and multi-determinant ansatzes, built as a linear combination of exponential, gaussian, or mixed-type function orbitals. QMeCha is capable of optimizing all variational parameters of the wave function by using either the SRC or SNR techniques integrated at VMC level. The code is published in a private repository[115].

2.4.2 LOWDIN code

The LOWDIN code is a MCMO computational package developed under the supervision of professor Dr. Andrés Reyes [116] following the formalism of the APMO approach. The code has been written in FORTRAN 2008 standard with C bindings to external libraries, following an object-oriented programming philosophy. Since its conception, the code was designed to perform MC-HF calculations for molecular systems containing any number of different quantum species with their charge and mass. LOWDIN can solve the coupled Roothan-Hall equations for all quantum particles under a self-consistent procedure, finding all the mean-field eigenvalues and eigenvectors, which are constructed as a linear combination of single-particle atomic orbitals. The HF and MP2 methods of Section 2.2 are implemented in the code, among other quantum chemistry methods and capabilities. The LOWDIN code is currently available under a GNU General Public License v3.0 [117].

Correlated Electron-Positron Wave Functions

Parts of this chapter have been published in this or similar form in:

J. Charry, M. Barborini, A. Tkatchenko. "Correlated Wave Functions for Electron-Positron Interactions in Atoms and Molecules" *J. Chem. Theory Comput.* **18**, 4, 2267-2280, 2022,

and have been produced in collaboration with the above authors.

For a quantum-mechanical description of positron-matter systems defined by the Hamiltonian of Eq. 2.2, the wave function ansatz should include the standard electronic correlation effects and cusp conditions, but also the electron-positron correlation interactions, satisfying the nucleus-positron, electron-positron and eventually positron-positron cusp conditions, together with the correct asymptotic behaviors as a function of the interparticle distances [96]. In order to fulfill these requirements, several ansatzes have been proposed in the literature, which can be essentially categorized into three different approaches: The first is to consider the electron-electron and electron-positron correlations directly into the determinantal part of the wave function [66, 67, 86, 96]; the second is to include these correlation effects through a two-body Jastrow factor, as a remodulating factor only, and constructing the single particle positronic orbital as a linear combination of an atomic centered basis set [87, 88, 118, 119], similarly to the case of electrons; the third is to include the correlation effects through an electron-positron orbital that explicitly depends on the two-particle distances, and that multiplies the purely electronic wave function [49, 82, 86]. The first approach, although the most accurate, is also the most complicated to generalize for a larger number of fermions, due to the antisymmetrization condition of the total wave function. The simplicity of the second approach relies on the fact that correlation effects are included in the Jastrow factor, which acts only as a re-modulating factor without affecting

the symmetry of the total wave function. While the third approach aims to combine the advantages of the previous two. Thus, this work compares the second and third types of wave function, discussing the crucial differences in recovering the electron-positron correlation and introducing a novel three-body Jastrow factor [120, 121] to describe the correlation between electrons and positrons in the field of the atomic nuclei, achieving a robust improvement in the description of the positron-matter interactions.

This chapter presents an efficient and transferable variational ansatz based on a combination of electron-positron geminal orbitals and a Jastrow factor that explicitly includes the electron-positron correlation in the field of the nuclei, which can be variationally optimized at the level of VMC and further employed as the trial wave function for a DMC calculation. This approach was applied to systematically study the binding energies of positron and positronium with the first row atoms, anions or cations (H^- , Li^+ , Li , Li^- , Be^+ , Be , B^- , C^- , O^- and F^-). In particular, for the largest positron-atom systems, PsB , PsC , PsO , and PsF , the QMC total energies presented here are lower than the results available in the literature. To further assess the performance towards molecular systems, this approach was also tested on the computation of the PES describing the bond formation of the repelling H^- anions mediated by one positron [71, 73, 122, 123, 124], demonstrating the robustness of the approach that can be generalized to larger electron-positron systems, and obtaining accurate estimations of its spectroscopic properties.

This chapter is organized as follows: Section 3.1 explicitly defines the construction of the electron-positron wave function. Next, Section 3.2 shows the total energies and the positron binding energies for several positronic atomic and molecular systems. Finally, Section 3.3 summarizes the results and provides concluding remarks.

3.1 Wave function

3.1.1 Generalized cusps conditions

The generalized cusp conditions described by Kato [125]

$$\frac{1}{\Psi} \frac{d\Psi}{dr} \Big|_{r=0} = \frac{2q_i q_j \mu_{ij}}{d \pm 1}, \quad (3.1)$$

establish the correct behavior of a fermionic wave function when two particles interacting through Coulomb potential find each other at the same point in space. There, q_i and q_j are the particles' charges in units of the electronic charge, $\mu_{ij} = m_i m_j / (m_i + m_j)$ is the reduced mass, and d is the dimensionality. The minus sign is used for distinguishable particles (anti-parallel-spin fermion, or different fermions like electron and positron), and the plus sign is for indistinguishable particles (parallel-spin fermions).

3.1.2 Electron–positron wave functions

The most general expression for many-electrons and a positron wave function $\Psi(\bar{\mathbf{x}}^e, \mathbf{x}^p; \bar{\mathbf{R}})$ explicitly describes the many-body correlation effects between the $4N_e$ electronic Cartesian and spin coordinates $\bar{\mathbf{x}}^e$ and the four positronic \mathbf{x}^p coordinates in the field of the nuclei $\bar{\mathbf{R}}$. A first approximation to this fully correlated state can be built by considering only the explicit correlation between particle pairs. The wave function is thus built as a symmetrized product (or a linear combination of symmetrized products) of two-particle functions, as proposed for example by Bressanini *et al.* in Ref. 126, describing the correlation between electron–electron, electron–positron, nucleus–electron, and nucleus–positron pairs. Clearly, this ansatz, although very accurate, is more computationally expensive when applied to large systems of many atoms and many positrons.

A way to further simplify the total wave function is to decouple it into a product

$$\Psi(\bar{\mathbf{x}}^e, \mathbf{x}^p; \bar{\mathbf{R}}) = \psi_e(\bar{\mathbf{x}}^e; \bar{\mathbf{R}})\psi_p(\mathbf{x}^p; \bar{\mathbf{x}}^e, \bar{\mathbf{R}})J(\bar{\mathbf{x}}^e, \mathbf{x}^p; \bar{\mathbf{R}}), \quad (3.2)$$

of two fermionic functions, an electronic one $\psi_e(\bar{\mathbf{x}}^e; \bar{\mathbf{R}})$ (such as a Slater determinant) and a positronic orbital $\psi_p(\mathbf{x}^p; \bar{\mathbf{x}}^e, \bar{\mathbf{R}})$, and a bosonic Jastrow factor that describes the correlation between the remaining particle pairs, eventually also including three or four body correlation effects, as later proposed in this work.

Assuming that the electronic wave function $\psi_e(\bar{\mathbf{x}}^e; \bar{\mathbf{R}})$ describes the spin and angular symmetries of the electrons in the field of the nuclei, the general positronic function $\psi_p(\mathbf{x}^p; \bar{\mathbf{x}}^e, \bar{\mathbf{R}})$ should depend on both the nuclear and electronic coordinates, being symmetric for the exchange of any electronic coordinate. In the literature, the $\psi_p(\mathbf{x}^p; \bar{\mathbf{x}}^e, \bar{\mathbf{R}})$ function has been further simplified, assuming it to be independent of $\bar{\mathbf{x}}^e$ [71, 76, 118, 124, 127] or from $\bar{\mathbf{R}}$ [86], the former chosen especially for computational reasons, since it is also simpler to implement and integrate with post-HF methods. The following sections discuss the three parts of the total wave function.

3.1.3 Electronic wave function

Because of the multiconfigurational nature of some of the electronic systems studied in this work, for example the Be atom and the Li^- anion, the electronic wave function is chosen to be the Antisymmetrized Geminal Power (AGP) [128] which corresponds to a more compact and constrained multideterminantal expansion[129]. For a closed shell system, the AGP is built as the determinant

$$\psi_e(\bar{\mathbf{x}}^e; \bar{\mathbf{R}}) = \det[\mathbf{G}], \quad (3.3)$$

of a $N_e^\uparrow \times N_e^\downarrow$ matrix \mathbf{G} , whose elements \mathbf{G}_{ij} describe the coupling of electronic pairs in a singlet state $|0, 0\rangle = \frac{1}{\sqrt{2}} (|\frac{1}{2}, \frac{1}{2}\rangle |\frac{1}{2}, -\frac{1}{2}\rangle - |\frac{1}{2}, -\frac{1}{2}\rangle |\frac{1}{2}, \frac{1}{2}\rangle)$, through the symmetric linear

combination of products of two atomic orbitals modulated by the coupling coefficients λ_{qp} :

$$\mathbf{G}_{ij} = \phi_G(\mathbf{r}_i^\uparrow, \mathbf{r}_j^\downarrow) = \sum_{q,p=1}^Q \lambda_{qp} \psi_q(\mathbf{r}_i^\uparrow) \psi_p(\mathbf{r}_j^\downarrow) |0, 0\rangle. \quad (3.4)$$

For a spin polarized systems ($N_e^\uparrow > N_e^\downarrow$), the geminal matrix can be generalized [130] by adding $N_e^u = N_e^\uparrow - N_e^\downarrow$ columns, each with N_e^\uparrow elements, containing unpaired molecular orbitals

$$\mathbf{G}_{ik} = \phi_k(\mathbf{r}_i^\uparrow) = \sum_{q=1}^Q l_q^k \varphi_q(\mathbf{r}_i^\uparrow) \quad \begin{array}{l} i \in [1, N_e^\uparrow] \\ k \in [N_e^\downarrow + 1, N_e^\uparrow] \end{array}, \quad (3.5)$$

occupied solely by the spin-up electrons, therefore, reconstructing a square \mathbf{G} matrix of $N_e^\uparrow \times N_e^\uparrow$ elements.

3.1.4 Positronic wave function

A very common approach in the literature [71, 76, 118, 124, 127] assumes that the positronic wave function is independent of the electronic coordinates and can be written as Positronic Molecular Orbitals (PMO), which are a linear combination

$$\psi_p(\mathbf{x}^p; \bar{\mathbf{R}}) = \sum_{q=1}^Q l_q \phi_q(\mathbf{x}^p), \quad (3.6)$$

of atomic orbitals $\phi_q(\mathbf{x}^p)$, which are centered on the nuclear coordinates, hidden here for simplicity. This kind of approach is well suited when describing the positron's interactions with atoms or anions, since its density is spherically distributed around the electronic charge. Yet, for molecules, such approach becomes deficient, since while the positron forms bound states with the electrons to which it is attracted, it does not form bound states with the atomic nuclei that repel it.

One way to solve this inconsistency is to construct the positron's orbital through a positronic basis set [86, 126] explicitly describing the bound states between electron-positron pairs. As a matter of fact, it can be easily shown that the ground state of a system of one electron and one positron, *i.e.* the Positronium (Ps), can be exactly described by an exponential function of the electron-positron distance $r^{ep} = |\mathbf{x}^e - \mathbf{x}^p|$:

$$\phi(\mathbf{x}^{ep}) = r^{ep} R(r^{ep}) Y_l^m(\theta^{ep}, \phi^{ep}). \quad (3.7)$$

where $R(r^{ep})$ is a radial function normalized with respect to the distance r^{ep} and $Y_l^m(\theta^{ep}, \phi^{ep})$ is a real spherical harmonic (centered on the positron) that is used to introduce an angular momentum [131].

Through these orbitals, one can construct a positronic wave function for many electrons and one positron as the product:

$$\psi_p(\mathbf{x}^p; \bar{\mathbf{x}}^e) = \prod_{i=1}^{N_e} \varphi_p(\mathbf{r}_i^{ep}), \quad (3.8)$$

of identical orbitals (so that the function is symmetric with respect to the exchange of the electronic coordinates), each dependent on the electron-positrons distance \mathbf{r}_i^{ep} , thus referred to as Electron-Positron Orbitals (EPO), that are defined as linear combinations

$$\varphi_p(\mathbf{r}^{ep}) = \sum_{q=1}^Q l_q \phi_q(\mathbf{r}^{ep}), \quad (3.9)$$

of the newly defined positronic orbitals.

It can be shown that the scaling of the computational cost with respect to the number of electrons, of both the PMO and the EPO wave functions, is negligible with respect to that of the electronic determinant. It is in fact known that through the Sherman-Morrison formula [132], the operations required for N_e consecutive updates of the electronic determinant scale at most as N_e^3 .

The PMO wave function, which is updated only when the positron's coordinates are changed, requires at most Q multiplications (being Q the length of the atomic basis set which is proportional to N_e), which is negligible with respect to the electronic determinant.

For the EPO, on the other hand, since the update of the wave function for the change of one electronic coordinate requires Q operations, N_e consecutive updates require $N_e Q$ multiplications, which is the same computational cost of the EPO update for the change of the positron's coordinates. Thus, the full configuration update will cost $2N_e Q$ operations where Q is the length of the positronic basis defined in Eq. 3.7, which can also be set to one and that in any case is lower than the number of electrons. Again this means that the computational cost of the update of the EPO is negligible with respect to the update of the electronic determinant. The next section compares the results obtained with both the PMO and the EPO based wave functions used in combination with a novel Jastrow factor to accurately recover the correlations between electron-positron pairs in the electrostatic field of the nuclei. This Jastrow factor is described in the next subsection.

3.1.5 Jastrow factor

The bosonic Jastrow factor [121] constructed in this work, that explicitly includes many-body correlations in the QMC wave functions, is inspired by the general form introduced

by Casula *et al.* in Ref. 128, as the linear combination of five terms

$$J(\bar{\mathbf{x}}^e, \mathbf{x}^p; \bar{\mathbf{R}}) = \exp \{ \mathcal{J}_c^{en}(\bar{\mathbf{r}}^e, \bar{\mathbf{R}}) + \mathcal{J}_c^{pn}(\mathbf{r}^p, \bar{\mathbf{R}}) + \mathcal{J}_c^{ee}(\bar{\mathbf{r}}^e) + \mathcal{J}_c^{ep}(\bar{\mathbf{r}}^e, \mathbf{r}^p) + \mathcal{J}_{3/4}(\bar{\mathbf{r}}^e, \mathbf{r}^p; \bar{\mathbf{R}}) \}, \quad (3.10)$$

which can be classified as one-body terms, $\mathcal{J}_c^{en}(\bar{\mathbf{r}}^e; \bar{\mathbf{R}})$ and $\mathcal{J}_c^{pn}(\mathbf{r}^p; \bar{\mathbf{R}})$ that are used to describe the fermion-nucleus cusps conditions, pure homogeneous two-body terms, $\mathcal{J}_c^{ee}(\bar{\mathbf{r}}^e)$ and $\mathcal{J}_c^{ep}(\bar{\mathbf{r}}^e, \mathbf{r}^p)$, that describe the pair correlations between electronic pairs and electron-positron pairs, and finally a many-body (or inhomogeneous) term $\mathcal{J}_{3/4}(\bar{\mathbf{r}}^e, \mathbf{r}^p; \bar{\mathbf{R}})$ that is used to describe the fermionic pair correlations in the field of the nuclei.

The one-body Jastrow factors are written as the sums

$$\mathcal{J}_c^{en}(\bar{\mathbf{r}}) = \sum_{i=1}^{N_e} \sum_{a=1}^{N_c} f_a^e(r_{ia}), \quad (3.11)$$

$$\mathcal{J}_c^{pn}(\bar{\mathbf{r}}) = \sum_{i=1}^{N_p} \sum_{a=1}^{N_c} f_a^p(r_{ia}), \quad (3.12)$$

of functions that only depend on the relative distances r_{ia} between the i th fermion and the a th nucleus, and are used to reproduce the nuclear cusp condition.

The functions used to describe the nuclear cusp condition are different for electrons and the positron, due to the corresponding attractive and repulsive nature of the interactions (see Section 3.1.1). For this reason, for the electron-nucleus cusp the following short-range function [128] was chosen

$$f_a^e(r_a) = \frac{Z_a}{\mathcal{A}_a} e^{-\mathcal{A}_a r_a} + \sum_{n=1}^N g_n^a e^{-\zeta_n^a r_{ia}^2}, \quad (3.13)$$

while the positron-nucleus cusp is given the long-range cusp[128]

$$f_a^p(r_a) = -\frac{Z_a}{\mathcal{A}_a (1 + \mathcal{A}_a r_a)} + \sum_{n=1}^N \gamma_n^a e^{-\xi_n^a r_{ia}^2}, \quad (3.14)$$

where $\mathcal{A}_a = (2Z_a)^{1/4} \mathcal{B}_a$ is a factor depending on the nuclear charge and a remodulating variational parameter \mathcal{B}_a that can depend on the atom. In all calculations, this variational parameter was simply fixed to one. The sums that appear in the two equations are a linear combination of Gaussian functions centered on the corresponding atom that are modulated by a set of coefficients g_n^a as well as γ_n^a and by the corresponding exponents ζ_n^a and ξ_n^a , that depend on the atom and are optimized.

The homogeneous two-body Jastrow factors that describe the correlation between electronic pairs and electron-positron pairs are also written as the sum of functions depending only on the distances between particle pairs:

$$\mathcal{J}_c^{ee}(\bar{\mathbf{r}}^e) = \sum_{j>i=1}^{N_e} f_{ee}(r_{ij}), \quad (3.15)$$

$$\mathcal{J}_c^{ep}(\bar{\mathbf{r}}^e, \mathbf{r}^p) = \sum_{i=1}^{N_e} f_{ep}(r_{ip}). \quad (3.16)$$

The functions used to describe the fermionic cusps conditions are different for the two types of particle pairs. For the repulsive electronic pairs, the following functions are employed

$$f_{ee}(r_{ij}) = \begin{cases} -\frac{1}{4b^p(1+b^p r_{ij})} + \sum_{n=1}^N g_n^p e^{-\zeta_n^p r_{ia}^2} & \text{indis.} \\ -\frac{1}{2b^a(1+b^a r_{ij})} + \sum_{n=1}^N g_n^a e^{-\zeta_n^a r_{ia}^2} & \text{dis.} \end{cases} \quad (3.17)$$

respectively for indistinguishable electrons (parallel spin) and distinguishable ones (antiparallel spin). The variational parameters b^p and b^a are related to the cusp functions, and are optimized independently [133]. The additional linear combination of Gaussian type orbitals works as a remodulating factor depending on the set of coefficients g_n^p and g_n^a as well as exponents ζ_n^p and ζ_n^a that are optimized. For the attractive electron-positron cusp, the short-range cusp function of the following form was used:

$$f_{ep}(r_{ij}) = \frac{1}{2b} e^{-br_{ip}} + \sum_{n=1}^N h_n e^{-\eta_n r_{ip}^2}, \quad (3.18)$$

where again b , the coefficients h_n and the exponents η_n are optimized variational parameters.

Finally, the last non-homogeneous term in the Jastrow factor is a three/four body term, written as the linear combination of products of two atomic orbitals:

$$\mathcal{J}_{3/4}(\bar{\mathbf{r}}^e, \mathbf{r}^p; \bar{\mathbf{R}}) = \sum_{j>i=1}^{N_e} \sum_{q,p=1}^{\mathcal{Q}} \gamma_{qp} \chi_q(\mathbf{r}_i) \chi_p(\mathbf{r}_j) + \sum_{i=1}^{N_e} \sum_{q,p=1}^{\mathcal{P}} \nu_{qp} \varpi_q(\mathbf{r}_i) \varpi_p(\mathbf{r}^p), \quad (3.19)$$

in which the first group of elements describes the correlation of two electrons in the field of one or two nuclei, and the second group of elements describes the correlation of the electron-positron pairs in the field of one or two nuclei. Here $\chi_q(\mathbf{r})$ and $\varpi_q(\mathbf{r})$ are a set of atomic orbitals and γ_{qp} and ν_{qp} are a set of coefficients that are fully optimized.

This Jastrow term is an extension to the one introduced for pure electronic systems by Casula *et al.* [128], and it is necessary to recover the dynamical correlation between fermionic

pairs, suppressing also nonphysical charge fluctuations [134]. Since the Jastrow factor must be symmetric with respect to the exchange of all the electrons, the γ_{qp} parameters satisfy the condition $\gamma_{qp} = \gamma_{pq}$. Also for simplicity, in this work the two atomic basis sets are chosen to be identical, so that $\chi_q(\mathbf{r}) = \varpi_q(\mathbf{r})$.

It is important to mention that the presence of one positron does not change the original computational cost of the purely electronic dynamical Jastrow factor. In fact, by partially storing intermediate matrix-vector operations, it can be shown that the update of this Jastrow factor for the change of the positronic coordinate requires QN_e multiplications which is the same computational cost of the update of the dynamical Jastrow factor that describes correlation between electronic pairs. Thus, the update of the dynamical Jastrow factor for the change of all the fermionic coordinates requires a number of multiplications that is proportional to $QN_e^2 \propto N_e^3$ and comparable to the computational cost required for N_e consecutive updates of the electronic determinant and of its inverse matrix.

3.1.6 Computational details

As discussed in the previous sections, to construct the electronic wave functions, the AGP ansatz was chosen with a basis set of contracted Gaussian Type Orbitals (GTOs). In particular, for the H atoms a 3s1p Gaussian primitives contracted in 1s1p orbitals were chosen, i.e. (3s1p)/[1s1p]. For Li, a basis set of (5s4p1d)/[2s1p1d] contracted GTOs, and for B, C, O and F a similar basis set of (6s4p1d)/[2s1p1d] contracted orbitals. These orbitals have been initialized before starting the full optimization by maximizing the overlap of the primitives' linear combinations together with the one-body cusp function in Eq. 3.11, with the contracted orbitals from the Slater type basis of Bunge *et al.*[135]. For the many-body Jastrow factor term described in Eq. 3.19, the $\chi_q(\mathbf{r})$ and $\varpi_q(\mathbf{r})$ orbitals are assumed to be the same. In particular, for the H atoms a (3s2p) uncontracted GTOs were used, while for all the heavier atoms one uncontracted d orbital was added, using the total basis of (3s2p1d) GTOs. Notice that during the optimization all the orbitals' parameters are relaxed.

The basis set used to construct the PMOs (Eq. 3.6) or the EPOs (Eq. 3.9) has been chosen to be simply made of contracted GTO functions with the same number of primitives [5s1p1d]/(1s1p1d). After the optimizations, higher angular momenta p and d were associated to very small coefficients, thus not contributing to the final wave function, as expected.

Finally, for all the cusp functions in Eqs. 3.11,3.12,3.15,3.16, the number of additional Gaussian functions have been chosen to be equal to $N = 5$.

Regarding the DMC calculations, a time-step extrapolation to the continuum was carried out to suppress the error in the energies due to time discretization, obtained with approximately 2000 walkers and with the following time-steps $dt = [0.015, 0.010, 0.005, 0.001]$.

3.2 Total Energies of Atomic-Positron System

3.2.1 Electron affinities

As known from previous computational investigations [26] of the neutral first-row atoms, only Li and Be are known to bind with e^+ . On the other hand, e^+ has been found to bind also with some of the anions such as H^- , Li^- , B^- , C^- , O^- and F^- . In order to compute the energetic stability of these positronic systems with QMC and to study the behavior of the implemented wave functions, it is first important to verify the convergence of the electronic wave functions by computing the total energies and by evaluating the Electron Affinity (EA) and the Ionization Potential (IP) for the different atoms.

The values of the total energies, obtained using the AGP wave function with the VMC and DMC methods are reported in Tables A1 and A2 of the appendix and compared to the accurate SD and Multideterminant (MD) calculations from refs. 136 and 137. To simplify the comparison, Figure 3.1 shows the correlation energy ratio recovered at the VMC level (panel a) and at the DMC level (panel b) defined as $\frac{E-E_{HF}}{(E_{exact}-E_{HF})}$, where the *exact* reference corresponds to the most accurate non-relativistic total energies of atoms obtained by Chakravorty *et al.* [138] who estimated the correlation energy from experimental ionization potentials and Complete Active Space (CAS) calculations. The differences in the energies of the two refs. 136 and 137 are due to two factors. For the SD wave functions, the authors used different basis sets and slightly different Jastrow factors. Regarding the differences within the two MD results, these are due to the fact that while Brown *et al.* [136] converged the energies as a function of the number of configurations, including a number of determinants ranging from 83 for Li to 499 for Ne, Buendía *et al.* [137] limited the number of configurations including only selective excitations involving 2p, 3s, 3p and 3d orbitals.

Since the AGP wave function is a constrained MD expansion, it is capable to include up to double excitations depending on the basis set. For this reason, the AGP energies of the Li and Be atoms, whose wave functions require the inclusion of the nearly degenerate p orbitals, are comparable to the most accurate MD calculations from Brown *et al.* [136]. For the heavier atoms and anions, on the other hand, the AGP wave function greatly outperforms the single determinant, and is comparable with the results of Maldonado *et al.* [137, 140] that only include a limited number of configurations. Given the aforementioned reasons, it is evident that the AGP gives results that are in between the SD calculations and the MD ones, for all the atoms and ions taken into consideration, and converges towards the MD results for the lighter atoms, or for those atoms in which the used MD space was kept small. Although these results seem to point towards rather accurate and converged estimations, some inconsistencies are observed when looking at energy differences such as EAs and IPs (Table A3 of the appendix).

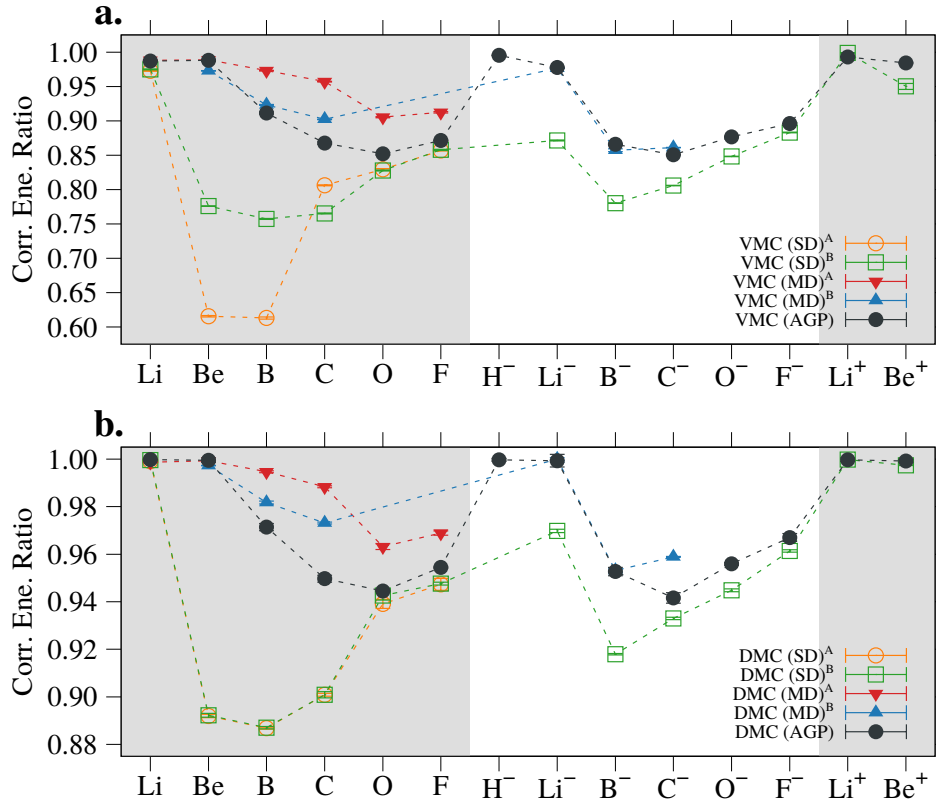


Figure 3.1: Correlation energy ratio defined as $\frac{E-E_{HF}}{(E_{exact}-E_{HF})}$, between the *exact* reference [138] and the correlation energies recovered by the wave function, compared to the single-determinant (SD) and multi-determinant (MD) results from Ref. 136 and Ref. 139 with VMC (panel a) and with DMC (panel b). ^A From Ref. 136, ^B From Ref. 139

According to the information compiled for this work, a complete analysis of the EA and the IP for SD and MD wave functions with QMC methods has been done only by Maldonado, Buendía and coworkers[140]. For this reason, from now, the comparison discussion will focus only against their calculations.

Again to simplify the understanding of the results, Table 3.1 collects the relative error, defined as $(E_{calc} - E_{exp})/E_{exp}$, between the calculated and experimental values in percentage. It can be seen that for H, Li, Be, O, and F, the values computed with the AGP wave function have an accuracy within 5% with respect to the experimental value with VMC and within less than 1% with DMC. Yet, for C and especially for B, the EA is greatly underestimated. The same discrepancy can also be observed for the MD wave function of Ref. 140 and can be explained by the inconsistency between the multi-configurational spaces of the neutral atom and its anion. This is due to the fact that, especially for the AGP wave function, the addition of one electron removes the possibility to include double p excitations in the ex-

Table 3.1: Values of the relative errors (in percentage), defined as $(E_{calc} - E_{exp})/E_{exp}$, for the electron affinities (EA) and ionization potentials (IP) of the various atoms, obtained with the AGP wave function and compared with the single-determinant (SD) and multi-determinant (MD) results (when present) of Ref. 140.^a

	VMC			DMC		
	SD[140]	MD[140]	AGP ^b	SD[140]	MD[140]	AGP ^b
EA _H			-0.52(3)			0.1(8)
EA _{Li}	-36.1(3)	-2.4(2)	-4.5(2)	-9.6(3)	0.2(2)	-0.2(8)
EA _B	-15(1)	-108(3)	-82(2)	21.5(7)	-44(1)	-32(3)
EA _C	2.1(3)	-22.4(2)	-14.8(6)	6.3(5)	-8.0(2)	-7(1)
EA _O	-11.0(4)		-5(1)	-6(1)		-0.6(3)
EA _F	-0.5(3)		0.2(2)	1.3(2)		1.3(5)
IP _{Li}	-0.55(2)		-0.14(2)	-0.01(2)		0.01(2)
IP _{Be}	-5.48(5)	-0.06(5)	-0.11(3)	-2.93(2)	-0.03(1)	-0.01(1)

^aValues of the IPs and EAs are reported in Table A3 of the appendix.

^bThis work.

pansion of the anion orbital space, that are in fact present in the atom. As a consequence, the wave function of the atom is more accurate, and the energy difference between the two states is underestimated. This inconsistency is also at the root of what was observed with the AGP wave function for more complex molecules in Ref. 141. A way to correct this inconsistency and to verify its effect, is to use for the Boron atom a single SD wave function that seems to give more consistent results.

The VMC and DMC energies computed with the SD wave function for B and B⁻ are reported in Tables A1 and A2 of the appendix. Even if these SD energies are slightly lower than those reported in Ref. 140, they give values for the EA that are absolutely comparable, obtaining a value of 0.273(4) eV for VMC and 0.341(8) eV with DMC (Table A3). This time, while the VMC results are quite accurate, the DMC results appear to overestimate the EA by nearly 50% of its value. Thus, since the B atom remains the most complicated system that requires careful attention, in the next section, when computing its binding energy with the positron, both the SD and AGP wave functions will be compared.

3.2.2 Total energies of atomic-positron system

Total energies for the positronic atoms are given in Table 3.2 at VMC and DMC levels employing the two positronic wave-function ansatzes PMO and EPO, while as electronic wave function the AGP was employed for all the atoms and the SD for the case of PsB,

Table 3.2: Non-relativistic total energies of the positron (e^+) and the positronium (Ps) interacting with the atomic systems. In parenthesis, the symmetry state of the electrons. All energies are reported in Hartree.^a

	$e^+\text{Li}(^2\text{S})$	$e^+\text{Be}(^1\text{S})$	PsH(^1S)	PsLi(^1S)	PsB(^3S)	PsC(^4S)	PsO(^2P)	PsF(^1S)
VMC SP [142]	-7.52510(10)		-0.786200(10)					
VMC MP [142]	-7.530180(10)		-0.788230(10)	-7.726160(80)				
VMC [86]				-7.498200(30)	-24.765(2)	-38.0030(20)	-75.1450(30)	-99.9960(30)
VMC SD/PMO					-24.84035(12)			
VMC SD/EPO					-24.84097(13)			
VMC AGP/PMO	-7.52302(11)	-14.6577(33)	-0.785600(37)	-7.722950(85)	-24.845635(81)	-38.06727(37)	-75.28046(81)	-100.02199(67)
VMC AGP/EPO	-7.52566(80)	-14.66386(18)	-0.786416(33)	-7.723921(87)	-24.846154(81)	-38.06800(39)	-75.28366(53)	-100.02490(58)
DMC SP [142]	-7.531650(80)		-0.789160(30)					
DMC MP [142]	-7.532290(20)		-0.789150(40)	-7.739529(60)				
DMC [86]				-7.737600(40)	-24.875(1)	-38.09590(60)	-75.31770(50)	-100.07190(80)
DMC SD/PMO					-24.87389(26)			
DMC SD/EPO					-24.87563(82)			
DMC AGP/PMO	-7.53072(95)	-14.66857(28)	-0.78901(13)	-7.73817(17)	-24.87796(83)	-38.09680(78)	-75.32739(20)	-100.07088(49)
DMC AGP/EPO	-7.53094(23)	-14.66931(36)	-0.7891191(31)	-7.73804(41)	-24.87819(37)	-38.09795(57)	-75.32969(63)	-100.07435(15)
CI			-0.78874(60) ^b		-24.83056 ^c	-38.05362 ^c	-75.28127 ^c	-100.001817 ^d
SVM	-7.532323[83]	-14.669042[83]	-0.789196[143]	-7.740208[144]				
Hylleras[145]			-0.7891967147(42)					

^aAGP and SD are related to the electronic wave function: they indicate respectively the antisymmetrized geminal power and the Slater determinant. SP, *i.e.* single-pairing, corresponds to one antisymmetrized explicitly correlated pairing function from ref. 142, while MP, *i.e.* multiple-pairing, corresponds to a linear combination of SP functions. For H the authors use a linear combination of 28 SP functions, while for Li they use 111.

^bFCI extrapolation from Ref. 71.

^cFCI limit with higher momentum corrections from Ref. 77.

^dMRCI calculation from Ref. 146.

which will be discussed later in detail in this section. Additionally, Table 3.2 collects the most accurate values present in literature obtained with other methods such as the SVM method [144, 147, 148], Multi-Reference Configuration Interaction (MRCI) [77, 146, 149] and Hylleraas functions [145].

As expected, the EPO wave function provides lower energies due to the fact that the dependency on the electron-positron distances is included explicitly into the wave function, differently from the PMO where these correlation effects are introduced only as re-modulating factors through the Jastrow term. Nevertheless, both the EPO and PMO energies are comparable at VMC level and are virtually identical at DMC level for these atomic systems. This is because in atomic systems, where the positronic orbital is spherically symmetric and localized around the electronic charge, the atomic basis set expansion used in the PMO becomes a reasonable approximation. This is clearly not the case in molecules, as will be shown in the next section.

Comparing the results with those obtained by Bressanini *et al.* in Ref. 86 for the PsLi, PsB,

PsC, PsO, and PsF systems, it can be seen that VMC energies with both EPO and PMO wave functions are always lower. This is explained by two facts. First, in their VMC calculations the variational parameters of the electronic wave function were optimized for the neutral atoms and kept frozen in the positronic complex, thus optimizing the positronic orbital but preventing the distortion in the electronic density which is polarized by the positron. Second, the authors only used a two-body Jastrow factor, compared to PMO and EPO wave functions that include dynamical correlation effects of the electron-positron pairs in the field of the nucleus, through the dynamical Jastrow factor described in Eq. 3.19. Despite this, their DMC energies are comparable to ones obtained in this work, indicating that DMC is capable to correct the electron-positron distribution, since most likely the positron does not drastically change the nodal surface of the electronic wave function.

The limitations of the wave function presented in Ref. 86 were fully discussed and improved by the same authors in a subsequent publication [142]. In their work, Bressanini and coworkers proposed the use of a more accurate trial wave function, written as the antisymmetrized product of two-body pairing functions constructed between all the fermionic or nuclear degrees of freedom in an Hylleraas-type ansatz. They construct the wave functions with only one of these antisymmetrized pairing functions, Single-Pairing (SP), and as linear combinations of many of these terms, Multi-Pairing (MP), applying them to compute the binding energies of the e^+Li , PsH, and PsLi spherical systems at both VMC and DMC level.

Interestingly, by comparing the SP results with the AGP/EPO wave function, it can be seen that at both VMC and DMC levels there is an agreement for both the e^+Li and PsH systems. This is because the AGP/EPO includes the pair correlation between all particles in a combination of Jastrow and EPO function, and it can be thought of as an explicitly correlated single pairing function.

On the other hand, the MP energies obtained by Bressanini and coworkers for the e^+Li and PsLi systems are 5 mHa more accurate at the VMC level and around 1-2 mHa more accurate at the DMC level when compared to the AGP/EPO wave function. Thus, in order to improve the current variational estimations, it would be needed to expand the variational ansatz in a combination of many AGP/EPO fermionic terms, which is beyond the scope of this investigation.

Another proof of the accuracy of the present approach can be found by examining the e^+Be system, for which the DMC energy is exceptionally lower than the accurate value obtained with SVM [144]. This is explained by the numerical difficulties the authors have faced to converge the ECG basis of 1275 functions. For this reason, they decided to focus their efforts into improving the frozen core SVM polarization wave function which led to an improvement of the total energy prediction for e^+Be , obtaining the value of -14.6705(1) Ha which is around 1 mHa lower than the current DMC estimation. Finally, for the anionic positronic

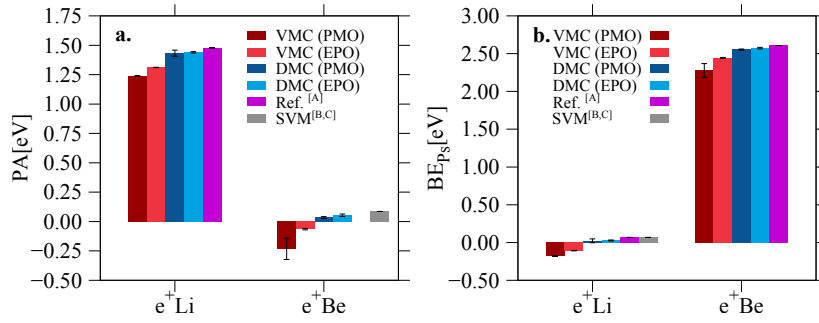


Figure 3.2: Positron affinities (PA) (panel a) and positronium binding energies (BE_{Ps}) (panel b) of the e^+X systems computed with the PMO and EPO wave functions using VMC and DMC methods. The results are compared to other references in the literature, ^A From Ref. 26, ^B From Ref. 147, ^C From Ref. 148.

atoms (PsB, PsC, PsO, PsF) the only references present in the literature are the VMC and DMC results of Bressanini *et al* from Ref. 86 and the extrapolated FCI energies of Saito in refs. 77, 146, 149. Regarding these last results, it is worth mentioning that their estimated total energies are 0.04 Ha higher than the EPO DMC predictions on average, probably due to the frozen core approximation employed and to the fact that the CI expansion is written in terms of single-particle atomic basis sets.

In summary, for e^+Li , e^+Be , PsH, and PsLi, the best results obtained at DMC AGP/EPO level are in good agreement with the highly accurate approaches based on explicitly correlated wave functions [142]. Moreover, for PsB, PsC, PsO, and PsF, since the present VMC and DMC values are always lower in energy with respect to the results previously published in the literature [77, 86, 146, 149], it can be concluded that they are the best energy references reported until now in the literature.

3.2.3 Positron affinities and positronium binding energies with atoms

Having compared the total energies of all atomic systems and assessing the quality of the overall results, the discussion will now focus on studying the binding energies of the positron, *i.e.* the Positron Affinity (PA), and of Positronium, *i.e.* Positronium binding energies (BE_{Ps}), with atoms.

The PA is related to the direct binding of the positron to the electronic system and it corresponds to the difference between the total energies of the system without and with the positron attached to it:

$$PA[X] = E[X] - E[e^+X], \quad (3.20)$$

similar to electron affinity. The BE_{Ps} is related to the separation of the electron/positron sys-

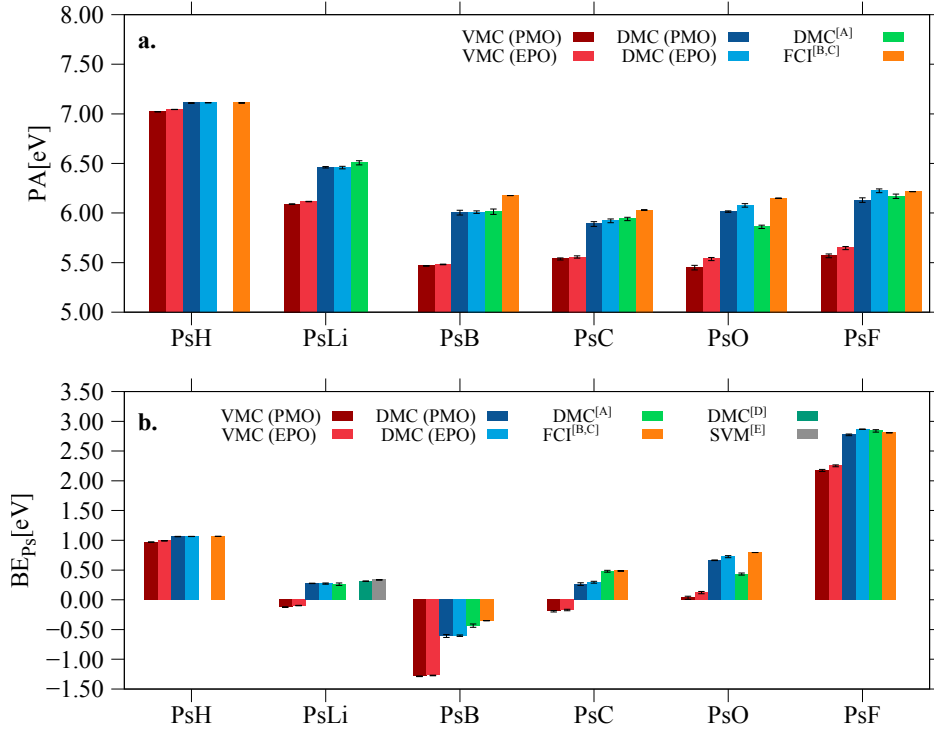


Figure 3.3: Positron affinities (PA) (panel **a**) and positronium binding energies (BE_{Ps}) (panel **b**) of the PsX systems computed with the PMO and EPO wave functions using VMC and DMC methods. The results are compared to other references in the literature. For clarity purposes, the scale of the BE_{Ps} plot is intentionally chosen to cutoff the under-estimated VMC values. ^A From Ref. 86, ^B From Ref. 146, ^C From Ref. 77, ^D From Ref. 142, ^E From Ref. 147.

tem into the electronic system with one less electron and Positronium (with a total energy of -0.25 Ha), being thus defined as the energy difference:

$$\text{BE}_{\text{Ps}}[\text{X}] = E[\text{X}^+] + E[\text{Ps}] - E[e^+\text{X}]. \quad (3.21)$$

Considering the above definitions, when both channels give positive binding energies the positronic atom can be considered energetically stable. On the contrary, when even one of the two has a negative value, this indicates that the system is predicted to dissociate according to that channel.

Table A4 of the appendix presents the computed binding energies for all the atomic systems studied in this work using both dissociation channels in Eq. 3.20 and Eq. 3.21 at VMC and DMC levels employing the two positronic wave-function ansatz PMO and EPO. For comparison, the same table also reports the best values present in literature, including those obtained with SVM [147, 148], MRCI [77, 146, 149], Hylleras functions [145], the predicted

values by Cheng *et al.* [25], the recommended values compiled by Harabati *et al.* [26], and those obtained through the VMC and DMC calculations done by Bressanini and coworkers [86, 142]. However, to simplify the discussion, Figs. 3.2 and 3.3 present the PA and BE_{Ps} data as bar plots.

Considering the performance obtained for the total energies, it could be assumed that the best estimation, within those presented in this work, corresponds to the bindings obtained at the DMC level with the AGP/EPO wave function. Based on these calculations, all the electron/positron systems are in fact stable with respect to both the dissociation channels, except for B^- for which the BE_{Ps} is negative, predicting it to dissociate in Ps and the neutral B atom. These binding energies are comparable to the most accurate DMC [86, 142], SVM [147, 148] or MRCI [77, 146, 149] calculations present in the literature for some of the systems.

Surprisingly, within the same QMC method, there are no appreciable differences between the binding energies obtained with the PMO or EPO wave functions. As discussed above, this is probably due to the fact that the positronic orbital is spherically symmetric and centered around the atoms, making the atomic basis set of the PMO wave function suitable to describe these systems, when used in conjunction with the present novel dynamical Jastrow factor. However, this is not the case for molecules.

The relevant differences can be found, on the other hand, between the binding energies estimated at the VMC level and those predicted by DMC. This is a reasonable result, since the binding depends on the strong correlation between the electronic cloud and a single positron. If this electron-positron correlation effect is not exactly described through the trial wave function (which is generally the case also in pure electronic systems), the binding predicted by VMC will be consistently underestimated.

In general though, VMC and DMC agree qualitatively well, except for the cases in which the binding energies are quite small, as for the BE_{Ps} of e^+Li PsLi, PsB, PsC and the PA of e^+Be , for which in some cases the stability is inverted.

Within this group of systems, e^+Li and e^+Be are two of the most challenging ones, since the rather weak positronic bond is explained by Li and Be atoms' low ionization potential, low electron affinities and large covalent radius [25]. Fortunately, due to the reduced number of fermions, they have been studied with the most accurate SVM methods [147, 148] that can serve as reference. Now, by comparing the accurate DMC (AGP/EPO) results with the SVM ones for the BE_{Ps} of e^+Li and the PA of e^+Be it can be seen that the former is lower by about 0.03 eV with respect to the latter. This is consistent with the corresponding total energies, that are compatible with the SP function [142], while Bressanini and coworkers have shown the necessity to converge the energy with a MP wave function of up to a linear combination of 111 pairing functions [142].

Another special case is PsB system, which is stable with respect to the PA dissociation channel, but unstable against the BE_{Ps} one. Moreover, as reported in the previous section, due to the size consistency problem of the AGP or MR approaches in the description of the B atom and its anion, the error in the estimation of the electron affinity can range between 20% and 100% of the total value. As a consequence, this affects the estimation of the BE_{Ps} energy introducing an error of about 0.08 eV for the AGP wave function at the DMC level (see Table A3 of the appendix). For this reason, the Boron PA and the BE_{Ps} were computed using also an SD wave function to describe the electronic correlation. Table 3.2 compares the total energies of the SD and AGP wave function, used in conjunction with the PMO and EPO positronic ones at both VMC and DMC level, and Table A4 of the appendix reports the numerical values of the PA and BE_{Ps} .

As expected, the PA is practically the same between all the wave functions ansatzes with VMC and DMC, since there is no change in the number of electrons between the atomic species in Eq. 3.20. On the contrary, the positronium dissociation channel involves the removal of one electron, which can be expressed in terms of the EA of the neutral atom as

$$BE_{Ps}[X] = PA[X] + EA[X] + E[Ps]. \quad (3.22)$$

For this reason, with the SD wave function the BE_{Ps} value is about 200 meV higher with respect to the AGP with both VMC and DMC. The BE_{Ps} DMC energy obtained with the SD/EPO wave function is of -0.4080(32) eV which is only 0.05 eV lower than the predicted FCI extrapolation value and more compatible with respect to the previous DMC estimations [126]. Qualitatively, it must be pointed out that also with the SD wave function, the PsB is still unstable with respect to the BE_{Ps} dissociation channel.

In light of these results, a similar effect is expected behind the underestimation of the binding energy observed for the same BE_{Ps} channel in PsC, where the best DMC value with AGP/EPO is 192 meV away from extrapolated FCI [77]. In fact, by taking a look at the electron affinity of carbon (reported in Table A3) it can be seen that the error is about 200 meV for VMC and 100 meV for DMC, which explains the discrepancy with the BE_{Ps} value predicted by the extrapolated FCI.

In conclusion, since the positron or positronium affinities are energy differences, it is not possible to argue that the present methodology actually obtains a better estimation of those quantities, nevertheless the DMC values are shown to be in good agreement with the other references obtained with QMC and CI [77, 142, 146, 149].

3.2.4 Dissociation channels of $e^+ \cdot H_2^{2-}$ molecule

As a first attempt to study molecular systems, the performance of the different wave functions was also tested on the dissociation channels of two hydrogen anions bound by one

positron [71, 73, 124]:

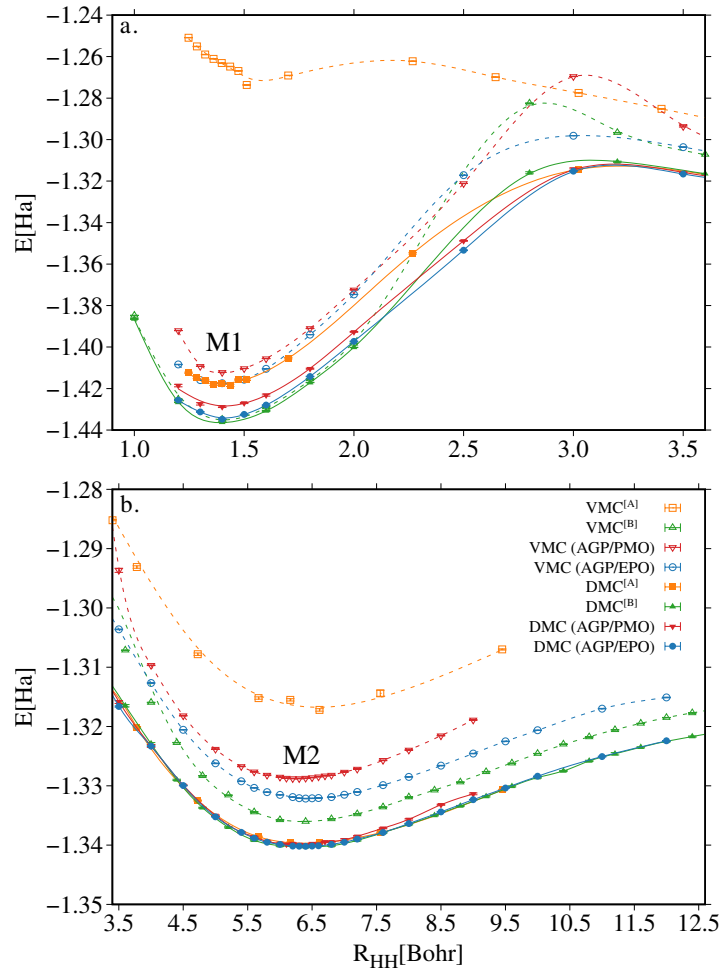
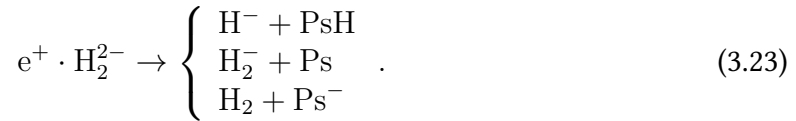


Figure 3.4: Comparison between the VMC and DMC potential energy surfaces of the $e^+ \cdot H_2^{2-}$ around the M1 minimum (panel a) and around second minimum M2 (panel b) obtained with the AGP/PMO and AGP/EPO wave functions and with other wave functions presented in the literature. ^A From Ref. 124, ^B From Ref. 73.

Figure 3.4 gathers all the PES of the $e^+ \cdot H_2^{2-}$ molecule as a function of the internuclear distance between the hydrogen atoms, calculated at VMC and DMC levels with the AGP/PMO and AGP/EPO wave functions, as well as the results previously reported in literature. As discussed by Ito *et al.* [124] and Bressanini [73], the PES of the $e^+ \cdot H_2^{2-}$ molecule has two minima: the first minimum appears at an internuclear distance equal to the equilibrium

distance of the two H atoms in the H_2 molecule, which is referred as M1 in panel **a** of Figure 3.4; the second minimum, which is defined as M2 in panel **b** of Figure 3.4, is observed at larger distances between 5.5 and 6.5 Bohr and is found to be stable with respect to the dissociation of $e^+ \cdot H_2^{2-}$ in PsH and H^- , yet, its total energy is higher than the M1 minimum.

From Figure 3.4, it is clear that at the VMC level the qualitative description of the PES strongly depends on the variational ansatz. The least accurate representation of the molecular dissociation is given by the wave function used by Ito *et al.* [124], which is composed of the product between a Slater determinant (for the electronic wave function), a PMO orbital for the positron, both optimized at the Hartree-Fock level, and a two-body Jastrow factor that recovers correlation between electron-electron, electron-nuclei and electron-positron pairs. Clearly, the two-body Jastrow factor, which is a function that tends to one as the interparticle distances increase, is not suitable to describe the long-range attraction between positrons and electrons, that form bound states. On the other hand, the most accurate wave function is the correlated SP wave function used by Bressanini [73], which explicitly includes two-particle correlation effects and has been used also for the PsH and PsLi and e^+Li atomic systems described in the section above.

Regarding the M2 minimum in Figure 3.4b it can be seen that the AGP/PMO wave function is better with respect to Ito's description, due to the combination of the full relaxation of the variational parameters within the VMC framework, and the use of the dynamical Jastrow factor that was introduced in Eq. 3.19. The AGP/EPO wave function on the other hand, gives results that are more accurate with respect to those of the AGP/PMO, but does not match the accuracy of Bressanini's SP wave function, differently for what was obtained for the atomic systems. Moreover, the estimated M2 energy minimum of the AGP/EPO wave function is more accurate with respect to that predicted by the AGP/PMO wave function which is slightly shifted towards shorter distances by 0.2 Bohr.

Interestingly, all DMC curves are practically equal for the M2 region, suggesting that the nodal surface is correctly described by all the trial wave functions.

The results around the M1 minimum require further discussion. Bressanini [73] demonstrated that the M1 minimum is actually the non-interacting state between the H_2 molecule and the Ps^- anion. In order to describe this region at the variational level, it is essential to have a wave function that can correctly factorize as the product of the two non interacting subspaces. This is in fact the type of wave function that Bressanini uses to describe this state in Ref. 73. This is clearly not the case for Ito's wave function and for the proposed AGP/PMO. Consequently, taking into account this fragmentation, it is clear why in this case the EPO ansatz is again superior than PMO, since the latter forces the positron to localize around the nuclei, while the EPO gives enough flexibility for the positron to adapt to the distribution of the electronic cloud. As a matter of fact, the relaxation of the AGP/EPO can qualitatively describe this region of space and is remarkably close to exact H_2 PES rescaled

by the energy of the Ps^- anion, yet, also this function cannot fully factorize to a product of the non-interacting subsystems, and this explains the slight error obtained at the VMC level, that disappears when using the higher DMC level of calculation (see also Figure 3.5).

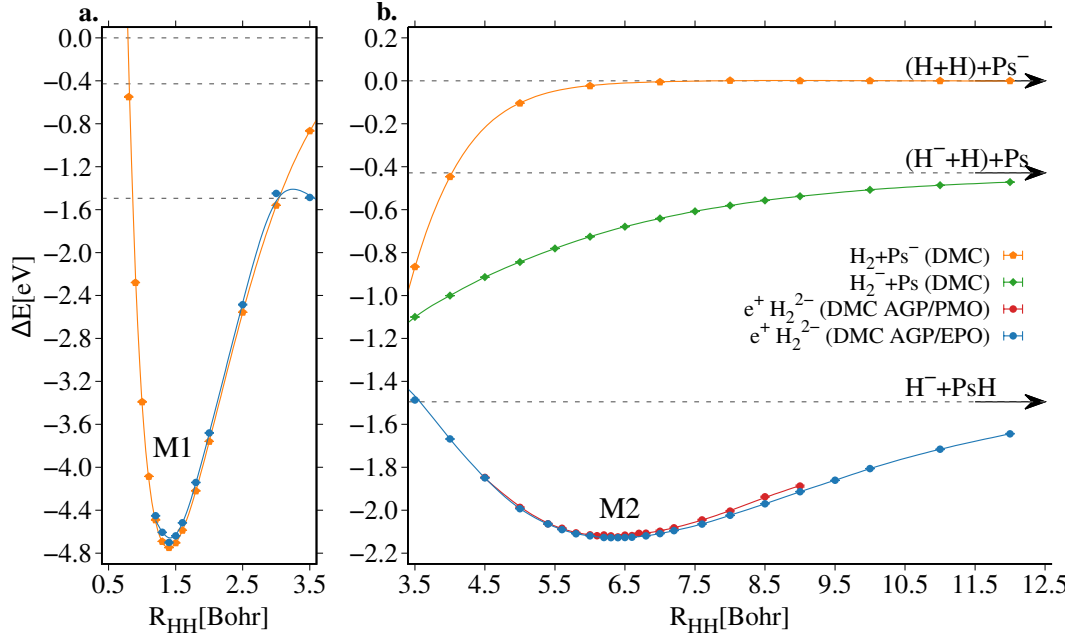


Figure 3.5: Potential energy surfaces (PESs) around the M1 minimum of $\text{H}_2 + \text{Ps}^-$ (panel a) and around the M2 minimum of $e^+ \cdot \text{H}_2^{2-}$ (panel b) obtained at the DMC level for the chemical systems consisting of two hydrogen atoms (H) plus the positronium anion (Ps^-). The dissociation energy of this system in $\text{H} + \text{H} + \text{Ps}^-$ fragments, equal to -1.262 Ha is assumed to be the reference. In orange, the potential energy curve of the H_2 molecule shifted by the energy of Ps^- (-0.262 Ha). The potential energy surface of the $e^+ \cdot \text{H}_2^{2-}$ molecule is shown for the AGP/EPO (blue circles) and for the AGP/PMO (full red circles). In green, the potential energy surface of the H_2^- anion shifted by the energy of Ps (-0.250 Ha).

Following the stability analysis proposed by Bressanini [73], Figure 3.5 plots the PES at DMC level for the $e^+ \cdot \text{H}_2^{2-}$ system as a function of the internuclear distance between the hydrogen atoms. In addition, this plot also includes the PES of H_2 shifted by the energy of Ps^- (-0.262 Ha) as well as the PES of H_2^- shifted by the energy of Ps (-0.250 Ha), that allow to discuss the vertical dissociation channels at each distance. In panel a of Figure 3.5 it can be seen that around 3.5 bohrs the PES of $\text{H}_2 + \text{Ps}^-$ and of the $e^+ \cdot \text{H}_2^{2-}$ positronic molecule intersect, thus $e^+ \cdot \text{H}_2^{2-}$ spontaneously dissociates in the $\text{H}_2 + \text{Ps}^-$ fragments.

This second M2 minimum of the $e^+ \cdot \text{H}_2^{2-}$ molecule, shown in panel b, observed at larger distances, around 6.0 to 6.5 Bohr, is found to be stable with respect to the dissociation in PsH and H^- from which it is separated by a potential barrier of 24 mHa, and also against the

vertical dissociations in $\text{H}_2 + \text{Ps}^-$ or $\text{H}_2^- + \text{Ps}$. For this minimum, the vibrational parameters were also calculated using perturbation theory [150] as also explained in Ref. 151, obtaining an equilibrium geometry of $R_{\text{HH}} = 6.367(5)$ Bohr, a dissociation energy with and without Zero Point Energy (ZPE) corrections equal to $D_0 = 22.31(1)$ mHa and $D_e = 23.35(1)$ mHa respectively, ZPE corrections of $229(2)$ cm^{-1} , harmonic vibrational frequency of $\omega_e = 461(3)$ cm^{-1} , and a first anharmonicity constant of $x_e\omega_e = 6(1)$ cm^{-1} . These are the most detailed results, reported up till now in the literature for the M2 minimum of the $e^+ \cdot \text{H}_2^-$ positronic molecule, and the dissociation energy without ZPE only slightly differs from the previous accurate predictions of Bressanini [73], of -0.2 mHa, and from those of Ito *et al.* [124], by about 0.6 mHa.

The nature of this particular bond and of the positronic bonds, in general, is still largely debated. In the literature, the M2 minimum is referred to as a positronic covalent bond [71, 122], since similarities are observed by comparing, for example, the covalently bound Li_2^+ cation (or $e^- \text{Li}_2^{2+}$) with the corresponding $e^+ \text{Li}_2^{2-}$ positronic molecule. The two molecules were seen to share properties such as equilibrium distances, vibrational frequencies, and binding energies, as well as similarities in the distributions of the electronic HOMO (for $e^- \text{Li}_2^{2+}$) and of the positron (for $e^+ \text{Li}_2^{2-}$) densities. Later, Goli and Shahbazian [122], using AIM analysis, confirmed that the dominant contribution to the bonding is the positron density in between the atoms, which acts as a mediator between the otherwise repulsive anions that do not share any electrons. Furthermore, the authors confirmed a recent study by Nascimento and coworkers [152] which demonstrated that there was no distinction between the mechanism responsible for the formation of one- and two-electron bonds. Despite this, for systems sharing positron pairs, such as the $(\text{PsH})_2$ molecule studied in a recent work by Bressanini [153], the author highlights relevant differences with the corresponding electronic bond formation in H_2 stating that: “It remains to be seen if the binding mechanism in $(\text{PsH})_2$ is the same as in the H_2 covalent bond or it is a completely different and new type of bond” [153]. Moreover, it must be added that the bond in the $e^+ \cdot \text{H}_2^-$ molecule shows intriguing similarities with a van der Waals minimum, such as the slow decay of the interaction energy, where two non-covalently bound atoms are energetically stabilized by a delicate balance between the Pauli repulsion and the attractive dispersion effects. For this reason, in the future it will be interesting to study in detail the electronic properties and their response to an external perturbation, which will shed more light on the bonding nature of positronic molecules.

Regarding the results presented in this section, it can be said that although at the DMC level both the AGP/EPO and AGP/PMO ansatzes agree in the description of the M2 minimum, it is evident that the AGP/PMO is overall less accurate. In fact, around the M1 minimum the AGP/PMO is not capable to correctly reproduce the nucleiless positronic bound state of the partitioned $\text{H}_2 + \text{Ps}^-$ system, which on the other hand is better described by the AGP/EPO wave function. Moreover, the AGP/EPO is also capable to give a good qualitative

description of the system at the level of VMC, due to the more efficient description of the electron-positron correlation effects, also enhanced by the novel dynamical Jastrow factor, which could be suitable to describe loosely Ps or Ps⁻ bound states as well as more localized positronic molecular systems. Finally, at the DMC level the AGP/EPO PES of the e⁺ · H₂²⁻ molecule has been described with a similar accuracy obtained by Bressanini[73] using DMC applied to an explicitly correlated ansatz. Thus, the new approach of this work, allows to provide the most detailed information regarding the vibrational properties of the M2 minimum.

3.3 Summary

This chapter presents a simple yet efficient correlated wave function to study the interaction of a positron with complex atomic and molecular systems. The wave function is constructed as a product of an electronic determinant, in this case the AGP or the SD, a positronic orbital, built on electron-positron correlation functions (the EPO), and a novel explicit Jastrow factor that includes the correlation between electron-positron pairs in the field of the nuclei. This approach was compared with the most commonly used methods in quantum chemistry, to study the binding energies of the positron with different atomic systems and with simple molecules for which accurate results have been obtained in the literature.

For atomic systems, the comparison between the two wave functions in conjunction with the Jastrow factor, demonstrates their accuracy and its important role in the recovery of the necessary correlation to obtain an excellent estimation of the binding energies at the level of VMC. The EPO and PMO results are in fact comparable at the VMC level and identical when doing DMC calculations. This agreement between VMC and DMC is explained by the isotropy of the positron wave function, which is centered around the electronic charge and thus can be represented correctly by a basis set composed of atom-centered orbitals.

Importantly, for the heaviest atoms, such as B, C, O and F, the total energies of the positronic systems PsB, PsC, PsO and PsF presented in this chapter are the most accurate in the literature so far and will serve as references for future investigations. For the lighter atoms, such as H, Li and Be, it has been shown that these approaches are comparable to the SD wave functions used by Bressanini in ref.142, yet easier to generalize also to heavier atoms and more complex molecules. Regarding the positron and positronium affinities, the accuracy analysis is not straightforward since these quantities are energy differences and the variational principle cannot be used as a guide, however the DMC values obtained in this chapter are in excellent agreement with other references present in the literature.

For molecular systems, the discrepancy between the EPO and PMO approaches becomes

more evident. As a matter of fact, at the VMC level the dissociation curves of the $e^+(\text{H}^-)_2$ molecular system, computed with the EPO and PMO wave functions, show a discrepancy in energies of about 0.005 Ha in favour of the former. Through the EPO wave function and using a dense grid of points to construct the PES of the M2 minimum, accurate spectroscopic properties for the $e^+(\text{H}^-)_2$ molecule were computed.

Dynamical Electron-Positron Jastrow Factor

Parts of this chapter will be published in this or similar form in:

J. Charry, M. Barborini, A. Tkatchenko. "Dynamical Jastrow factor for electron-positron interactions" *In preparation*.

and have been produced in collaboration with the above authors.

Chapter 3 described which type of fermionic wave functions can be used in QMC to successfully describe the ground states of positronic atomic and molecular systems [91]. Apart from the computational advantages of the QMC methods, such as the third order scaling with the number of fermions, and the intrinsic parallelization of the algorithms, their main effectiveness lies in the possibility of integrating the Schrödinger equation over intricate trial wave functions that explicitly include few-body correlation factors. Commonly, in QMC, these correlation factors are introduced through a multiplicative function, the Jastrow factor [121, 154, 155], and can be enhanced by more complex and computationally expensive back-flow transformations [156, 157, 158] or Neural Networks [159, 160, 161, 162, 163] ansatz functions.

The Jastrow term is a factor that multiplies a fermionic wave function, such as a Slater determinant, without directly influencing its spatial and spin symmetries, and thus it is always a positive bosonic term. As such, it is usually expressed as a function of two-particle distances that remodulates the wave function amplitudes when two or more particles come close to each other. Its purpose is to describe the correct fermion-fermion and nucleus-fermion cusp conditions of the exact wave function, and secondly to recover explicit dynamical correlation between few-particles in the non-homogeneous Coulomb field of the molecular nuclei (Section 3.1.1). Many different expressions of the Jastrow factors [121, 154, 155, 164] have

been presented in the literature for purely electronic systems including at most four-body correlations between particles.

For positronic systems, on the other hand, a first three- and four-body Jastrow factor was introduced in Ref. 91, built as an extension of the electronic one proposed in Ref. 164. This factor is based on a linear combination of products of non-normalized atomic orbitals, and it has the advantage of being relatively simple and fast to compute. Yet, being expressed in terms of atomic orbitals, the Jastrow factor is inefficient in describing the correlation between the attractive electron-positron pairs and requires further improvements, such as a dependency on the electron-positron distances. For that reason, this chapter investigates the effectiveness of previously introduced dynamical Jastrow factor by including all three- and four-body terms that arise from the linear combinations of products not only of atomic but also of positronic orbitals [91], that are written as a function of the fermion-nuclei and electron-positron distances, respectively. Through both sets of orbitals, it is possible to explicitly describe the distance and angular correlation of the positrons with respect to the electrons, and vice-versa, preserving the overall spatial and spin symmetry of the wave function. In particular, this chapter presents a systematic study of the contributions of the various Jastrow terms to the variational and diffusion Monte Carlo estimations of the total and positronic binding energies, also investigating the effects on the relaxation of the nodal structure once the Jastrow factor is optimized together with the fermionic parameters. In order to enhance the Jastrow factor's capability to recover correlation, this approach is used in combination with a simple Slater determinant that does not include explicit correlation between particles and is most commonly used in quantum chemistry. This total wave function is applied to describe a set of one positron (PsH , $e^+\text{Li}$, PsLi , PsO , and $e^+\text{LiH}$) and two positrons ($e^+\text{PsH}$, $(\text{PsH})_2$, and Ps_2O) systems, that have been chosen due to their challenging description of the electronic and positronic structures, and for the availability of highly accurate reference values in the literature.

The chapter is organized as follows. The electron-positron wave function used in this work is briefly summarized in Section 4.1, Section 4.2 describes the construction of the extended dynamical Jastrow factor for the electron-positron systems. Afterward, Section 4.3 reports and discusses the results, focusing mainly on the total energies and the lowest positronic dissociation energies of the several positronic systems examined. Finally, Section 4.4 provides concluding remarks.

4.1 Electron-positron wave functions

In the literature, many ansatzes have been proposed to describe the many-electrons and many-positrons wave function $\Psi_T(\bar{\mathbf{x}}^p, \bar{\mathbf{x}}^e; \bar{\mathbf{R}})$, where $\bar{\mathbf{x}}^e = \{\bar{\mathbf{r}}^e, \sigma^e\}$ and $\bar{\mathbf{x}}^p = \{\bar{\mathbf{r}}^p, \sigma^p\}$ are the set of Cartesian and spin coordinates for the electrons and positrons, respectively. Whereas $\bar{\mathbf{R}}$ is the vector of the nuclear positions. Ideally, the most general expression of the wave function should explicitly include all particle correlation effects, including the nuclei, while establishing the correct spatial and spin symmetries for both the electrons and positrons [74, 86].

This study employs the most straightforward trial wave function, written as the product of determinants and a Jastrow factor

$$\Psi_T(\bar{\mathbf{x}}^p, \bar{\mathbf{x}}^e; \bar{\mathbf{R}}) = \det[\mathbf{S}_\uparrow^e] \det[\mathbf{S}_\downarrow^e] \det[\mathbf{S}_\uparrow^p] \det[\mathbf{S}_\downarrow^p] e^{\mathcal{J}(\bar{\mathbf{r}}^e, \bar{\mathbf{r}}^p; \bar{\mathbf{R}})}, \quad (4.1)$$

where \mathbf{S}_\uparrow^e and \mathbf{S}_\downarrow^e are the Slater matrices for the spin-up and spin-down electrons, \mathbf{S}_\uparrow^p and \mathbf{S}_\downarrow^p are the corresponding matrices for the positrons, and $\mathcal{J}(\bar{\mathbf{r}}^e, \bar{\mathbf{r}}^p; \bar{\mathbf{R}})$ is the Jastrow factor.

Several QMC studies have employed similar trial wave functions [91, 118, 119, 124, 165, 166] based on products of determinants constructed via atomic basis sets since they are simpler to implement and to integrate with traditional quantum chemistry methods based on HF or DFT. The determinantal part of the wave function defined in Eq. 4.1 correctly describes the total spin and spatial symmetry for many-fermionic systems but completely disregards the correlation of the attracting electron-positron couples.

Although more efficient correlated fermionic wave functions have been proposed in the literature [86, 91, 96], the use of this simple determinantal part has the scope of enhancing the correlation effects recovered by the dynamical Jastrow factor between the fermions in the field of the nuclei, thus rendering more evident its effectiveness.

4.2 Electron-positron Jastrow factor

The bosonic Jastrow factor constructed in this work can be written as the sum of two many-body terms

$$\mathcal{J}(\bar{\mathbf{r}}^e, \bar{\mathbf{r}}^p; \bar{\mathbf{R}}) = \mathcal{J}_c(\bar{\mathbf{r}}^e, \bar{\mathbf{r}}^p; \bar{\mathbf{R}}) + \mathcal{J}_d(\bar{\mathbf{r}}^e, \bar{\mathbf{r}}^p; \bar{\mathbf{R}}), \quad (4.2)$$

the first term describes the fermion-nucleus and fermion-fermion cusps conditions of the exact wave function, while the second term is the one containing few-body correlations between the various particles, also with respect to the nuclear positions, and is responsible for the recovery of dynamical correlation.

The $\mathcal{J}_c(\bar{\mathbf{r}}^e, \bar{\mathbf{r}}^p; \bar{\mathbf{R}})$ term is extensively discussed in Refs. 72, 91 and Chapter 3.1.3. This chapter will focus on the dynamical Jastrow factor $\mathcal{J}_d(\bar{\mathbf{r}}^e, \bar{\mathbf{r}}^p; \bar{\mathbf{R}})$ and its extension.

A first version of the dynamical Jastrow factor for electron-positron systems, inspired by the purely electronic that of Casula *et al.* in Ref. 128, was introduced in Ref. 91, simply written as a linear combination of products of atomic orbitals centered on the nuclei. Although this is not the most common expression of the three-/four-body correlation term [121, 154], the advantages of this formulation lie in its simplicity and computational efficiency [128]. Yet, this Jastrow explicitly depends only on the distances between the nuclei and the fermions. While this is a reasonable correlation factor in describing the attraction between nuclei and electrons, it becomes less efficient for the positrons that are attracted by the electrons.

In order to further generalize this Jastrow factor, the atomic orbitals will be coupled with a set of positronic orbitals, that explicitly depend on the relative distances between electrons and positrons. Therefore, the new dynamical Jastrow factor is built as a combination of three groups of terms

$$\mathcal{J}_d(\bar{\mathbf{r}}^e, \bar{\mathbf{r}}^p; \bar{\mathbf{R}}) = \mathcal{A}(\bar{\mathbf{r}}^e, \bar{\mathbf{r}}^p; \bar{\mathbf{R}}) + \mathcal{G}(\bar{\mathbf{r}}^e, \bar{\mathbf{r}}^p) + \mathcal{M}(\bar{\mathbf{r}}^e, \bar{\mathbf{r}}^p; \bar{\mathbf{R}}), \quad (4.3)$$

which correspond to the atomic Jastrow $\mathcal{A}(\bar{\mathbf{r}}^e, \bar{\mathbf{r}}^p; \bar{\mathbf{R}})$, built purely from the combination of atomic orbitals as previously used in Refs. 72, 91, a set of terms $\mathcal{G}(\bar{\mathbf{r}}^e, \bar{\mathbf{r}}^p)$ constructed only from the positronic orbitals, and a mixed term that combines both orbital sets, $\mathcal{M}(\bar{\mathbf{r}}^e, \bar{\mathbf{r}}^p; \bar{\mathbf{R}})$.

The following sections describe the various terms and explain their relative importance in constructing the full set of four-body correlations included in the Jastrow factor. A schematic representation of the total number of terms is anticipated in Figure 4.1.

4.2.1 Atomic dynamical Jastrow factor

The first part of the dynamical Jastrow, already introduced for multi-positronic systems in Ref. 91, is built on a basis set of Q non-normalized atomic orbitals $\chi_\nu(\mathbf{r})$, that are centered on different atoms (the atomic index is included in the orbital index μ or ν and will always be omitted in the following sections).

For a system comprised of N_e electrons and N_p positrons, this part of the Jastrow factor consists of the sum of three groups of correlation functions,

$$\mathcal{A}(\bar{\mathbf{r}}^e, \bar{\mathbf{r}}^p; \bar{\mathbf{R}}) = \sum_{j>i}^{N_e} \mathcal{A}^{ee}(\mathbf{r}_i^e, \mathbf{r}_j^e; \bar{\mathbf{R}}) + \sum_{h>t}^{N_p} \mathcal{A}^{pp}(\mathbf{r}_h^p, \mathbf{r}_t^p; \bar{\mathbf{R}}) + \sum_i^{N_e} \sum_h^{N_p} \mathcal{A}^{ep}(\mathbf{r}_i^e, \mathbf{r}_h^p; \bar{\mathbf{R}}), \quad (4.4)$$

all written as linear combinations of products of two atomic orbitals. The first set will

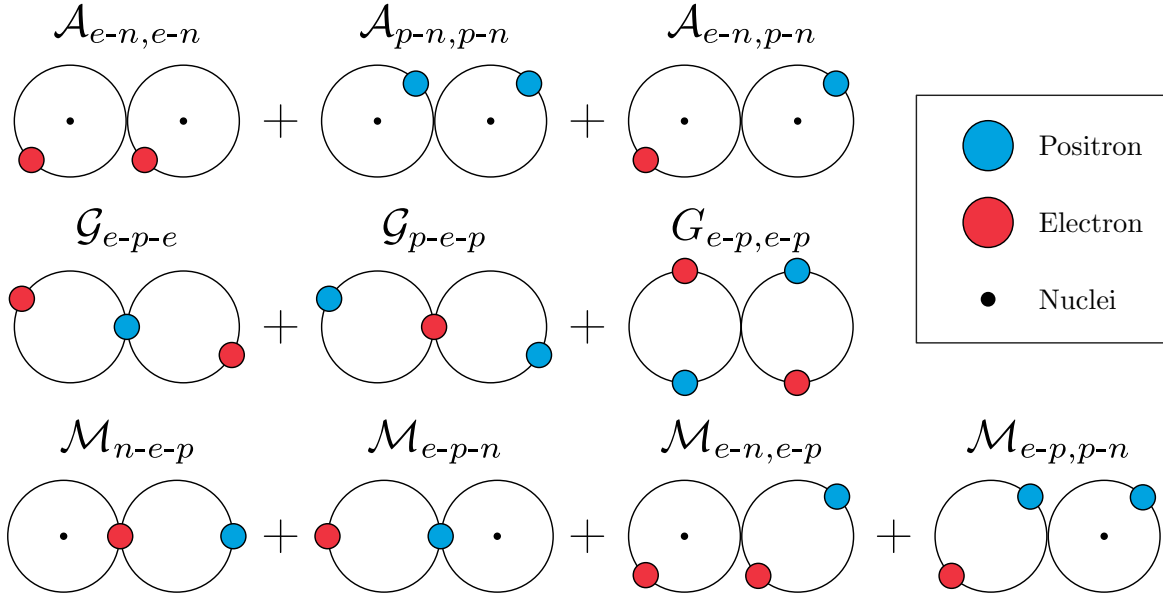


Figure 4.1: Schematic representation of the dynamical Jastrow factor. \mathcal{A} terms correspond to the Atomic dynamical Jastrow, \mathcal{G} terms for Germinal Electron-Positron dynamical Jastrow, and finally the \mathcal{M} terms for the Mixed Atomic and Geminal dynamical Jastrow. The *hyphen* mark is used to represent the distance between two particles within an orbital and the *comma* symbol to indicate a product of two uncoupled orbitals.

correlate two electrons

$$\mathcal{A}^{ee}(\mathbf{r}_i^e, \mathbf{r}_j^e; \bar{\mathbf{R}}) = \sum_{\mu, \nu}^Q A_{\mu\nu}^{ee} \chi_{\mu}(\mathbf{r}_i^e) \chi_{\nu}(\mathbf{r}_j^e), \quad (4.5)$$

the second set will correlate two positrons

$$\mathcal{A}^{pp}(\mathbf{r}_h^p, \mathbf{r}_t^p; \bar{\mathbf{R}}) = \sum_{\mu, \nu}^Q A_{\mu\nu}^{pp} \chi_{\mu}(\mathbf{r}_h^p) \chi_{\nu}(\mathbf{r}_t^p), \quad (4.6)$$

and the third set will correlate one electron and one positron

$$\mathcal{A}^{ep}(\mathbf{r}_i^e, \mathbf{r}_h^p; \bar{\mathbf{R}}) = \sum_{\mu, \nu}^Q A_{\mu\nu}^{ep} \chi_{\mu}(\mathbf{r}_i^e) \chi_{\nu}(\mathbf{r}_h^p). \quad (4.7)$$

Here the square matrices \mathbf{A}^{ee} , \mathbf{A}^{pp} , and \mathbf{A}^{ep} contain the linear coefficients of the expansions, $A_{\mu\nu}^{ee}$, $A_{\mu\nu}^{pp}$, and $A_{\mu\nu}^{ep}$, respectively. Those matrices describe the coupling between the various atomic orbitals occupied by different fermionic pairs. To avoid spin contamination, the \mathbf{A}^{ee}

and \mathbf{A}^{pp} matrices must be symmetric, *i.e.* $A_{\mu\nu}^{ee} = A_{\nu\mu}^{ee}$ and $A_{\mu\nu}^{pp} = A_{\nu\mu}^{pp}$, allowing the Jastrow factor to be invariant with respect to the exchange of two electrons or two positrons, no matter their spin.

Despite the quality of the results presented in Refs. 72, 91, these Jastrow terms only contain functions of the electron-nuclei and positron-nuclei distances with no explicit correlation between the two attractive fermionic particles (electrons and positrons). Yet, the correlation effects arising from explicit electron-positron terms are crucial, especially when describing homogeneous systems of pure electron-positron pairs, or for systems with large numbers of electrons where the positron particle is not in general spherically distributed around an atom [71, 72, 73, 74, 91, 153]. For this reason, the following sections will introduce additional Jastrow components based on electron-positron (or positronic) orbitals [82, 91].

4.2.2 Geminal dynamical Jastrow factor

As previously discussed, the dynamical Jastrow factor constructed as a linear combination of atomic orbitals does not explicitly include the correlation between electron-positron pairs. These pair correlation functions are essential, for example, when describing homogeneous systems of pure electrons and positrons, such as the positronium anion (Ps^-) or the positronium dimer (Ps_2), or in those cases in which the positronic wave function is not spherically symmetric around the nuclei, such as in molecular systems.

For this reason, additional terms will be introduced, indicated as the Geminal Jastrow factor, which is built through a set of K non-normalized positronic orbitals $\varphi_\eta(\mathbf{r}_{ih}^{ep})$ [91], that depends on the distance vector $\mathbf{r}_{ih}^{ep} = \mathbf{r}_i^e - \mathbf{r}_h^p$ connecting the electron-positron pair. For convention, the center of these positronic orbitals is considered to be on the positron's position.

As for the atomic Jastrow factor, the coupled three-/four- body correlations between two pairs of electron-positron are built as the sum of three sets of correlation functions

$$\mathcal{G}(\bar{\mathbf{r}}^e, \bar{\mathbf{r}}^p) = \sum_{j>i}^{N_e} \sum_h^{N_p} \mathcal{G}^{epe}(\mathbf{r}_i^e, \mathbf{r}_h^p, \mathbf{r}_j^e) + \sum_{t>h}^{N_p} \sum_i^{N_e} \mathcal{G}^{pep}(\mathbf{r}_h^p, \mathbf{r}_i^e, \mathbf{r}_t^p) + \sum_{j>i}^{N_e} \sum_{t>h}^{N_p} \mathcal{G}^{epep}(\mathbf{r}_i^e, \mathbf{r}_h^p, \mathbf{r}_j^e, \mathbf{r}_t^p), \quad (4.8)$$

each written as the linear combination of products of two positronic orbitals. Here, the first

$$\mathcal{G}^{epe}(\mathbf{r}_i^e, \mathbf{r}_h^p, \mathbf{r}_j^e) = \sum_{\eta,\tau}^K G_{\eta\tau}^{epe} \varphi_\eta(\mathbf{r}_{ih}^{ep}) \varphi_\tau(\mathbf{r}_{jh}^{ep}), \quad (4.9)$$

and second

$$\mathcal{G}^{pep}(\mathbf{r}_h^p, \mathbf{r}_i^e, \mathbf{r}_t^p) = \sum_{\eta, \tau}^K G_{\eta\tau}^{pep} \varphi_\eta(\mathbf{r}_{ih}^{ep}) \varphi_\tau(\mathbf{r}_{it}^{ep}), \quad (4.10)$$

sets of terms represent three fermion correlations respectively between two electrons and one positron (Eq. 4.9) and two positrons and one electron (Eq. 4.10).

Since the Jastrow factor must be invariant with respect to the exchange of two same-spin electronic or positronic coordinates, the square matrices of the coefficients that define the two expansions, \mathbf{G}^{epe} and \mathbf{G}^{pep} , must be symmetric, *i.e.* $G_{\eta\tau}^{epe} = G_{\tau\eta}^{epe}$ and $G_{\eta\tau}^{pep} = G_{\tau\eta}^{pep}$.

The third set of terms describes the correlation between four different fermions: two electrons and two positrons, again as a product of two geminal orbitals,

$$\mathcal{G}^{ep ep}(\mathbf{r}_i^e, \mathbf{r}_h^p, \mathbf{r}_j^e, \mathbf{r}_t^p) = \sum_{\eta, \tau}^K G_{\eta\tau}^{ep ep} [\varphi_\eta(\mathbf{r}_{ih}^{ep}) \varphi_\tau(\mathbf{r}_{jt}^{ep}) + \varphi_\eta(\mathbf{r}_{jh}^{ep}) \varphi_\tau(\mathbf{r}_{it}^{ep})]. \quad (4.11)$$

As for the last two terms, the four-particle correlation function must be symmetric with respect to the exchange of both electrons and positrons, and in order to impose this not only the coupling matrix $\mathbf{G}^{ep ep}$ must be symmetric, *i.e.* $G_{\eta\tau}^{ep ep} = G_{\tau\eta}^{ep ep}$, but also to impose symmetrization to the exchange of both electron pairs and positron pairs. For this reason, they should be written as the sum of the two contributions $\varphi_\eta(\mathbf{r}_{ih}^{ep}) \varphi_\tau(\mathbf{r}_{jt}^{ep}) + \varphi_\eta(\mathbf{r}_{jh}^{ep}) \varphi_\tau(\mathbf{r}_{it}^{ep})$.

4.2.3 Mixed atomic-geminal dynamical Jastrow factor

The atomic and geminal Jastrow factors defined in the previous sections do not exhaust the four-body correlations that can be described with the atomic and positronic basis sets. While the atomic part neglects the pair correlation between electron-positron pairs and the Geminal part neglects the influence of the nuclei, a third term exploits the possibility of describing the correlation of two or three fermions in the field of one nucleus, as products of positronic and atomic orbitals.

The first option is to describe a three-body coupling of the i th electron with the h th positron in the field of the nuclear positions. This correlation is constructed as the sum of two combinations, the first of which is the term

$$\mathcal{M}^{nep}(\mathbf{r}_i^e, \mathbf{r}_h^p; \bar{\mathbf{R}}) = \sum_{\nu}^Q \sum_{\eta}^K M_{\nu\eta}^{nep} \chi_{\nu}(\mathbf{r}_i^e) \varphi_{\eta}(\mathbf{r}_{ih}^{ep}), \quad (4.12)$$

that correlates the i th electron with the nuclear coordinates through the atomic basis set and the h th positron through the positronic basis set. The second term inverts the couplings,

correlating the positron with the atomic basis and with the electron through the positronic basis set:

$$\mathcal{M}^{epn}(\mathbf{r}_i^e, \mathbf{r}_h^p; \bar{\mathbf{R}}) = \sum_{\nu}^Q \sum_{\eta}^K M_{\nu\eta}^{epn} \varphi_{\eta}(\mathbf{r}_{ih}^{ep}) \chi_{\nu}(\mathbf{r}_h^p). \quad (4.13)$$

Following the same procedure, it is possible to build terms correlating three fermions in the field of the nuclei. The first set of terms will correlate two electrons and a positron in the field of the nuclei,

$$\mathcal{M}^{enep}(\mathbf{r}_i^e, \mathbf{r}_j^e, \mathbf{r}_h^p; \bar{\mathbf{R}}) = \sum_{\nu}^Q \sum_{\eta}^K M_{\nu\eta}^{enep} \chi_{\nu}(\mathbf{r}_i^e) \varphi_{\eta}(\mathbf{r}_{jh}^{ep}), \quad (4.14)$$

while the second set of terms will correlate two positrons and one electron:

$$\mathcal{M}^{eppn}(\mathbf{r}_i^e, \mathbf{r}_h^p, \mathbf{r}_t^p; \bar{\mathbf{R}}) = \sum_{\nu}^Q \sum_{\eta}^K M_{\nu\eta}^{eppn} \varphi_{\eta}(\mathbf{r}_{ih}^{ep}) \chi_{\nu}(\mathbf{r}_t^p). \quad (4.15)$$

Since the first two sets of terms are two-body correlation functions coupling an electron and a positron, no symmetries have to be imposed in the rectangular matrices, \mathbf{M}^{nep} and \mathbf{M}^{epn} . The same holds for the rectangular matrices \mathbf{M}^{enep} and \mathbf{M}^{eppn} that appear in the last two three-body terms. Yet, the invariance of the Jastrow factor should be guaranteed for the exchange between the two electrons in Eq. 4.14 and the two positrons in Eq. 4.15. To this end, it is sufficient to extend the sums to all pairs of different fermions. Therefore, using Eqs. 4.12, 4.13, 4.14, and 4.15, the total mixed atomic-geminal dynamical factor is expressed as:

$$\begin{aligned} \mathcal{M}(\bar{\mathbf{r}}^e, \bar{\mathbf{r}}^p; \bar{\mathbf{R}}) &= \sum_i^{N_e} \sum_h^{N_p} \mathcal{M}^{nep}(\mathbf{r}_i^e, \mathbf{r}_h^p; \bar{\mathbf{R}}) + \sum_i^{N_e} \sum_h^{N_p} \mathcal{M}^{epn}(\mathbf{r}_i^e, \mathbf{r}_h^p; \bar{\mathbf{R}}) \\ &+ \sum_{j \neq i}^{N_e} \sum_h^{N_p} \mathcal{M}^{enep}(\mathbf{r}_i^e, \mathbf{r}_j^e, \mathbf{r}_h^p; \bar{\mathbf{R}}) + \sum_i^{N_e} \sum_{t \neq h}^{N_p} \mathcal{M}^{eppn}(\mathbf{r}_i^e, \mathbf{r}_h^p, \mathbf{r}_t^p; \bar{\mathbf{R}}). \end{aligned} \quad (4.16)$$

Finally, Figure 4.1 summarizes all the dynamical Jastrow factors in a simple yet illustrative schematic picture.

4.2.4 Computational details

A single Slater determinant was employed for the electronic and positronic wave functions, built with a linear combination of atomic-centered orbitals as a sum contracted GTOs. In particular, the H atoms basis employed a 3s1p Gaussian primitives contracted in the 1s1p

orbitals, that is, (3s1p)/[1s1p]. For Li, a basis set of (5s4p1d)/ [2s1p1d] contracted GTOs, and for O atom, a similar basis set of (6s4p1d)/[2s1p1d] contracted orbitals was employed. For simplicity, the same set of orbitals is used for both the positronic and fermionic wave function determinant parts. The initialization of the exponents and contraction coefficients is fully described in a previous work [91]. The dynamical Jastrow factor uses a (3s2p) uncontracted and not normalized GTOs centered on each atom to construct the atomic part, while the positronic basis was built from a single set of (3s2p) uncontracted electron-positron GTOs.

In the present work, all the parameters are optimized simultaneously, including the contracted exponents and coefficients, the molecular orbitals coefficients, the cusps parameters, and the linear and orbital parameters of the dynamical Jastrow factor.

For LiH, e^+ LiH, and (PsH)₂ molecular systems, the calculations have been done using equilibrium distances of respectively 3.015[67], 3.458[67], and 6.000[153] Bohr, consistent with the reference calculations present in the literature.

Regarding the DMC calculations, each optimized VMC wave function was taken as the guiding function, and the estimation of the DMC energy was performed with 6400 walkers divided into 4000 blocks, each 2000 steps long, for a time step of 0.001 atomic units. All computed VMC and DMC energies with their associated estimates error are reported in Table B1 of the appendix.

Table 4.1: Variational Monte Carlo (VMC) and diffusion Monte Carlo (DMC) total energies (in Hartree) of the three-/four- body systems of the form $[e^-, e^-, e^+]$ and $[e^-, e^-, e^+, e^+]$ with variable positronic mass m_{e^+} . Here, m_H is the mass of the Hydrogen atom, which is set to $m_H = 1836 m_{e^-}$.

	Ps ⁻ $m_{e^+} = m_{e^-}$	H ⁻ (QN) $m_{e^+} = m_H$	H ⁻ (CN) $m_{e^+} = \infty$	Ps ₂ $m_{e^+} = m_{e^-}$	H ₂ (QN) $m_{e^+} = m_H$	H ₂ (CN) $m_{e^+} = \infty$
VMC \mathcal{J}_c	-0.252856(16)	-0.521290(34)	-0.521622(25)	-0.502504(24)	-1.145409(66)	-1.170694(31)
VMC $\mathcal{J}_c + \mathcal{J}_d$	-0.2610146(73)	-0.526716(42)	-0.5272118(78)	-0.513893(16)	-1.162724(55)	-1.1743590(94)
DMC \mathcal{J}_c	-0.26175(12)	-0.527340(76)	-0.527525(86)	-0.51590(20)	-1.16341(24)	-1.174471(52)
DMC $\mathcal{J}_c + \mathcal{J}_d$	-0.261941(34)	-0.527398(26)	-0.527756(18)	-0.515990(55)	-1.16368(15)	-1.1744693(86)
Reference ^a	-0.26200507	-0.527445881093	-0.527751016523	-0.516003790416 ^b	-1.164025024 ^c	-1.17447593140021 ^d

^a From Ref. 167, ^b From Ref. 19, ^c From Ref. 168, and ^d 169

4.3 Results and discussion

4.3.1 Pure electron-positron systems

In order to understand the purpose of the Geminal Jastrow factor (Section 4.2.2), an initial study was performed on systems of only electrons and positrons, as well as the molecular ones derived from the variation of the positronic mass m_{e^+} . More specifically, this test considers the three-particle system $[e^-, e^-, e^+]$ that corresponds to Ps^- when $m_{e^+} = m_{e^-}$ (m_{e^-} is the mass of the electron that is set to 1), to H^- with quantum nucleus (QN) when $m_{e^+} = 1836 m_{e^-} = m_H$) and to H^- with classical nucleus (CN) if $m_{e^+} = \infty$. Similarly, it was considered the four particle system $[e^-, e^-, e^+, e^+]$ that corresponds to the positronium dimer Ps_2 with $m_{e^+} = m_{e^-}$, to the Hydrogen molecule H_2 with quantum nuclei if $m_{e^+} = 1836 m_{e^-} = m_H$, and to the Hydrogen molecule with classical nuclei if again $m_{e^+} = \infty$.

These purely fermionic systems, Ps^- and Ps_2 , as well as for their analogs H^- and H_2 with quantum nuclei, require a fermionic wave function representation that cannot be based on fixed nuclear positions. Therefore, for these systems, the fermionic part was built using the electron-positron orbital ansatz proposed in a previous work [91]

$$\psi_p(\bar{\mathbf{r}}^p; \bar{\mathbf{r}}^e) = \prod_{i=1}^{N_e} \prod_{j=1}^{N_p} \varphi(\mathbf{r}_{ij}^{ep}),$$

where $\varphi(\mathbf{r}_{ij})$ are molecular orbitals identical for each electron-positron pair, built as a linear combination of positronic orbitals. On the other hand, for comparing infinite mass cases in the classical H^- and H_2 molecules, the simple Slater determinant function was employed (Eq. 2.6).

In all cases, the Jastrow factor is written as the sum of the two body cusp functions \mathcal{J}_c , (see Eqs. 3.15, 3.11, 3.16) that are optimized for each system, and the dynamical term \mathcal{J}_d responsible for the three and four body correlation effects between the particles. Clearly, for the purely fermionic systems, Ps^- and Ps_2 , and for their analogs H^- and H_2 with quantum nuclei, the three- and four-body correlation effects can only be described through the geminal Jastrow factor described in Section 4.2.2, due to the fixed center's absence. Albeit, for the infinite mass cases, the dynamical Jastrow factor is constructed only through the atomic orbital terms described in Section 4.2.1.

The VMC and DMC energies obtained for these systems with and without the dynamical Jastrow factors are reported in Table 4.1. In all cases, it can be observed that the addition of the dynamical Jastrow factor reduces the absolute error of the VMC energies by one order of magnitude from 10 mHa to 1 mHa on average, compared to the accurate reference values obtained with fully explicitly correlated Gaussian functions [19, 167, 168, 169]. At

the DMC level, on the other hand, since all systems consist of distinguishable particles, the total energies are always converged, yet remarkably, the use of the dynamical Jastrow factor significantly reduces the absolute errors with respect to the reference values, since the Jastrow factor remodulates the amplitude of the wave function towards the exact solution. This can be observed by comparing the differences between the VMC and DMC total energies that are greatly reduced with the use of the dynamical Jastrow factor.

The above results indicate that the geminal Jastrow factorw introduced in Section 4.2.2 plays the same role as the atomic one (Section 4.2.1) used for purely electronic systems, and it is necessary to recover the three- and four-body correlations between electrons and positrons in systems of many electrons and positrons.

Yet, while the atomic Jastrow factor correlates the fermionic pairs with the nuclei and the Geminal Jastrow correlates fermionic pairs of opposite charge, a Jastrow factor capable of considering explicit electron-positron pair correlation in the non-homogeneous field of the nuclei is still missing. This is the reason to introduce the mixed Jastrow factor (Section 4.2.3), whose effects are studied in the following sections through positronic molecules.

4.3.2 Jastrow basis set effect

The dynamical Jastrow factor (Eq. 4.3) is built in terms of either atomic-centered orbitals or electron-positron geminal orbitals, therefore it is important to analyze the basis set convergence exploring the dependency of the total VMC energy with respect to the number of Gaussian type functions (GTFs) and their angular momentum.

Considering the simplest positronic atom, Positronium hydride (PsH) using classical proton, with the full dynamical Jastrow factor that includes the atomic, geminal and mixed terms, Table 4.2 reports the convergence of the VMC energy combining basis sizes of (1s), (3s), (3s2p), and (3s2p1d) uncontracted GTFs.

Subsequently, by analyzing the energy difference with respect to the highest energy obtained, which corresponds to the smallest basis combination 1s/1s as expected, it can observe a convergence of the VMC energy gain around 3.8 mHa after using a set of 3s2p GTFs for both the atomic Jastrow basis and the geminal one. Further addition of d-GTFs does not lower the variational energy significantly. Now, by analyzing the convergence of both basis sizes individually, it can be observed that the effect of the geminal basis size is slower than the atomic basis; for example, all combinations of 1s atomic basis with 3s,3s2p, and 3s2p1d geminal orbitals provide almost the same energy gain of just 0.5 mHa. On the other hand, for the 1s geminal basis, the variation from 1s to 3s and then to 3s2p provides an energy change of 1.6 and 1.2mHa respectively. This behavior will be further discussed in the following sections by analyzing the contribution of each dynamical Jastrow term individually.

In addition, this converged Jastrow basis with p-GTF functions should be adequate for systems where the spatial symmetry has to be broken, in a similar fashion to how polarization GTFs are added in standard quantum chemical methods to describe the polarization of the electron density of atoms in molecular systems [170]. For all the above reasons mentioned, further calculations on this work employed the 3s2p/3s2p dynamical Jastrow basis for the atomic and geminal Jastrow orbitals, respectively.

Table 4.2: Effect of the size of the atomic Jastrow basis and Geminal electron-positron basis on the VMC energy for PsH (in Hartree units) using the full dynamical Jastrow (atomic, geminal and mixed) according to Eq. 4.3. The ΔE column corresponds to the energy difference between each basis set combination and the highest energy obtained.

\mathcal{A}	\mathcal{G}	VMC	ΔE
Basis	Basis	[Ha]	[mHa]
1s	1s	-0.784278(19)	0.0
1s	3s	-0.784856(19)	-0.6
1s	3s2p	-0.784797(18)	-0.5
1s	3s2p1d	-0.784794(19)	-0.5
3s	1s	-0.785832(16)	-1.6
3s	3s	-0.786660(19)	-2.4
3s	3s2p	-0.786674(12)	-2.4
3s	3s2p1d	-0.786675(15)	-2.4
3s2p	1s	-0.787104(14)	-2.8
3s2p	3s	-0.787620(15)	-3.3
3s2p	3s2p	-0.788107(12)	-3.8
3s2p	3s2p1d	-0.788111(10)	-3.8
3s2p1d	1s	-0.787131(14)	-2.9
3s2p1d	3s	-0.787630(16)	-3.4
3s2p1d	3s2p	-0.788159(9)	-3.9
3s2p1d	3s2p1d	-0.788203(13)	-3.9

4.3.3 Atoms and molecules

Once a reasonable Jastrow basis set size has been determined, the next step is to analyze the contribution of each dynamical Jastrow term of Eq. 4.3 to the description of electron-positron correlation by systemically performing individual wave function variational optimizations, by switching on or off the atomic electron-positron term \mathcal{A}^{ep} , the geminal \mathcal{G} terms, and the mixed one \mathcal{M} in all possible combinations. All tests employed a Slater determinant for the fermionic part except for e^+Li and $PsLi$ where a constrained multi-

determinantal [91] was chosen, in addition to the one- and two-body cusp Jastrow, and the pure electronic atomic dynamical Jastrow term \mathcal{A}^{ee} , note that in the present approach, all the variational parameters are optimized in order to see their relaxation effect and to provide lower variational energies at VMC level. This study presents results for eight of the most relevant positronic systems previously studied in the literature with highly accurate methods, more precisely: PsH, which is the most studied system due to its small size [171]. The $e^+\text{Li}$ and PsLi, which are characterized by their very low dissociation energies [57, 83, 142], therefore one of the most challenging systems, and $e^+\text{LiH}$ as the most studied small positronic molecule [75]. Regarding two positronic systems: $e^+\text{PsH}$, the simplest two positronic atom [84], the two positron bond in $(\text{PsH})_2$ [153], and the positronic water molecule Ps_2O which was hypothesized to be one of the fewest two-positron systems that can be experimentally observed due to their stability [45], in addition to Ps_2 .

Figure 4.2 compares the VMC energies employing different combinations of dynamical Jastrow terms of Eq. 4.3 for the aforementioned positronic systems. All the data in these plots are also presented as a table in the appendix, B1. Overall, the effect of each term on the total correlation energy seems to be consistent for this set of systems. First of all, the calculations employing only the electron-electron atomic dynamical Jastrow \mathcal{A}^{ee} can be seen as the starting point since the electron-positron correlation effects are only considered in the two-body Jastrow term, which is presented for all calculations. Next, it is observed that the addition of the \mathcal{G} terms has the lowest contribution for improving the total energy, and even in the cases of PsH, $e^+\text{Li}$ the improvement is almost absent, while for the other systems the energy gain is at most around half of the correlation energy that the other terms can add. This low contribution could indicate that there is no need to describe Ps^- formation into the wave function for PsH and $e^+\text{Li}$, a process that will require breaking the stable $1s^2$ shell. On the contrast, these terms provide a better description in the following cases: two positronic systems as $e^+\text{PsH}$ and $(\text{PsH})_2$, positronic distribution far from the nuclei like in $e^+\text{LiH}$ and $(\text{PsH})_2$, or negatively charged atoms with high nuclei charge as in PsLi, PsO, and Ps_2O .

Regarding the \mathcal{M} dynamical Jastrow factor, its mere addition provides one of the largest contributions to lower the VMC energy, indicating the importance of including in the wave function the formation of Ps, Ps^- or anti- Ps^- species in the vicinity of the nuclei. Furthermore, the addition of both \mathcal{G} and \mathcal{M} combined does not significantly improve further than \mathcal{M} alone, suggesting that the electron-positron correlation effects described by \mathcal{G} are fully covered in the mixed terms, in other words, the coupling with the atomic orbitals for electrons in the field of the nuclei.

The next Jastrow term in the current analysis is the \mathcal{A}^{ep} , which displays a slightly better performance (in $e^+\text{Li}$, $e^+\text{LiH}$, PsO) than the mixed Jastrow \mathcal{M} , suggesting that the positronic distribution can be improved as a simple linear combination of coupled atomic-centered orbitals. On the contrary, for $e^+\text{PsH}$, PsLi, $(\text{PsH})_2$ the \mathcal{M} outperforms \mathcal{A}^{ep} indicating the

importance of the explicitly Ps geminal orbitals coupled to atomic orbitals.

Similarly to the $\mathcal{G} + \mathcal{M}$ case, for $\mathcal{A}^{ep} + \mathcal{G}$ there is no significant change in the reduction of the VMC energy, indicating again that the contribution \mathcal{G} can be either included in the atomic \mathcal{A}^{ep} or \mathcal{M} mixed Jastrow factor.

Consequently, the next significant improvement of the variational energy is obtained with $\mathcal{A}^{ep} + \mathcal{M}$. Here it is important to note that the combination of both is not accumulative. Therefore the final contribution is not the sum of the independent terms, indicating that some of the missing electron-positron correlation effects can be described by both terms, and the further improvements are probably due to the explicit Ps Jastrow orbital and the coupled Ps^- in the mixed term \mathcal{M} .

Lastly, as expected, all terms combined provide the lowest variational energy, but once more the addition of \mathcal{G} on top of $\mathcal{A}^{ep} + \mathcal{M}$ does not significantly decrease the energies, reinforcing the present observations of the low impact for the geminal dynamical Jastrow factor compared to the atomic and mixed one.

The optimized VMC wave functions for each dynamical Jastrow combination were further taken as guiding functions in the DMC calculations, these results are gathered in Figure 4.3. Overall, there is a decrease in the standard deviation of the mean according to the same trend observed in the total VMC energies for each Jastrow factor, indicating that the correlation effects included in the dynamical Jastrow factors allow a correct relaxation of the nodal structure in the fermionic part. For the systems: PsH, $e^+\text{PsH}$, $(\text{PsH})_2$, and $e^+\text{LiH}$ the differences with respect to reference values are lower than 0.5 mHa, with no significant differences between Jastrow combinations. As the number of electrons increases, so does the absolute error on the total energies in $e^+\text{Li}$, PsLi , PsO , and Ps_2O , except in $e^+\text{LiH}$ where the dominant electrostatic interaction is simpler to describe than polarization effects due to its permanent dipole moment [29].

4.3.4 Dissociation energies

For positronic systems, the energy of the dissociation channels should also be addressed in order to establish a true bound state, since in some cases the most energetically stable species corresponds to the ejection of a positron, Ps , Ps^- or even Ps_2 . Therefore, the following lines discuss the lowest dissociation channels for all the Jastrow combinations and systems presented in Figure 4.4. For the two positron systems, the dissociation energies calculations employ the energies for each corresponding Jastrow in the one positron counterpart.

First, for PsH the lowest dissociation channel is $\text{H} + \text{Ps}$, therefore any variational energies lower than -0.75 Hartree means a bound state, which is the case for all Jastrow combinations

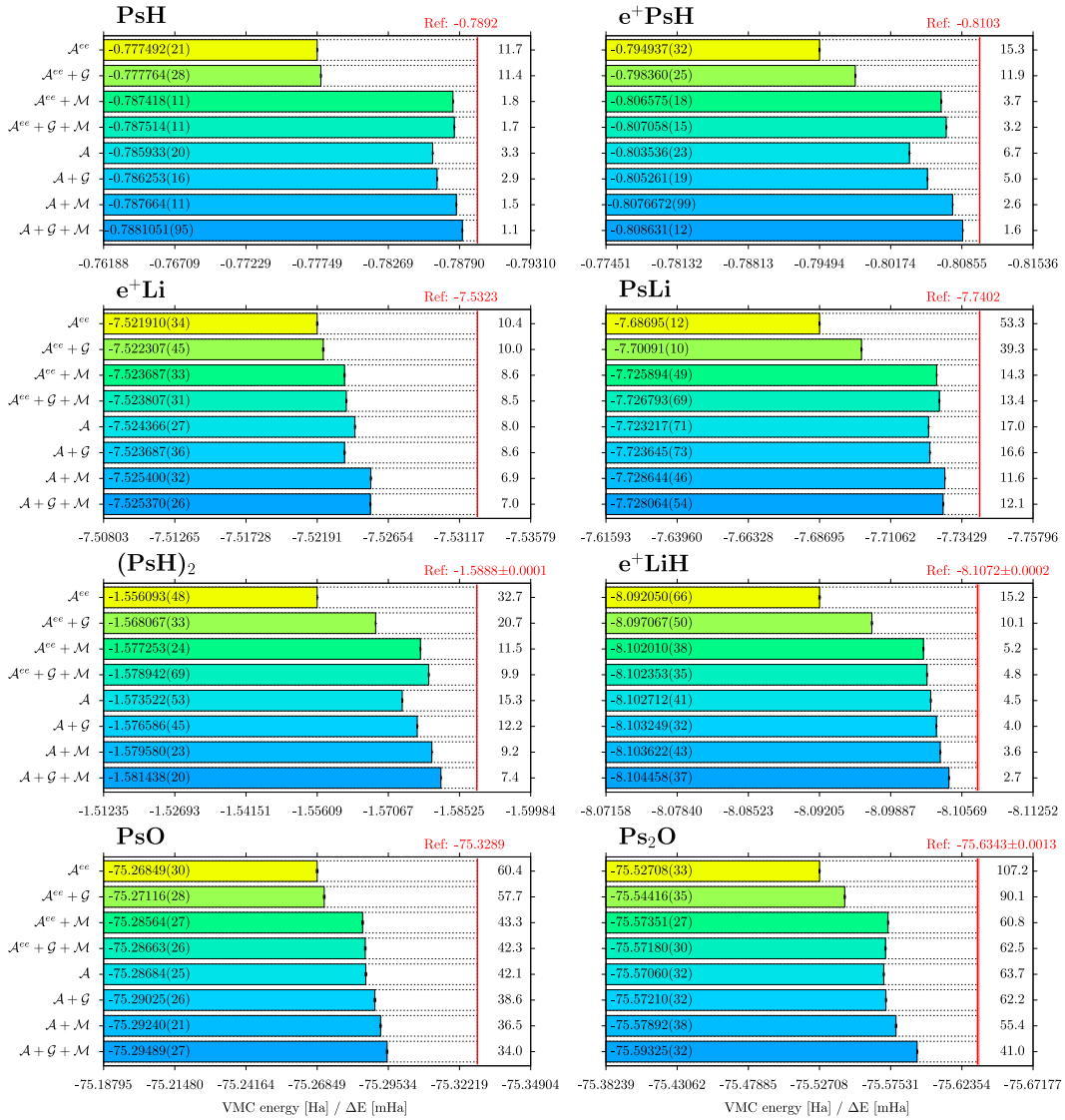


Figure 4.2: Comparison of the VMC energies for different combinations of the atomic, geminal, and mixed electron-positron dynamical Jastrow terms for one- and two-positron systems. Energy differences (in mHa) are displayed on the right side of each bar against the reference value, indicated by a red vertical.

(see Figure 4.2), therefore the same trends are observed as in the total energies. The analysis in $e^+\text{PsH}$ is also trivial since the lowest channel is the ejection of one positron as $e^+\text{PsH} \rightarrow \text{PsH} + e^+$, then any energy lower than PsH gives a bound state as seen in Figure 4.2. However, for the $\mathcal{A}^{ee} + \mathcal{G}$ Jastrow, the corresponding binding energies seem to be higher

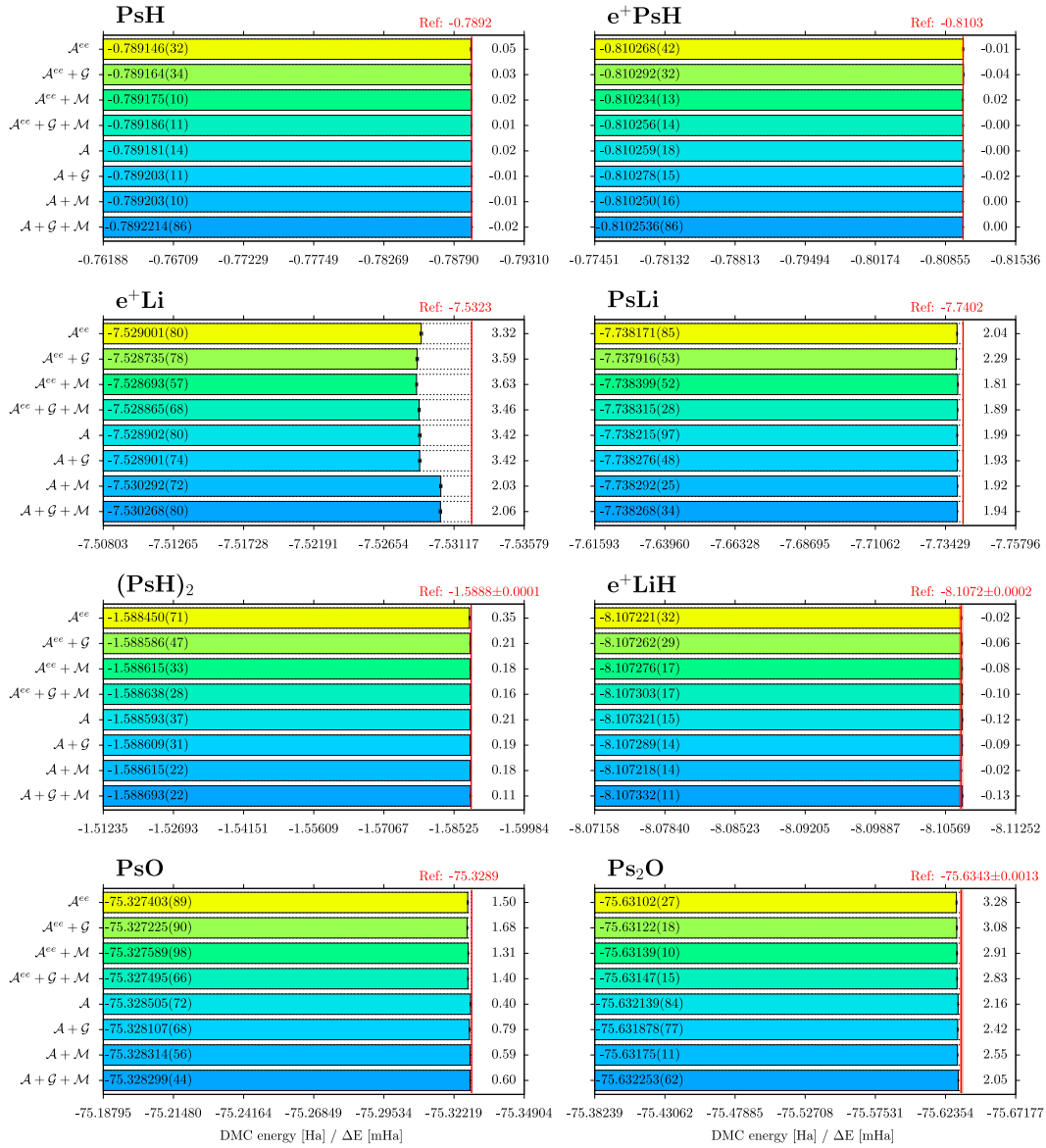


Figure 4.3: Comparison of the DMC energies (in Ha) with a time step of 0.001 a.u for different combinations of the atomic, geminal, and mixed electron-positron dynamical Jastrow terms for one- and two-positron systems. Energy differences (in mHa) are displayed on the right side of each bar against the reference value, indicated by a red vertical.

than expected. This discrepancy is caused by the poor performance of the geminal term in PsH, which for the case of e^+PsH is compensated by the anti-positronium anion term \mathcal{G}^{pep} , and by the dipositronium term $\mathcal{G}^{ep ep}$, clearly indicating that these two Jastrow factors cannot be comparable at the same level, although the absolute error is just 0.02 eV.

Next, for e^+Li all Jastrow combinations fail to predict the bound state, this system is the most challenging one due to its low binding energy attributed to the large electronic volume in the Li atom. Additionally, it has been already reported that at large distances from the Lithium nucleus the probability distribution of the valence electron and positron have combined to form a Ps cluster [83], which can probably only be correctly described with explicit electron-electron and electron-positron correlation into the fermionic wave function [142].

In PsLi, using only the atomic \mathcal{A}^{ep} and mixed \mathcal{M} terms, it is possible to attain a bound state, although the binding energy is far from the accurate reference by one order of magnitude. The structure of the ground state of PsLi was recently studied by Bressanini, finding that introducing explicitly the positronium wave function of the form $\Psi(Li)\Psi(Ps)f(Li, Ps)$ is capable to surpass the energy threshold of $Li + Ps$, opposite to the form $\Psi(Li^-)\Psi(e^+)f(Li^-, e^+)$, which is more similar to our ansatz. Nevertheless, this work will focus only on the description at the level of the Jastrow factor [57].

Regarding the dissociation channels in $(PsH)_2$ as demonstrated by Bressanini [153], due to the instability of the two repulsive H^- , the potential energy curve of $(PsH)_2$ intersects with the energy curve of multiple dissociation channels at short distances. Therefore the analysis there is more complex and goes beyond the scope of this work. For that reason, only the dissociation at long internuclear distances of two PsH will be considered in this work. Surprisingly, even with the full dynamical Jastrow, the dissociation energy has an error of 50%, indicating that at VMC level the positronic structure of PsH is better described than in the dimer. This is explained by the different type of interactions, in the case of PsH [83] the positron probability densities is spherically symmetric around the nuclei following the electronic density with a maximum at 3 Bohr of distance, while in PsH_2 [153] it is localized in the internuclear region between the two H^- where the electronic density goes to a minimum. Therefore in the latter case it would be better described by using an auxiliary orbital centered in the middle region (ghost center) or by an explicit geminal [91], as can be seen on the more consistent results for all the other Jastrow factors based on geminal orbitals. Similarly to the e^+PsH case, for PsH_2 there is an overestimation of the dissociation energy $\mathcal{A}^{ee} + \mathcal{G}$ Jastrow factor, which is also explained by the unbalanced description in PsH with this Jastrow factor.

The diatomic system of e^+LiH is an interesting case because the vertical binding energy obtained with only \mathcal{A}^{ee} of 0.6720(22) eV is more than triple the previously reported VMC value of 0.15(2) eV [86] were the authors employed a similar wave function to ours but keeping frozen the parameters of the one- and two-body Jastrow factor with respect to LiH. Thus, indicating the importance of relaxing those parameters in the calculation of the positronic complexes. On the other hand, the other Jastrow factors significantly improve the binding energies to only less than 0.2 eV error for the Geminal Jastrow \mathcal{G} and less than 0.06 eV for the others. For PsO, both the atomic \mathcal{A}^{ep} and mixed \mathcal{M} correctly reach a bound

state by lowering the energy in 0.4 eV, whereas both the purely electronic Jastrow and geminal alone are not enough to breach the dissociation threshold, although for the others the binding is still underestimated by 0.5 eV. Finally, for Ps_2O all Jastrow combinations manage to correctly predict the bound state, however it should be noted here that the binding can be closer to the reference due to the missing correlation effects on PsO with the same Jastrow factor. Nevertheless, the \mathcal{A}^{ep} and mixed \mathcal{M} ones improve the binding energy by a considerable amount of 0.7 eV.

The dissociation energies calculated at DMC level are gathered in Figure 4.5. For the systems PsH , $e^+\text{PsH}$, $(\text{PsH})_2$, $e^+\text{LiH}$, and Ps_2O , there is a good agreement against the reference values within the error bars. For $e^+\text{Li}$, most of the Jastrow factors cannot provide a qualitatively good guiding wave function, since they still predict an unbound state, except for the combination of atomic \mathcal{A} and mixed \mathcal{M} Jastrow factors, although their predicted energy is strongly underestimated. Additionally, all DMC calculations proved to be unstable for $e^+\text{Li}$. For example, Figure B1 of the appendix shows the estimated error as a function of the block length in the reblocking technique, observing no convergence with long blocks sizes, indicating an underestimation of the error bars [85]. In PsLi , the bound state is correctly achieved, nevertheless, the energies are far away from the reference data by 75 meV on average. For PsO , the gap to the reference is attributed to the missing multireference character from single-determinant DMC calculations for Oxygen atom, evidenced by an error of 80 meV in its electron affinities compared to experimental value [77, 91], which is already accounted in the multireference configuration interaction calculation performed by Saito for estimating the Positronium binding energy [77]. In the case of Ps_2O , this multireference error is not present since the reference value also corresponds to a single determinant DMC calculation.

4.3.5 Scaling

Finally, the next lines discuss the scaling of each Jastrow factor with respect to the number of variational parameters. As shown in Equations 4.4, 4.8, and 4.16, the scaling with respect to the size of the Jastrow basis sets is Q^2 for the atomic \mathcal{A} , K^2 for the geminal \mathcal{G} , and QK for the mixed Jastrow \mathcal{M} . For practical applications, the size of the atomic Jastrow basis will increase proportionally to number $Q \propto (N_A)$, while the geminal basis will be fixed to a certain number of geminal orbitals $K \propto (n_{gem})$. Therefore the scaling will be simplified to N_A^2 for atomic, n_{gem}^2 for geminal, and $n_{gem}N_A$ for the mixed Jastrow factor. Considering that for large systems $N_A \gg n_{gem}$, and the performance discussed in the previous sections, the mixed Jastrow alone outperforms the others by reaching the lowest VMC energies with only a linear scaling with respect to the number of atoms, contrary to the atomic Jastrow having slightly lower performance with quadratic scaling, on the other hand, the geminal Jastrow factor provides a non-negligible energy gain without scaling with the number of

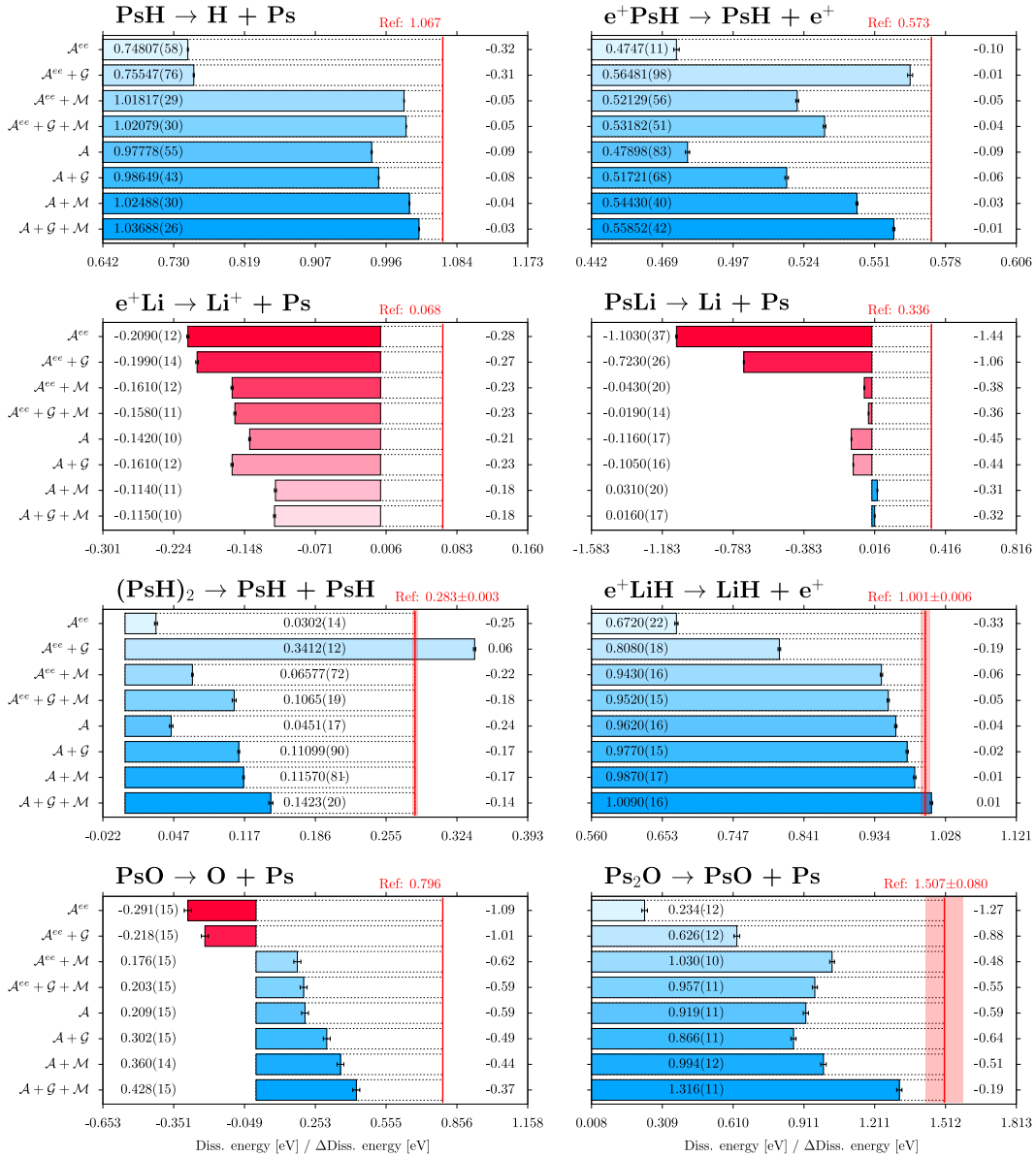


Figure 4.4: Comparison of the lowest dissociation energies at VMC level for different combinations of the atomic, geminal, and mixed electron-positron dynamical Jastrow terms for selected one- and two-positron systems. The vertical red line indicates the reference values. Unbound and bound values are associated with red and blue color bars, respectively.

atoms.

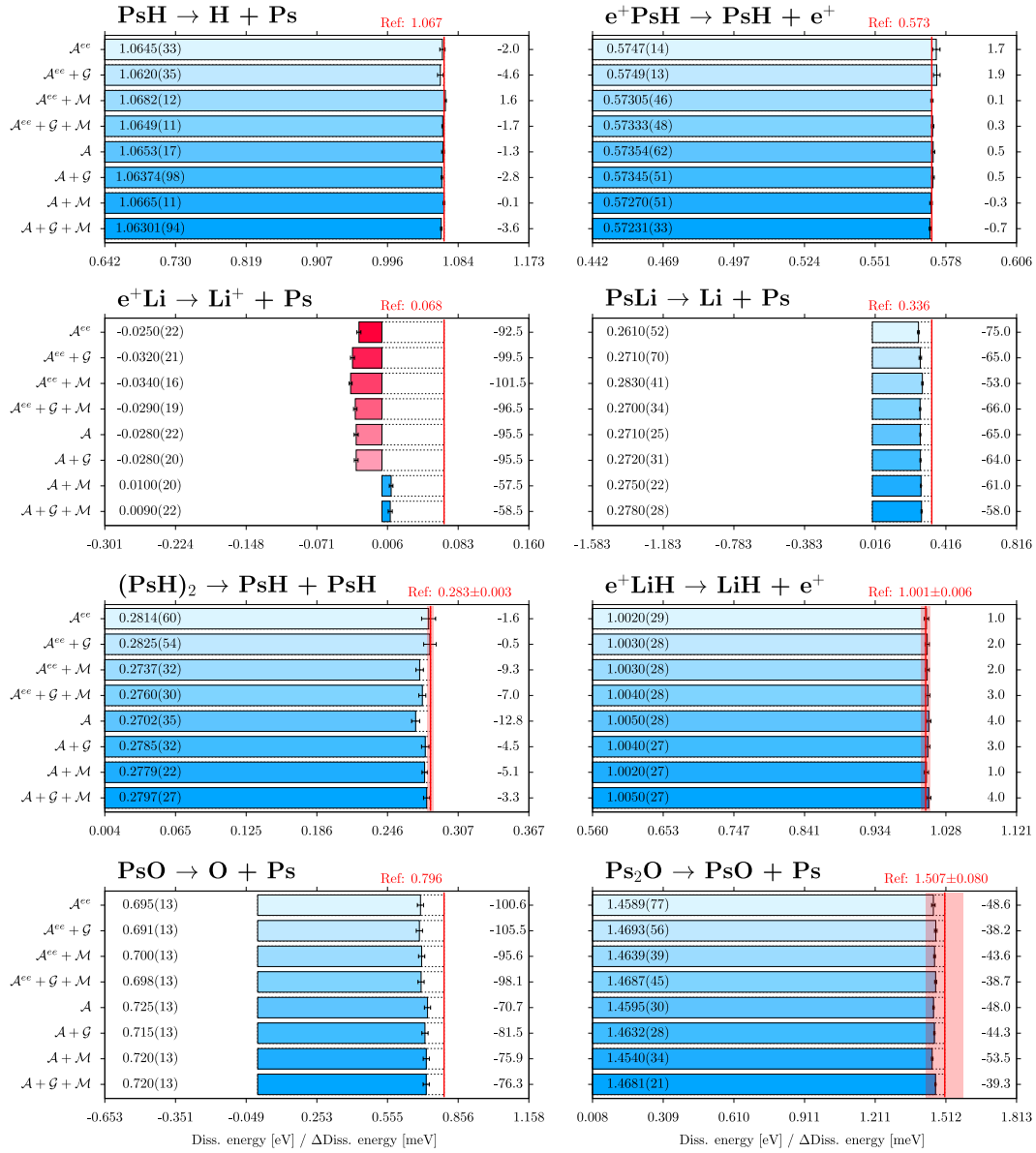


Figure 4.5: Comparison of the lowest dissociation energies at DMC level for different combinations of the atomic, geminal, and mixed electron-positron dynamical Jastrow terms for selected one- and two-positron systems. The vertical red line indicates the reference values. Unbound and bound values are associated with red and blue color bars, respectively.

4.4 Summary

This chapter has introduced a set of homogeneous and non-homogeneous dynamical Jastrow factors to account for three- and four-body electron-positron correlation effects in the field of nuclei. This new Jastrow factor is built as a linear combination of products of atomic and geminal orbitals, which can be grouped together in three different types: fully atomic Jastrow terms, fully geminal orbitals, or a mixed term combining products of both types of orbitals.

As demonstrated for the three and four-body systems Ps^- and Ps_2 , by changing the mass of the positive particle this generalized Jastrow factor successfully connects the extreme cases of positron mass, finite nuclear mass, and infinite nuclear mass by lowering the absolute error in VMC from 10 mHartree to only 1 mHartree.

In order to test the effects of this dynamical Jastrow in the description of electron-positron interactions, total and dissociation energies were computed for selected positronic complexes at VMC and DMC levels, relaxing all variational parameters of the fermionic and bosonic wave function. The atomic and mixed terms alone provide the biggest improvement to the total and dissociation energies at VMC level, and the combinations of both further improve by some extra mHa with respect to the most accurate data available in the literature. Nevertheless, the mixed Jastrow factor only scales linearly with respect to the number of atoms, preserving an optimal balance between accuracy and the number of variational parameters to optimize, making it the most suitable term for larger systems. The geminal Jastrow factor shows the smallest energy gain, although this term could be relevant for positronic distributions far from the nuclei and poses the best scaling compared to the other terms since it depends on a fixed number of positronic orbitals.

Despite the significant improvement in the variational VMC energies, for $e^+\text{Li}$ and PsLi systems, their lowest dissociation channels are still wrongly predicted as an unbound state, due to an insufficient description of the electronic and positronic distributions at long distances from the nuclei. Nevertheless, the positronic atoms are the most challenging systems; on the contrary, positronic molecular systems should be simpler to describe correctly due to their ability to have permanent or induced dipole moment enhancing the electron-positron interactions.

Electric Response Properties of Positronic Systems

Parts of this chapter will be published in this or similar form in:

J. Charry, M. Barborini, A. Tkatchenko. "Electric response properties of positronic atom and molecules" *In preparation*.

and have been produced in collaboration with the above authors.

While Chapters 3 and 4 have focused on the development of a QMC methodology to study the ground state and binding energies of isolated positronic systems, the present chapter explores how to unveil the electron-positron wave function structure and the positron binding mechanism through the evaluation of their response properties to an external electric field, computed by QMC techniques.

The effect of an external electric field on electronic and positronic systems has been known for many decades and can be classified according to its intensity. In the strong electric field regime, the recent advances in laser technology are aimed at the generation of electron-positron pairs from vacuum, that are predicted in quantum electrodynamics (QED) [172, 173, 174, 175]. For moderate fields, the main goal is to explore how the electric field can increase the positronium lifetimes [176, 177, 178, 179, 180], thus controlling the annihilation dynamics [181, 182]. Since the electron-positron annihilation rates depend on the overlap of their wave functions [183], the long-lived matter-antimatter systems are explained by the increase of the electron-positron distance induced by the electric field, in which the probability density contact is reduced. On the other hand, low electric fields are used to study the response properties of the electron-positron systems, which can be generated, for example, by an external atom or molecule of the environment surrounding the positronic complex.

Most of the computational studies focus in particular on the evaluation of binding energies and annihilation rates of the isolated positronic complex, but other electronic and positronic properties, or their interactions with external atoms and molecules, are an almost unexplored topic [59] due to the difficulty of correctly capturing the correlated motions of electrons and positrons. In addition, for such properties, the wave function should be versatile enough to describe the small polarization effects that break the spatial symmetry caused by the electric field. Nevertheless, there are a few reports on the calculation of the polarizability of PsH using explicitly correlated ansatz [58, 59, 60, 184], as a first step towards understanding the interaction of PsH with external potentials. For some years, there was a discrepancy between the first reported dipole polarizability of 123 a.u. by Le Sech and Silvi [58], compared to the estimate of 49 a.u. reported by Mella *et al.* [67].

Other response properties reported in the literature for positronic systems are the two-body dispersion coefficients, mainly the C_6 , corresponding to the dipole-dipole term r^{-6} of the multipole expansion of the long-range interaction potential between two atoms. In particular, these coefficients were computed for PsH [59, 60], Ps with a few neutral atoms [61, 63], Ps and H in all combinations [62], and Ps₂ with atoms [63]. Those studies assumed that the interatomic interaction is repulsive at short distances due to the Pauli exclusion principle, which repels the same spin electron between atoms. In contrast, at long distances between atoms, the interaction should be attractive due to the dispersion interaction between the electronic clouds. However, this assumption ignores the effects on the positron wave function at the typical equilibrium distances for regular non-covalent electronic interactions. This premise was recently proven inadequate in the case of two interacting PsH. By performing QMC calculations at several internuclear distances, Bressanini [153] found that the two positrons can induce the formation of a chemical bond between two otherwise repelling ions, similarly to the case of one positron [71].

Even though QMC techniques have proven to yield accurate absolute and relative energies for regular electronic [90, 95, 100] and positronic systems [67], their application to computing polarizabilities is more challenging because of the stochastic error that comes with these approaches, causing the computation of accurate second-order derivatives to be quite demanding [185, 186, 187]. On the contrary, although HF based methods can more easily provide accurate polarizabilities for electronic systems [188], for positronic ones, the lack of explicit correlation greatly affects the accuracy of total and binding energies [29], and has repercussions on the estimation of all electronic properties.

Motivated by the above challenges and by the lack of data regarding the response properties of positronic systems, this chapter explores at VMC and DMC levels, the computation of dipole polarizabilities and the effects of an external electric field to the annihilation rates and expectation values of the interparticle distances for Ps, Ps₂, PsH and (PsH)₂. Those quantities are analyzed in order to shed light into the structure of their electronic and positronic wave functions, revealing non-trivial scaling of the dipole polarizability with

respect to the number of interacting particles.

This chapter is organized as follows: Section 5.1 briefly describes the wave function employed, as well as describing the computation of the response properties. Next, Section 5.2 shows and analyzes the total energies, dipole moment, annihilation rates, density changes, and interparticle distances for a few positronic atoms and their dimers. Finally, Section 5.3 summarizes the results and provides concluding remarks.

5.1 Methods

This study considers electrons and positrons as quantum particles and atomic nuclei as point charges within the Born-Oppenheimer approximation described by the Hamiltonian in Eq. 2.2. All molecular properties were computed using the VMC and DMC methods as described in Section 2.3.

5.1.1 Wave function

The general trial wave function employed for this work is written as the product of a fermionic part and a bosonic component, the Jastrow factor, used to describe the explicit correlation between particles, expressed as

$$\Psi(\bar{\mathbf{x}}^e, \bar{\mathbf{x}}^p; \bar{\mathbf{R}}) = \psi_e(\bar{\mathbf{x}}^e; \bar{\mathbf{R}}) \psi_p(\bar{\mathbf{x}}^e, \bar{\mathbf{x}}^p) \text{Exp}[\mathcal{J}(\bar{\mathbf{x}}^e, \bar{\mathbf{x}}^p; \bar{\mathbf{R}})]. \quad (5.1)$$

For multielectronic systems, ψ_e is built as a Slater determinant (Eq. 2.6), whereas the positronic wave function is described by the EPO orbitals in Eq. 3.7 but generalized for two positronic systems as

$$\psi_p(\bar{\mathbf{x}}^e, \bar{\mathbf{x}}^p) = \prod_{i=1}^{N_e} \prod_{j=1}^{N_p} \varphi(\mathbf{r}_{ij}^{ep}), \quad (5.2)$$

based on identical orbitals $\varphi(\mathbf{r}_{ij}^{ep})$ (so that the function is symmetric with respect to the exchange of the electronic coordinates) that depend on the electron-positron distance \mathbf{r}_i^{ep} . The generalization for multipositronic systems will require the introduction of an antisymmetry operator. The orbitals φ are built as linear combinations

$$\varphi(\mathbf{r}^{ep}) = \sum_{q=1}^Q l_q \phi_q(\mathbf{r}^{ep}), \quad (5.3)$$

of electron-positron orbitals

$$\phi(\mathbf{x}^{ep}) = r^{ep} R(r^{ep}) Y_l^m(\theta^{ep}, \phi^{ep}). \quad (5.4)$$

Finally, the Jastrow factor consists of the two-body terms between fermions and fermion-nuclei to describe their cusp conditions and pair correlations, together with the full three- and four-body dynamical Jastrow described in Eq. 4.3 to account for homogeneous and non-homogeneous two-body correlations in the field of the nuclei or positrons as

$$\mathcal{J}(\bar{\mathbf{r}}^e, \bar{\mathbf{r}}^p; \bar{\mathbf{R}}) = \mathcal{J}_c^{en}(\bar{\mathbf{r}}^e, \bar{\mathbf{R}}) + \mathcal{J}_c^{pn}(\bar{\mathbf{r}}^p, \bar{\mathbf{R}}) + \mathcal{J}_c^{ee}(\bar{\mathbf{r}}^e) + \mathcal{J}_c^{pp}(\bar{\mathbf{r}}^p) + \mathcal{J}_c^{ep}(\bar{\mathbf{r}}^e, \bar{\mathbf{r}}^p) + \mathcal{J}_{3/4}(\bar{\mathbf{r}}^e, \bar{\mathbf{r}}^p; \bar{\mathbf{R}}). \quad (5.5)$$

All the parameters of the wave functions are optimized with the SRC method [189, 190], as described in Section 2.3.

5.1.2 External electric field

The dipole moment operator for a system with N_n number of particles [191], is defined as

$$\hat{\mu}_a = \sum_i^{N_n} q_i r_{ia} \quad a = \{x, y, z\}, \quad (5.6)$$

where q_i is the charge of a particle i and its position in the cartesian component a is described by $r_{i,a}$. Given that, in the QMC formalism (Section 2.3), the local dipole moment corresponds simply to:

$$\mu_{a,loc}(\bar{\mathbf{r}}) = \frac{\hat{\mu} \Psi_T(\bar{\epsilon}; \bar{\mathbf{r}})}{\Psi_T(\bar{\epsilon}; \bar{\mathbf{r}})} = \sum_i^{N_p} q_i r_{i,a}. \quad (5.7)$$

The Hamiltonian of a quantum system in a weak static electric field [191] is described by

$$\hat{H} = \hat{H}_0 - \sum_a \hat{\mu}_a F_a - \frac{1}{3} \sum_{ab} \Theta_{ab} F_{ab} - \dots \{a, b = x, y, z\}, \quad (5.8)$$

where \hat{H}_0 is the unperturbed Hamiltonian, F_a is the strength of the electric field, Θ is the quadrupole moment, and F_{ab} is the field gradient. However, for the present calculations, it will be considered only uniform electric fields, such that $F_{ab} = 0$. Taking into account the expressions from Eq. 5.7 for the local dipole moment, the local energy of this type of perturbed system can be computed as [186]

$$E_{loc}^F(\bar{\epsilon}; \bar{\mathbf{r}}) = E_{loc}^0(\bar{\epsilon}; \bar{\mathbf{r}}) - \sum_a \mu_{a,loc}(\bar{\mathbf{r}}) F_a - \frac{1}{2} \sum_a a, b \alpha_{a,b} F_a F_b - \dots \{a, b = x, y, z\}. \quad (5.9)$$

Here, it should be noted that the contributions from the external field do not depend explicitly on the set of variational parameters $\bar{\epsilon}$ of the trial wave function $\Psi_T(\bar{\epsilon}; \bar{\mathbf{r}})$, but its sampling will depend on the probability distribution according to the trial wave function.

5.1.3 Polarizabilities

Considering that the energy of a system under a weak external electric field can be expanded in a power series with respect to the strength of the electric field [191] as

$$E(F) = E_0 - \sum_a \mu_a^{(0)} F_a - \frac{1}{2} \sum_{a,b} \alpha_{ab} F_a F_b - \dots, \quad (5.10)$$

then, the dipole polarizability α_1 (from now on simplified as α , and its cartesian component α_{ab}), is defined as the second derivative with respect to the strength of the field when this one goes to zero [184]

$$\alpha_{ab} = - \left(\frac{\partial}{\partial F_a} \left(\frac{\partial E(F)}{\partial F_b} \right) \right)_{F=0}. \quad (5.11)$$

Analogously, the dipole moment can be expanded as

$$\mu_a(F) = \mu_a^{(0)} + \sum_b \alpha_{ab} F_b + \dots, \quad (5.12)$$

leading to defining the polarizability as the first derivative of the dipole moment

$$\alpha_{aa} = \left(\frac{\partial \mu_a(F_b)}{\partial F_b} \right)_{F=0}. \quad (5.13)$$

The first or second derivative can be obtained by numerical differentiation with respect to different applied electric fields [192]. Vrbik *et al.*[193] proposed an alternative method to compute the estimate of the polarizability, as well as any first and higher derivatives of the expectation value of an operator with respect to one or more physical parameters. Within that approach, finite differences of an unknown exact wave function are determined by analytical averaged expressions involving only the total serial correlation of known quantities, such as the local dipole moment. However, that approach will not be discussed in this thesis.

In this work, the dipole polarizabilities were computationally estimated by performing a quadratic or linear fitting of the total energies or dipole moment, respectively, for a set of different strengths of a uniform external electric field F , according to

$$E(F_a) = -\alpha_{aa}/2 \cdot F_a^2 + b \cdot F_a + E_0, \quad (5.14)$$

where α_{aa} , b , and E_0 are the fitting parameters. Therefore, the quadratic function's second derivative at $F = 0$ corresponds to the dipole polarizability. Similarly, from the dipole

$$\mu(F_a) = \alpha_{aa} \cdot F_a + \mu_0, \quad (5.15)$$

where α_{aa} and μ_0 are the fitting parameters, and the first derivative at $F = 0$ of the linear function corresponds to the dipole polarizability.

5.1.4 Annihilation rate

For a closed-shell electronic and positronic system, the dominant annihilation path is the two-photon process. Thus, the rate at which an electron and a positron in a singlet state come into direct contact is given by the two-photon annihilation rate [183]

$$\Gamma_2 = \pi r_0^2 c \langle \delta_{ep} \rangle, \quad (5.16)$$

which is proportional to the electron-positron contact density, related to the probability of finding the electron and the positron at a certain point in space

$$\langle \delta_{ep} \rangle = \left\langle \Psi(\mathbf{r}_p, \mathbf{r}_e) \left| \sum_{i=1}^{N_e} \sum_{j=1}^{N_p} \delta(\mathbf{r}_i - \mathbf{r}_j) \right| \Psi(\mathbf{r}_p, \mathbf{r}_e) \right\rangle. \quad (5.17)$$

here c is the speed of light in vacuum and r_0 is the classical electron radius, which is connected to the Bohr radius a_0 by $r_0 = \alpha_{fsc}^2 a_0$, where α_{fsc} is the fine structure constant. In VMC and DMC, it is extremely expensive to properly sample the coalescence integral because of the low number of configurations for which an electron and a positron are located at the same point, or close to it. For that reason, it is preferred to use the simple extrapolation technique proposed by Jiang *et al.* in Ref. [45], where the coalescence $\delta(\mathbf{r}_i - \mathbf{r}_j)$ is replaced by

$$\delta_a(x_i - x_j) = \begin{cases} \frac{3}{4\pi a^3}, & \text{for } |x_i - x_j| \leq a \\ 0, & \text{otherwise} \end{cases}. \quad (5.18)$$

Therefore, the quantity $\Gamma_2(a)$ should be computed and stored for a set of different distance values a by summing the contribution of each walkers with an electron-positron distance lower than a . Afterward, the QMC averages of $\Gamma_2(a)$ are extrapolated to $a = 0$ by doing a standard linear fit considering the standard error of the averages. However, it should be noted that when a is small, the deviation of the counts becomes larger because the counts are few.

5.1.5 Computational details

For systems with fixed nuclei, a single Slater determinant was employed for the electronic wave functions, built with a linear combination of atomic-centered orbitals as a sum of contracted GTOs. In particular, the H atoms basis is built with a 3s1p Gaussian primitives contracted in the 1s1p orbitals, that is, (3s1p)/[1s1p]. The dynamical Jastrow factor uses a (3s2p) uncontracted and not normalized GTOs centered on each atom to construct the atomic part, while the positronic basis is built from a single set of (3s2p) uncontracted electron-positron GTOs. In the present work, all the parameters are optimized simultaneously, including the

contracted exponents and coefficients, the molecular orbitals coefficients, the cusps parameters, and the linear and orbital parameters of the dynamical Jastrow factor. Regarding the DMC calculations, each optimized VMC wave functions were taken as the guiding function, and the estimation of the DMC energy was performed with 6400 walkers divided into 4000 blocks, each 2000 steps long, for a time step of $0.001 \text{ hartree}^{-1}$. For the systems without fixed charged nuclei, namely Ps and Ps_2 , a ghost 1s orbital was added for the electronic wave function. This ghost center with a fixed delocalized exponent allows constraining the sampling over a center, stabilizing the optimization procedure.

5.2 Results and discussion

5.2.1 Dipole polarizabilities

Figure 5.1 plots the quadratic and linear fitting for Ps, Ps_2 , PsH, and $(\text{PsH})_2$ computed at VMC and DMC levels. For the Ps atom, a great accuracy can be achieved for the energies of the perturbed systems. Nevertheless, since in this approach the dipole polarizability is computed as a second-order quantity, small fluctuations can greatly impact the accuracy of the polarizabilities. This issue is due to the fact that the energy differences are smaller or equal to the error bars for small electric fields, whereas, for large electric fields, the optimization of the variational parameters becomes more unstable. On the other hand, for the estimates obtained through the first derivative of the dipole moment, the fluctuations of the dipole averages are larger than the fluctuations of the energies with the same sampling. Therefore, in both approaches, the accuracy of polarizability estimates is greatly affected by different causes, explaining the high uncertainties for that property prediction, which can be improved by increasing the sampling. The same behavior is observed for all the other systems studied here.

Table 5.1 reports all the computed quantities for dipole polarizabilities, expectation values of interparticle distances, and two-photon annihilation rates (ns^{-1}) for the unperturbed (no external field) Ps, Ps_2 , PsH and $(\text{PsH})_2$ systems computed at VMC and DMC levels. Except for $(\text{PsH})_2$, in all cases, the computed polarizability is slightly smaller at VMC than at DMC despite the error bars, which might indicate that, within the fixed-node approximation and imaginary time discretization, the correct description of the wave function is more polarizable than the trial wave function. Within the error bars, the Ps polarizability agrees with the analytical value for VMC and DMC levels. The Ps_2 polarizability is also in good agreement with the reported value, which was obtained using a field-free estimator from Path-Integral Monte Carlo (PIMC) method [63]. Unfortunately, the error bars are too large to discern if the polarizability is larger or smaller than the sum of the polarizability of two non-interacting Ps atoms. Nevertheless, it is interesting the small variation in the

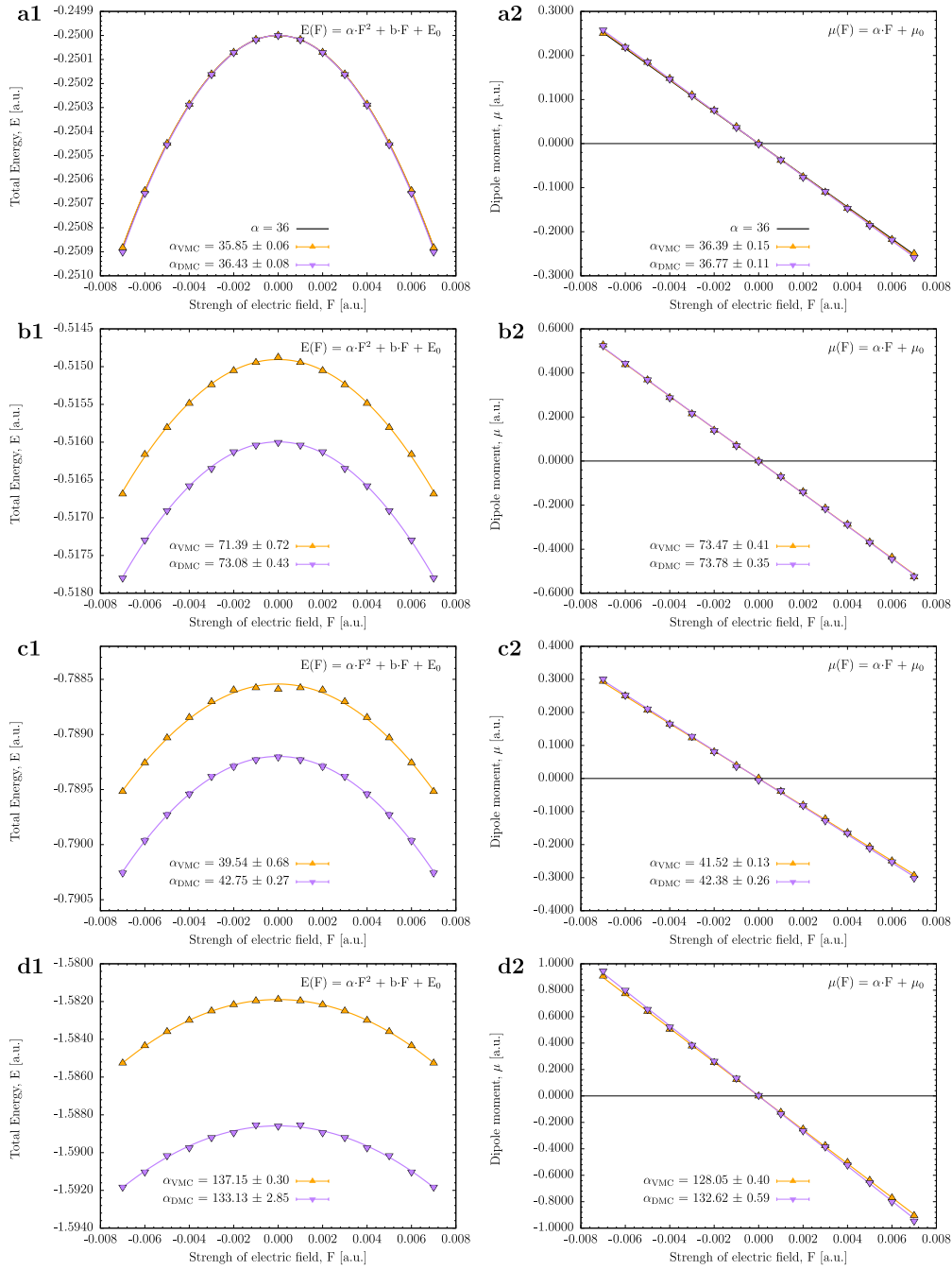


Figure 5.1: Total energies (first column) and dipole moment (second column) as a function of the strength of an external electric field for **a:** Ps, **b:** Ps_2 , **c:** PsH and **d:** $(\text{PsH})_2$ (parallel component) computed at VMC (orange) and DMC (purple) levels. Solid lines indicate the quadratic or linear fit.

Table 5.1: Dipole polarizabilities (a.u.), expectation values of Interparticle distances (bohr), and two-photon annihilation rates (ns^{-1}) for Ps, Ps_2 , PsH and $(\text{PsH})_2$ systems computed at VMC and DMC levels. Reference values for Ps_2 and PsH were taken from the ECG values of Ref. [171], and the DMC energy of $(\text{PsH})_2$ was taken from Ref. [153].

Property	Ps	Ps_2	PsH	$(\text{PsH})_2$
E_{VMC}	-0.249999970(10)	-0.5148778(44)	-0.7885914(31)	-1.5818902(94)
E_{DMC}	-0.249999920(10)	-0.5160019(90)	-0.789204(20)	-1.588591(68)
E_{ref}	-0.25	-0.516004	-0.7891967100(42)	-1.58880(10)
α_{VMC} [E]	35.850(60)	71.39(72)	39.54(68)	137.15(30)
α_{VMC} [μ]	36.39(15)	73.47(41)	41.52(13)	128.05(40)
α_{DMC} [E]	36.430(80)	73.08(43)	42.75(27)	133.1(28)
α_{DMC} [μ]	36.77(11)	73.78(35)	42.38(26)	132.62(59)
α_{ref}	36.0	71.70(20)	42.28360(50)	-
$\langle r_{ee} \rangle_{\text{VMC}}$	-	5.92592(81)	3.51261(30)	5.53093(20)
$\langle r_{ee} \rangle_{\text{DMC}}$	-	5.9928(40)	3.5490(23)	5.5490(17)
$\langle r_{ee} \rangle_{\text{ref}}$	-	6.03321	3.574788	-
$\langle r_{pp} \rangle_{\text{VMC}}$	-	5.92626(84)	-	6.94941(44)
$\langle r_{pp} \rangle_{\text{DMC}}$	-	5.9929(40)	-	6.9756(39)
$\langle r_{pp} \rangle_{\text{ref}}$	-	6.03321	-	-
$\langle r_{ep} \rangle_{\text{VMC}}$	3.00080(18)	4.43607(44)	3.45129(22)	5.11751(21)
$\langle r_{ep} \rangle_{\text{DMC}}$	3.00228(95)	4.4683(20)	3.4674(25)	5.1266(17)
$\langle r_{ep} \rangle_{\text{ref}}$	3.0	4.487155	3.480273	-
$\Gamma_{2,\text{VMC}}$	2.013(15)	4.587(63)	2.399(10)	4.507(13)
$\Gamma_{2,\text{DMC}}$	2.0092(20)	4.5221(19)	2.4675(35)	4.746(14)
$\Gamma_{2,\text{ref}}$	2.0	4.465106	2.471406	-

polarizability of the interacting dimer, despite the relatively large binding of 0.4 eV and the significant change in the average electron-positron distance (from 3.0 to 4.48 bohr), suggesting that their electric response is very similar to the one in Ps, probably compensated by the balance between the attraction and repulsion forces in Ps_2 . For PsH, the estimated value of the polarizability is close to the highly accurate value of Yan *et al.* obtained with Hylleraas functions [60], corroborating all previous calculations, in contrast to the first reported value of 123 a.u. [58]. For the recently observed PsH dimer, there is no reported polarizability. According to the present results, the polarizability (in its parallel component) is considerably larger than the sum of two non-interacting PsH ($84.6 = 2 \times 42.3$ a.u.), indicating that there is a significant redistribution of the wave function in the bound state, similar to what is observed for covalently bonded diatomic systems at equilibrium distance [194, 195, 196]. Figure 5.2 elaborates on the latter idea by plotting the parallel, α_{\parallel} and perpendicular α_{\perp} polarizabilities of PsH dimer as a function of the internuclear distance. The

α_{\parallel} displays a non-trivial behavior; at short distances, the high polarizability is attributed to the dissociated state of Ps_2 and H_2 [153], then rapidly decreases until increasing to a maximum near the equilibrium distance, followed by a slow second decrease converging to the polarizability of two non-interacting PsH. The α_{\perp} exhibits similar behavior to the α_{\parallel} , but the magnitude of the changes is significantly smaller and close to the estimated error bars. Therefore, it is almost constant compared to the sum of two PsH.

Figure 5.2 also shows the results of Li_2 for comparison purposes due to the previous similarities observed between positron-bond systems and alkali metals [71, 72, 123]. Even though the form of the curves is similar to that of the PsH dimer, there are significant differences. Firstly, the absolute and relative changes of the polarizabilities are larger compared to the two non-interacting Li atoms. Secondly, the maximum polarizability is attained at much larger distances. Lastly, at their respective equilibrium distances, the dipole polarizability for Li dimer is smaller than two Li atoms, while in PsH dimer it is larger than the one of the sum of two PsH. Therefore, considering the above, the response properties of $(\text{PsH})_2$ and Li_2 are significantly different.

In order to have a better understanding of the polarizabilities of the PsH dimer as a function of the internuclear distance, Figure 5.3 shows the positronic density differences between an unperturbed system and the perturbed system with an electric field of 0.007 (a.u.), computed at DMC level. First of all, in Figure 5.3a, it can be seen how the electric field produces an accumulation of the positronic density towards the same dimensional axis of the applied field, and the consequent reduction of the positronic density in the opposite side, with a nodal surface at the nuclei position, thus forming a dipole. Next, Figure 5.3b shows the density change induced by an electric field perpendicular to the nuclear axis in PsH dimer, displaying an equivalent density redistribution as the one observed for PsH, but for two adjacent PsH. On the other hand, Figures 5.3c and 5.3d display the effect of an electric field parallel to the nuclear axis in the positronic density of PsH dimer. At the equilibrium distance, Figure 5.3c, the electric field induces an accumulation of positronic density over one side of one nucleus facing away from the other nucleus, while the opposite effect is produced at the other hydrogen atom. Overall, this effect forms a dipole between the two hydrogen nuclei, thus depending on the internuclear distance. Although, at longer distances like 9.0 a.u., the electric field forms two collinear dipoles, one at each hydrogen nuclei, as seen in Figure 5.3d, explaining the dissociation limit of the polarizability as the sum of polarizabilities of two non-interacting fragments. An analogous behavior is observed for Li_2 (see Figure C1 in appendix) with remarkable differences close to the nuclei surroundings due to the repulsion with the core electrons [71, 123].

Since the dipole moment in Eq. 5.6 is a one-particle operator, it can be decomposed into electronic

$$\hat{\mu}^{e^-} = - \sum_i^{N^{e^-}} r_i, \quad (5.19)$$

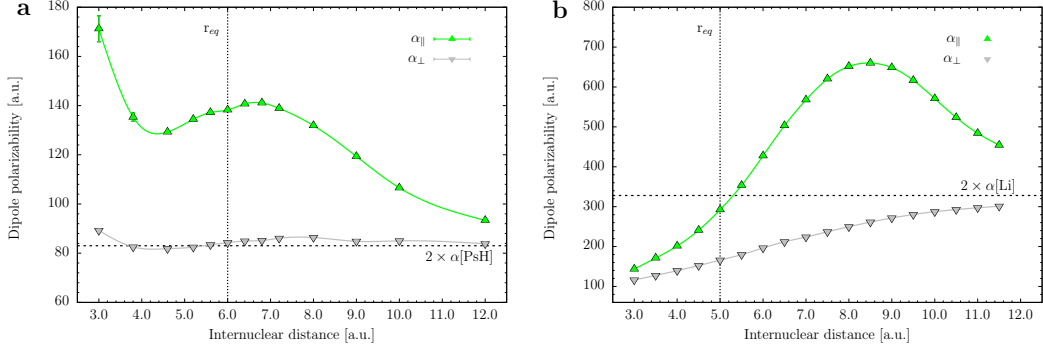


Figure 5.2: Dipole polarizability parallel (α_{\parallel}) and perpendicular component (α_{\perp}) as a function of the internuclear distance for **a:** (PsH)₂ at DMC level, and **b:** for Li₂ at CCSD(T)/aug-cc-pVQZ level. Vertical dotted lines indicate the equilibrium distance.

and positronic parts

$$\hat{\mu}^{e^+} = \sum_i^{Ne^+} r_i. \quad (5.20)$$

For neutral-charged or homonuclear diatomic systems like PsH and (PsH)₂, the net contribution from the fixed point charges is zero. Thus, the above separation allows to express the dipole probability as the first derivative of the electronic and positronic contribution to the dipole moment

$$\alpha_{aa} = \left(\frac{\partial \mu(F_a)}{\partial F_a} \right)_{F_a=0} = \left(\frac{\partial \mu^{e^-}(F_a)}{\partial F_a} \right)_{F_a=0} + \left(\frac{\partial \mu^{e^+}(F_a)}{\partial F_a} \right)_{F_a=0} = \alpha_{aa}^{e^-} + \alpha_{aa}^{e^+}. \quad (5.21)$$

Figure 5.4 displays such decomposition of the dipole moment for PsH and (PsH)₂ at DMC level as a function of the strength of the external electric field, with their corresponding calculated dipole polarizabilities obtained from a linear fitting regression. From such decomposition, it is evident that for PsH and (PsH)₂, the largest contribution to the dipole polarizability comes from the positronic wave function, while the electronic part is almost zero. These results suggest that from the point of view of their response properties, the system can be interpreted as a positronic cloud surrounding an H anion, fully screening its electronic response, since on the contrary, an isolated H anion exhibits a large polarizability of 203 a.u. [59] explained by the loosely bound electrons that can be more easily distorted.

This effect is similar to the case of regular atoms, where the main contribution to the polarizability comes from the electronic valence orbital, while the core orbitals are barely affected by an external electric field [197]. This observation contradicts the arguments of Yan [60], who proposed that a simple estimate of the polarizabilities of PsH (42.3 a.u.) as a weakly bound state between Ps and H atoms (40.5 = 36 + 4.5 a.u.), but confirms previous studies

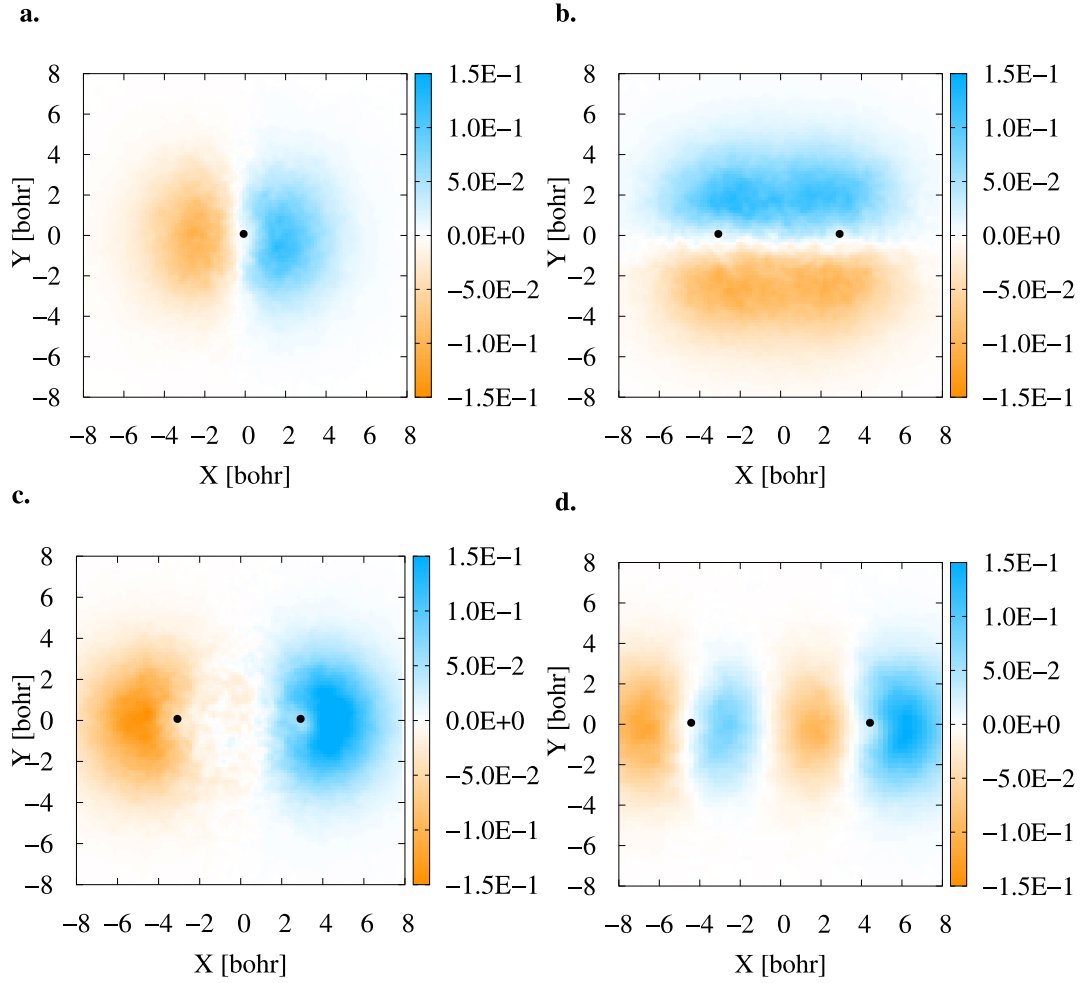


Figure 5.3: 2D cuts of the positronic density difference between unperturbed system and the perturbed system with an electric field of 0.007 (a.u.). All densities were obtained as histograms of the number of particles inside voxels (width=0.08 bohr) disposed along an internuclear axis. Panel **a**: PsH, Panel **b**: $(\text{PsH})_2$ at $R_{\text{H-H}} = 6.0$ a.u. perturbed with a field perpendicular to the internuclear axis. Panel **c** and **d**, are for $(\text{PsH})_2$ at $R_{\text{H-H}} = 6.0$ a.u. and $R_{\text{H-H}} = 9.0$ a.u. respectively, both perturbed by an electric field parallel to the internuclear axis. Black circles are used to represent the hydrogen nuclei positions.

based on the wave functions distributions, which concludes that the structure of PsH as an H anion slightly perturbed by a positron [96]. In the PsH dimer, a similar effect is observed. The main contribution to the polarizability also comes from the positronic dipole fluctuations. However, in this system, the electronic contribution is higher than the one observed in PsH by a factor of ten. This larger contribution can be explained by the electronic and positronic density analysis [153], which indicates that even if the positronic density distri-

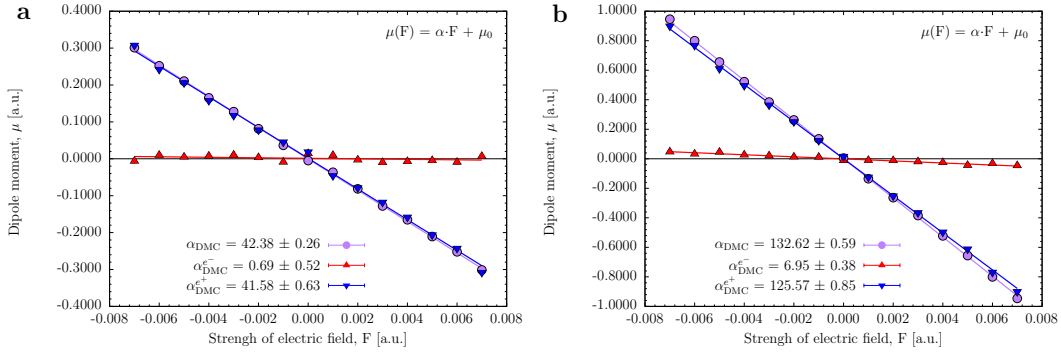


Figure 5.4: Decomposition of the dipole moment (purple) into electronic (red) and positronic (blue) displacement from the nuclei as a function of the strength of an external electric field for **a:** PsH and **b:** (PsH)₂ (parallel component) at DMC level.

bution is mainly localized in the internuclear regions, it is still capable to partially screen the hydrogen anions.

5.2.2 Interparticle expectation distances and annihilation rates

Table 5.1 also reports all expectation values of the distances and annihilation rates at zero electric field. For all the systems and distances, there is excellent agreement at VMC and DMC with respect to accurate reference values corroborating the good description of the wave function in addition to their total variational energies. Nevertheless, their response to the external electric field exhibits small fluctuations compared to the larger changes observed in the dipole moment, as seen for example in PsH dimer in Figure 5.5. In the case of the distances between same type of fermions (electron-electron and positron-positron), there is no clear trend. However, this situation is expected since an external electric field will tend to move together all particles with the same electric charge. On the contrary, for oppositely charged pairs, the electric field will force the oppositely charged particles to displace in opposite directions, producing the observed subtle increment of the electron-positron distances as a function of the strength of the field. Consequently, the decrease in annihilation rates is also attributed to the increase of the average electron-positron distances, which lowers their contact probability density (see Eq. 5.16). Nevertheless, the variations of those averages are too small compared to their estimated errors. Thus, it is not possible to draw conclusions with this methodology for those properties, and further analysis is required.

Among the possible causes, it could be attributed to an inefficient sampling of the fermionic distances averages, a serial correlation problem in the walkers moves, or constraints of the two body-cusps conditions.

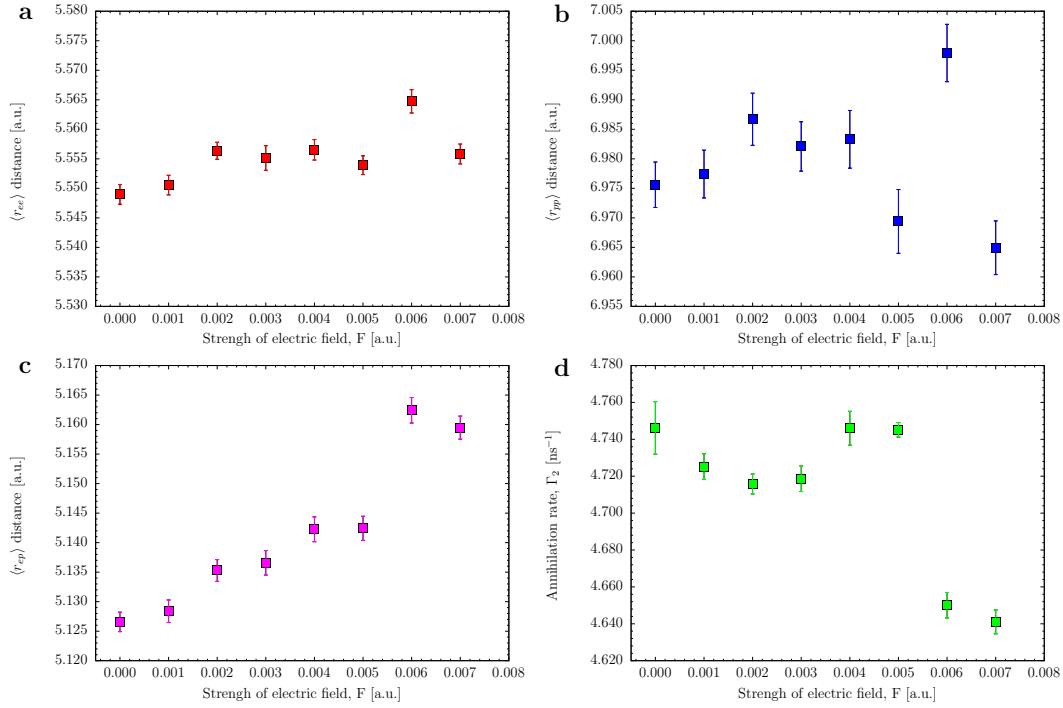


Figure 5.5: Expectation values of **a**: electron-electron distance, **b**: positron-positron, **c**: electron-positron, and **d**: two-photon annihilation rates, as functions of the strength of an external electric field for $(\text{PsH})_2$ in the parallel component at DMC level.

5.3 Summary

This chapter has presented the computation and analysis of the response properties of positronic systems, focusing in particular on the dipole polarizability, and the effect of the external electric field on the expectation values of the interparticle distances, and on the two-photon annihilation rates. A comparison with previously reported values reveals that at the QMC level, the fermionic wave function and Jastrow factors presented in Chapter 3 and 4 can provide comparable results to highly accurate and precise all particle explicitly correlated wave functions. Specifically, for the case of dipole polarizabilities, a good agreement with the reference values was obtained, either through the finite numerical evaluation of the second derivative of the energy or from the first derivative of the dipole moment under the effect of finite external electric fields. In particular, for PsH, the current methodology provides a dipole polarizability value of 42 a.u., corroborating all the estimations that followed the first result of 123 a.u. reported by Le Sech [58]. The polarizability of Ps_2 is again found to be close to twice the polarizability of Ps, suggesting that in an electric field, Ps_2 behaves like two non-interacting Ps. On the contrary, for the PsH dimer, its parallel

component of the polarizability is vastly greater than that of two PsH systems due to the formation of a bound state with a different positronic probability distribution. Thus, it is revealed by the present work a non-trivial and non-linear scale of the polarizability with respect to the number of particles and internuclear separation.

This chapter also analyzed the decomposition of the dipole polarizability in terms of independent electronic and positronic dipole fluctuations. For PsH and (PsH)₂, the main contributions come from the positronic component, which can screen the electronic response to the external potential. Therefore, from the point of view of the electric response properties, PsH and its dimer can be understood as one or two positrons surrounding one or two hydrogen anions, respectively. The expectation values of the distances and annihilation rates at zero electric fields are also in excellent agreement at VMC and DMC with respect to the reference values present in the literature. However, with the current QMC methodology, the variation of those averages is too small to provide conclusive trends, at least for the weak electric fields employed here.

Three-center Two-positron Bond

Parts of this chapter have been published in this or similar form in:

J. Charry, F. Moncada, M. Barborini, L. Pedraza-González, M. T. do N. Varella, A. Tkatchenko, A. Reyes. "The three-center two-positron bond" *Chem. Sci.* **13**, 13795, 2022.

and have been produced in collaboration with the above authors. Based on the CRediT standardised author contribution description, the author contribution corresponds to: Conceptualization, Formal Analysis, Investigation, Methodology, Resources, Software, Visualization, Writing - original draft, Writing - review & editing. The full description of each author's contribution can be found in the published paper.

In the field of positronic chemistry, most of the research focuses on the study of the positron interactions with a previously stable atom or molecule [29, 39]. Recently, the existence of a different kind of positronic molecules was theoretically predicted by Charry *et al.* [71] based on computational quantum chemical simulations at Full Configuration Interaction (FCI) level. The authors found that two otherwise repelling hydride anions can be bound by a positron, and the analysis of the positronic orbital suggested the formation of a positronic bond. Subsequent computational studies pointed out that similar bonds should also exist in positronic dihalides [123].

The positronic dihydride system, denoted as $e^+[\text{H}_2^{2-}]$, has attracted considerable attention. Goli and Shahbazian [122] addressed the nature of the interaction employing Multi-Component Quantum Theory of Atoms in Molecules (MC-QTAIM). The authors concluded that the accumulation of positron density between the two nuclei would underlie the bonding process, acting as "a positronic glue" that converts the repulsive H_2^{2-} system into a stable one, and no electronic covalent bond is conceivable in between. The energy stability of positron-bonded dihydrides was further confirmed by QMC calculations performed by Ito *et al.* [124], Bressanini [73] and Charry *et al.* [72]. Bressanini also concluded that the

bonding is not limited to one positron and in later works [153] he showed that two singlet-coupled positrons can form a bond between two hydride anions, thus giving rise to the $2e^+[\text{H}_2^-]$ molecule, or simply $(\text{PsH})_2$. The equilibrium internuclear distance was reduced from 6.4 bohr to 6.0 bohr as the number of positrons was increased from 1 to 2. Unexpectedly, the bond length shortening was accompanied by a reduction in the Bond Energy (BE), from $23.5 mE_h$ to $10.4 mE_h$.

These fascinating theoretical results raise questions on how complex positron-bonded compounds can become, or on how far the analogy between electronic and positronic bonds can be stretched. Bressanini has conjectured that a system analogous to H_3^+ with three protons, six electrons, and two positrons, could be stable [74, 153]. In this direction, the present study further explores positronic bonding mechanisms beyond the previously studied two-center to three-center systems. More specifically, to study the stabilisation of three repelling hydride anions by the addition of two positrons. Based on the QMC simulations performed in this chapter, it is conjectured the existence of an energetically stable system denoted as $2e^+[\text{H}_3^{3-}]$. Such hypothetical Three-center Two-positron (3c2p) bond is further compared against the analogous Three-center Two-electron (3c2e) bond, which is a well-established bonding mechanism found in purely electronic molecules [198, 199, 200, 201].

The H_3^+ molecule is probably the best known example of 3c2e bonds [201], in view of its astrochemical relevance [202, 203, 204]. While the trihydrogen cation could be rated the closest analogue of $2e^+[\text{H}_3^{3-}]$ at first glance, previous studies have consistently shown that the properties of electronic and positronic bonds are closest when the systems have isoelectronic ion cores [71, 123]. Therefore, this chapter also considers Li_3^+ as an alternative purely electronic analogue of the di-positronic tri-hydride compound for comparison of the bonding properties.

This chapter is organised as follows: In Section 6.1 the methods and numerical procedures are described. Next, the properties of the di-positronic system and the purely electronic analogues are presented and discussed in Section 6.2. Finally, the concluding remarks and perspectives for future work are outlined in Section 6.3.

6.1 Methods

This study considers electrons and positrons as quantum particles and atomic nuclei as point charges within the Born-Oppenheimer approximation described by the Hamiltonian in Eq. 2.2. Exploratory studies of the PES of the $2e^+[\text{H}_3^{3-}]$ system were performed at the MP2 level of theory. The MP2 expressions for systems composed of electrons and positrons can be found in Eq. 2.18 and more detailed described in Refs. 76, 127. The MP2 equilibrium energies and geometries were further refined with the VMC and DMC methods as described

in Sections 2.3 and 3.1.

6.1.1 Quantum Monte Carlo wave function

As previously discussed, QMC methods are stochastic techniques employed to integrate the TISE for a given trial wave function, the most common of which are VMC and DMC [85, 100, 106].

The energy functional is evaluated over a trial wave function which is written as the product of a fermionic part, such as a Slater determinant, and a bosonic component, the Jastrow factor, used to describe explicit correlation between particles. The trial wave function used in this study of electron-positron systems is written as the product

$$\Psi = \det[\mathbf{S}_{e\uparrow}] \det[\mathbf{S}_{e\downarrow}] \det[\mathbf{S}_{p\uparrow}] \det[\mathbf{S}_{p\downarrow}] e^{\mathcal{J}(\bar{\mathbf{r}}^e, \bar{\mathbf{r}}^p; \bar{\mathbf{R}})}, \quad (6.1)$$

where $\mathbf{S}_{e\uparrow}$ and $\mathbf{S}_{e\downarrow}$ are the electronic Slater matrices associated to the two spin populations, $\mathbf{S}_{p\uparrow}$ and $\mathbf{S}_{p\downarrow}$ are the corresponding matrices for the positrons, and $e^{\mathcal{J}}$ is the Jastrow factor. Several QMC studies have employed similar trial wave functions [72, 118, 119, 124, 166, 205] based on products of determinants constructed via atomic basis sets. This particular Jastrow factor was introduced in Ref. 72 and Chapter 2 of this thesis. Here it is now generalized for two-positron systems in the present work. The Jastrow factor is built as the sum

$$\begin{aligned} \mathcal{J}(\bar{\mathbf{r}}^e, \bar{\mathbf{r}}^p; \bar{\mathbf{R}}) = & \mathcal{J}_c^{en}(\bar{\mathbf{r}}^e, \bar{\mathbf{R}}) + \mathcal{J}_c^{pn}(\bar{\mathbf{r}}^p, \bar{\mathbf{R}}) + \mathcal{J}_c^{ee}(\bar{\mathbf{r}}^e) + \\ & + \mathcal{J}_c^{pp}(\bar{\mathbf{r}}^p) + \mathcal{J}_c^{ep}(\bar{\mathbf{r}}^e, \bar{\mathbf{r}}^p) + \mathcal{J}_{3/4}(\bar{\mathbf{r}}^e, \bar{\mathbf{r}}^p; \bar{\mathbf{R}}), \end{aligned} \quad (6.2)$$

of five functions describing respectively the electron-nucleus ($\mathcal{J}_c^{en}(\bar{\mathbf{r}}^e, \bar{\mathbf{R}})$), positron-nucleus ($\mathcal{J}_c^{pn}(\bar{\mathbf{r}}^p, \bar{\mathbf{R}})$), electron-electron ($\mathcal{J}_c^{ee}(\bar{\mathbf{r}}^e)$), positron-positron ($\mathcal{J}_c^{pp}(\bar{\mathbf{r}}^p)$) and electron-positron ($\mathcal{J}_c^{ep}(\bar{\mathbf{r}}^e, \bar{\mathbf{r}}^p)$) cusps, and a term that describes the dynamical correlation between the fermionic particles in the field of the nuclei ($\mathcal{J}_{3/4}(\bar{\mathbf{r}}^e, \bar{\mathbf{r}}^p; \bar{\mathbf{R}})$), which is an extension of the one defined in Ref. 120. The functions used to describe the cusp conditions are of two types. For particle pairs with the same charge the slowly decaying functions [206] are employed together with a linear combination of Gaussian Type Function (GTF)s,

$$\mathcal{J}_c^{ee}(\bar{\mathbf{r}}^e) = \sum_{i>j=1}^{N_e} \left(-\frac{\Gamma}{\beta_0^{ee}(1 + \beta_0^{ee}|\mathbf{r}_i^e - \mathbf{r}_j^e|)} + \sum_{g=1}^G \beta_g^{ee} e^{-\zeta_g^{ee}|\mathbf{r}_i^e - \mathbf{r}_j^e|^2} \right), \quad (6.3)$$

$$\mathcal{J}_c^{pp}(\bar{\mathbf{r}}^p) = \sum_{i>j=1}^{N_p} \left(-\frac{\Gamma}{\beta_0^{pp}(1 + \beta_0^{pp}|\mathbf{r}_i^p - \mathbf{r}_j^p|)} + \sum_{g=1}^G \beta_g^{pp} e^{-\zeta_g^{pp}|\mathbf{r}_i^p - \mathbf{r}_j^p|^2} \right), \quad (6.4)$$

$$\mathcal{J}_c^{pn}(\bar{\mathbf{r}}^p, \bar{\mathbf{R}}) = \sum_{i=1}^{N_p} \sum_{I=1}^{N_n} \left(-\frac{Z_I}{\beta_0^{pI}(1 + \beta_0^{pI}|\mathbf{r}_i^p - \mathbf{R}_I|)} + \sum_{g=1}^G \beta_g^{pI} e^{-\zeta_g^{pI}|\mathbf{r}_i^p - \mathbf{R}_I|^2} \right), \quad (6.5)$$

while for particles with opposite charges, the faster decaying cusp functions [207] were used along with the linear combination of GTFs,

$$\mathcal{J}_c^{en}(\bar{\mathbf{r}}^e, \bar{\mathbf{R}}) = \sum_{i=1}^{N_e} \sum_{I=1}^{N_n} \left(\frac{Z_I}{\beta_0^{eI}} e^{-\beta_0^{eI} |\mathbf{r}_i^e - \mathbf{R}_I|} + \sum_{g=1}^G \beta_g^{eI} e^{-\zeta_g^{eI} |\mathbf{r}_i^e - \mathbf{R}_I|^2} \right), \quad (6.6)$$

$$\mathcal{J}_c^{ep}(\bar{\mathbf{r}}^e, \bar{\mathbf{r}}^p) = \sum_{j=1}^{N_p} \sum_{i=1}^{N_e} \left(\frac{\Gamma}{\beta_0^{ep}} e^{-\beta_0^{ep} |\mathbf{r}_i^e - \mathbf{r}_j^p|} + \sum_{g=1}^G \beta_g^{ep} e^{-\zeta_g^{ep} |\mathbf{r}_i^e - \mathbf{r}_j^p|^2} \right). \quad (6.7)$$

Here β and ζ are sets of variational parameters, Z_I are the nuclear charges, and Γ is a constant that is equal to 1/2 and 1/4 respectively for distinguishable and indistinguishable particles to correctly describe the cusp conditions. In this investigation, the number of GTFs used in the cusps expansions is $G = 5$. To reduce the variance in the wave function, the variational parameters for distinguishable or indistinguishable electronic and positronic pairs are optimized separately, also reducing the eventual spin contamination.[133]

Finally, the dynamical Jastrow factor [72, 120] is written as a linear combination of products of non-normalized atomic orbitals χ_q , which corresponds to the atomic dynamical Jastrow defined in Eq. 3.19 of Chapter 3

$$\begin{aligned} \mathcal{J}_{3/4}(\bar{\mathbf{r}}^e, \bar{\mathbf{r}}^p; \bar{\mathbf{R}}) = & \sum_{j>i=1}^{N_e} \sum_{q,p=1}^Q \gamma_{qp} \chi_q(\mathbf{r}_i^e) \chi_p(\mathbf{r}_j^e) + \\ & + \sum_{j>i=1}^{N_p} \sum_{q,p=1}^Q \mu_{qp} \chi_q(\mathbf{r}_i^p) \chi_p(\mathbf{r}_j^p) + \sum_{i=1}^{N_e} \sum_{j=1}^{N_p} \sum_{q,p=1}^Q \nu_{qp} \chi_q(\mathbf{r}_i^e) \chi_p(\mathbf{r}_j^p), \end{aligned} \quad (6.8)$$

where Q is the total length of the basis set, while γ_{qp} , μ_{qp} and ν_{qp} are coupling parameters that are fully optimized. To further avoid the spin contamination introduced by the Jastrow factor, the γ_{qp} and μ_{qp} parameters, which respectively describe correlation between electron pairs and positron pairs, are symmetric ($\gamma_{qp} = \gamma_{pq}$ and $\mu_{qp} = \mu_{pq}$). In this investigation, (3s2p1d) uncontracted GTFs were employed as the χ_q orbitals.

All the parameters of the wave functions are optimized with the Stochastic reconfiguration method [189, 190], as described in Section 2.3, using the Correlated Sampling technique [208] to stabilize the convergence if necessary. To better describe the dynamical correlation between the particles, the DMC [100] method was employed with the Fixed-Node approximation [108] from the optimized VMC trial wave function.

6.1.2 Computational details

MP2 calculations for the positronic systems were carried out with the LOWDIN software [116] using the standard aug-cc-pVTZ basis set [170] for electrons with an uncontracted set

of (6s4p3d2f) GTFs, denoted as PSX-TZ, for positrons [123]. VMC and DMC calculations were performed with the QMeCha [72, 115] QMC package, published privately on GitHub, see Section 2.4. The electronic and positronic Slater determinants for the QMC calculations of H systems were constructed from (7s3p2d) primitive GTFs contracted to [4s3p2d], with the initial values of the exponents and contraction coefficients taken from the aug-cc-pVTZ basis set [170, 209, 210, 211]. In the VMC calculations, orbital coefficients, basis set contraction coefficients, and GTF exponents were variationally optimized with the Stochastic Reconfiguration Optimization method [120], amounting to 1152 non-zero parameters for $2e^+[\text{H}_3^{3-}]$ in the singlet state, and 837 for $2e^+[\text{H}_3^{3-}]$ in the triplet state. The VMC optimized wave functions were taken as guiding functions in the fixed-node DMC calculations [108] performed with 6000 walkers divided into 5000 blocks, each 100 steps long, for a total of 3×10^9 sampled configurations. Calculations were repeated with a time step of 0.005 a.u. to verify the accuracy of the DMC results. Statistical agreement was observed between the results computed with two time steps. The DMC density plots were obtained by counting the number of particles of each weighted configuration in a three-dimensional grid. The final bonding properties such as energy minimum, equilibrium distances, and forces constants, were estimated by fitting the VMC and DMC energy values to a 4th-degree polynomial with respect to one of the internuclear distances.

6.2 Results and discussion

6.2.1 Energy stability analysis

To study the $2e^+[\text{H}_3^{3-}]$ system, it was assumed the electrons to be in a closed shell singlet state, while for the positrons both the singlet and triplet states were investigated. An initial exploratory study of the PES is performed at the MP2 level of theory according to the coordinates $R_1 = R_2 = R$ and θ described in Figure 6.1a, to preserve the symmetry of the charge distribution. The two-dimensional potential energy surfaces obtained for both the singlet and triplet positronic states in that system of coordinates (constrained to C_{2v} symmetry) are shown in Figure 6.2, together with the contours paths for configurations with R_3 constant value that are represented as dashed lines. The singlet state displays a single energy minimum with D_{3h} symmetry (see Figure 6.1b), corresponding to a triangular configuration with $\theta = 60^\circ$ and $R \approx 6$ bohr. In contrast, the triplet state has a minimum at a linear conformation with $D_{\infty h}$ symmetry (see Figure 6.1d) and $R \approx 6$ bohr. Further analysis of the PESs in Figure 6.2 reveals that both the singlet and triplet states display two regions with low energies (blue color). The first region follows a dissociation path along the R coordinate in the C_{2v} configuration, with the R_3 coordinate constrained to 6 bohr. The second region corresponds to the transition between the D_{3h} and $D_{\infty h}$ configurations

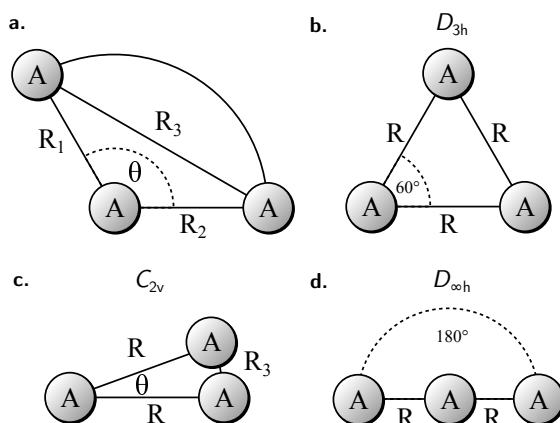


Figure 6.1: Panel **a** shows the coordinates for the molecules with three atomic centers. The other panels illustrate relevant particular cases: **b** equilateral triangle (D_{3h} symmetry), **c** isosceles triangle (C_{2v} symmetry), and **d** collinear geometry ($D_{\infty h}$ symmetry).

along the angle coordinate, for constant R . For comparison purposes, the 2D PES of Li_3^+ was also computed at MP2 level for both singlet and triplet electronic states, as shown in Figure 6.2. Qualitatively, it can be appreciated that at MP2 level, the PES of $2e^+[\text{H}_3^{3-}]$ system reassembles the same shape and features of the one obtained for Li_3^+ , further comparisons between both systems will be analyzed later in this chapter.

The optimal MP2 geometries were further refined with the VMC and DMC methods for both the singlet and triplet states. The minima were located for geometries constrained to D_{3h} and $D_{\infty h}$ symmetries. The results shown in Table 6.1 corroborate the singlet D_{3h} state as the most stable one. Therefore, from now the discussion will focus on the lowest-energy $2e^+[\text{H}_3^{3-}]$ singlet state.

Table 6.1: Equilibrium energies and distances computed with the VMC and DMC methods for the singlet and triplet states of the $2e^+[\text{H}_3^{3-}]$ system. The symmetry of the potential energy minima is also indicated.

Positronic State	Symmetry	Method	Energy [E_h]	R_{eq} [bohr]
Singlet	D_{3h}	VMC	-2.1489(1)	6.15(1)
		DMC	-2.1652(2)	6.11(1)
Triplet	$D_{\infty h}$	VMC	-2.1266(1)	6.77(2)
		DMC	-2.1401(4)	6.62(1)

Once the minimum was found, the thermodynamic stability of $2e^+[\text{H}_3^{3-}]$ is explored with

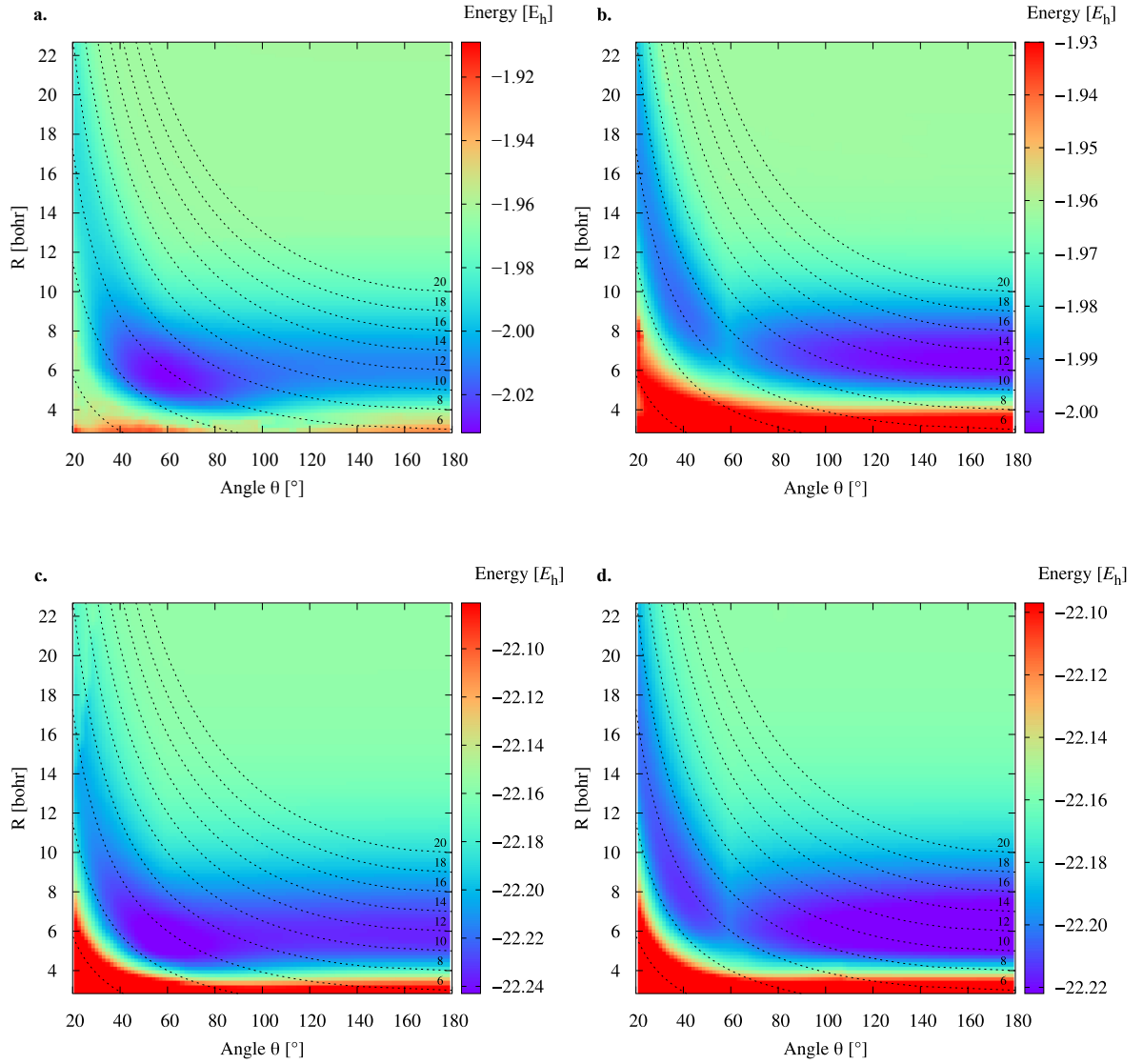
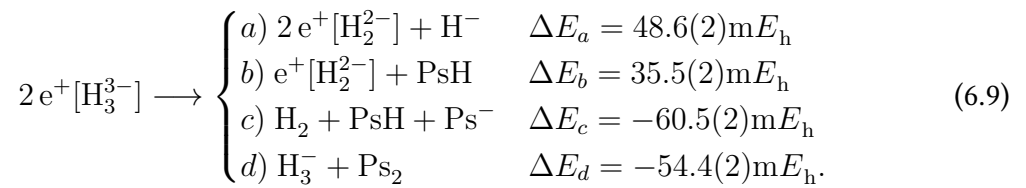


Figure 6.2: Potential energy surfaces for the singlet (a) and triplet (b) positronic states of the $2e^+[\text{H}_3^{3-}]$ system, and for the singlet (c) and triplet (d) electronic states of the Li_3^+ system. The energies were computed at the MP2 level using the aug-cc-pVTZ/PSX-TZ combination of electronic and positronic basis sets centered at the hydrogen nuclei. The dashed lines correspond to constant R_3 paths obtained for C_{2v} conformations.

respect to the lowest dissociation channels given below,



An expanded list of predicted dissociation channels into chemical meaningful species is given in the Tables D4 and D5 of the appendix. The dissociation energies of channels 6.9a-6.9d were calculated employing the DMC results of Table 6.1 and the energy data reported in Table D3. The negative ΔE of channels 6.9c and 6.9d reveal that $2e^+[\text{H}_3^{3-}]$ is thermodynamically unstable with respect to these dissociation products. It is therefore clear that the lowest energy arrangement of a set of three protons, six electrons, and two positrons consists of a sum of dissociated species rather than the bonded D_{3h} structure. Here it must be added that the fixed-node errors of the DMC calculations are negligible in the computation of the binding energies, because the nodal surfaces of the purely electronic systems and of the electron-positron ones are described at the same level of theory, leading to a cancellation of errors when computing the energy differences. Moreover, the wave function optimization of the full set of variational parameters in the presence of the correlating Jastrow factor tends to reduce the fixed-node error also in the total energies.

A similar situation was found for positron bonded dihydrides. Previous studies pointed out that I) $e^+[\text{H}_2^{2-}]$ [72, 73, 124], II) $2e^+[\text{H}_2^{2-}]$ [153], and III) $3e^+[\text{H}_2^{2-}]$ [74] are thermodynamically unstable with respect to dissociation into I') $\text{H}_2 + \text{Ps}^-$, II') $\text{H}_2 + \text{Ps}_2$, and III') $\text{H}_2 + \text{Ps}_2 + e^+$, respectively. The local range of stability for the systems I, II, and III was explored by comparing the Potential Energy Curve (PEC) for the (I, I'), (II, II'), and (III, III') pairs. The PEC pairs were found to intersect at internuclear distances considerably shorter than the equilibrium distances of the corresponding positron bonded dihydrides. Those studies further confirmed the kinetic (or local) energy stability of the dihydrides I-III, since their energy barriers, calculated at the crossing points of the potential curves, were found to be sufficiently high to support a few vibrational states.

Along similar lines, the local stability of $2e^+[\text{H}_3^{3-}]$ was further explored around the D_{3h} minimum. For this purpose, it was necessary to compute at VMC and DMC levels all the dissociated species in the four lowest-energy vertical detachment channels given by

$$2e^+[\text{H}_3^{3-}] \longrightarrow \begin{cases} a) 2e^+[\text{H}_3^{2-}] + e^- & \Delta E_a = 72.8(2)mE_h \\ b) e^+[\text{H}_3^{2-}] + \text{Ps} & \Delta E_b = 68.1(2)mE_h \\ c) e^+[\text{H}_3^-] + \text{Ps}^- & \Delta E_c = 116.8(2)mE_h \\ d) \text{H}_3^- + \text{Ps}_2 & \Delta E_d = 107.4(2)mE_h. \end{cases} \quad (6.10)$$

Here, positive ΔE values confirm the stability of $2e^+[\text{H}_3^{3-}]$ against vertical detachments.

Figure 6.3 presents PECs along the R coordinate constraining the system to preserve the D_{3h} symmetry, and along the θ coordinate imposing C_{2v} symmetry with $R = 6.1$ bohr. Panel 6.3a reveals that the energy of $2e^+[\text{H}_3^{3-}]$ along the R coordinate is always lower than those computed for the 6.10a-6.10d channels, and no curve crossings were found. In contrast, panel 6.3b reveals that the PEC of $2e^+[\text{H}_3^{3-}]$ intersects the 6.10c potential around 20° and $R_3 = 2.1$ bohr. The stabilization of the 6.10c channel as the R_3 distance decreases is

consistent with the formation of a H_2 molecule ($R = 1.40$ bohr) in the adiabatic channel 6.9c. Although the 6.9c channel energy lies below the $2e^+[\text{H}_3^{3-}]$ energy, the intersections are separated from the D_{3h} minimum by a rather high ($\approx 20 mE_h$) and broad ($\theta \approx 30^\circ$) energy barrier across the $2e^+[\text{H}_3^{3-}]$ potential. The PECs in Figures 6.3a and 6.3b therefore corroborate the local (kinetic) energy stability of the $2e^+[\text{H}_3^{3-}]$ species.

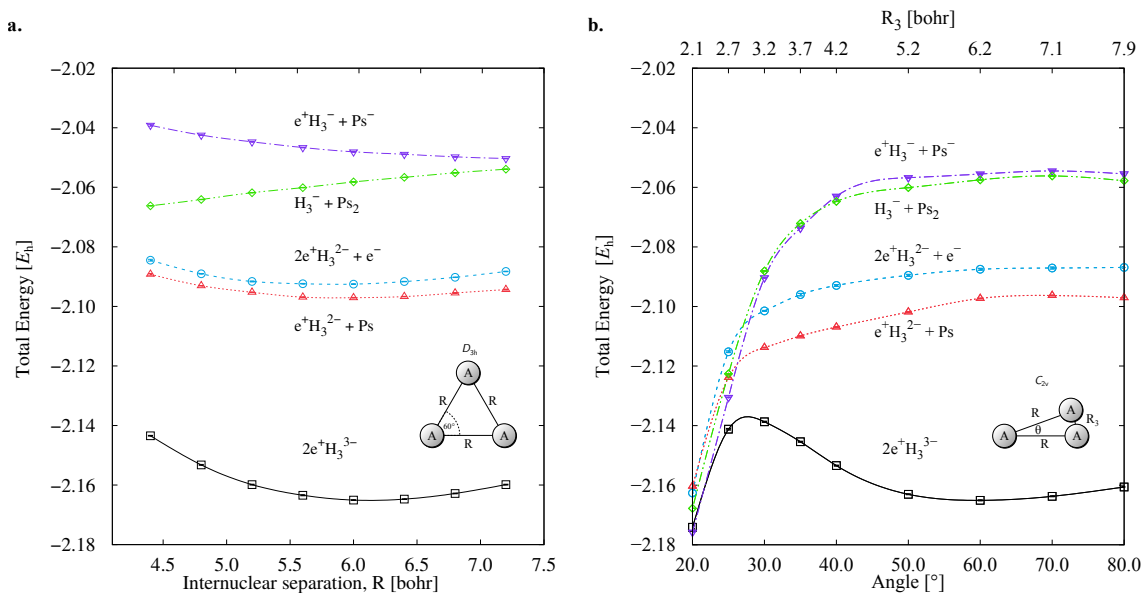


Figure 6.3: Potential energy curves for the $2e^+[\text{H}_3^{3-}]$ system and the vertical detachment channels 6.10a-6.10d. The energies were computed with the DMC method as functions of the R coordinate in the D_{3h} symmetry (a), and of the ϑ coordinate in the C_{2v} symmetry (b) fixing $R=6.1$ bohr. The lowest variation energies for Ps^- and Ps_2 were employed from references [171, 212], and the exact value for Ps is $-0.25 E_h$.

6.2.2 Comparison with analogous purely electronic systems

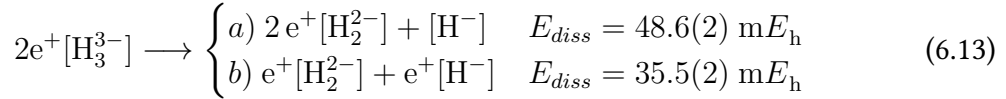
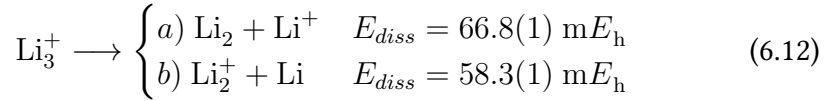
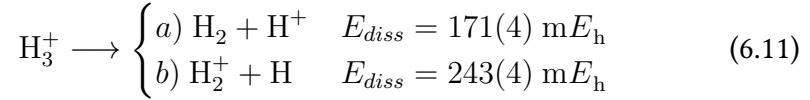
As in previous studies of positron bonded dihydrides[71] and dihalides[123], it is relevant to compare the properties of the $2e^+[\text{H}_3^{3-}]$ system with a fully electronic counterpart of two $3c2e$ bonded systems, i.e., H_3^+ and Li_3^+ . Specifically, by comparing the equilibrium distances and the force constants for the symmetric stretching (ν_1) and bending (ν_2) vibrational modes of the D_{3h} ground states, calculated with the DMC method, and shown in Table 6.2. These results indicate that the equilibrium distance of the positronic molecule ($R = 6.11$ bohr) is much closer to that of Li_3^+ ($R = 5.64$ bohr) than H_3^+ ($R = 1.63$ bohr). This observation is consistent with previous studies, which pointed out that purely electronic molecules with isoelectronic cores are the closest analogues to positron bonded systems. Although, larger discrepancies are found for the vibrational frequencies of $2e^+[\text{H}_3^{3-}]$ and Li_3^+ (roughly a factor

of 2), they are still much closer if compared to the frequencies of H_3^+ , having different orders of magnitude.

Table 6.2: Total energies (in E_h), equilibrium distance (in bohr) and force constants (in a.u.) for the symmetric stretching ν_1 mode and bending ν_2 mode of triatomic systems in D_{3h} symmetry calculated at DMC level.

System	E	R	k_{ν_1}	k_{ν_2}
H_3^+	-1.346(4)	1.63(3)	0.57(5)	0.16(2)
Li_3^+	-22.3419(1)	5.645(7)	0.0254(3)	0.0110(4)
$2e^+[H_3^{3-}]$	-2.1652(2)	6.11(1)	0.0114(4)	0.0047(7)

The longer equilibrium distances and lower vibrational frequencies also indicate a weaker 3c2p bond compared to the 3c2e analogs. In addition, it is possible to contrast the energy stability of $2e^+[H_3^{3-}]$ with equivalent dissociation species of the purely electronic Li_3^+ , and H_3^+ , in essence, by considering the dissociation channels of Li_3^+ , and H_3^+ into the following chemically meaningful products



The energies of channels 6.11 and 6.12 were calculated employing the DMC energy data reported in Table D3. It can be observed that the lowest energy dissociation channel for H_3^+ ($E_{diss} = 171.84mE_h$) involves the formation of a neutral molecule and a proton. Contrastingly, for Li_3^+ ($E_{diss} = 58.27mE_h$) and $2e^+[H_3^{3-}]$ ($E_{diss} = 35.54mE_h$), it involves the formation of a neutral atom, and an ionic single particle bonded molecule. It is worth noticing that E_{diss} of Li_3^+ and $2e^+[H_3^{3-}]$ are of the same order and differ considerably from that of H_3^+ for all dissociation channels considered here.

6.2.3 Densities

To gain further insight into the 3c2p bond formation, the positron (ρ_{e^+}) and electron (ρ_{e^-}) densities of $2e^+[H_3^{3-}]$ were computed. One-dimensional (1D) cuts of the electron densities

obtained for the unbound $[\text{H}_3^{3-}]$ trianion and the bound $2e^+[\text{H}_3^{3-}]$ compound are shown in Figure 6.4. The densities are remarkably similar, thus pointing out that the binding mechanism in $2e^+[\text{H}_3^{3-}]$ is not electronic, as previously observed for positronic bonds [71, 122]. In contrast, the positron density prominently accumulates between the H nuclei, balancing the otherwise repulsive interaction between the anions and producing a slight increase of the electronic density in that region.

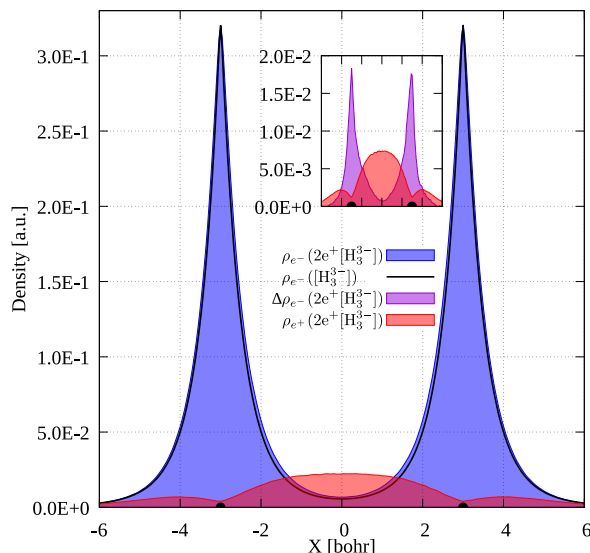


Figure 6.4: 1D cuts of the electronic density of $[\text{H}_3^{3-}]$ (black line), as well as the electronic (blue) and positronic (red) densities of $2e^+[\text{H}_3^{3-}]$. The inset panel displays the electronic density difference, $\Delta\rho_{e^-}$, between $2e^+[\text{H}_3^{3-}]$ and $[\text{H}_3^{3-}]$ (violet). The density of the unstable $[\text{H}_3^{3-}]$ system was constructed as the sum of the densities of three H^- anions at the equilibrium positions of $2e^+[\text{H}_3^{3-}]$. The densities were obtained as histograms of the number of particles inside voxels (width=0.08 bohr) disposed along an internuclear axis.

A comparison between the two-particle bonding densities in three-center systems is carried out in Figure 6.5. In H_3^+ the bonding density presented in panel a) is the total electron density, ρ_{e^-} . ρ_{e^-} in H_3^+ has maxima on top of the nuclei and accumulates around the centroid of the system, where ρ_{e^-} has a local minimum. For Li_3^+ the bonding density, $\Delta\rho_{e^-}$, displayed in panel b), was obtained as the ρ_{e^-} difference between the $[\text{Li}_3^+]$ and $[\text{Li}_3^{3+}]$ systems, both calculated at the same geometry. $\Delta\rho_{e^-}$ in Li_3^+ also displays maxima around the nuclei and accumulates around the centroid, but in this case, it has a local maximum at that point. The symmetric accumulation of electronic density in the centroid of the system is a signature of 3c2e bonding. In turn, in $2e^+[\text{H}_3^{3-}]$ the bonding density is the total positron density, ρ_{e^+} portrayed in panel c). ρ_{e^+} in $2e^+[\text{H}_3^{3-}]$ is depleted around the nuclei, as expected from the Coulomb interaction, gradually accumulates at the internuclear region and peaks at

the centroid, clearly resembling $\Delta\rho_{e^-}$ of Li_3^+ in that region. Therefore, this accumulation around the centroid of $2e^+[\text{H}_3^{3-}]$ can be viewed as the formation of a 3c2p bond.

The densities (Figure 6.5), vibrational properties (Table 6.2) and bond energies (Eqs. 6.9 and 6.12) provide strong evidence that similar three-center two-particle bonding mechanisms are present in Li_3^+ and in $2e^+[\text{H}_3^{3-}]$.

Now that it was established the local stability of $2e^+[\text{H}_3^{3-}]$, its bonding properties, and its similarities with Li_3^+ , it is worth exploring the chemistry of the latter to gain further insight into the chemical implications of the three-center two-positron bond.

Previous studies of the nature of the 3c2e bond in Li_3^+ based on topological analyses of the electronic density [213, 214] and an Interference Energy analysis [215] have concluded that Li_3^+ can be considered as the smallest metallic cluster, where the valence electrons in the centroid act as free metallic electrons. Additionally, to explain the relative stability and structure of Li_3^+ , the presence of σ -aromatic or σ -antiaromatic states is still widely discussed [213, 215, 216, 217]. Based on the reported similarities of the bonding densities of $2e^+[\text{H}_3^{3-}]$ and Li_3^+ , it can be speculated that the positrons in $2e^+[\text{H}_3^{3-}]$ could also be considered as ‘pseudo’-metallic in character and that the positronic delocalization in $2e^+[\text{H}_3^{3-}]$ could provide in the future evidence of a new type of positronic σ -aromaticity or σ -antiaromaticity. Clearly, exploring the extension of the metallic bond and aromaticity concepts to positronic molecules would require a more in-depth analysis of the bonding nature. For instance, by employing energy decomposition, quantum interference [215] or multicomponent atoms-in-molecules [122, 218, 219] analyses. However, those studies are beyond the scope of the present work.

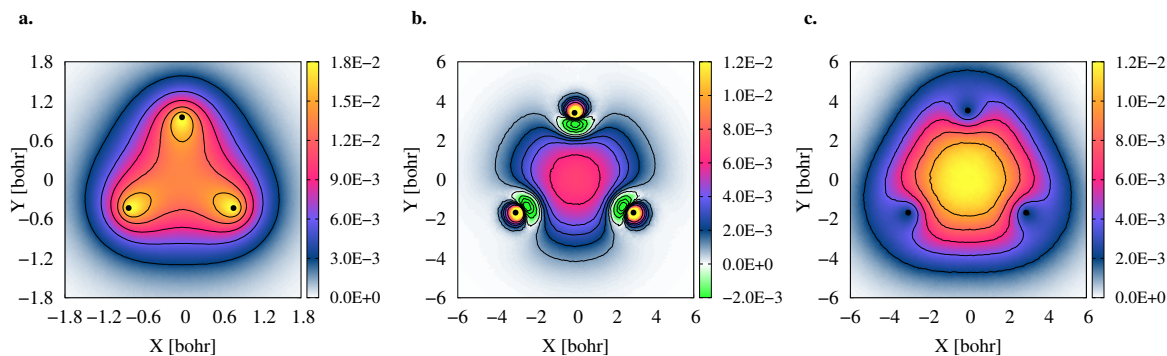


Figure 6.5: Comparison of three-center two-particle bonding densities. Electronic density of $2e^-[\text{H}_3^{3+}]$ (a), electronic bonding density of Li_3^+ (b), and positronic bonding density of $2e^+[\text{H}_3^{3-}]$ (c). The densities were obtained with the DMC method as histograms of the number of particles inside voxels (width=0.08 bohr) disposed along the molecular plane. In all panels, the atomic nuclei are represented as black dots.

Remarkably, the similarities between $2e^+[H_3^{3-}]$ and Li_3^+ are also observed for their triplet positronic and electronic states, respectively. Figure 6.6 shows the bonding densities of both species in their equilibrium minimum for the triplet state, which is characterized by a linear configuration. Again, it can be appreciated that both density distributions share similar features in the internuclear region, while being fundamentally distinct at the nuclei. However, these bonding densities indicate another type of bonding interaction, different from the 3c2p bond, which could be interesting for further investigations.

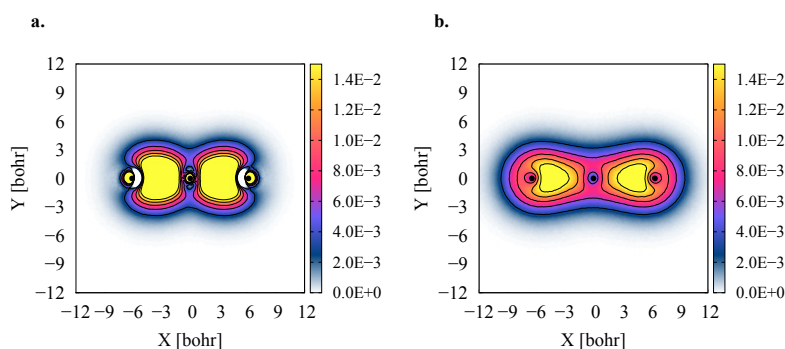


Figure 6.6: Comparison of three-center two-particle bonding densities. Electronic bonding density of Li_3^+ (a), and positronic bonding density of $2e^+[H_3^{3-}]$ (b) on triplet electronic and triple positronic states, respectively. The densities were obtained with the DMC method as histograms of the number of particles inside voxels (width=0.08 bohr) disposed along the molecular plane. In all panels, the atomic nuclei are represented as black dots.

6.3 Summary

Based on the research performed in this work, it has been found that two positrons can form a locally stable bound state with three hydride anions in a D_{3h} configuration and singlet positronic spin state. The results suggest the formation of a 3c2p bond, pointing out that the chemical bond concept reaches beyond the positron covalent bonds in two-center molecules, as addressed in previous studies. The dissociation products $H_2 + PsH + Ps^-$ correspond to the lowest-energy configuration of the system comprising two positrons, six electrons, and three hydrogen nuclei. Nevertheless, the vertical detachment and adiabatic energy dissociation analysis confirm the local stability of $2e^+[H_3^{3-}]$ around the D_{3h} equilibrium geometry. A comparative analysis reveals that the positronic molecule is similar to the trilithium cation with isoelectronic atomic cores, and remarkably different from the trihydrogen cation. Similarities were found for the equilibrium geometries, force constants in the symmetric stretch and bending modes, and also dissociation energies trends. The positronic species has slightly longer bond lengths, weaker force constants, and lower

bond energies than the trilithium cation, which can be viewed as the analog purely electronic system. In addition, the electronic (Li_3^+) and positronic ($2e^+[\text{H}_3^{3-}]$) bonding densities are similar around the internuclear region and equally spread among all three atomic centers, suggesting strong similarities between the 3c2p and 3c2e bonds.

Positron-Bonded Diatomics: Estimating the Size of Interacting Atoms

Parts of this chapter will be published in this or similar form in:

J. Charry, M. Barborini, A. Tkatchenko. "Positron-bonde diatomics: Estimating atomic size" *In preparation*.

J. Charry, D. V. Fedorov, A. Tkatchenko. "van der Waals radius for Hydrogen atom" *In preparation*.

and have been produced in a collaboration of the above authors.

Defining the size of an atom is one of the most fundamental questions in physics and chemistry. However, there is no unique answer to this question due to the quantum nature of the electrons in an atom since its boundary is not physically defined. Despite the ambiguity in the concept of size of an atom, numerous empirical definitions have been proposed for establishing a consistent size for all atoms in the periodic table [220, 221, 222, 223, 224, 225, 226]. The most common examples are the covalent radii, determined from the equilibrium internuclear distance between two atoms covalently bonded in molecules and crystals; van der Waals (vdW) radii, defined in terms of the distance of closest approach of non-covalently bonded atoms; ionic radii, determined from inter-ionic distances in crystals; metallic radii, obtained from the internuclear distances in a metal. However, determining such atomic radii presents many difficulties since most of them are inferred from a system of many interacting atoms, rather than as isolated entities. Therefore, the presence of any other atom will modify the electron density cloud associated with an atomic nucleus in different manners: shape, size, and direction. Despite this, the key aspect of defining an atomic size

relies on establishing a consistent and relative size definition for all atoms that can satisfy the group and periodic trends of the periodic table for selected types of interactions, such as the ones observed in molecules or crystals. Following these ideas, the aforementioned atomic size concepts have been employed in chemistry for a century to provide qualitative and quantitative descriptions and predictions for many phenomena and properties.

This chapter presents a tentative alternative to estimate the size of an interacting atom based on a positronically bonded diatomic molecule, similar to the three-positron bond system studied in Chapter 6, where the positrons were identified to be responsible for the bonding rather than electrons.

7.1 Methods

MP2 calculations for the positronic diatomic systems were carried out with the LOWDIN software [116], as described in Section 2.2. The standard def2-TZVPPD basis set was employed for electrons [227] centered at each nuclei, while an uncontracted set of (6s4p3d2f) GTFs for positrons [123] in three different centers: two at each nucleus, and one additional in the midpoint. The basis set choice follows the one used in the previous work for positron-bonded dihalides [123]. In the reported MP2 calculations, all electrons were taken into account, as well as all virtual orbitals from the basis set employed.

7.2 Positron-bond systems

One common feature in all studied positron-bonded systems [71, 123] is the small change in the electronic density distribution of the repulsive anionic atoms by the addition of the positron, as observed in the hydrides $e^+[\text{H}^- \text{H}^-]$ and halides $e^+[\text{X}^- \text{Y}^-]$ ($\text{X}^-, \text{Y}^- = \text{F}^-, \text{Cl}^-, \text{Br}^-$). Further analysis based on Quantum Theory of Atoms In Molecules (QTAIM) elucidated that the electron exchange phenomenon is virtually non-existent between the two atoms, and no electronic covalent bond is conceivable in between [122]. Given that, it is worth exploring a possible atomic size definition based on the interatomic distance of those positron systems, which will be driven by the positronic bonds and not regular electronic bonds as in the case of covalent, van der Waals or anionic radii.

First of all, Table 7.1 shows different atomic radii for the atoms previously found to form a positron-bonded [71, 123, 228]. Here, it is important to notice the difference between crystallographic radii and effective or equilibrium radii. The former is usually derived from the closest approach of atoms in crystal structures, while the latter is more suitable to describe equilibrium distances between atoms in molecular systems.

Table 7.1: Comparison of different atomic radii (in Angstroms) for selected elements, where (*crys.*) stands for crystallographic values

Atom	R_{vdW} (<i>crys.</i>) ^a	R_{vdW} (equilibrium) ^a	$R_{anionic}$ (<i>crys.</i>) ^b	$R_{anionic}$ (effective) ^b	$R_{covalent}$ (<i>crys.</i>) ^c
H	1.1	1.66 ^d	-	1.40	0.31
Li	2.2	2.63	-	-	1.28
F	1.5	1.65	1.19	1.33	0.57
Cl	1.8	2.05	1.81	1.81	1.02
Br	1.9	2.1	1.82	1.96	1.20

a Recommended value from [224]

b Recommended value from [222]

c Recommended value from [226]

d Recommended value from [229]

For this work, the previously known positron-bond diatomics were recomputed at MP2 level, in order to have a consistent value of the equilibrium distance. All the PECs are available in Figure E1 of the appendix. Table 7.2 collects and compares all equilibrium MP2 distances with respect to previously reported values in literature. For $e^- [\text{H}^- \text{H}^-]$, a good agreement is observed between MP2 and FCI data, with a slight difference of just 0.1 Å compared to DMC. For $e^- [\text{Li}^- \text{Li}^-]$, there is also a good agreement against CISD. Although, Ito *et al.* [228] observed at DMC level the appearance of a global energy minimum at closer distances, featuring a bound state described as a delocalized Ps orbiting a Li_2^- , distinct from the $e^- [\text{X}^- \text{Y}^-]$ bond. Thus, that minimum structure will not be considered for this work. Furthermore, for the positron bond halides $e^- [\text{X}^- \text{Y}^-]$, MP2 results exhibit a constant shift of 0.3 Å due to the lack of electron-positron correlation effects compared to the more accurate renormalized third-order propagator theory correction (RENPP3) [78, 127].

The data of Table 7.2 is further expanded by calculating the MP2 equilibrium distance of all the remaining combinations of anions not considered in previous works; namely, between $\text{H}^- \text{Li}^-$, $\text{H}^- \text{F}^-$, $\text{H}^- \text{Cl}^-$, $\text{H}^- \text{Br}^-$, $\text{Li}^- \text{F}^-$, $\text{Li}^- \text{Cl}^-$, $\text{Li}^- \text{Br}^-$.

Therefore, and based on the information compiled for atomic radii, Table 7.3 compares the newly calculated MP2 equilibrium distances of positron bond systems of the form $e^+ [\text{A}^- \text{B}^-]$ with the sum of atomic radii for each constituent atom. From that data, it is evident that the equilibrium distance is much longer than the sum of electronic covalent radii, confirming once more that there is no electronic covalent bond formation [122]. In order to simplify the comparison, the two closest radii values are compared in Figure 7.1, which is split into two categories for a clear visual comparison: equilibrium van der Waals radii and effective

Table 7.2: Comparison of equilibrium distances of positron-bond diatomics obtained with several methods. All values in Angstroms. The last column indicates the difference between MP2 results and the most accurate data from the literature.

System AB	MP2 ^a	CI	CC-PT ^d	DMC	ΔR_{eq}
H-H	3.27	3.26 ^b	-	3.38(2) ^e	0.11(2)
Li-Li	5.57	5.51 ^c	-	3.06 ^c	-0.058
F-F	3.42	-	3.088	-	-0.330
F-Cl	3.82	-	3.545	-	-0.280
F-Br	3.96	-	3.709	-	-0.253
Cl-Cl	4.15	-	3.869	-	-0.282
Cl-Br	4.30	-	4.019	-	-0.281
Br-Br	4.43	-	4.149	-	-0.281

^a This work

^b FCI [71]

^c CISD and DMC [228]

^d Electronic CCSD(T)/CBS + RENPP3 [123]

^e DMC [73]

anionic radii.

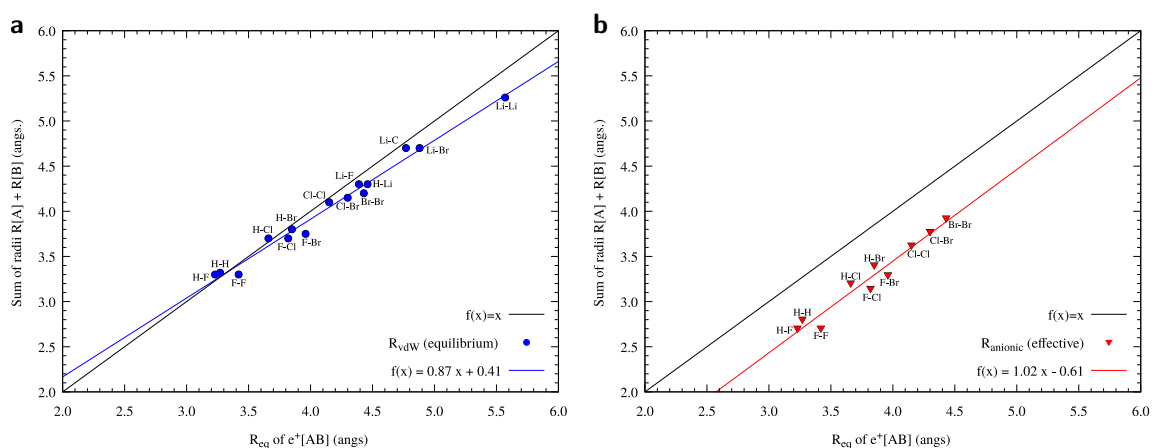


Figure 7.1: Sum of atomic radii versus equilibrium distance of positron-bonded diatomic system of the form $e^+[A^-B^-]$. Panel **a** for equilibrium van der Waals radii and panel **b** for effective anionic radii.

The equilibrium positron bond distance seems to follow the same trends of crystallographic vdW radii for halides slightly shifted towards higher distances, but there is a large discrepancy for hydrogen. On the other hand, the sum of anionic crystallographic radii does not

Table 7.3: Comparison between the equilibrium distance of positron bond diatomic system and the sum of radii of their constituent atoms. All distances in Angstrom units.

System AB	R_{eq} $e^+[A^-B^-]$	R_{vdW} (crys.)	R_{vdW} (equilibrium)	$R_{anionic}$ (crys.)	$R_{anionic}$ (effective)	R_{cov} (crys.)
H-H	3.27	2.2	3.32	-	2.80	0.62
H-Li	4.46	3.3	4.29	-	-	1.59
H-F	3.23	2.6	3.31	-	2.73	0.88
H-Cl	3.66	2.9	3.71	-	3.21	1.33
H-Br	3.85	3.0	3.8	-	3.36	1.51
Li-Li	5.57	4.4	5.26	-	-	2.56
Li-F	4.39	3.7	4.28	-	-	1.85
Li-Cl	4.77	4.0	4.68	-	-	2.30
Li-Br	4.88	4.1	4.7	-	-	2.48
F-F	3.42	3.0	3.30	2.38	2.66	1.14
F-Cl	3.82	3.3	3.70	3.00	3.14	1.59
F-Br	3.96	3.4	3.8	3.01	3.29	1.77
Cl-Cl	4.15	3.6	4.10	3.62	3.62	2.04
Cl-Br	4.30	3.7	4.2	3.63	3.77	2.22
Br-Br	4.43	3.8	4.2	3.64	3.92	2.40

follow a clear linear trend, mainly given by the slight difference between Cl^- and Br^- radii. Additionally, Shannon [222] pointed out the wide variations in the observed radius of H^- , attributed to its large polarizability and for changes in interatomic distances due to covalence effects of Hydrides, therefore the author did not consider useful to report a unique anionic radius for H^- . On the contrary, a better correlation is observed when comparing against effective anion radii (Figure 7.1) following the same trends of the equilibrium distance but shifted by a constant value of 0.6 Å. This shift in the distances could be reduced by including more attractive electron-positron correlation effects, missing in MP2, and by extrapolation to the complete basis set limit [71, 127]. The effective radii were empirically proposed to closely reproduce interatomic distances in solids based on the assumption of a fixed value for oxygen and fluorine in metal-oxygen and metal-fluorine bonds. Furthermore, a closer resemblance is obtained with the sum of equilibrium vdW radii, with further deviations for larger radii, which can be explained by the difficulty of capturing long-range electron-positron correlation effects at MP2 level using single-particle orbitals. Unfortunately, such deviations cannot be observed for the anionic radii, since there are no estimated values for lithium atom, which is the one with larger radius.

The similarity between vdW radii of neutral atoms and their anionic radii was initially observed by Pauling [220]. He considered that a covalently bonded closed-shell atom behaves

similarly to its anionic atom, therefore for nonmetallic elements, their vdW radii were approximated to their anionic radii counterpart. The case of positron-bond systems seems to share similar features with those observed for regular electronic systems, employed to define either an anionic or vdW radii. For the former, the anionic radii are derived from interatomic distance in ionic bonds. Hence, it depends on the attractive interaction between a cation and anion, but in this case, the cation is replaced by the positron. For the vdW radius, the radii are established in terms of the distance at which the Pauli repulsion balances the attraction forces between the non-covalently bonded closed-shell atoms [230], while in the positronic bonded case would correspond to the distance at which the electrostatic repulsive force of the non-covalently closed-shell atoms balances the attractive electrostatic force introduced by the positronic density distribution spread between the anions. In both cases, the positron is acting as the attractive force between two otherwise repulsive closed-shell anions, until reaching the inter-penetrability limit of the electronic atoms.

The main advantage of defining an atomic radius with positron-bonded systems lies in the fact that the anionic atoms are isolated and there are not covalently bonded. Thus they are not affected by a chemical environment, as opposed to previous definitions on other atomic radii [222, 224, 226].

The numerical evidence of Figure 7.1 supports this hypothesis, although further studies are required for constructing a new interacting atomic size definition. In essence, one needs to i) Calculate the equilibrium distance with a highly accurate method such as QMC; ii) corroborate that the type of interactions is consistent for all systems, either fully positronic, fully electronic, or a mixture; iii) expand the study to more anionic atoms, either isolated or in a molecule, so far the atom studied here share a common feature, all of them are closed shell atoms, they have positive electron affinities, thus the anion is stable, and are capable of forming positronium atom [72]; iv) explore the equilibrium distances of two positron-bonded system, in singlet and triplet positronic spin state.

Summary and Outlook

In the last decades, experimental and theoretical evidence has accumulated for the formation of metastable states between atoms and molecules with positrons, raising interest in understanding their binding mechanisms, examining new compounds with unique molecular properties, and studying their physical and chemical processes. Yet, the field of positron-matter interactions is still vastly unexplored.

The description of metastable positron-matter states represents a difficult challenge for quantum-chemical methods due to the need to describe the strong attractive correlation effects between the electronic cloud and the positrons. In this direction, QMC methods are a powerful tool since they can easily incorporate sophisticated wave functions with the ability to explicitly include the correlation effects between particles. Naturally, even in QMC, it is necessary to find a balance between simplicity and accuracy of wave functions in order to be applicable to compute large molecular systems without introducing prohibitive computational costs.

This thesis contributes to the theoretical development and computational implementation of correlated electron-positron wave function ansatzes. The main challenge for quantum chemistry methods lies essentially in the employment of single-particle atom-centered basis sets to describe the positronic orbitals. Since the positron does not form bound states with the nuclei, the natural basis should be based on an expansion of electron-positron orbitals, which explicitly capture the correlation between electron-positron pairs. The wave function ansatz proposed in Chapter 3 has been shown to be efficient in reaching a quantitative description of the binding properties for positronic atoms and molecules with rather small basis sets and lower computational effort with respect to the converged limits of traditional quantum-chemistry approaches. It was demonstrated that electron-positron orbitals deliver a suitable and efficient ansatz, which provides the lowest reported variational energies for PsB, PsC, PsO, and PsF, at VMC and DMC level. Moreover, the presented wave function is general enough to be applied to larger molecular compounds, taking advantage

of the scalability of the QMC methods.

Furthermore, the dynamical Jastrow framework presented in Chapter 4 in conjunction with the relaxed fermionic part and the one- and two-body Jastrow factor, stands as a simple and efficient scheme to construct an improved VMC guiding wave function for DMC calculations, reducing the number of configurations needed for a desired variance. The proposed improved version of the Jastrow factor demonstrates the importance of including three- and four-body correlations between pairs of positive charges (positrons, nuclei) and pairs of negative charges (electrons), which can be described by introducing a set of products of atomic and positronic orbitals.

For these reasons, the Jastrow factor presented in Chapter 4 in conjunction with a correlated fermionic wave function, like an electron-positron geminal of Chapter 3, can be applied to study the positron-matter interactions on larger and more complex polar and non-polar molecules.

The proposed methodologies were implemented in the QMeCha computational package [115] (see Section 2.4). Even if the aforementioned developments are focused on studying positronic systems, the methodology is general enough to be applied to studying other positively charged quantum particles, such as positive muons or quantum nuclei. The latter is particularly crucial in the case of Hydrogen atoms to study nuclear quantum effects (NQEs) in many phenomena, such as proton transfer reactions, zero-point vibrations, tunneling, resonance, isotope effects [76]

Once the methodology was established to accurately compute positronic-matter systems, as described in Chapters 3 and 4, the following chapters focused on examining the physical and chemical properties of selected systems. Chapter 5 showed how QMC and the wave functions developed in this work can be used for positronic systems to compute other properties such as expectation values of interparticle distances, two-photon annihilation rates, and dipole polarizabilities, in addition to showing the physical insights that can be inferred from analyzing those properties. Good agreement was obtained in comparison to highly accurate and precise reference data, despite the numerical challenges of estimating polarizabilities through finite difference derivatives of averaged quantities with a statistical error introduced by the stochastic nature of QMC techniques.

Therefore, the current methodology can be employed to explore dipole polarizability of other molecules, which is a valuable physical quantity that is related to the ability of a system to respond to an external potential, and related to dispersion forces, all essential concepts to the understanding of intermolecular interactions with regular electronic or positronic systems. Although here it should be remarked that intramolecular positronic interactions are just being discovered, for example, for many decades the dimer of PsH was assumed to be formed through van der Waals interactions [59], but the possibility to form a bound state electrostatically stabilized by a large redistribution of the positronic cloud

has been just recently discovered [71, 153]. Chapter 5 also introduced a dipole polarizability decomposition in terms of independent electronic and positronic dipole fluctuations. For PsH and (PsH)₂, it was revealed that the main contributions come from the positronic component. Therefore, from the perspective of response functions, PsH and (PsH)₂ can be understood as a highly polarizable positronic cloud in the nuclei's outer regions, screening the electrons' response to the external potential. Such simple decomposition can be computed for other positronic systems to better understand their electronic and positronic structure. In addition, the polarizability of PsH dimer exhibits a non-trivial and non-linear scaling with respect to the interatomic length, a similar quantum effect observed in regular electronically bonded diatomic.

Chapter 6 described one of the first applications of the electron-positron wave function ansatz presented in this thesis under QMC methodology discussed before. The present results revealed that two positrons are capable of bonding three otherwise repelling atomic anions, forming a three-center positronic bond, extending the findings of previous theoretical studies that have evidenced the formation of locally stable systems composed of two repelling atomic anions and one-to-three positrons. On such systems, the antiparticles are mainly responsible for the conformers' stabilization, thus expanding the definition of chemical bonding beyond the ordinary purely electronic systems [71, 72, 73, 74, 122, 124, 153]. Positron-bonded systems are fundamentally distinct from those formed by positron attachment to previously stable atoms and molecules. Therefore, these results will hopefully stimulate further theoretical and experimental research on novel physical and chemical processes involving this kind of bond. The two-positron three-center bond was found to be remarkably similar to the two-electron three-center bond observed in Li₃⁺. This comparison encourages to further explore the chemistry of lithium, and alkali metals, in order to find more exciting positronic counterparts. Additionally, such similarities could also give further hints on the nature of electronic bonds, benefiting the understanding of both positronic and electronic bonds.

The investigations performed for the positron-bonded systems led to an appealing observation: half the equilibrium distance of positron-bonded dimers is approximately the sum of their isolated atomic radii. Therefore, positronically bonded system could serve as an alternative to estimate the size of interacting atoms, numerically similar to the anionic or van der Waals radii, and sharing features with both definitions. However, further studies are required to construct a new atomic size definition consistent for several atoms, based on accurate equilibrium distances for a larger number of positron-bond systems and a deeper understanding of the type of interactions, either electronic or positronic, or both of them.

As concluding remarks, the main developments and findings discussed in this thesis for the study of positron interactions with atoms, molecules, and electric fields, are the following:

- A new efficient fermionic VMC wave function ansatz based on explicitly correlated

electron-positron orbitals.

- An improved Jastrow factor that accounts for three- and four-body electron-positron correlation effects in the field of the nuclei.
- Benchmarking total variational and binding energies for selected positronic atoms and molecules at VMC and DMC level.
- Elucidating the electron-positron wave function structure by computing the dipole polarizability decomposed as electronic and positronic contributions, revealing non-trivial scaling with respect to the size of the system, and positronic screening effects to an external field.
- The stability of three hydrogen anions by two positrons, forming a three-center two-positron bond in analogy to three-center two-electron bonds.
- The equilibrium distance of positron-bonded diatomic systems is connected to the sum of van der Waals radii of the corresponding neutral atoms, and to their anionic radii, which serves as an alternative approach to defining atomic sizes.

The developments and findings reported in this thesis can serve as valuable tools for boosting the investigation of positron-matter interactions on a wider variety of systems and phenomena, encouraging further experimental and theoretical studies. There are many possible directions for the latter. For example, the methodology developed here can be a powerful tool to predict new molecular systems that could bind a positron, and to explain a large amount of experimental data that remains unexplained; namely, alkanes, alkenes, aromatic compounds, halogenated hydrocarbons, alcohols, or acetates [29]. In addition, the developed methodology can be used to further understand the relationship between positron binding and molecular properties such as dipole moment, polarizability, and aromaticity, among others [29], helping to develop simple yet efficient physical models. Also, this approach would aid in finding the molecular region that is more energetically favorable for the positron binding to occur, as well as the fragmentation products upon the annihilation, in order to establish if a positron can be used as “molecular scissors” with a unique fragmentation pattern, therefore as an alternative ionization tool in mass spectrometry [231].

Another challenge that can be handled with the proposed methodology is the possibility of efficiently exploring complex PES of positronic complexes, allowing to study the coupling of the positron binding with the vibrational motion of a molecule, a crucial step to elucidate the resonant annihilation mechanism, which is the main phenomena exploited in the Vibrational Feshbach Resonance (VFR) technique to obtain positron binding energies experimentally. In addition, accurate PES are required to describe the effect of a positron on complex chemical processes, such as chemical reactions [69] and molecular dynamics simulations [70], fields that are still highly unexplored due to the lack of accurate and efficient computational methodologies.

On the other hand, due to the high accuracy delivered by QMC techniques, the variational ansatz proposed in this work can be employed to generate accurate benchmark data for total or binding energies of positronic compounds, serving as reference values to develop and parametrize efficient model potentials. For example, Gribakin and coworkers [50] proposed to include a model-potential between a positron and a molecule expressed with a simple asymptotic form $\frac{\alpha_A}{r^6}$, where α_A is the polarizability of an atom A within a molecule at a distance r_A from the positron, very similar to a van der Waals interaction in regular electronic systems [232]. Within a DFT scheme, electron-positron correlation functionals have not yet been widely explored [89, 102, 103, 233]. Therefore, this kind of correlation functionals can be derived in an analytical form by studying the physical behavior of positrons with the aid of highly accurate methods, like QMC.

All the aforementioned aspects and the developments reported in this thesis could potentially lead to the discovery of breakthrough applications based on matter-antimatter interactions, a fascinating emerging field in chemical physics.

Appendix A: Correlated Electron-Positron Wave Functions

Part of the results presented in the following section have been reproduced from the Supporting Material of Reference [91]

Table A1: Non-relativistic total energies of the atoms obtained with Single determinant (SD) and multi determinantal (MD) wave functions. In parenthesis, the electronic state of the system. All energies are reported in Hartree.

	Li(² S)	Be(¹ S)	B(² P)	C(³ P)	O(³ P)	F(² P)
VMC SD[136]	-7.47683(3)	-14.6311(1)	-24.6056(2)	-37.8147(1)	-75.0233(3)	-99.6874(3)
VMC SD[137]	-7.47693(3)	-14.64622(1)	-24.62361(9)	-37.8083(1)	-75.0229(2)	-99.6877(3)
VMC MD[137]		-14.66480(3)	-24.64432(8)	-37.82972(8)		
VMC MD[136]	-7.47752(3)	-14.66630(4)	-24.65055(6)	-37.8383(1)	-75.0429(2)	-99.7054(3)
VMC AGP ^a	-7.477478(26)	-14.66624(11)	-24.64287(19)	-37.82430(27)	-75.02917(48)	-99.69212(24)
VMC SD ^a			-24.62860(10)			
DMC SD[136]	-7.478 02(1)	-14.65717(7)	-24.63978(5)	-37.8295(1)	-75.0516(5)	-99.7167(8)
DMC MD[136]	-7.478 00(1)	-14.66729(1)	-24.65325(5)	-37.84317(7)	-75.0578(3)	-99.7237(3)
DMC AGP ^a	-7.47805252(60)	-14.667315(90)	-24.65034(19)	-37.83713(22)	-75.0529960(65)	-99.719018(95)
DMC SD ^a			-24.64062(24)			
HF[234]	-7.432726931	-14.57302317	-24.52906073	-37.68861896	-74.80939847	-99.40934939
Exact[138]	-7.47806	-14.66736	-24.65391	-37.8450	-75.0673	-99.7338

^aThis work.

Table A2: Non-relativistic total energies of the atomic ions. All energies are reported in Hartree.

	H ⁻ (¹ S)	Li ⁻ (¹ S)	B ⁻ (³ S)	C ⁻ (⁴ S)	O ⁻ (² P)	F ⁻ (¹ S)	Li ⁺ (¹ S)	Be ⁺ (² S)
VMC SD[140]		-7.49145(6)	-24.63235(6)	-37.85566(8)	-75.0707(1)	-99.8121(2)	-7.279880(10)	-14.32241(18)
VMC MD[140]		-7.49909(2)	-24.6435(3)	-37.8657(1)				
VMC AGP ^b	-0.5275729(51)	-7.49916(36)	-24.644739(85)	-37.86381(11)	-75.08019(18)	-99.81738(22)	-7.279624(27)	-14.324014(35)
VMC SD ^b			-24.63863(12)					
DMC SD[140]		-7.498 58(5)	-24.65230(5)	-37.8788(1)	-75.1027(2)	-99.8434(2)	-7.2799100(50)	-14.3246360(40)
DMC MD[140]		-7.50077(4)	-24.6574(1)	-37.88351(4)				
DMC AGP ^b	-0.527741(23)	-7.50072(19)	-24.65734(26)	-37.88037(40)	-75.10639(19)	-99.84561(66)	-7.279905(32)	-14.324723(31)
DMC SD ^b			-24.65317(19)					
HF[234]		-7.42823206	-24.5192214	-37.7088436	-74.7897459	-99.4594539	-7.23641520	-14.2773948
Exact[138]	-0.527751 ^a	-7.50077	-24.6642	-37.8910	-75.1210	-99.8588	-7.27992	-14.32476

^aSVM calculation from Ref. 83. ^bThis work.

Table A3: Electron affinities (EA) and Ionization potentials (IP). All values are in eV.

	H	Electron affinities [eV]					Ionization potentials [eV]	
		Li	B	C	O	F	Li	Be
VMC		0.395(2)	0.238(3)	1.289(4)	1.301(6)	3.385(9)	5.362(1)	8.812(5)
SD[140]								
VMC		0.603(1)	-0.022(8)	0.979(3)				9.317(5)
MD[140]								
VMC SD ^a			0.273(4)					
VMC AGP ^a	0.7503(2)	0.590(1)	0.051(6)	1.075(7)	1.388(15)	3.409(6)	5.384(1)	9.312(3)
DMC		0.559(2)	0.340(2)	1.342(6)	1.37(2)	3.445(8)	5.391(1)	9.050(2)
SD[140]								
DMC		0.619(1)	0.158(3)	1.161(2)				9.320(1)
MD[140]								
DMC SD ^a			0.341(8)					
DMC AGP ^a	0.7549(6)	0.617(5)	0.190(9)	1.177(12)	1.453(5)	3.445(18)	5.392(1)	9.322(1)
Exp.	0.754195(19)	0.618049(22)	0.279723(25)	1.2621226(11)	1.461112(3)	3.4011895(25)	5.3917149(4)	9.322699(7)
Ref. Exp.	[235]	[236]	[237]	[238]	[239]	[240]	[241]	[242]

^aThis work.

Table A4: Positron affinity (PA) calculated as $PA[X] = E[X] - E[e^+X]$ and Positronium binding energy $BE_{Ps}[X] = E[X^+] + E[Ps] - E[e^+X]$. All energies are in eV. The energies of Hydrogen and Positronium atoms correspond to the exact values of -0.5 and -0.25 Hartree, respectively.

	PA	BE_{Ps}		PA	BE_{Ps}
	H^-			Li	
VMC AGP/PMO ^a	7.0213(10)	0.9687(10)	VMC AGP/PMO ^a	1.2392(32)	-0.1798(32)
VMC AGP/EPO ^a	7.04347(92)	0.99092(91)	VMC AGP/EPO ^a	1.3112(26)	-0.1078(23)
DMC AGP/PMO ^a	7.1094(35)	1.0614(35)	DMC AGP/PMO ^a	1.433(26)	0.022(26)
DMC AGP/EPO ^a	7.11248(62)	1.064485(86)	DMC AGP/EPO ^a	1.4390(63)	0.0280(63)
MRCI[149]	7.110	1.066	Ref.[26]	1.477	
Hylleras[145]		1.0666	SVM[147]		0.0675
	Li^-			Be	
VMC AGP/PMO ^a	6.0896(26)	-0.1232(24)	VMC AGP/PMO ^a	-0.232(90)	2.277(90)
VMC AGP/EPO ^a	6.1160(26)	-0.0968(24)	VMC AGP/EPO ^a	-0.0646(58)	2.4449(50)
DMC AGP/PMO ^a	6.4613(69)	0.2753(44)	DMC AGP/PMO ^a	0.0340(81)	2.5536(78)
DMC AGP/EPO ^a	6.458(12)	0.272(11)	DMC AGP/EPO ^a	0.054(10)	2.5740(98)
VMC[86]	0.460(16)	-6.1171(82)	Ref.[26]	0.086	2.608
DMC[86]	6.506(22)	0.261(22)	SVM[148]	0.086	
DMC[46]		0.3137(16)			
SVM [148]		0.330564			
	B^-			C^-	
VMC AGP/PMO ^a	5.4667(32)	-1.2854(61)	VMC AGP/PMO ^a	5.536(10)	-0.191(12)
VMC AGP/EPO ^a	5.4808(32)	-1.2713(61)	VMC AGP/EPO ^a	5.556(11)	-0.171(13)
DMC AGP/PMO ^a	6.003(24)	-0.609(23)	DMC AGP/PMO ^a	5.890(24)	0.263(22)
DMC AGP/EPO ^a	6.010(12)	-0.603(11)	DMC AGP/EPO ^a	5.921(19)	0.294(17)
VMC SD/PMO ^a	5.48908(46)	-1.04074(42)			
VMC SD/EPO ^a	5.50594(47)	-1.0239(44)			
DMC SD/PMO ^a	6.00605(87)	-0.45546(94)			
DMC SD/EPO ^a	6.0535(23)	-0.4080(32)			
VMC[86]	3.837(54)	-2.667(54)	VMC[86]	4.354(82)	-1.170(82)
DMC[86]	6.014(27)	-0.435(27)	DMC[86]	5.940(16)	0.479(16)
MRCI[77]	6.176	-0.350	MRCI[77]	6.029	0.486
	O^-			F^-	
VMC AGP/PMO ^a	5.449(23)	0.035(26)	VMC AGP/PMO ^a	5.567(19)	2.173(19)
VMC AGP/EPO ^a	5.536(16)	0.122(19)	VMC AGP/EPO ^a	5.647(16)	2.253(16)
DMC AGP/PMO ^a	6.0138(76)	0.6639(55)	DMC AGP/PMO ^a	6.130(22)	2.772(14)
DMC AGP/EPO ^a	6.076(18)	0.726(17)	DMC AGP/EPO ^a	6.224(19)	2.8663(48)
VMC[86]	2.286(82)	-3.157(82)	VMC[86]	5.306(82)	2.122(82)
DMC[86]	5.861(16)	0.433(16)	DMC[86]	6.169(22)	2.838(22)
MRCI[77]	6.150	0.796	MRCI[146]	6.215	2.806

^aThis work.

Appendix B: Dynamical Jastrow Factor for Electron-Positron Interactions

Table B1: VMC and DMC energies (in Ha) for different combinations of the atomic, geminal, and mixed electron-positron dynamical Jastrow terms for one- and two-positron systems.

Jastrow	PsH		e ⁺ PsH		e ⁺ Li		PsLi	
	VMC	DMC	VMC	DMC	VMC	DMC	VMC	DMC
\mathcal{A}^{ee}	-0.777492(21)	-0.789146(32)	-0.794937(32)	-0.810268(42)	-7.521910(34)	-7.529001(80)	-7.68695(12)	-7.738171(85)
$\mathcal{A}^{ee} + \mathcal{G}$	-0.777764(28)	-0.789164(34)	-0.798360(25)	-0.810292(32)	-7.522307(45)	-7.528735(78)	-7.70091(10)	-7.737916(53)
$\mathcal{A}^{ee} + \mathcal{M}$	-0.787418(11)	-0.789175(10)	-0.806575(18)	-0.810234(13)	-7.523687(33)	-7.528693(57)	-7.725894(49)	-7.738399(52)
$\mathcal{A}^{ee} + \mathcal{G} + \mathcal{M}$	-0.787514(11)	-0.789186(11)	-0.807058(15)	-0.810256(14)	-7.523807(31)	-7.528865(68)	-7.726793(69)	-7.738315(28)
\mathcal{A}	-0.785933(20)	-0.789181(14)	-0.803536(23)	-0.810259(18)	-7.524366(27)	-7.528902(80)	-7.723217(71)	-7.738215(97)
$\mathcal{A} + \mathcal{G}$	-0.786253(16)	-0.789203(11)	-0.805261(19)	-0.810278(15)	-7.523687(36)	-7.528901(74)	-7.723645(73)	-7.738276(48)
$\mathcal{A} + \mathcal{M}$	-0.787664(11)	-0.789203(10)	-0.807667(99)	-0.810250(16)	-7.525400(32)	-7.530292(72)	-7.728644(46)	-7.738292(25)
$\mathcal{A} + \mathcal{G} + \mathcal{M}$	-0.7881051(95)	-0.7892214(86)	-0.808631(12)	-0.8102536(86)	-7.525370(26)	-7.530268(80)	-7.728064(54)	-7.738268(34)

Jastrow	PsH ₂		e ⁺ LiH		PsO		Ps ₂ O	
	VMC	DMC	VMC	DMC	VMC	DMC	VMC	DMC
\mathcal{A}^{ee}	-1.556093(48)	-1.588450(71)	-8.092050(66)	-8.107221(32)	-75.26849(30)	-75.327403(89)	-75.52708(33)	-75.63102(27)
$\mathcal{A}^{ee} + \mathcal{G}$	-1.568067(33)	-1.588586(47)	-8.097067(50)	-8.107262(29)	-75.27116(28)	-75.327225(90)	-75.54416(35)	-75.63122(18)
$\mathcal{A}^{ee} + \mathcal{M}$	-1.577253(24)	-1.588615(33)	-8.102010(38)	-8.107276(17)	-75.28564(27)	-75.327589(98)	-75.57351(27)	-75.63139(10)
$\mathcal{A}^{ee} + \mathcal{G} + \mathcal{M}$	-1.578942(69)	-1.588638(28)	-8.102353(35)	-8.107303(17)	-75.28663(26)	-75.327495(66)	-75.57180(30)	-75.63147(15)
\mathcal{A}	-1.573522(53)	-1.588593(37)	-8.102712(41)	-8.107321(15)	-75.28684(25)	-75.328505(72)	-75.57060(32)	-75.632139(84)
$\mathcal{A} + \mathcal{G}$	-1.576586(45)	-1.588609(31)	-8.103249(32)	-8.107289(14)	-75.29025(26)	-75.328107(68)	-75.57210(32)	-75.631878(77)
$\mathcal{A} + \mathcal{M}$	-1.579580(23)	-1.588615(22)	-8.103622(43)	-8.107218(14)	-75.29240(21)	-75.328314(56)	-75.57892(38)	-75.63175(11)
$\mathcal{A} + \mathcal{G} + \mathcal{M}$	-1.581438(20)	-1.588693(22)	-8.104458(37)	-8.107332(11)	-75.29489(27)	-75.328299(44)	-75.59325(32)	-75.632253(62)

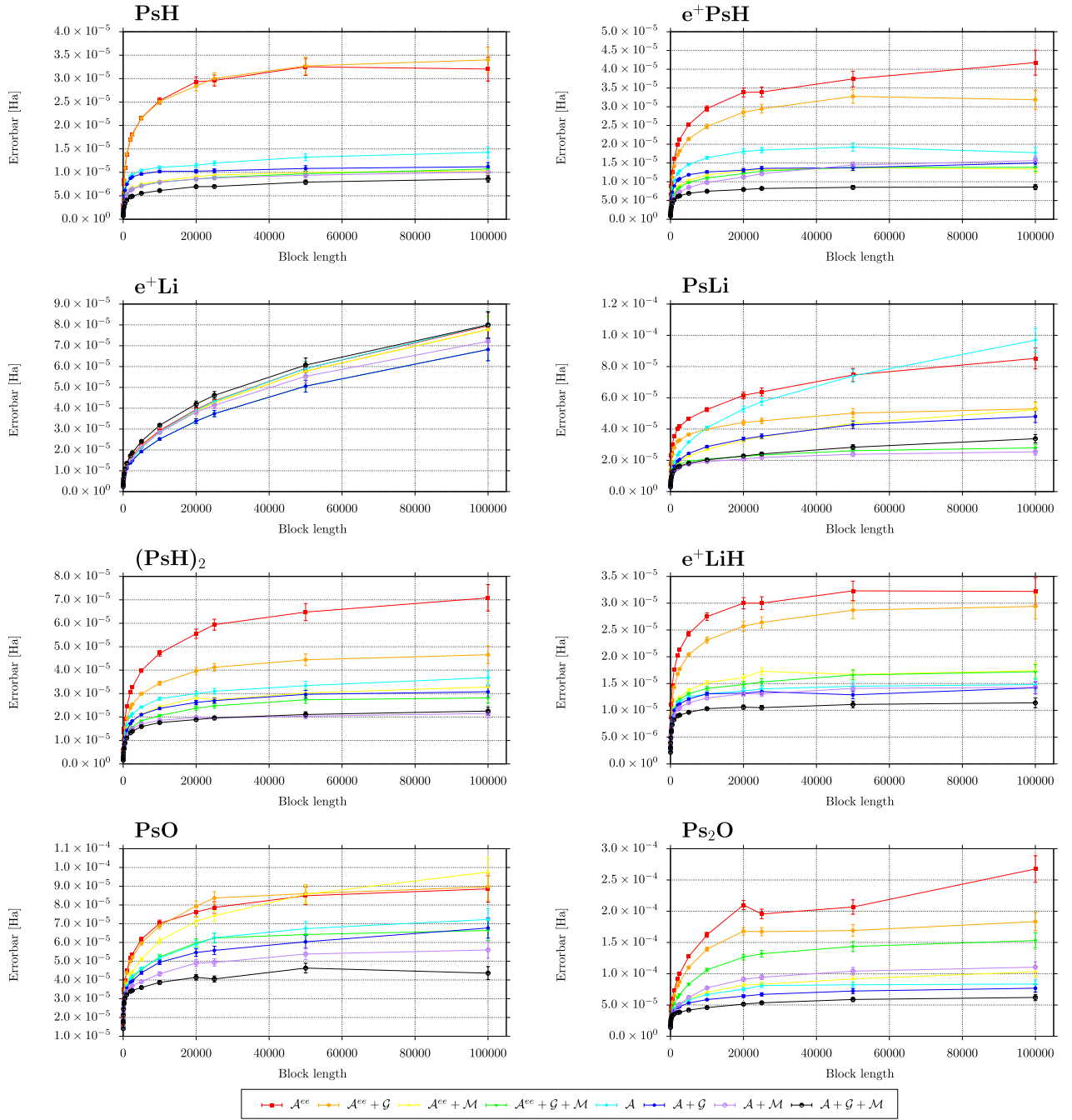


Figure B1: The DMC (dt 0.001) errorbar estimated with the reblocking technique as a function of the block length for all the positronic systems studied comparing with different combination of the dynamical Jastrow factor.

Appendix C: Electric Response Properties of Positronic Systems

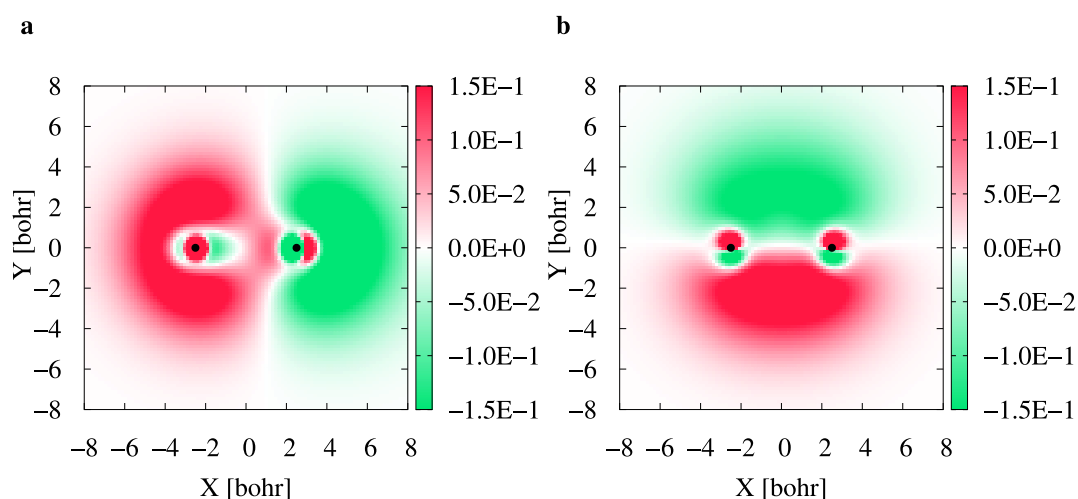


Figure C1: 2D cuts of the electronic density difference between unperturbed system and the perturbed system with an electric field of 0.007 (a.u.). All densities were obtained at CCSD/aug-cc-pVQZ level. Panel **a** and panel **b** for Li_2 at $R_{\text{Li-Li}} = 5.0$ a.u. perturbed with a field parallel and perpendicular to the internuclear axis, respectively. Black circles are used to represent the lithium nuclei positions.

Appendix D: The Three-Center Two-Positron Bond

Part of the results presented in the following section have been reproduced from the Supporting Material of Reference [72].

Table D1: Total energies (in E_h), equilibrium distance (in Bohr) and force constant (in a.u.) of triatomic systems for D_{3h} symmetry calculated at VMC level

System	E	r_{eq}	k_{ν_1}
$2 e^- [H_3^{3+}] S$	-1.347(4)	1.64(3)	0.56(6)
$2 e^- [Li_3^{3+}] S$	-22.3345(2)	5.687(10)	0.0248(4)
$2 e^+ [H_3^{3-}] S$	-2.1489(1)	6.149(10)	0.0110(4)
$2 e^- [Li_3^{3+}] T$	-22.3105(2)	5.950(7)	0.0175(3)
$2 e^+ [H_3^{3-}] T$	-2.1266(1)	6.78(2)	0.0085(6)

Table D2: Total energies (in E_h), equilibrium distance (in Bohr) and force constant (in a.u.) of triatomic systems for D_{3h} symmetry calculated at DMC level.

System	E	r_{eq}	k_{ν_1}	k_{ν_2}
$2 e^- [H_3^{3+}] S$	-1.346(4)	1.63(3)	0.57(5)	0.16(2)
$2 e^- [Li_3^{3+}] S$	-22.34190(10)	5.645(7)	0.0254(3)	0.0110(4)
$2 e^+ [H_3^{3-}] S$	-2.1652(2)	6.11(1)	0.0114(4)	0.0047(7)
$2 e^- [Li_3^{3+}] T$	-22.31280(7)	5.937(7)	0.0168(2)	-
$2 e^+ [H_3^{3-}] T$	-2.1401(4)	6.62(1)	0.0080(4)	-

Table D3: Total energies (in E_h) of atomic, diatomic, and triatomic species along with diatomic and triatomic equilibrium distances (in bohrs)

System	E(DMC)		E(Ref.)	
Ps	-		-0.25 ^a	
Ps ⁻	-		-0.262005 [212]	
Ps ₂	-		-0.516004 [171]	
H ⁻	-0.52759(4)		-0.52779(3) [124]	
PsH	-0.78919(4)		-0.78907(7) [124]	
Li ⁺	-7.27992(1)		-7.279910(5) [140]	
Li	-7.47801(2)		-7.47802(1) [136]	
System	E(DMC)	R(DMC)	E(Ref.)	R(Ref)
H ₂ ⁺	-		-0.602635 [243]	2.00
H ₂	-		-1.174476 [169]	1.40
H ₃ ^{+b}	-1.346(4)	1.63(3)	-1.343426 [244]	1.65
H ₃ ^{-c}	-		-1.703511 [245]	1.42, 6.07
Li ₂ ⁺	-14.80562(2)	5.90	-14.80562(1) [246]	5.877
Li ₂	-14.99175(6)	5.05	-14.9952(1) [247]	5.051
Li ₃ ^{+b}	-22.3419(1)	5.645(7)	-	
Li ₃ ^{+d}	-22.31280(7)	5.937(7)	-	
e ⁺ [H ₂ ²⁻]	-1.3403(1)	6.39(3)	-1.3403(1) [73]	6.4(4)
2e ⁺ [H ₂ ²⁻]	-1.5885(1)	6.003(7)	-1.5888(1) [153]	6.0(4)
2e ⁺ [H ₃ ³⁻] ^b	-2.1652(2)	6.11(1)		
2e ⁺ [H ₃ ³⁻] ^d	-2.1401(4)	6.62(1)		

^a Exact^b Singlet D_{3h} symmetry^c Singlet C_{∞v} symmetry^d Triplet D_{∞h} symmetry

Table D4: Vertical dissociation channels for the $2e^+H_3^{3-}$ system into two subsystems A without nuclei and B with the three hydrogen atom nuclei at the internuclear separation near the equilibrium geometry of $2e^+H_3^{3-}$. The column "Estimated Energy" (in E_h) corresponds to the estimated energy according to the species described in the column "Estimation." The dissociated species are highlighted in red with a total charge larger or smaller than +1 or -1 for subsystems A and B . In pink color, all rows where subsystem A dissociates in more than one species.

ID	A	B	Estimation	Estimated Energy	Total charge of A	# Species A	Total charge of B
1	e^+	$1e^+H_3^{3-}$	$H^- + e^+H_2^{2-}$	-1.868	1	1	-2
2	$2e^+$	H_3^{3-}	$3H^- + 3/r$	-1.093	2	2	-3
3	e^-	$2e^+H_3^{2-}$	$H + 2e^+H_2^{2-}$	-2.089	-1	1	0
4	Ps	$1e^+H_3^{2-}$	$Ps + H + e^+H_2^{2-}$	-2.090	0	1	-1
5	$2e^+e^- (=Ps^-)$	H_3^{2-}	$H + 2H^- + Ps^-$	-1.817	1	1	-2
6	$2e^-$	$2e^+H_3^-$	$2H + PsHe^+$	-1.810	-2	2	1
7	Ps^-	$1e^+H_3^-$	$PsH + 2H + Ps^-$	-2.051	-1	1	0
8	Ps_2	H_3^-	$H^- + 2H + Ps_2$	-2.044	0	1	-1
9	$3e^-$	$2e^+H_3$	$3H$	-1.500	-3	3	2
10	$Ps^- + e^-$	e^+H_3	$3H + Ps^-$	-1.762	-2	2	1
11	$Ps^- + Ps$	H_3	$3H + Ps^- + Ps$	-2.012	-1	2	0
12	$Ps_2 + e^-$	H_3	$3H + Ps_2$	-2.016	-1	2	0
13	$4e^-$	$2e^+H_3^+$	$2H$	-1.000	-4	4	3
14	$Ps^- + 2e^-$	$e^+H_3^+$	$2H + Ps^-$	-1.262	-3	3	2
15	$2Ps^-$	H_3^+	$2H + 2Ps^-$	-1.524	-2	2	1
16	$Ps_2 + 2e^-$	H_3^+	$2H + Ps_2$	-1.516	-2	3	1

Table D5: Adiabatic dissociation channels for the $2 e^+ H_3^{3-}$ system after the vertical dissociation into two subsystems A without nuclei and B with the three hydrogen atom nuclei, which later dissociates again in subsystem B_1 with one nucleus and B_2 with two nuclei. The column "Estimated Energy" (in E_h) corresponds to the estimated energy according to the species described in the columns A , B_1 , and B_2 .

ID	A	B	B ₁ (1H)	B ₂ (2H)	Estimated Energy, A+B ₁ +B ₂
1	e^+	$1 e^+ H_3^{3-}$	H_3^-	Ps^-	-1.966
2	$2 e^+$	H_3^{3-}	H^-	$H_2 + 2 e^-$	-1.702
3	e^-	$2 e^+ H_3^{2-}$	PsH	$H_2 + Ps$	-2.214
4	Ps	$1 e^+ H_3^{2-}$	PsH	$H_2 + e^-$	-2.214
5	$2 e^+ e^- (=Ps^-)$	H_3^{2-}	H^-	$H_2 + e^-$	-1.964
6	$2 e^-$	$2 e^+ H_3^-$	PsHe ⁺	H_2	-1.985
7	Ps^-	$1 e^+ H_3^-$	PsH	H_2	-2.226
8	Ps_2	H_3^-	-	H_3^-	-2.220
9	$3 e^-$	$2 e^+ H_3$	H	$H_2 + 2 e^+$	-1.674
10	$Ps^- + e^-$	$e^+ H_3$	H	$H_2 + e^+$	-1.936
11	$Ps^- + Ps$	H_3	H	H_2	-2.186
12	$Ps_2 + e^-$	H_3	H	H_2	-2.190
13	$4 e^-$	$2 e^+ H_3^+$	-	$H_3^+ + 2 e^+$	-1.343
14	$Ps^- + 2 e^-$	$e^+ H_3^+$	-	$H_3^+ + e^+$	-1.605
15	$2 Ps^-$	H_3^+	-	H_3^+	-1.867
16	$Ps_2 + 2 e^-$	H_3^+	-	H_3^+	-1.859

Appendix E: Positron-Bonded Diatomics: Estimating the Size of Interacting Atoms

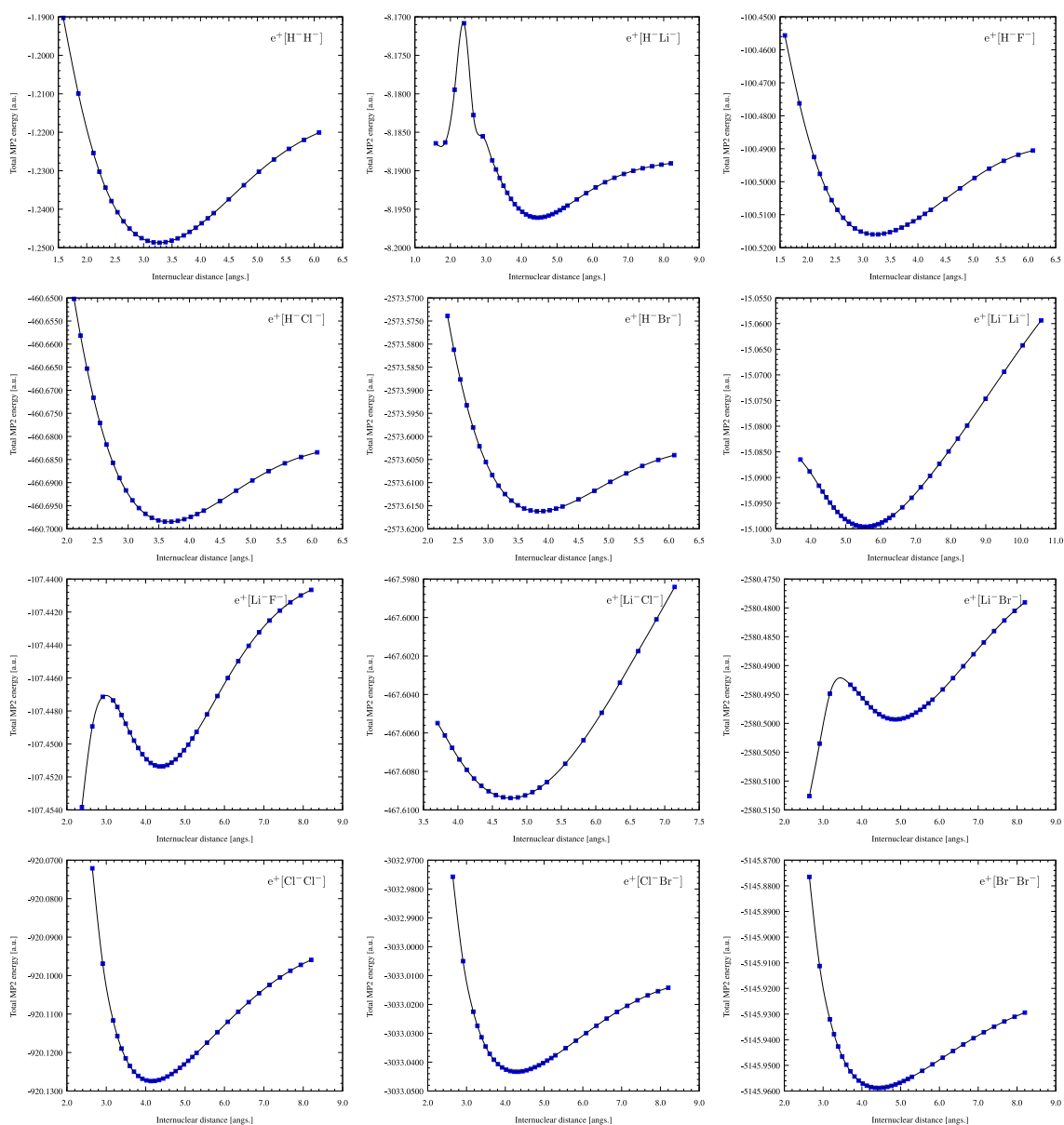


Figure E1: Potential energy curves of positron-bond diatomics of the form $e^+[A^-B^-]$ computed at MP2/def2-TZVPPD//6s4p3d2f Gaussian-type

Bibliography

- [1] C. D. Anderson. “The production and properties of positrons”. *Nobel Lecture (1936)*. Available at <https://www.nobelprize.org/prizes/physics/1936/anderson/lecture/>.
- [2] C. D. Anderson. “The positive electron”. *Phys. Rev* **43**, 491 (1933).
- [3] P. A. M. Dirac. “The Quantum Theory of the Electron”. *Proc. R. Soc. London. Ser. A* **117**, 610 (1928).
- [4] D. Griffiths. *Introduction to Elementary Particles* (John Wiley & Sons, Inc., 1987).
- [5] R. P. Feynman. “The Theory of Positrons”. *Phys. Rev.* **70**, 749 (1949).
- [6] F. Joliot. “Preuves expérimentales de l’annihilation des électrons positifs”. *J. Phys. Radium* **5**, 299 (1934).
- [7] J. Thibaud. “Positive Electrons: Focussing of Beams, Measurement of Charge-to-Mass Ratio, Study of Absorption and Conversion into Light”. *Phys. Rev.* **45**, 781 (1934).
- [8] Y. C. Jean, P. E. Mallon & D. M. Schrader. *Principles and Applications of Positron and positronium chemistry*, vol. 1 (World Scientific, 2003).
- [9] P. A. Dirac. “On the Annihilation of Electrons and Protons”. *Math. Proc. Camb. Philos. Soc.* **26**, 361 (1930).
- [10] R. Wahl & J. Buchanan. *Principles and Practice of Positron Emission Tomography* (Lippincott Williams & Wilkins, 2002).
- [11] G. Muehllehner & J. S. Karp. “Positron emission tomography”. *Phys. Med. Biol.* **51**, r117 (2006).
- [12] J. J. Vaquero & P. Kinahan. “Positron Emission Tomography: Current Challenges and Opportunities for Technological Advances in Clinical and Preclinical Imaging Systems”. *Annu. Rev. Biomed. Eng.* **17**, 385 (2015).

- [13] D. W. Gidley, H. G. Peng & R. S. Vallery. “Positron annihilation as a method to characterize porous materials”. *Annu. Rev. Mater. Res.* **36**, 49 (2006).
- [14] E. Kubicz. “Potential for biomedical applications of positron annihilation lifetime spectroscopy (PALS)”. *AIP Conf. Proc* **2182**, 050004 (2019).
- [15] S. Mohorovičić. “Möglichkeit neuer Elemente und ihre Bedeutung für die Astrophysik”. *Astron. Nachrichten.* **253**, 93 (1934).
- [16] M. Deutsch. “Evidence for the Formation of Positronium in Gases”. *Phys. Rev.* **83**, 866 (1951).
- [17] J. A. Wheeler. “Polyelectrons”. *Ann. N. Y. Acad. Sci* **48**, 219 (1946).
- [18] E. A. Armour, J. M. Richard & K. Varga. “Stability of few-charge systems in quantum mechanics”. *Phys. Rep.* **413**, 1 (2005).
- [19] E. Mátyus. “On the calculation of resonances in pre-born-oppenheimer molecular structure theory”. *J. Phys. Chem. A* **117**, 7195 (2013).
- [20] A. P. Mills. “Observation of the positronium negative ion”. *Phys. Rev. Lett.* **46**, 717 (1981).
- [21] D. B. Cassidy & A. P. Mills Jr. “The production of molecular positronium”. *Nature* **449**, 7159 (2007).
- [22] S. Bubin, O. V. Prezhdo & K. Varga. “Instability of tripositronium”. *Phys. Rev. A* **87**, 054501 (2013).
- [23] R. J. Drachman. “Why positron physics is fun”. *AIP Conf. Proc* **360**, 369 (1996).
- [24] M. J. Brunger, D. B. Cassidy, S. Dujko, D. Marić, J. Marler, J. P. Sullivan & J. Fedor. “Recent studies with electrons, positrons and positronium”. *Eur. Phys. J. D* **74**, 158 (2020).
- [25] X. Cheng, D. Babikov & D. M. Schrader. “Binding-energy predictions of positronium-atom systems”. *Phys. Rev. A - At. Mol. Opt. Phys.* **85**, 012503 (2012).
- [26] C. Harabati, V. A. Dzuba & V. V. Flambaum. “Identification of atoms that can bind positrons”. *Phys. Rev. A* **89**, 022517 (2014).
- [27] D. M. Schrader, F. M. Jacobsen, N. P. Frandsen & U. Mikkelsen. “Formation of positronium hydride”. *Phys. Rev. Lett.* **69**, 57 (1992).
- [28] S. J. Gilbert, L. D. Barnes, J. P. Sullivan & C. M. Surko. “Vibrational-Resonance Enhancement of Positron Annihilation in Molecules”. *Phys. Rev. Lett.* **88**, 043201 (2002).

- [29] G. F. Gribakin, J. A. Young & C. M. Surko. “Positron-molecule interactions: Resonant attachment, annihilation, and bound states”. *Rev. Mod. Phys.* **82**, 2557 (2010).
- [30] Y. Sugiura, T. Takayanagi, Y. Kita & M. Tachikawa. “Positron binding to hydrocarbon molecules : calculation using the positron – electron correlation polarization potential”. *Eur. Phys. J. D* **73**, 162 (2019).
- [31] M. R. Natisin, J. R. Danielson, G. F. Gribakin, A. R. Swann & C. M. Surko. “Vibrational Feshbach Resonances Mediated by Nondipole Positron-Molecule Interactions”. *Phys. Rev. Lett.* **119**, 113402 (2017).
- [32] S. Ghosh, J. R. Danielson & C. M. Surko. “Resonant Annihilation and Positron Bound States in Benzene”. *Phys. Rev. Lett.* **129**, 123401 (2022).
- [33] J. R. Danielson, S. Ghosh & C. M. Surko. “Enhancement of positron binding energy in molecules containing π bonds”. *Phys. Rev. A* **106**, 032811 (2022).
- [34] R. S. B. Alfredo Dupasquier, Allen P. Mills, R. S. Brusa (ed.) *Physics with Many Positrons* (IOS Press, 2010).
- [35] J. R. Danielson, D. H. Dubin, R. G. Greaves & C. M. Surko. “Plasma and trap-based techniques for science with positrons”. *Rev. Mod. Phys.* **87**, 247 (2015).
- [36] A. P. Mills Jr. “Positronium Bose-Einstein condensation in liquid ^4He bubbles”. *Phys. Rev. A* **100**, 063615 (2019).
- [37] D. B. Cassidy. “Experimental progress in positronium laser physics”. *Eur. Phys. J. D* **72**, 53 (2018).
- [38] C. Amsler *et al.* “Velocity-selected production of 2^3S metastable positronium”. *Phys. Rev. A* **99**, 033405 (2019).
- [39] J. Hofierka, B. Cunningham, C. M. Rawlins, C. H. Patterson & D. G. Green. “Many-body theory of positron binding to polyatomic molecules”. *Nature* **606**, 688 (2022).
- [40] J. Mitroy & I. A. Ivanov. “Semiempirical model of positron scattering and annihilation”. *Phys. Rev. A* **65**, 042705 (2002).
- [41] L. Chiari, A. Zecca, S. Girardi, A. Defant, F. Wang, X. G. Ma, M. V. Perkins & M. J. Brunger. “Positron scattering from chiral enantiomers”. *Phys. Rev. A* **85**, 052711 (2012).
- [42] A. R. Swann & G. F. Gribakin. “Model-potential calculations of positron binding, scattering, and annihilation for atoms and small molecules using a Gaussian basis”. *Phys. Rev. A* **101**, 022702 (2020).

- [43] M. M. Billah, M. M. Khatun, M. M. Haque, M. Y. Ali, M. H. Khandker, A. K. Haque, H. Watabe & M. A. Uddin. “A Theoretical Study of Scattering of Electrons and Positrons with a CO₂ Molecule”. *Atoms* **10**, 31 (2022).
- [44] L. A. Poveda, M. I. Muniz & J. R. Mohallem. “Chaos and resonances in the classical scattering of a positron by a model diatomic molecule”. *J. Mol. Model.* **29**, 29 (2023).
- [45] N. Jiang & D. M. Schrader. “Diffusion quantum Monte Carlo calculation of the binding energy and annihilation rate of positronium hydride, PsH”. *J. Chem. Phys.* **109**, 9430 (1998).
- [46] M. Mella, S. Chiesa & G. Morosi. “Annihilation rate in positronic systems by quantum Monte Carlo: e⁺LiH as test case”. *J. Chem. Phys.* **116**, 2852 (2002).
- [47] J. M. Campillo Robles, E. Ogando & F. Plazaola. “Positron lifetime calculation for the elements of the periodic table”. *J. Phys. Condens. Matter* **19**, 176222 (2007).
- [48] M. M. Wołczyrz, K. Strasburger & H. Chojnacki. “Two-photon annihilation rate of the positronic HCN molecule”. *Mol. Phys.* **111**, 345 (2013).
- [49] K. R. Brorsen, M. V. Pak & S. Hammes-Schiffer. “Calculation of Positron Binding Energies and Electron-Positron Annihilation Rates for Atomic Systems with the Reduced Explicitly Correlated Hartree-Fock Method in the Nuclear-Electronic Orbital Framework”. *J. Phys. Chem. A* **121**, 515 (2017).
- [50] A. R. Swann & G. F. Gribakin. “Calculations of positron binding and annihilation in polyatomic molecules”. *J. Chem. Phys.* **149**, 244305 (2018).
- [51] Y. Iwabata, R. Aiba, T. Iwanade, H. Nishizawa, F. Wang & H. Nakai. “Quantum chemical approach for positron annihilation spectra of atoms and molecules beyond plane-wave approximation”. *J. Chem. Phys.* **148**, 184110 (2018).
- [52] M. Ozaki, D. Yoshida, Y. Kita, T. Shimazaki & M. Tachikawa. “Positron Binding and Annihilation Properties of Amino Acid Systems”. *ACS Omega* **6**, 29449 (2021).
- [53] A. M. Frolov. “Bound-state properties, positron annihilation and hyperfine structure of the four-body positronium hydrides”. *Mol. Phys.* **120**, e2019337 (2022).
- [54] R. J. Buenker, H. P. Liebermann, L. Pichl, M. Tachikawa & M. Kimura. “Role of the electric dipole moment in positron binding to the ground and excited states of the BeO molecule”. *J. Chem. Phys.* **126**, 1 (2007).
- [55] M. W. Bromley & J. Mitroy. “Excited, bound and resonant positron-atom systems”. *J. Phys. Conf. Ser.* **199**, 012011 (2010).

- [56] D. Bressanini. “Positron binding to lithium excited states”. *Phys. Rev. Lett.* **109**, 1 (2012).
- [57] D. Bressanini. “Structure of LiPs ground and excited states”. *Phys. Rev. A* **97**, 012508 (2018).
- [58] C. Le Sech & B. Silvi. “Study of positronium hydride with a simple wavefunction: Application to the Stark effect of PsH”. *Chem. Phys.* **236**, 77 (1998).
- [59] M. Mella, D. Bressanini & G. Morosi. “Variational Monte Carlo calculation of dynamic multipole polarizabilities and van der Waals coefficients of the PsH system”. *Phys. Rev. A* **63**, 024503 (2001).
- [60] Z.-c. Yan. “Polarizabilities and dispersion coefficients of positronium hydride”. *J. Phys. B At. Mol. Opt. Phys.* **35**, 345 (2002).
- [61] J. Mitroy & M. W. Bromley. “Van der Waals coefficients for positronium-atom interactions”. *Phys. Rev. A* **68**, 3 (2003).
- [62] S. Kar & Y. K. Ho. “Dispersion coefficients for interactions between positronium and light atoms with pure Coulomb and screened Coulomb potentials”. *Nucl. Instr. and Meth. in Phys. Res. B* **266**, 526 (2008).
- [63] J. Tiihonen, I. Kylänpää & T. T. Rantala. “Computation of Dynamic Polarizabilities and van der Waals Coefficients from Path-Integral Monte Carlo”. *J. Chem. Theory Comput.* **14**, 5750 (2018).
- [64] Y. Suzuki, S. Hagiwara & K. Watanabe. “Time-Dependent Multicomponent Density Functional Theory for Coupled Electron-Positron Dynamics”. *Phys. Rev. Lett.* **121**, 133001 (2018).
- [65] F. Carelli, J. Franz & F. A. Gianturco. “Dipole-driven dynamics for near-threshold electron/positron interactions with pyrimidinic DNA bases: A path to compound formations”. *Mol. Phys.* **114**, 213 (2016).
- [66] M. Mella, G. Morosi & D. Bressanini. “A diffusion Monte Carlo accurate interaction potential between H and PsH”. *J. Chem. Phys.* **112**, 1063 (2000).
- [67] M. Mella, G. Morosi, D. Bressanini & S. Elli. “Positron and positronium chemistry by quantum Monte Carlo. V. The ground state potential energy curve of e^+LiH ”. *Chem. Phys.* **113**, 6154 (2000).
- [68] Y. Sugiura, K. Suzuki, T. Takayanagi, Y. Kita & M. Tachikawa. “Reduction of OH vibrational frequencies in amino acids by positron attachment”. *J. Comput. Chem.* **39**, 2060 (2018).

- [69] K. Suzuki, Y. Sugiura, T. Takayanagi, Y. Kita & M. Tachikawa. “Hydration Effect on Positron Binding Ability of Proline: Positron Attachment Induces Proton-Transfer to Form Zwitterionic Structure”. *J. Phys. Chem. A* **123**, 1217 (2019).
- [70] M. Bergami, A. L. Santana, J. Charry Martinez, A. Reyes, K. Coutinho & M. T. N. Varella. “Multicomponent Quantum Mechanics/Molecular Mechanics Study of Hydrated Positronium”. *J. Phys. Chem. B* **126**, 2699 (2022).
- [71] J. Charry, M. T. N. Varella & A. Reyes. “Binding Matter with Antimatter: The Covalent Positron Bond”. *Angew. Chem* **57**, 8859 (2018).
- [72] J. Charry, F. Moncada, M. Barborini, L. Pedraza-González, M. T. d. N. Varella, A. Tkatchenko & A. Reyes. “The three-center two-positron bond”. *Chem. Sci.* **13**, 13795 (2022).
- [73] D. Bressanini. “The stability of $e^+(H^-)_2$ ”. *J. Chem. Phys.* **154**, 224306 (2021).
- [74] D. Bressanini. “ $e^+(PsH)_2$: A three-positron molecule with a positronic chemical bond”. *J. Chem. Phys.* **156**, 154302 (2022).
- [75] R. J. Buenker, Heinz-Peter Liebermann, Vladlen Melnikov, M. Tachikawa, L. Pichl & M. Kimura. “Positron Binding Energies for Alkali Hydrides”. *J. Phys. Chem. A* **109**, 5956 (2005).
- [76] A. Reyes, F. Moncada & J. Charry. “The any particle molecular orbital approach: A short review of the theory and applications”. *Int. J. Quantum Chem.* **119**, e25705 (2019).
- [77] S. L. Saito. “Multireference configuration interaction calculations for complexes of positronium and B, C, N, and O atoms”. *Theor. Chem. Acc* **115**, 281 (2006).
- [78] J. Romero, J. a. Charry, R. Flores-Moreno, M. T. D. N. Varella & A. Reyes. “Calculation of positron binding energies using the generalized any particle propagator theory”. *J. Chem. Phys.* **141**, 114103 (2014).
- [79] J. Ludlow & G. Gribakin. “Many-body theory calculations of positron binding to negative ions”. *Int. Rev. At. Mol. Physics*, **1**, 73 (2010).
- [80] K. Strasburger. “Adiabatic positron affinity of LiH”. *J. Chem. Phys.* **114**, 615 (2001).
- [81] S. Bubin & L. Adamowicz. “Non-Born-Oppenheimer study of positronic molecular systems: e^+LiH ”. *J. Chem. Phys.* **120**, 6051 (2004).
- [82] C. Swalina, M. V. Pak & S. Hammes-Schiffer. “Analysis of electron-positron wavefunctions in the nuclear-electronic orbital framework”. *J. Chem. Phys.* **136**, 164105 (2012).

- [83] G. G. Ryzhikh, J. Mitroy & K. Varga. “The structure of exotic atoms containing positrons and positronium”. *J. Phys. B At. Mol. Opt. Phys.* **31**, 3965 (1998).
- [84] J.-Y. Zhang & J. Mitroy. “Expectation values of the e^+PsH system”. *Phys. Rev. A* **76**, 014501 (2007).
- [85] F. Becca & S. Sorella. *Quantum Monte Carlo approaches for correlated systems* (Cambridge University Press, 2017).
- [86] D. Bressanini, M. Mella & G. Morosi. “Positronium chemistry by quantum Monte Carlo. I. Positronium-first row atom complexes”. *J. Chem. Phys.* **108**, 4756 (1998).
- [87] E. Boroński. “Investigation of electron-positron correlations by Monte Carlo simulation”. *Acta Phys. Pol* **107**, 576 (2005).
- [88] Y. Kita, M. Tachikawa, N. D. Drummond & R. J. Needs. “A variational monte carlo study of positronic compounds using inhomogeneous backflow transformations”. *Chem. Lett.* **39**, 1136 (2010).
- [89] N. D. Drummond, P. López Ríos, R. J. Needs & C. J. Pickard. “Quantum monte carlo study of a positron in an electron gas”. *Phys. Rev. Lett.* **107**, 207402 (2011).
- [90] R. J. Needs, M. D. Towler, N. D. Drummond, P. L. Rios & J. R. Trail. “Variational and Diffusion Quantum Monte Carlo Calculations with the CASINO Code”. *J. Chem. Phys.* **152**, 154106 (2020).
- [91] J. A. Charry Martinez, M. Barborini, A. Tkatchenko, J. Alfonso, C. Martinez, M. Barborini & A. Tkatchenko. “Correlated Wave Functions for Electron-Positron Interactions in Atoms and Molecules”. *J. Chem. Theory Comput* **18**, 2267 (2022).
- [92] D. M. Schrader. “Bound states of positrons with atoms and molecules: Theory”. *Nucl. Instr. and Meth. in Phys. Res. B* **143**, 209 (1998).
- [93] Y. Kita & M. Tachikawa. “Quantum Monte Carlo Study of the Binding of a Positron to Polar Molecules”. In *Advances in Quantum Monte Carlo*, chap. 13, 157–173 (2012).
- [94] K. A. Simula, J. E. Muff, I. Makkonen & N. D. Drummond. “Quantum Monte Carlo Study of Positron Lifetimes in Solids”. *Phys. Rev. Lett* **129**, 166403 (2022).
- [95] K. Nakano *et al.* “TurboRVB: A many-body toolkit for ab initio electronic simulations by quantum Monte Carlo”. *J. Chem. Phys* **152**, 204121 (2020).
- [96] D. Bressanini & G. Morosi. “Compact boundary-condition-determined wave function for positronium hydride (PsH)”. *J. Chem. Phys* **119**, 7037 (2003).

- [97] M. Born & R. Oppenheimer. “Born Oppenheimer”. *Ann. Phys. (Berl.)* **457–484** (1927).
- [98] P. Popelier. *Solving the Schrödinger equation Has everything been tried?* (World Scientific, 2011).
- [99] N. S. O. Attila Szabo. *Modern Quantum Chemistry: Introduction to Advanced Electronic Structure Theory* (Dover Publications, New York, United States, 1996).
- [100] W. M. C. Foulkes, L. Mitas, R. J. N. Rajagopal & G. “Quantum Monte Carlo simulations of solids”. *Rev. Mod. Phys* **73**, 33 (2001).
- [101] B. M. Austin, D. Y. Zubarev & W. A. Lester. “Quantum monte carlo and related approaches”. *Chem. Rev.* **112**, 263 (2012).
- [102] E. Boroński & R. M. Nieminen. “Electron-positron density-functional theory”. *Phys. Rev. B* **34**, 3820 (1986).
- [103] F. Moncada & A. Reyes. “Multicomponent wavefunction-in-DFT embedding for positronium molecules”. *J. Chem. Phys* **158**, 134101 (2023).
- [104] N. Metropolis, A. W. Rosenbluth, M. N. Rosenbluth, A. H. Teller & E. Teller. “Equation of state calculations by fast computing machines”. *J. Chem. Phys* **21**, 1087 (1953).
- [105] H. Flyvbjerg & H. G. Petersen. “Error estimates on averages of correlated data”. *J. Chem. Phys* **91**, 461 (1989).
- [106] M. H. Kalos & P. A. Whitlock. *Quantum Monte Carlo*, chap. 8 (John Wiley & Sons, Ltd, 2000).
- [107] R. M. Fye. “Study of trotter-like approximations”. *J. Stat. Phys* **43**, 827 (1986).
- [108] P. J. Reynolds, D. M. Ceperley, B. J. Alder & W. A. Lester. “Fixed-node quantum Monte Carlo for molecules”. *J. Chem. Phys* **77**, 5593 (1982).
- [109] T. A. Anderson & C. J. Umrigar. “Nonlocal pseudopotentials and time-step errors in diffusion Monte Carlo”. *J. Chem. Phys* **154** (2021).
- [110] C. J. Umrigar, M. P. Nightingale & K. J. Runge. “A diffusion Monte Carlo algorithm with very small time-step errors”. *J. Chem. Phys* **99**, 2865 (1993).
- [111] R. Assaraf, M. Caffarel & A. Khelif. “Diffusion Monte Carlo methods with a fixed number of walkers”. *Phys. Rev. E* **61**, 4566 (2000).
- [112] A. Zen, S. Sorella, M. J. Gillan, A. Michaelides & D. Alfè. “Boosting the accuracy and speed of quantum Monte Carlo: Size consistency and time step”. *Phys. Rev. B.* **93**, 241118(R) (2016).

- [113] M. D. Towler. “The quantum Monte Carlo method”. *Phys. Status Solidi B* **243**, 2573 (2006).
- [114] M. Casula, C. Filippi & S. Sorella. “Diffusion Monte Carlo method with lattice regularization”. *Phys. Rev. Lett.* **95**, 100201 (2005).
- [115] M. Barborini. “Quantum Mecha (QMeCha) package α .0.3.0 (private repository july, 2021)”. Available at <https://github.com/QMeCha>.
- [116] R. Flores-Moreno, E. Posada, F. Moncada, J. Romero, J. Charry, M. Díaz-Tinoco, S. A. González, N. F. Aguirre & A. Reyes. “LOWDIN: The any particle molecular orbital code”. *Int. J. Quantum Chem.* **114**, 50 (2014).
- [117] A. Reyes Velasco. “openlowdin quantum chemistry package”. Available at <https://github.com/efposadac/openLOWDIN>.
- [118] Y. Kita, R. Maezono, M. Tachikawa, M. Towler & R. J. Needs. “Ab initio quantum Monte Carlo study of the positronic hydrogen cyanide molecule.”. *J. Chem. Phys* **131**, 134310 (2009).
- [119] Y. Yamada, Y. Kita, M. Tachikawa, M. D. Towler & R. J. Needs. “Quantum Monte Carlo and high-level ab initio molecular orbital investigation of dissociation channels of the positronic alkali-metal hydrides, $[XH;e^+]$ ($X = \text{Li, Na, and K}$)”. *Eur. Phys. J. D* **68**, 63 (2014).
- [120] M. Casula & S. Sorella. “Geminal wave functions with Jastrow correlation: A first application to atoms”. *J. Chem. Phys* **119**, 6500 (2003).
- [121] N. D. Drummond, M. D. Towler & R. J. Needs. “Jastrow correlation factor for atoms, molecules, and solids”. *Phys. Rev. B* **70**, 235119 (2004).
- [122] M. Goli & S. Shahbazian. “On the Nature of the Positronic Bond”. *ChemPhysChem* **20**, 831 (2019).
- [123] F. Moncada, L. Pedraza-González, J. Charry, M. T. do N. Varella & A. Reyes. “Covalent bonds in positron dihalides”. *Chem. Sci* **11**, 44 (2020).
- [124] S. Ito, D. Yoshida, Y. Kita & M. Tachikawa. “First-principles quantum Monte Carlo studies for prediction of double minima for positronic hydrogen molecular dianion”. *J. Chem. Phys* **153**, 224305 (2020).
- [125] T. Kato. “On the eigenfunctions of many-particle systems in quantum mechanics”. *Commun. Pure Appl.* **10**, 151 (1957).

- [126] D. Bressanini, M. Mella & G. Morosi. “Stability and positron annihilation of positronium hydride states: A quantum Monte Carlo study”. *Phys. Rev. A* **57**, 1678 (1998).
- [127] J. Charry, J. Romero, M. T. do N. Varella & A. Reyes. “Calculation of positron binding energies of amino acids with the any-particle molecular-orbital approach”. *Phys. Rev. A*. **89**, 052709 (2014).
- [128] M. Casula, C. Attaccalite & S. Sorella. “Correlated geminal wave function for molecules: An efficient resonating valence bond approach”. *J. Chem. Phys.* **121**, 7110 (2004).
- [129] A. Zen, Y. Luo, S. Sorella & L. Guidoni. “Molecular properties by quantum Monte Carlo: An investigation on the role of the wave function ansatz and the basis set in the water molecule”. *J. Chem. Theory Comput* **9**, 4332 (2013).
- [130] A. J. Coleman. “Structure of fermion density matrices. II. Antisymmetrized geminal powers”. *J. Math. Phys.* **6**, 1425 (1965).
- [131] R. Brown, Q. Prigent, A. R. Swann & G. F. Gribakin. “Effective radius of ground- and excited-state positronium in collisions with hard walls”. *Phys. Rev. A* **95**, 032705 (2017).
- [132] J. Sherman & W. J. Morrison. “Adjustment of an Inverse Matrix Corresponding to a Change in One Element of a Given Matrix”. *Ann. Math. Stat.* **21**, 124 (1950).
- [133] C. J. Huang, C. Filippi & C. J. Umrigar. “Spin contamination in quantum Monte Carlo wave functions”. *J. Chem. Phys.* **108**, 8838 (1998).
- [134] F. Sterpone, L. Spanu, L. Ferraro, S. Sorella & L. Guidoni. “Dissecting the hydrogen bond: A quantum monte carlo approach”. *J. Chem. Theory Comput* **4**, 1428 (2008).
- [135] C. Bunge, J. Barrientos & A. Bunge. “Roothaan-Hartree-Fock Ground-State Atomic Wave Functions: Slater-Type Orbital Expansions and Expectation Values for $Z = 2-54$ ”. *At. Data Nucl. Data Tables* **53**, 114 (1993).
- [136] M. D. Brown, J. R. Trail, P. L. Ríos & R. J. Needs. “Energies of the first row atoms from quantum Monte Carlo”. *J. Chem. Phys.* **126**, 224110 (2007).
- [137] E. Buendía, F. J. Gálvez, P. Maldonado & A. Sarsa. “Quantum Monte Carlo ground state energies for the atoms Li through Ar”. *J. Chem. Phys.* **131**, 044115 (2009).
- [138] S. J. Chakravorty, S. R. Gwaltney & E. R. Davidson. “Ground-state correlation energies for atomic ions with 3 to 18 electrons”. *Phys. Rev. A* **47**, 3469 (1993).

- [139] E. Buendía, F. J. Gálvez & A. Sarsa. “Jastrow correlations and near degeneracy effects in neutral atoms and cations with 3 le Z le 36”. *Chem. Phys. Lett.* **436**, 352 (2007).
- [140] P. Maldonado, A. Sarsa, E. Buendía & F. J. Gálvez. “Quantum Monte Carlo ground state energies for the singly charged ions from Li through Ar”. *J. Chem. Phys.* **133**, 064102 (2010).
- [141] M. Barborini & E. Coccia. “Investigating Disjoint Non-Kekulé Diradicals with Quantum Monte Carlo: The Tetramethyleneethane Molecule through the Jastrow Antisymmetrized Geminal Power Wave Function”. *J. Chem. Theory Comput.* **11**, 5696 (2015).
- [142] M. Mella, G. Morosi & D. Bressanini. “Positron and positronium chemistry by quantum Monte Carlo. IV. Can this method accurately compute observables beyond energy?”. *J. Chem. Phys.* **111**, 108 (1999).
- [143] J. Mitroy. “Energy and expectation values of the PsH system”. *Phys. Rev. A* **73**, 054502 (2006).
- [144] J. Mitroy & G. G. Ryzhikh. “Improved binding energies for LiPs, e⁺Be, NaPs and e⁺Mg”. *J. Phys. B At. Mol. Phys.* **34**, 2001 (2001).
- [145] Z. C. Yan & Y. K. Ho. “Ground state and S-wave autodissociating resonant states of positronium hydride”. *Phys. Rev. A - At. Mol. Opt. Phys.* **59**, 2697 (1999).
- [146] S. L. Saito. “Multireference configuration interaction calculations for positronium halides”. *J. Chem. Phys.* **122**, 054302 (2005).
- [147] J. Mitroy. “Expectation values of the e⁺Li system”. *Phys. Rev. A* **70**, 25 (2004).
- [148] J. Mitroy. “Structure of the LiPs and e⁺Be systems”. *J. At. Mol. Sci.* **1**, 275 (2010).
- [149] S. L. Saito. “Multireference configuration interaction calculations of some low-lying states of positronium hydride”. *J. Chem. Phys.* **118**, 1714 (2003).
- [150] L. D. Landau & E. M. Lifshitz. *Quantum Mechanics - Non-Relativistic Theory - Vol. 3* (2nd ed. Pergamon Press Inc., 44-01 21st Street, Long Island City, New York 11101, 1965).
- [151] M. Barborini. “Neutral, Anionic, and Cationic Manganese Dimers through Density Functional Theory”. *J. Phys. Chem. A* **120**, 1716 (2016).
- [152] D. W. O. D. Sousa & M. A. C. Nascimento. “Are One-Electron Bonds Any Different from Standard Two-Electron Covalent Bonds?”. *Acc. Chem. Res.* **50**, 2264 (2017).

- [153] D. Bressanini. “Two positrons can form a chemical bond in $(\text{PsH})_2$ ”. *J. Chem. Phys.* **155**, 054306 (2021).
- [154] S. F. Boys & N. C. Handy. “Calculation for Energies and Wavefunctions for States of Neon With Full Electronic Correlation Accuracy”. *Proc. R. Soc. Lond. A* **310**, 63 (1969).
- [155] K. E. Schmidt & J. W. Moskowitz. “Correlated Monte Carlo wave functions for the atoms He through Ne”. *J. Chem. Phys.* **93**, 4172 (1990).
- [156] P. López Ríos, A. Ma, N. D. Drummond, M. D. Towler & R. J. Needs. “Inhomogeneous backflow transformations in quantum Monte Carlo calculations”. *Phys. Rev. E.* **74**, 066701 (2006).
- [157] M. Ruggeri, S. Moroni & M. Holzmann. “Nonlinear Network Description for Many-Body Quantum Systems in Continuous Space”. *Phys. Rev. Lett* **120**, 205302 (2018).
- [158] M. Holzmann & S. Moroni. “Orbital-dependent backflow wave functions for real-space quantum Monte Carlo”. *Phy. Rev. B* **99**, 085121 (2019).
- [159] J. Hermann, Z. Schätzle & F. Noé. “Deep-neural-network solution of the electronic Schrödinger equation”. *Nat. Chem* **12**, 891 (2020).
- [160] D. Pfau, J. S. Spencer, A. G. Matthews & W. M. Foulkes. “Ab initio solution of the many-electron Schrödinger equation with deep neural networks”. *Phys. Rev. Res* **2**, 033429 (2020).
- [161] G. Cassella, H. Sutterud, S. Azadi, N. D. Drummond, D. Pfau, J. S. Spencer & W. M. Foulkes. “Discovering Quantum Phase Transitions with Fermionic Neural Networks”. *Phys. Rev. Lett.* **130**, 36401 (2023).
- [162] M. T. Entwistle, Z. Schätzle, P. A. Erdman, J. Hermann & F. Noé. “Electronic excited states in deep variational Monte Carlo”. *Nat. Commun.* **14**, 274 (2023).
- [163] W. Ren, W. Fu & J. Chen. “Towards the ground state of molecules via diffusion Monte Carlo on neural networks”. *Nat. Commun.* **14**, 1860 (2023).
- [164] M. Marchi, S. Azadi, M. Casula & S. Sorella. “Resonating valence bond wave function with molecular orbitals: Application to first-row molecules”. *J. Chem. Phys.* **131**, 154116 (2009).
- [165] T. Yoshida & G. Miyako. “Diffusion quantum Monte Carlo calculations of positronium hydride and positron lithium”. *Phys. Rev. A* **54**, 4571 (1996).
- [166] Y. Yamada, Y. Kita & M. Tachikawa. “Theoretical prediction of the binding of a positron to a formaldehyde molecule using a first-principles calculation”. *Phys. Rev. A* **89**, 062711 (2014).

- [167] A. M. Frolov & V. H. Smith. “One-photon annihilation in the Ps^- ion and the angular (e^-, e^-) correlation in two-electron ions”. *Phys. Rev. A* **49**, 3580 (1994).
- [168] A. Muolo, E. Mátyus & M. Reiher. “Generalized elimination of the global translation from explicitly correlated Gaussian functions”. *J. Chem. Phys.* **148**, 084112 (2018).
- [169] W. Cencek & K. Szalewicz. “Ultra-High Accuracy Calculations for Hydrogen Molecule and Helium Dimer”. *Int. J. Quantum Chem.* **111**, 4020 (2011).
- [170] T. H. Dunning Jr. “Gaussian basis sets for use in correlated molecular calculations. I. The atoms boron through neon and hydrogen”. *J. Chem. Phys.* **90**, 1007 (1989).
- [171] S. Bubin & L. Adamowicz. “Nonrelativistic variational calculations of the positronium molecule and the positronium hydride”. *Phys. Rev. A* **74**, 052502 (2006).
- [172] B. S. Xie, Z. L. Li & S. Tang. “Electron-positron pair production in ultrastrong laser fields”. *Matter Radiat. at Extremes* **2**, 225 (2017).
- [173] A. Chervyakov & H. Kleinert. “On Electron–Positron Pair Production by a Spatially Inhomogeneous Electric Field”. *Phys. Part. Nucl.* **49**, 374 (2018).
- [174] L. F. Granz, O. Mathiak, S. Villalba-Chávez & C. Müller. “Electron-positron pair production in oscillating electric fields with double-pulse structure”. *Phys. Lett. B* **793**, 85 (2019).
- [175] J. K. Koga, M. Murakami, A. V. Arefiev, Y. Nakamiya, S. S. Bulanov & S. V. Bulanov. “Electron-positron pair creation in the electric fields generated by micro-bubble implosions”. *Phys. Lett. A* **384**, 126854 (2020).
- [176] W. R. Falk, P. H. R. Orth & G. Jones. “Effect of Electric Field on Positron Lifetimes in Argon and Helium”. *Phys. Rev. Lett.* **14**, 447 (1965).
- [177] G. F. Lee & G. Jones. “Electric Field and Temperature Dependence of Positron Annihilation in Argon Gas”. *Can. J. Phys.* **52**, 17 (1974).
- [178] I. Pepe, D. A. Paul, J. Steyaer, F. Gimeno-Nogues, J. Deutsch & R. Prieels. “Positron annihilation in liquid helium and liquid argon under an electric field”. *J. Phys. B* **28**, 3643 (1995).
- [179] J. Ackermann, J. Shertzer & P. Schmelcher. “Long-lived states of positronium in crossed electric and magnetic fields”. *Phys. Rev. Lett.* **78**, 199 (1997).
- [180] H. F. Mohamed. “Study of the effect of electric field on positron annihilation parameters in polymers”. *Radiat. Phys. Chem.* **68**, 449 (2003).

- [181] A. M. Alonso, B. S. Cooper, A. Deller, S. D. Hogan & D. B. Cassidy. “Controlling Positronium Annihilation with Electric Fields”. *Phys. Rev. Lett.* **115**, 183401 (2015).
- [182] T. E. Wall, A. M. Alonso, B. S. Cooper, A. Deller, S. D. Hogan & D. B. Cassidy. “Selective production of Rydberg-stark states of positronium”. *Phys. Rev. Lett.* **114**, 173001 (2015).
- [183] R. A. Ferrell. “Theory of positron annihilation in solids”. *Rev. Mod. Phys.* **28**, 308 (1956).
- [184] J. Tiihonen, I. Kylänpää & T. T. Rantala. “General polarizability and hyperpolarizability estimators for the path-integral Monte Carlo method applied to small atoms, ions, and molecules at finite temperatures”. *Phys. Rev. A* **94**, 032515 (2016).
- [185] C. Amovilli & F. M. Floris. “Study of dispersion forces with quantum Monte Carlo: Toward a continuum model for solvation”. *J. Phys. Chem. A* **119**, 5327 (2015).
- [186] E. Coccia, O. Chernomor, M. Barborini, S. Sorella & L. Guidoni. “Molecular electrical properties from quantum Monte Carlo calculations: Application to ethyne”. *J. Chem. Theory Comput.* **8**, 1952 (2012).
- [187] E. Ospadov, D. G. Oblinsky & S. M. Rothstein. “Ground-state properties of LiH by reptation quantum Monte Carlo methods”. *Phys. Chem. Chem. Phys.* **13**, 8031 (2011).
- [188] P. Schwerdtfeger & J. K. Nagle. “2018 Table of static dipole polarizabilities of the neutral elements in the periodic table*”. *Mol. Phys.* **117**, 1200 (2019).
- [189] S. Sorella. “Generalized Lanczos algorithm for variational quantum Monte Carlo”. *Phys. Rev. B* **64**, 024512 (2001).
- [190] S. Sorella. “Wave function optimization in the variational Monte Carlo method”. *Phys. Rev. B* **71**, 241103 (2005).
- [191] A. D. Buckingham. “Permanent and Induced Molecular Moments and Long-Range Intermolecular Forces”. *Adv. Chem. Phys.* **12**, 107 (1967).
- [192] J. Kobus, D. Moncrieff & S. Wilson. “Comparison of the polarizabilities and hyperpolarizabilities obtained from finite basis set and finite difference Hartree-Fock calculations for diatomic molecules”. *J. Phys. B* **34**, 5127 (2001).
- [193] J. Vrbik, D. A. Legare & S. M. Rothstein. “Infinitesimal differential diffusion quantum Monte Carlo: Diatomic molecular properties”. *J. Chem. Phys.* **92**, 1221 (1990).
- [194] J. Rychlewski. “An accurate calculation of the polarizability of the hydrogen molecule and its dependence on rotation, vibration and isotopic substitution”. *Mol. Phys.* **41**, 833 (1980).

- [195] G. Gopakumar, M. Abe, M. Hada & M. Kajita. “Dipole polarizability of alkali-metal (Na, K, Rb)-alkaline-earth-metal (Ca, Sr) polar molecules: Prospects for alignment”. *J. Chem. Phys.* **140**, 224303 (2014).
- [196] E. Miliordos & K. L. Hunt. “Dependence of the multipole moments, static polarizabilities, and static hyperpolarizabilities of the hydrogen molecule on the H-H separation in the ground singlet state”. *J. Chem. Phys.* **149**, 234103 (2018).
- [197] P. Szabó, S. Góger, J. Charry, M. R. Karimpour, D. V. Fedorov & A. Tkatchenko. “Four-Dimensional Scaling of Dipole Polarizability in Quantum Systems”. *Phys. Rev. Lett.* **128**, 070602 (2022).
- [198] R. M. Lobayan, R. C. Bochicchio, A. Torre & L. Lain. “Electronic structure and effectively unpaired electron density topology in closo -Boranes: Nonclassical three-center two-electron bonding”. *J. Chem. Theory Comput* **7**, 979 (2011).
- [199] J. C. Green, M. L. Green & G. Parkin. “The occurrence and representation of three-centre two-electron bonds in covalent inorganic compounds”. *Chem. Commun* **48**, 11481 (2012).
- [200] E. S. Smirnova & A. M. Echavarren. “A hexanuclear gold cluster supported by three-center-two-electron bonds and aurophilic interactions”. *Angew. Chem* **52**, 9023 (2013).
- [201] J. J. Duchimaza Heredia, A. D. Sadow & M. S. Gordon. “A Quasi-Atomic Analysis of Three-Center Two-Electron Zr-H-Si Interactions”. *J. Phys. Chem. A* **122**, 9653 (2018).
- [202] E. Herbst, P. Trans & R. S. Lond. “The astrochemistry of H_3^+ ”. *Philos. T. Roy. Soc. A.* **358**, 2523 (2000).
- [203] S. Miller *et al.* “The role of H_3^+ in planetary atmospheres”. *Philos. Trans. R. Soc. A* **358**, 2485 (2000).
- [204] T. Oka. “Interstellar H_3^+ ”. *Chem. Rev* **113**, 8738 (2013).
- [205] T. Yoshida, G. Miyako, N. Jiang & D. M. Schrader. “Diffusion quantum Monte Carlo calculation of the binding energy of positronium hydroxide”. *Phys. Rev. A* **54**, 964 (1996).
- [206] S. Fahy, X. W. Wang & S. G. Louie. “Variational quantum Monte Carlo nonlocal pseudopotential approach to solids: Formulation and application to diamond, graphite, and silicon”. *Phys. Rev. B* **42**, 3503 (1990).
- [207] M. S. Becker, A. A. Broyles & T. Dunn. “A parametric approach to the ground-state energy of an electron gas”. *Phys. Rev.* **175**, 224 (1968).

- [208] C. Filippi & C. Umrigar. “Correlated sampling in quantum Monte Carlo: A route to forces”. *Phys. Rev. B* **61**, R16291 (2000).
- [209] R. A. Kendall, T. H. Dunning & R. J. Harrison. “Electron affinities of the first-row atoms revisited. Systematic basis sets and wave functions”. *J. Chem. Phys* **96**, 6796 (1992).
- [210] D. E. Woon & T. H. Dunning. “Gaussian basis sets for use in correlated molecular calculations. III. The atoms aluminum through argon”. *J. Chem. Phys* **98**, 1358 (1993).
- [211] A. K. Wilson, D. E. Woon, K. A. Peterson & T. H. Dunning. “Gaussian basis sets for use in correlated molecular calculations. IX. The atoms gallium through krypton”. *J. Chem. Phys* **110**, 7667 (1999).
- [212] V. I. Korobov. “Coulomb three-body bound-state problem: Variational calculations of nonrelativistic energies”. *Phys. Rev. A* **61**, 3 (2000).
- [213] R. W. Havenith, F. De Proft, P. W. Fowler & P. Geerlings. “ σ -Aromaticity in H_3^+ and Li_3^+ : Insights from ring-current maps”. *Chem. Phys. Lett.* **407**, 391 (2005).
- [214] C. Foroutan-Nejad & P. Rashidi-Ranjbar. “Chemical bonding in the lightest tri-atomic clusters; H_3^+ , Li_3^+ and B_3^- ”. *Comput. Theor. Chem.* **901**, 243 (2009).
- [215] D. W. O. de Sousa & M. A. C. Nascimento. “Three-centre two-electron bonds from the quantum interference perspective”. *Phys. Chem. Chem. Phys* **24**, 15958 (2022).
- [216] A. N. Alexandrova & A. I. Boldyrev. “ σ -Aromaticity and σ -antiaromaticity in alkali metal and alkaline earth metal small clusters”. *J. Phys. Chem. A* **107**, 554 (2003).
- [217] X. He, C. Guo, M. Li, S. Zhong, X. Wan, C. Rong, P. K. Chattaraj & D. Zhao. “Revisiting the trapping of noble gases (He–Kr) by the triatomic H_3^+ and Li_3^+ species: a density functional reactivity theory study”. *J. Mol. Model.* **28**, 122 (2022).
- [218] M. Goli & S. Shahbazian. “The quantum theory of atoms in positronic molecules: A case study on diatomic species”. *Int. J. Quantum Chem.* **111**, 1982 (2011).
- [219] M. Gharabaghi & S. Shahbazian. “Incorporating nuclear vibrational energies into the “atom in molecules” analysis: An analytical study”. *J. Chem. Phys* **146**, 154106 (2017).
- [220] L. Pauling, C. University & C. U. Press. *The Nature of the Chemical Bond and the Structure of Molecules and Crystals: An Introduction to Modern Structural Chemistry*. George Fisher Baker Non-Resident Lecture Series (Cornell University Press, 1960).
- [221] R. J. Boyd. “The relative sizes of atoms”. *J. Phys. B* **10**, 2283 (1977).

- [222] R. D. Shannon. “Revised effective ionic radii and systematic studies of interatomic distances in halides and chalcogenides.”. *Acta Cryst.* **32**, 751 (1976).
- [223] M. Rahm, R. Hoffmann & N. W. Ashcroft. “Atomic and Ionic Radii of Elements 1–96”. *Chem. Eur. J* **22**, 14625 (2016).
- [224] S. S. Batsanov. “van der Waals Radii of Elements”. *Inorg. Mater.* **37**, 1031 (2001).
- [225] M. Mantina, A. C. Chamberlin, R. Valero, C. J. Cramer & D. G. Truhlar. “Consistent van der Waals radii for the whole main group”. *J. Phys. Chem. A* **113**, 5806 (2009).
- [226] B. Cordero, V. Gómez, A. E. Platero-Prats, M. Revés, J. Echeverría, E. Cremades, F. Barragán & S. Alvarez. “Covalent radii revisited”. *J. Chem. Soc. Dalton Trans.* 2832–2838 (2008).
- [227] D. Rappoport & F. Furche. “Property-optimized Gaussian basis sets for molecular response calculations”. *J. Chem. Phys.* **133**, 134105 (2010).
- [228] S. Ito, D. Yoshida, Y. Kita, T. Shimazaki & M. Tachikawa. “Stability and bonding nature of positronic lithium molecular dianion”. *J. Chem. Phys.* **158**, 204303 (2023).
- [229] A. Tkatchenko & M. Scheffler. “Accurate molecular van der Waals interactions from ground-state electron density and free-atom reference data”. *Phys. Rev. Lett.* **102**, 073005 (2009).
- [230] A. Bondi. “Van der waals volumes and radii”. *J. Phys. Chem.* **68**, 441 (1964).
- [231] D. L. Donohue, L. D. Hulett, S. A. McLuckey, G. L. Glish & H. S. Mckown. “Positron ionization mass spectrometry. I: instrumentation”. *Int. J. Mass Spectrom.* **97**, 227 (1990).
- [232] J. Hermann, R. A. DiStasio & A. Tkatchenko. “First-Principles Models for van der Waals Interactions in Molecules and Materials: Concepts, Theory, and Applications”. *Chem. Rev.* **117**, 4714 (2017).
- [233] M. J. Puska, A. P. Seitsonen & R. M. Nieminen. “Electron-positron Car-Parrinello methods: Self-consistent treatment of charge densities and ionic relaxations”. *Phys. Rev. B* **52**, 10947 (1995).
- [234] T. Koga, S. Watanabe, K. Kanayama, R. Yasuda & A. J. Thakkar. “Improved Roothaan-Hartree-Fock wave functions for atoms and ions with N less equal than 54”. *J. Chem. Phys.* **103**, 3000 (1995).
- [235] K. R. Lykke, K. K. Murray & W. C. Lineberger. “Threshold photodetachment of H⁻”. *Phys. Rev. A.* **43**, 6104 (1991).

- [236] G. Haefliger, D. Hanstorp, I. Kiyan, A. E. Klinkmüller, U. Ljungblad & D. J. Pegg. “Electron affinity of Li: A state-selective measurement”. *Phys. Rev. A* **53**, 4127 (1996).
- [237] M. Scheer, R. C. Bilodeau, H. K. Haugen & H. K. Haugen. “Negative ion of boron: An experimental study of the 3P ground state”. *Phys. Rev. Lett* **80**, 2562 (1998).
- [238] D. Bresteau, C. Drag & C. Blondel. “Isotope shift of the electron affinity of carbon measured by photodetachment microscopy”. *Phys. Rev. A* **93**, 013414 (2016).
- [239] C. Blondel, C. Delsart, C. Valli, S. Yiou, M. R. Godefroid & S. Van Eck. “Electron affinities of ^{16}O , ^{17}O , ^{18}O , the fine structure of $^{16}O^-$ and the hyperfine structure of $^{17}O^-$ ”. *Phys. Rev. A* **64**, 052504 (2001).
- [240] C. Blondel, C. Delsart & F. Goldfarb. “Electron spectrometry at the μeV level and the electron affinities of Si and F”. *J. Phys. B* **34**, L281 (2001).
- [241] B. A. Bushaw, W. Nörtershäuser, G. W. Drake & H. J. Kluge. “Ionization energy of $^{6,7}Li$ determined by triple-resonance laser spectroscopy”. *Phys. Rev. A* **75**, 052503 (2007).
- [242] R. Beigang, D. Schmidt & P. J. West. “Laser spectroscopy of high Rydberg states of light alkaline-earth elements: Be and Mg”. *J. phys., Colloq.* **44**, 229 (1983).
- [243] X. Guan, B. Li & K. T. Taylor. “Strong parallel magnetic field effects on the hydrogen molecular ion”. *J. Phys. B* **36**, 3569 (2003).
- [244] A. V. Turbiner & J. C. Lopez Vieyra. “Ground state of the H_3^+ molecular ion: Physics behind”. *J. Phys. Chem. A* **117**, 10119 (2013).
- [245] M. Ayouz, O. Dulieu, R. Gúrout, J. Robert & V. Kokoouline. “Potential energy and dipole moment surfaces of H_3^- molecule”. *J. Chem. Phys* **132**, 194309 (2010).
- [246] S. Nasiri & M. Zahedi. “A benchmark study of Li_2^+ , Li_2^- , LiH^+ and LiH^- : Quantum Monte-Carlo and coupled-cluster computations”. *Comput. Theor. Chem.* **1114**, 106 (2017).
- [247] D. Bressanini, G. Morosi & S. Tarasco. “An investigation of nodal structures and the construction of trial wave functions”. *J. Chem. Phys* **123**, 204109 (2005).

